




This is to certify that the
dissertation entitled
METAL-METAL BONDED COMPLEXES IN EXTENDED
MOLECULAR ARRAYS
presented by

Stuart L. Bartley

has been accepted towards fulfillment
of the requirements for

Ph.D. degree in Chemistry


Major professor

Date August 26, 1993

LIBRARY

Michigan State University

PLACE IN RETURN BOX to remove this checkout from your record.
TO AVOID FINES return on or before date due.

DATE DUE	DATE DUE	DATE DUE
OCT 04 2009 041709	_____	_____
_____	_____	_____
_____	_____	_____
_____	_____	_____
_____	_____	_____
_____	_____	_____
_____	_____	_____

**METAL-METAL BONDED COMPLEXES IN EXTENDED
MOLECULAR ARRAYS**

By

Stuart L. Bartley

A DISSERTATION

**Submitted to
Michigan State University
in partial fulfillment of the requirements
for the degree of**

DOCTOR OF PHILOSOPHY

Department of Chemistry

1993

ABSTRACT

METAL-METAL BONDED COMPLEXES IN EXTENDED MOLECULAR ARRAYS

By

Stuart L. Bartley

Metal-metal bonded dinuclear complexes that are redox active and coordinatively unsaturated are targeted as building blocks in the synthesis of new materials that may exhibit interesting optical, magnetic, or conductive properties. The reactions of dimetal donor compounds (e.g. $M_2Cl_4(PR_3)_4$; $M = Re, Mo$) with polycyano organic acceptor compounds lead to the formation of covalently linked complexes. The tetranuclear compound $[Re_2Cl_4(dppm)_2]_2(\mu\text{-TCNQ})$ (dppm = bis(diphenylphosphino)-methane, TCNQ = 7,7,8,8-tetracyanoquinodimethane) was characterized and is the first structurally characterized example of a complex containing a bridging TCNQ unit. Similar results were obtained using a variety of substituted dicyanoquinodiimines (DCNQI's). An alternative route to the direct ligation of redox active ligands to a metal center was accomplished using the tetrathiafulvalenyl-*ortho*-bisphosphine compound, $Ph_2P\text{-TTF-PPh}_2$. The reactions of chemically or electrochemically reduced forms of the polycyano acceptors with solvated metal-metal bonded complexes (e.g. $[Rh_2(NCCH_3)_{10}](BF_4)_4$) also lead to covalently linked complexes.

Another approach to the synthesis of polymeric materials incorporating metal-metal bonds is the reaction of solvated dimetal cations with homoleptic dinuclear metal-cyanide anions. Several metal-cyanide compounds, including $[\text{Bu}^n_4\text{N}]_4[\text{Mo}_2(\text{CN})_8]$, were synthesized and spectroscopically and structurally characterized. In general, the chemistry of cyanide with dinuclear compounds has not been well examined, therefore, the chemistry of cyanide with several metal-metal bonded complexes was studied.

To my wife Robin and my children Rebecca and Benjamin.

ACKNOWLEDGEMENTS

I would like to first thank Professor Kim R. Dunbar for her guidance and support during these past several years. It is primarily because of her enthusiasm and outstanding ability to teach that I was able to accomplish my goals. I also want to thank all of the past and present Dunbar group students, especially Steven Haefner, Laura Pence, and Sue-Jane Chen, for their excellent help and training when I first began in the lab. It was a pleasure to be able to spend three years in the same lab with Jui-Sui "Alice" Sun as she always had the answers for all of the tough questions. Also, thanks to John Matonic, Anne Quillevere, Gary Finniss, Xiang "Sean" Ouyang, Kemal Catalan, Calvin Ulzemeier, Vijay Saharan and Susan Baker for their help and friendship.

Many thanks go to Michigan State University, the Department of Chemistry and the Center for Fundamental Materials Research, and the Council for Graduate Students for financial support. I would also like to thank Dr. Donald Ward for his help with many crystallographic problems and Professors Thomas J. Pinnavaia, James E. Jackson and Eugene LeGoff for being on my Dissertation committee.

I want to thank my parents for their support, for having confidence in me and for giving me the freedom to do as I choose. I want to thank my mother- and father-in-law for easing the pressures of graduate school by giving me those needed weekend getaways to Grand Rapids and for helping to care for my children when I needed time for my studies.

Finally, a special thanks to my wife Robin for being there for me every step of the way regardless of the circumstances and for making this experience a pleasurable one.

TABLE OF CONTENTS

	page
LIST OF TABLES	xvii
LIST OF FIGURES	xx
LIST OF SYMBOLS AND ABBREVIATIONS	xxiv
LIST OF COMPOUNDS	xxviii
 CHAPTER I	
INTRODUCTION	1
A. The Synthesis of Molecular Metals and Magnets from Charge-Transfer Reactions.	2
B. Complexes That Contain Covalently linked Donors or Acceptors.	6
C. The Design of Magnetic Materials.	8
D. Inorganic-Organic Hybrid Polymers.	9
E. Metal-Metal Bonds in Extended Arrays.	10
 CHAPTER II	
REACTIVITY STUDIES OF $\text{Re}_2\text{Cl}_4(\text{dppm})_2$ WITH TCNE, TCNQ, AND TNAP.	19
1. Introduction	20
2. Experimental.	21
A. Synthesis	21
(1) Preparation of $\text{Re}_2\text{Cl}_4(\text{dppm})_2$	21

(2) 1:1 Reactions of $\text{Re}_2\text{Cl}_4(\text{dppm})_2$ with TCNQ.....	23
(i) Preparation of (1)-A	23
(ii) Preparation of (1)-B	23
(iii) Preparation of (1)-C	24
(iv) Preparation of (1)-D	24
(3) Preparation of $[\text{Re}_2\text{Cl}_4(\text{dppm})_2]_2(\mu\text{-TCNQ})$ (2)	24
(i) Bulk Reaction	24
(ii) Slow Diffusion Reaction	25
(4) 1:1 Reactions of $\text{Re}_2\text{Cl}_4(\text{dppm})_2$ with TCNE.....	25
(i) Preparation of (3)-A	25
(ii) Preparation of (3)-B	26
(iii) Refluxing Reaction in Toluene.....	26
(5) Reactions of $\text{Re}_2\text{Cl}_4(\text{dppm})_2$ with TNAP	27
(i) Preparation of $[\text{Re}_2\text{Cl}_4(\text{dppm})_2](\text{TNAP})$ (4)	27
(ii) Preparation of $[\text{Re}_2\text{Cl}_4(\text{dppm})_2]_2(\mu\text{-TNAP})$ (5).....	27
B. X-Ray Crystallography	28
(1) $[\text{Re}_2\text{Cl}_4(\text{dppm})_2]_2(\text{TCNQ})\cdot 8\text{THF}$, (2) $\cdot 8\text{THF}$	30
(i) Data Collection and Reduction.....	30
(ii) Structure Solution and Refinement.....	30
3. Results and Discussion.....	31
A. Reactions of $\text{Re}_2\text{Cl}_4(\text{dppm})_2$ with TCNQ.....	31
(1) Preparation.....	31
(2) Spectroscopic Properties	32

(3) X-ray Crystal Structure of $[\text{Re}_2\text{Cl}_4(\text{dppm})_2]_2(\mu\text{-TCNQ})\cdot 8\text{THF}$ (2)·8THF	42
(4) Magnetic and Electrical Properties.....	53
B. Reactions of $\text{Re}_2\text{Cl}_4(\text{dppm})_2$ with TCNE	56
(1) Preparation and Spectroscopic Properties	56

CHAPTER III

THE USE OF N,N'-DICYANOQUINONEDIIMINES AS LINKING UNITS FOR THE DINUCLEAR COMPOUND $\text{Re}_2\text{Cl}_4(\text{dppm})_2$

1. Introduction	75
2. Experimental.....	75
A. Synthesis	75
(1) Preparation of DCNPQI.....	77
(2) Reaction of $\text{Re}_2\text{Cl}_4(\text{dppm})_2$ with DM-CNQMI.....	78
(3) Reactions of $\text{Re}_2\text{Cl}_4(\text{dppm})_2$ with DCNQI.....	78
(i) Preparation of $[\text{Re}_2\text{Cl}_4(\text{dppm})_2]_2(\mu\text{-DCNQI})$	78
(ii) 1:4 $\text{Re}_2\text{Cl}_4(\text{dppm})_2$:DCNQI Stoichiometric Reaction.	79
(4) Reactions of $\text{Re}_2\text{Cl}_4(\text{dppm})_2$ with DM-DCNQI.....	79
(i) 1:1 Reactions	79
(a) Preparation of $[\text{Re}_2\text{Cl}_4(\text{dppm})_2](\text{DM-DCNQI})$ (6)-A	79
(b) Preparation of $[\text{Re}_2\text{Cl}_4(\text{dppm})_2](\text{DM-DCNQI})$ (6)-B	80
(c) Reaction of 1:1 $\text{Re}_2\text{Cl}_4(\text{dppm})_2$ and DM-DCNQI in Toluene.....	80

(ii) Preparation of $[\text{Re}_2\text{Cl}_4(\text{dppm})_2]_2(\mu\text{-DM-DCNQI})$ (7)	81
(a) Slow Diffusion Reaction	81
(b) Bulk Reaction	81
(5) Reactions of $\text{Re}_2\text{Cl}_4(\text{dppm})_2$ with DCNNQI	82
(i) 2:1 $\text{Re}_2\text{Cl}_4(\text{dppm})_2$:DCNNQI Reaction	82
(ii) 1:1 Reaction	82
(6) Reactions of $\text{Re}_2\text{Cl}_4(\text{dppm})_2$ with DCNAQI	83
(i) 1:2 $\text{Re}_2\text{Cl}_4(\text{dppm})_2$:DCNAQI Reaction	83
(ii) 2:1 $\text{Re}_2\text{Cl}_4(\text{dppm})_2$:DCNAQI Reaction	83
(7) 2:1 Reaction of $\text{Re}_2\text{Cl}_4(\text{dppm})_2$ with DC-DCNAQI	84
(8) 2:1 Reaction of $\text{Re}_2\text{Cl}_4(\text{dppm})_2$ with DCNPQI	84
(9) Reaction of $[\text{Re}_2\text{Cl}_4(\text{dppm})_2]_2(\text{DM-DCNQI})$ (7) with DM-CNQMI.	85
B. X-ray Crystallography	85
(1) $[\text{Re}_2\text{Cl}_4(\text{dppm})_2]_2(\text{DM-DCNQI})\cdot 4\text{THF}$, (7) $\cdot 4\text{THF}$	85
(i) Data Collection and Reduction	86
(ii) Structure Solution and Refinement	86
3. Results	87
A. Reactions of $\text{Re}_2\text{Cl}_4(\text{dppm})_2$ with DM-DCNQI	88
(1) Preparation and spectroscopic properties	88
(2) X-ray crystal structure of $[\text{Re}_2\text{Cl}_4(\text{dppm})_2]_2(\text{DM-DCNQI})\cdot 4\text{THF}$, (7) $\cdot 4\text{THF}$	89
(3) Magnetic properties	92

B. Reactions of $\text{Re}_2\text{Cl}_4(\text{dppm})_2$ with other DCNQIs.....	92
4. Conclusions.....	99

CHAPTER IV

REACTIONS OF $\text{M}_2\text{Cl}_4(\text{PR}_3)_4$, $\text{M}_2\text{Cl}_4(\text{P}\sim\text{P})_2$ ($\text{M} = \text{Mo}, \text{Re}$; $\text{R} = \text{Et}$, Pr^n ; $\text{P}\sim\text{P} = \text{dppm}, \text{dmpm}, \text{dppe}$), AND $[\text{M}_2(\text{NCCH}_3)_{10}][\text{BF}_4]_4$ ($\text{M} = \text{Mo}, \text{Rh}$) WITH POLYCYANO ACCEPTORS.....	102
1. Introduction.....	103
2. Experimental.....	103
A. Synthesis.....	103
(1) Reactions of $\text{Re}_2\text{Cl}_4(\text{PEt}_3)_4$ with TCNQF_4	103
(2) Reaction of $\text{Re}_2\text{Cl}_4(\text{PEt}_3)_4$ with TCNQ	104
(3) Reaction of $\text{Re}_2\text{Cl}_4(\text{PEt}_3)_4$ with DM-DCNQI.....	104
(4) Reactions of $\text{Mo}_2\text{Cl}_4(\text{dppe})_2$ with TCNQ	104
(i) 1:2 $\text{Mo}_2\text{Cl}_4(\text{dppe})_2$: TCNQ Reaction.....	104
(ii) 2:1 $\text{Mo}_2\text{Cl}_4(\text{dppe})_2$: TCNQ Reaction.....	105
(iii) 4:1 $[\text{Mo}_2\text{Cl}_4(\text{dppe})_2$: $\text{TCNQ}]$ Reaction.....	105
(5) Reaction of $\text{Mo}_2\text{Cl}_4(\text{dppe})_2$ with TCNE	106
(6) Reaction of $\text{Mo}_2\text{Cl}_4(\text{dppe})_2$ with TCNQF_4	106
(7) Reaction of $\text{Mo}_2\text{Cl}_4(\text{dppe})_2$ with DM-DCMQI.....	106
(8) Reaction of $\text{Mo}_2\text{Cl}_4(\text{dppm})_2$ with TCNQ	107
(9) Reaction of $\text{Mo}_2\text{Cl}_4(\text{dppm})_2$ with TCNE	107
(10) Reaction of $\text{Mo}_2\text{Cl}_4(\text{PEt}_3)_4$ with TCNQ	107
(11) Reaction of $\text{Mo}_2\text{Cl}_4(\text{PEt}_3)_4$ with TCNQF_4	108
(12) Reaction of $\text{Mo}_2\text{Cl}_4(\text{dmpm})_2$ with TCNQ	108

(13) Reaction of $\text{Mo}_2\text{Cl}_4(\text{dmpm})_2$ with TCNE.....	108
(14) Reaction of $\text{Re}_2\text{Cl}_4(\text{dppm})_2$ with TCNQF_4	108
(15) Reaction of $\text{Re}_2\text{Cl}_4(\text{PPr}^n_3)_4$ with DM-DCNQI.....	109
(16) Reaction of $[\text{Rh}_2(\text{NCCH}_3)_{10}][\text{BF}_4]_4$ with [Bu^n_4N] TCNQ	109
(17) Reaction of $[\text{Rh}_2(\text{NCCH}_3)_{10}][\text{BF}_4]_4$ with LiTCNQ	109
(18) Reaction of $[\text{Rh}_2(\text{NCCH}_3)_{10}][\text{BF}_4]_4$ with LiTCNQ in H_2O	110
(19) Electrochemical preparation of " $\text{Rh}(\text{TCNQ})_2$ ".....	110
(20) Reaction of $[\text{Rh}_2(\text{NCCH}_3)_{10}][\text{BF}_4]_4$ with $\text{Li}[\text{DM-DCNQI}]$	110
(21) Electrochemical Preparation of " $[\text{Rh}(\text{DM-DCNQI})_2]$ "	112
(22) Reaction of $[\text{Mo}_2(\text{NCCH}_3)_{10}][\text{BF}_4]_4$ with [Bu^n_4N] $[\text{TCNQ}]$	112
3. Results and Discussion.....	112
A. Reactions of Dinuclear Complexes with Polycyano Acceptors	112
B. Reactions of Solvated Metal Cations with Reduced Forms of Polycyano Acceptors.....	118
4. Conclusions.....	123
CHAPTER V	
METAL-METAL BONDED COMPOUNDS WITH CYANIDE LIGANDS.	
1. Introduction	128
2. Experimental.....	128
A. Synthesis	128

(1) Starting Materials.....	128
(2) Synthesis of $[\text{Bu}^n_4\text{N}]_4[\text{Mo}_2(\text{CN})_8]$ (8).....	129
(3) Synthesis of $[\text{Bu}^n_4\text{N}]_3[\text{Mo}_2(\text{O}_2\text{CCH}_3)(\text{CN})_6]$ (9).....	129
(4) Synthesis of $[\text{Et}_4\text{N}]_4[\text{Mo}_2(\text{CN})_8]$ (10).....	130
(i) Method i	130
(ii) Method ii	130
(iii) Method iii	130
(5) Synthesis of $[\text{Bu}^n_4\text{N}]_2[\text{Re}_2(\text{CN})_6(\text{dppm})_2]$ (11).....	131
(6) Preparation of " $\text{Mo}_2(\text{CN})_4(\text{NCCH}_3)_x$ "	131
(7) Reaction of $[\text{Et}_4\text{N}]_4[\text{Mo}_2(\text{CN})_8]$ with $[\text{Rh}_2(\text{NCCH}_3)_{10}][\text{BF}_4]_4$	132
(8) Reaction of $[\text{Et}_4\text{N}]_4[\text{Mo}_2(\text{CN})_8]$ with $[\text{Re}_2(\text{NCCH}_3)_{10}][\text{BF}_4]_4$	132
(9) Reaction of $[\text{Et}_4\text{N}]_4[\text{Mo}_2(\text{CN})_8]$ with $[\text{Fe}(\text{NCCH}_3)_6][\text{BF}_4]_2$	132
(10) Reaction of $[\text{Bu}^n_4\text{N}]_3[\text{Mo}_2(\text{O}_2\text{CCH}_3)(\text{CN})_6]$ with $[\text{Rh}_2(\text{NCCH}_3)_{10}][\text{BF}_4]_4$	133
(B). X-ray Crystallography	133
(1) $[\text{Bu}^n_4\text{N}]_4[\text{Mo}_2(\text{CN})_8] \cdot 8\text{CHCl}_3$ (8) $\cdot 8\text{CHCl}_3$	133
(i) Data Collection and Reduction.....	133
(ii) Structure Solution and Refinement.....	137
(2) $[\text{Bu}^n_4\text{N}]_3[\text{Mo}_2(\text{O}_2\text{CCH}_3)(\text{CN})_6]$ (9).....	137
(i) Data Collection and Reduction.....	137
(ii) Structure Solution and Refinement.....	138

(3) [Bu ⁿ ₄ N] ₂ [Re ₂ (CN) ₆ (dppm) ₂].8CH ₂ Cl ₂ (11).8CH ₂ Cl ₂	139
(i) Data Collection and Reduction.....	139
(ii) Structure Solution and Refinement.....	139
3. Results and Discussion.....	140
A. Preparation of Cyanide Compounds from Carboxylate and Chloride Compounds.	140
(1) Preparation of Dimolybdenum-cyanide Complexes.	140
(2) Preparation of [Bu ⁿ ₄ N] ₂ [Re ₂ (CN) ₆ (dppm) ₂] (11).....	141
B. Spectroscopy.....	142
C. Molecular Structures	144
(1) Crystal structure of [Bu ⁿ ₄ N] ₄ [Mo ₂ (CN) ₈].8CHCl ₃ (8).8CHCl ₃	144
(2) Crystal structure of [Bu ⁿ ₄ N] ₃ [Mo ₂ (O ₂ CCH ₃)(CN) ₆] (9).	144
(3) Crystal structure of [Bu ⁿ ₄ N] ₂ [Re ₂ (CN) ₆ (dppm) ₂].8CH ₂ Cl ₂ (11).8CH ₂ Cl ₂	149
D. Reactivity of Mo ₂ (CN) ₈ ⁴⁻ towards solvated metal cations.....	156

CHAPTER VI

REACTIONS OF METAL-METAL BONDED COMPLEXES WITH PHOSPHINE-FUNCTIONALIZED TETRATHIAFULVALENE DONORS.....	165
1. Introduction	166
2. Experimental.....	166
A. Synthesis	166
(1) Preparation of [Rh{Me ₂ (PPh ₂) ₂ TTF}] ₂ [BF ₄] (12).....	167

(2) Preparation of $\text{ReCl}_2[\text{Me}_2(\text{PPh}_2)_2\text{TTF}]_2$ (13)	167
(3) Reactions of $\text{Mo}_2(\text{O}_2\text{CCR}_3)_4$ ($\text{R} = \text{H}, \text{F}$) with $\text{Me}_2(\text{PPh}_2)_2\text{TTF}$	168
(4) Reaction of $[\text{Rh}_2(\text{NCCH}_3)_{10}](\text{BF}_4)_4$ with $\text{Me}_3(\text{PPh}_2)\text{TTF}$	168
(5) Reaction of $[\text{Bu}_4^n\text{N}]_2\text{Re}_2\text{Cl}_8$ with $\text{Me}_3(\text{PPh}_2)\text{TTF}$	169
(6) Reaction of $[\text{Rh}_2(\text{NCCH}_3)_{10}][\text{BF}_4]_4$ with $(\text{PPh}_2)_4\text{TTF}$	169
(7) Reaction of $\text{Re}_2\text{Cl}_6(\text{PBu}_3^n)_2$ with $(\text{PPh}_2)_4\text{TTF}$	170
B. X-ray Crystallography.....	170
(i) Data Collection and Reduction.....	171
(ii) Structure Solution and Refinement.....	171
3. Results and Discussion.....	172
A. Synthesis and Spectroscopy.	172
(1) Reactions of $\text{Me}_2(\text{PPh}_2)_2\text{TTF}$	172
(2) Reactions of $\text{Me}_3(\text{PPh}_2)\text{TTF}$	178
(3) Reactions of $(\text{PPh}_2)_4\text{TTF}$	178
B. X-ray Crystal Structure	179
 CHAPTER VII	
REACTIONS OF THE ELECTRON-RICH TRIPLY BONDED COMPOUND $\text{Re}_2\text{Cl}_4(\text{dppm})_2$ WITH DIOXYGEN.	
1. Introduction	183

2. Experimental Section	183
A. Synthesis	183
(1) Synthesis of $\text{Re}_2(\mu\text{-O})(\mu\text{-Cl})\text{OCl}_3(\text{dppm})_2 \cdot (14)$	184
(i) Method A	184
(ii) Method B	184
(2) Synthesis of $\text{Re}_2(\mu\text{-O})\text{O}_2\text{Cl}_4(\text{dppm})_2 (15)$	185
(i) Method A	185
(ii) Method B	185
(iii) Rigorous Exclusion of H_2O	186
B. X-ray Crystallographic Procedures	186
(1) $\text{Re}_2(\mu\text{-O})(\mu\text{-Cl})\text{OCl}_3(\text{dppm})_2 \cdot (\text{CH}_3)_2\text{CO}$ $(14) \cdot (\text{CH}_3)_2\text{CO}$	187
(2) $\text{Re}_2(\mu\text{-O})\text{O}_2\text{Cl}_4(\text{dppm})_2 \cdot 2(\text{CH}_3)_2\text{CO}$ $(15) \cdot 2(\text{CH}_3)_2\text{CO}$	189
3. Results and Discussion	191
A. Synthesis	191
B. Spectroscopy	194
CHAPTER VIII	
CONCLUSIONS	207
APPENDIX	211

LISTS OF TABLES

		page
1.	Summary of crystallographic data for [Re ₂ Cl ₄ (dppm) ₂] ₂ (μ-TCNQ)·8THF, (2)·8THF.	29
2.	Comparison of the C≡N and C=C stretching frequencies of various TCNQ containing products.....	34
3.	Comparison of the electronic spectral data of various TCNQ and TCNE complexes.....	38
4.	Selected bond distances(Å), bond angles(°) and torsion angles(°) for [Re ₂ Cl ₄ (dppm) ₂] ₂ (μ-TCNQ)·8THF, (2)·8THF.	46
5.	Comparison of selected bond distances and angles of dirhenium complexes exhibiting an unsymmetrical M ₂ L ₉ geometry.....	49
6.	Comparison of bond distances (Å) and angle (°) of several TCNQ containing products.	52
7.	Comparison of ν(C≡N) stretching frequencies for various TCNE containing complexes.....	61
8.	Comparison of the infrared spectral features of the TCNQ and TNAP products.	67
9.	Summary of crystallographic data for [Re ₂ Cl ₄ (dppm) ₂] ₂ (μ-DMDCNQI)·4THF (7)·4THF.	86
10.	Selected bond distances(Å), bond angles(°) and torsion angles(°) for [Re ₂ Cl ₄ (dppm) ₂] ₂ (μ-DM-DCNQI)·4THF, (7)·4THF.....	97
11.	Tabulation of ν(C≡N) stretching frequencies for the products from reactions of Re ₂ Cl ₄ (dppm) ₂ with DCNQIs.	100

12.	Comparison of the $\nu(\text{C}\equiv\text{N})$ stretching frequencies for products from reactions of dinuclear donor complexes with TCNQ.....	114
13.	Comparison of the $\nu(\text{C}\equiv\text{N})$ stretching frequencies for products from reactions of dinuclear donor complexes with TCNE.	115
14.	Comparison of the $\nu(\text{C}\equiv\text{N})$ stretching frequencies for products from reactions of dinuclear donor complexes with TCNQF ₄	116
15.	Comparison of the $\nu(\text{C}\equiv\text{N})$ stretching frequencies for products from reactions of dinuclear donor complexes with DM-DCNQL.....	117
16.	Summary of crystallographic data for [Bu ⁿ N] ₄ [Mo ₂ (CN) ₈]·8CHCl ₃ (8)·8CHCl ₃	134
17.	Summary of crystallographic data for [Bu ⁿ N] ₃ [Mo ₂ (O ₂ CCH ₃)(CN) ₆] (9).	135
18.	Summary of crystallographic data for [Bu ⁿ N] ₂ [Re ₂ (CN) ₆ (dppm) ₂]·8CH ₂ Cl ₂ (11)·8CH ₂ Cl ₂	136
19.	Selected Bond Distances (Å) and Bond Angles (°) for [Bu ⁿ N] ₄ [Mo ₂ (CN) ₈]·8CHCl ₃ , (8)·8CHCl ₃	146
20.	Comparison of the Mo-Mo bond distances of selected quadruply bonded dimolybdenum complexes.....	147
21.	Selected Bond Distances (Å) and Bond Angles (°) for [Bu ⁿ N] ₃ [Mo ₂ (O ₂ CCH ₃)(CN) ₆] (9).	150
22.	Selected Bond Distances (Å) and Bond Angles (°) for [Bu ⁿ N] ₂ [Re ₂ (CN) ₆ (dppm) ₂]·8CH ₂ Cl ₂ , (11)·8CH ₂ Cl ₂	154
23.	Comparison of $\nu(\text{C}\equiv\text{N})$ bands for mixed metal cyanide materials prepared in this study.....	157
24.	Summary of crystallographic data for Re ₂ (μ-O)(μ-Cl)(O)Cl ₃ (dppm) ₂ ·(CH ₃) ₂ O. (14)·(CH ₃) ₂ O.	190

25.	Summary of crystallographic data for $\text{Re}_2(\mu\text{-O})(\text{O})_2\text{Cl}_3(\text{dppm})_2 \cdot 2(\text{CH}_3)_2\text{O}$, (15)·2(CH ₃) ₂ O.	192
26.	Selected Bond Distances (Å) and Bond Angles (°) for $\text{Re}_2(\mu\text{-O})(\mu\text{-Cl})\text{OCl}_3(\text{dppm})_2 \cdot (\text{CH}_3)_2\text{O}$, (14)·(CH ₃) ₂ O.	200
27.	Selected Bond Distances (Å) and Bond Angles (°) for $\text{Re}_2(\mu\text{-O})\text{O}_2\text{Cl}_4(\mu\text{-dppm})_2 \cdot 2(\text{CH}_3)\text{CO}$, (15)·2(CH ₃)CO.	204
28.	Atomic positional parameters and equivalent isotropic displacement parameters (Å ²) and their estimated standard deviations for $[\text{Re}_2\text{Cl}_4(\text{dppm})_2]_2(\mu\text{-TCNQ}) \cdot 8\text{THF}$, (2)·8THF.	211
29.	Atomic positional parameters and equivalent isotropic displacement parameters (Å ²) and their estimated standard deviations for $[\text{Re}_2\text{Cl}_4(\text{dppm})_2]_2(\mu\text{-DMDCNQI}) \cdot 4\text{THF}$ (7)·4THF.	215
30.	Atomic positional parameters and equivalent isotropic displacement parameters (Å ²) and their estimated standard deviations for $[\text{Bu}_4^{\text{N}}]_4[\text{Mo}_2(\text{CN})_8] \cdot 8\text{CHCl}_3$ (8)·8CHCl ₃	218
31.	Atomic positional parameters and equivalent isotropic displacement parameters (Å ²) and their estimated standard deviations for $[\text{Bu}_4^{\text{N}}]_3[\text{Mo}_2(\text{O}_2\text{CCH}_3)(\text{CN})_6]$ (9).	221
32.	Atomic positional parameters and equivalent isotropic displacement parameters (Å ²) and their estimated standard deviations for $[\text{Bu}_4^{\text{N}}]_2[\text{Re}_2(\text{CN})_6(\text{dppm})_2] \cdot 8\text{CH}_2\text{Cl}_2$ (11)·8CH ₂ Cl ₂	224
33.	Atomic positional parameters and equivalent isotropic displacement parameters (Å ²) and their estimated standard deviations for $[\text{Rh}\{\text{Me}_2(\text{Ph}_2\text{P})_2\text{TTF}\}_2][\text{BF}_4]$ (12).	227
34.	Atomic positional parameters and equivalent isotropic displacement parameters (Å ²) and their estimated standard deviations for $\text{Re}_2(\mu\text{-O})(\mu\text{-Cl})\text{OCl}_3(\text{dppm})_2 \cdot (\text{CH}_3)_2\text{CO}$ (14)·(CH ₃) ₂ CO.	228
35.	Atomic positional parameters and equivalent isotropic displacement parameters (Å ²) and their estimated standard deviations for $\text{Re}_2(\mu\text{-O})\text{O}_2\text{Cl}_4(\text{dppm})_2 \cdot 2(\text{CH}_3)_2\text{CO}$ (15)·2(CH ₃) ₂ CO.	230

LIST OF FIGURES

		page
1.	Side view of the stack in (TMTSF) ₂ (ClO ₄).....	3
2.	Packing diagram of [(C ₅ Me ₅) ₂ Mn][TCNQ].....	5
3.	Selected precursors used for charge-transfer chemistry.....	22
4.	Pathway of the 1:1 reaction between Re ₂ Cl ₄ (dppm) ₂ and TCNQ	33
5.	Infrared spectral monitoring of the conversion of (1)-A to (1)-B in CH ₂ Cl ₂	36
6.	Infrared spectral monitoring of the decomposition of a CH ₂ Cl ₂ solution containing [Re ₂ Cl ₄ (dppm) ₂](μ-TCNQ).(2).....	39
7.	Electronic absorption spectrum of [Re ₂ Cl ₄ (dppm) ₂](μ-TCNQ) (2) in CH ₂ Cl ₂	41
8.	ORTEP representation of [Re ₂ Cl ₄ (dppm) ₂](μ-TCNQ)·8THF, (2)·8THF	43
9.	Pluto representation without dppm ligands of [Re ₂ Cl ₄ (dppm) ₂](μ-TCNQ)·8THF, (2)·8THF	45
10.	Plot of μ _{eff} (B.M.) vs. temperature (K) of [Re ₂ Cl ₄ (dppm) ₂](μ-TCNQ) (2).	54
11.	Plot of μ _{eff} (B.M.) vs. temperature (K) of [Re ₂ Cl ₄ (dppm) ₂](TCNQ) (1)-A.	55
12.	Single crystal EPR spectrum of [Re ₂ Cl ₄ (dppm) ₂](μ-TCNQ) (2) at -160°C.....	57
13.	Packing diagram of [Re ₂ Cl ₄ (dppm) ₂](μ-TCNQ)·8THF, (2)·8THF. View down C axis.....	58

14.	Variable temperature ^{31}P $\{^1\text{H}\}$ NMR (CDCl_3) spectra of $[\text{Re}_2\text{Cl}_4(\text{dppm})_2](\text{TCNE})$ (3)-A.....	63
15.	Cyclic voltammogram of $[\text{Re}_2\text{Cl}_4(\text{dppm})_2](\text{TCNE})$ (3)-A in 0.1 M TBABF $_4$ /CH $_2$ Cl $_2$.versus Ag/AgCl at a Pt disk electrode.....	64
16.	Synthetic route to DCNQI molecules and their cyclic voltammetric properties.	76
17.	Electronic absorption spectrum of $[\text{Re}_2\text{Cl}_4(\text{dppm})_2]_2(\mu\text{-DM-DCNQI})$ (7) in CH $_2$ Cl $_2$	90
18.	ORTEP representation of $[\text{Re}_2\text{Cl}_4(\text{dppm})_2]_2(\mu\text{-DM-DCNQI})\cdot 4\text{THF}$, (7) $\cdot 4\text{THF}$	91
19.	Pluto view without dppm ligands of $[\text{Re}_2\text{Cl}_4(\text{dppm})_2]_2(\mu\text{-DM-DCNQI})\cdot 4\text{THF}$, (7) $\cdot 4\text{THF}$	93
20.	Stick modle packing diagram of $[\text{Re}_2\text{Cl}_4(\text{dppm})_2]_2(\mu\text{-DM-DCNQI})\cdot 4\text{THF}$, (7) $\cdot 4\text{THF}$ viewed along the c axis.....	94
21.	Plot of μ_{eff} (B.M.) vs. temperature (K) of $[\text{Re}_2\text{Cl}_4(\text{dppm})_2]_2(\mu\text{-DM-DCNQI})$ (7).	95
22.	Solid state EPR spectrum of $[\text{Re}_2\text{Cl}_4(\text{dppm})_2]_2(\mu\text{-DM-DCNQI})$ (7) at -160°C.....	96
23.	Schematic drawing of the electrolysis cell used in the electrochemical synthesis of "Rh(TCNQ) $_2$ " and "Rh(DM-DCNQI) $_2$ ".....	111
24.	Plot of μ_{eff} and $1/\chi$ vs. temperature (K) of the product from the reaction of Mo $_2$ Cl $_4$ (dppe) $_2$ with TCNQF $_4$	119
25.	Proposed polymeric structure of "Rh(DM-DCNQI) $_2$ "	124
26.	ORTEP depiction of the molecular anion $[\text{Mo}_2(\text{CN})_8]^{4-}$ with atoms represented by their 50% probability ellipsoids.....	145

27.	Molecular structure of $[\text{Mo}_2(\text{O}_2\text{CCH}_3)(\text{CN})_6]^{3-}$ with the atom labeling scheme. With the exception of the H atoms, the atoms are represented by their 50% probability ellipsoids.	148
28.	ORTEP plot of a molecule of $[\text{Re}_2(\text{CN})_6(\text{dppm})_2]^{2-}$ with non-hydrogen atoms represented by their 50% probability ellipsoids.	152
29.	View looking down on the equatorial plane of the anion $[\text{Re}_2(\text{CN})_6(\text{dppm})_2]^{2-}$ emphasizing the unsymmetrical arrangement of the bridging CN group.....	153
30.	Thermogravimetric analysis of " $\text{Mo}_2(\text{CN})_4(\text{NCCH}_3)_x$ "	159
31.	Thermogravimetric analysis of " $\text{Rh}_2\text{Mo}_2(\text{CN})_8(\text{NCCH}_3)_x$ "	160
32.	Thermogravimetric analysis of " $\text{Re}_2\text{Mo}_2(\text{CN})_8(\text{NCCH}_3)_x$ "	161
33.	Thermogravimetric analysis of " $\text{Fe}_2\text{Mo}_2(\text{CN})_8(\text{NCCH}_3)_x$ "	162
34.	Pluto representation of $[\text{Rh}\{\text{Me}_2(\text{Ph}_2\text{P})_2\text{TTF}\}_2][\text{BF}_4]$ (12).....	173
35.	Stick packing diagram of $[\text{Rh}\{\text{Me}_2(\text{Ph}_2\text{P})_2\text{TTF}\}_2][\text{BF}_4]$ (12).....	174
36.	Cyclic voltammogram of $[\text{Rh}\{\text{Me}_2(\text{Ph}_2\text{P})_2\text{TTF}\}_2][\text{BF}_4]$ (12) in 0.1 M TBABF ₄ /CH ₂ Cl ₂ vs Ag/AgCl at a Pt disk electrode.....	176
37.	Cyclic voltammogram of $\text{Re}_2(\mu\text{-O})(\mu\text{-Cl})\text{OCl}_3(\text{dppm})_2$ (14) in 0.1 M TBABF ₄ /CH ₂ Cl ₂ vs Ag/AgCl at a Pt disk electrode.....	195
38.	Cyclic voltammogram of $\text{Re}_2(\mu\text{-O})\text{O}_2\text{Cl}_4(\text{dppm})_2$ (15) in 0.1 M TBABF ₄ /CH ₂ Cl ₂ vs Ag/AgCl at a Pt disk electrode.....	198
39.	ORTEP representation of $\text{Re}_2(\mu\text{-O})(\mu\text{-Cl})\text{OCl}_3(\text{dppm})_2 \cdot (\text{CH}_3)_2\text{CO}$ (14) $\cdot (\text{CH}_3)_2\text{CO}$ with 35% probability ellipsoids. Phenyl ring atoms are shown as 0.1 Å radius spheres.....	199

40.	ORTEP representation of $\text{Re}_2(\mu\text{-O})\text{O}_2\text{Cl}_4(\text{dppm})_2 \cdot 2(\text{CH}_3)_2\text{CO}$ (15) $\cdot 2(\text{CH}_3)_2\text{CO}$ with 40% probability ellipsoids. Phenyl ring atoms are shown as 0.1 Å radius spheres.	203
-----	-----------------------------------------------------------------------------------------------------------------------------------------------------------------------------------------------------------------------------------------------------------------------------	-----

LIST OF SYMBOLS AND ABBREVIATIONS

Å	Ångström
Ag/AgCl	silver-silver chloride reference
B.M.	Bohr magneton
br	broad
Bu ⁿ	<i>n</i> -butyl
<i>ca.</i>	circa, about
cm	centimeter
cm ⁻¹	wavenumber
CV	cyclic voltamogram
°C	degree centigrade
DC-DCNAQI	1,5-dichloro-N,N'-dicyano-9,10-anthraquinonediimine
DCNAQI	N,N'-dicyano-9,10-anthraquinonediimine
DCNNQI	N,N'-dicyano-1,4-naphthaquinonediimine
DCNPQI	N,N'-dicyano-6,13-pentacenequinonediimine
DCNQI	N,N'-dicyano-1,4-benzoquinonediimine
DM-CNQMI	2,6-dimethyl-N-cyano-1,4-benzoquinone-4-imine
DM-DCNQI	2,5-dimethyl-N,N'-dicyano-1,4-benzoquinonediimine

d	doublet
δ	parts per million (ppm)
dmpm	bis(dimethylphosphino)methane
dppm	bis(diphenylphosphino)methane
dppe	bis(diphenylphosphino)ethane
ε	molar extinction coefficient
<i>E</i>_{p,a}	anodic peak potential
<i>E</i>_{p,c}	cathodic peak potential
emu	electromagnetic unit
EPR	electron paramagnetic resonance
esd	estimated standard deviation
Et	ethyl
FAB	Fast Atom Bombardment
g	EPR g-value, gram
G	Gauss
h	hour
Hz	Hertz
IR	infrared
K	Kelvin
L	liter
λ	wavelength
m	medium
M	moles per liter
Me	methyl

mg	milligram
min.	minute
mL	milliliter
mm	millimeter
mmol	millimole
mult	multiplet
μ	bridging ligand
μ L	microliter
nm	nanometer
v	frequency
NMR	nuclear magnetic resonance
Ω	ohm
ox	oxidation
ppm	parts per million
Pr ⁿ	<i>n</i> -propyl
R	resistivity
red	reduction
r.t.	room temperature
s	singlet (NMR), strong (IR)
sh	shoulder
SQUID	Superconducting Quantum Interference Device
T	temperature
TCNE	tetracyanoethylene

TCNQ	7,7,8,8-tetracyanoquinodimethane
TCNQF ₄	7,7,8,8-tetracyano-2,3,5,6-tetrafluoroquinodimethane
TGA	thermogravimetric analysis
TNAP	11,11,12,12-tetracyanonapthaquinodimethane
TTF	tetrathiafulvalene
t	triplet
TBABF ₄	tetra- <i>n</i> -butylammonium tetrafluoroborate
THF	teterahydrofuran
TMS	tetramethylsilane
UV	ultraviolet
V	Volt
vs	versus, very strong
w	weak
X	halide ligand

LIST OF COMPOUNDS

- (1) -----[Re₂Cl₄(dppm)₂](TCNQ)
- (2) -----[Re₂Cl₄(dppm)₂]₂(μ-TCNQ)
- (3) -----[Re₂Cl₄(dppm)₂](TCNE)
- (4) -----[Re₂Cl₄(dppm)₂](TNAP)
- (5) -----[Re₂Cl₄(dppm)₂]₂(μ-TNAP)
- (6) -----[Re₂Cl₄(dppm)₂](DM-DCNQI)
- (7) -----[Re₂Cl₄(dppm)₂]₂(μ-DM-DCNQI)
- (8) -----[Buⁿ₄N]₄[Mo₂(CN)₈]
- (9) -----[Buⁿ₄N]₃[Mo₂(O₂CCH₃)(CN)₆]
- (10) -----[Et₄N]₄[Mo₂(CN)₈]
- (11) -----[Buⁿ₄N]₂[Re₂(CN)₆(dppm)₂]
- (12) -----[Rh{Me₂(PPh₂)₂TTF}₂][BF₄]
- (13) -----ReCl₂[Me₂(PPh₂)₂TTF]₂
- (14) -----Re₂(μ-O)(μ-Cl)OCl₃(dppm)₂
- (15) -----Re₂(μ-O)O₂Cl₄(dppm)₂

CHAPTER I

INTRODUCTION

A. Th

Charge-

Th

conduct

operation

receptor

process

other p

receptor

usually

which d

station I

structure

compon

partial

charge-

potential

station

TFE D

which I

related

amount

structural

other

descri

volume

A. The Synthesis of Molecular Metals and Magnets from Charge-Transfer Reactions.

There is considerable interest in the design and synthesis of conducting organic charge-transfer salts, organic metals, and organic superconductors.¹ Low-dimensional molecular solids comprised of donor-acceptor (D-A) stacks exhibit a variety of properties depending on the precursors and the stacking arrangement. Most charge-transfer solids either possess segregated stacking arrangements in which donors and acceptors are aligned in separate stacks, for example (TTF)(TCNQ), and usually exhibit electrical conductivity, or mixed stack arrangements in which the stacks contain alternating donors and acceptors and usually exhibit interesting optical as well as magnetic properties.² The segregated structural motif allows for electrical conductivity provided at least one component is in a non-integral oxidation state (i.e., "mixed valence," "partial oxidation," "incomplete charge transfer"). It has been shown that charge-transfer complexes, in which the difference between redox potentials between the donor and acceptor are small, result in products that exhibit the highest electrical conductivities. Such is the case for (TTF)(TCNQ) with well matched oxidation and reduction potentials that result in a material comprised of partially oxidized TTF and partially reduced TCNQ.² Infrared spectroscopy is a useful tool for ascertaining the amount of charge transfer in these complexes.³ In the segregated stack structures, conduction bands form as the result of intermolecular π -overlap, thereby providing a pathway for charge mobility. In some cases superconductivity is even observed as in (TMTSF)₂ClO₄ (TMTSF = tetramethyltetraselenafulvalene) whose structure (Figure 1) contains *partially* oxidized TMTSF molecules in one-dimensional stacks.² Due to

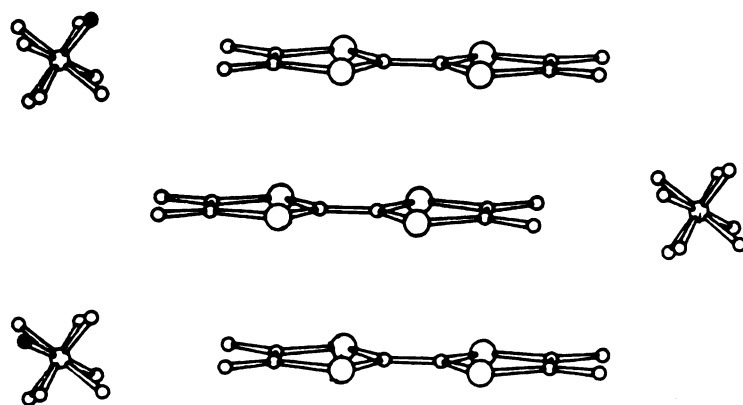


Figure 1. Side view of the stack in $(\text{TMTSF})_2(\text{ClO}_4)$

their st

that =

condit

I

metal

Rh₂O

molecu

inged

A

charge

A 147

magne

ICNE

and I

Encom

CSM

immed

track

CSM

imp

Encom

De or

Amag

1920

1920

1920

1920

1920

1920

their similarity to TTF, $M(\text{bdt})_2$ (bdt = bis-dithiolene) and $M(\text{dmit})_2$ (dmit = 1,3-dithiol-2-thione-4,5-dithiolate) units have been used to form conductive complexes with both inorganic and organic ions.⁴

In several examples, TTF itself was determined to bind directly to metal complexes through its S atom.^{4(b)} The complex $[\text{Rh}_2(\text{O}_2\text{CCH}_3)_4(\text{TTF})_2]$ was structurally characterized and contains TTF molecules bonded through its S atom to the Rh axial positions in which the doped version $[\text{Rh}_2(\text{O}_2\text{CCH}_3)_4(\text{TTF})_2] \cdot \text{I}_3$ showed electrical conductivity.⁵

A large body of research in the field of ferromagnetic molecular charge-transfer complexes has been carried out by Miller *et al.* at Dupont. A variety of substituted $(\text{C}_5\text{R}_5)_2\text{Fe}$ donors have been reported to form magnetically interesting solids when combined with acceptors such as TCNE, TCNQ, Bis(dithiolato)-metalates, $\text{C}_4(\text{CN})_6$.⁶ The charge-transfer solid $[(\text{C}_5\text{Me}_5)_2\text{Fe}][\text{TCNE}]$ forms a mixed stack arrangement and exhibits ferromagnetism below 4.8 K.⁶ The manganocene derivative $[(\text{C}_5\text{Me}_5)_2\text{Mn}][\text{TCNQ}]$, shown in Figure 2, exhibits ferromagnetism with a critical temperature (T_c) of 6.2 K which was considered to be a breakthrough at its time.⁷ Later, the charge transfer salt $[(\text{C}_5\text{Me}_5)_2\text{Mn}][\text{TCNE}]$ was discovered to have a T_c of 8.8 K.⁸ The complexes $[(\text{C}_6\text{R}_6)_2\text{Cr}][\text{TCNE}]$ ⁹ and $[(\text{C}_5\text{R}_5)_2\text{Cr}][\text{TCNE}]$ ¹⁰ are also ferromagnetic, while $[(\text{C}_6\text{R}_6)_2\text{Cr}][\text{TCNQ}]$ complexes are diamagnetic.⁵⁴ The iron and ruthenium derivatives of $[(\text{C}_6\text{Me}_6)_2\text{M}][\text{TCNQ}]_x$ exhibited diamagnetic behavior and were poor conductors when $x = 2$, but were paramagnetic and electrically conductive when $x = 4$.¹¹ Materials comprised of $[(\text{C}_5\text{Me}_5)_2\text{Fe}]^+$ with molecules other than cyano-containing organic moieties, such as $[\text{Fe}(\text{C}_5\text{Me}_5)_2][\text{Ni}(\text{bds})_2]$ (bds = bis(dichalcogolene)), have been found to exhibit ferromagnetic behavior.¹²

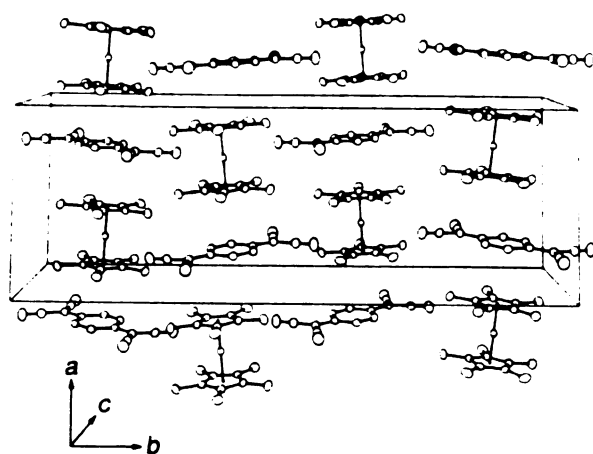


Figure 2. Packing diagram of $[(C_5Me_5)_2Mn][TCNQ]$

While s

known

stacked

B. C

Accept

A

shown

organer

0-0000

the me

TCNQ

The cor

di-z-py

for TC

the ele

in the

reacts

over s

$X = E$

this ar

a few e

ca. 1.6

A

from el

comp

through

and w

While several other theories have been proposed, Miller cites the well-known McConnell model to explain the ferromagnetism in these mixed stacked metallocene-donor/ π -acceptor complexes.^{6(a),13}

B. Complexes That Contain Covalently linked Donors or Acceptors.

Acceptor molecules such as TCNQ and TCNE have recently been shown to undergo charge transfer reactions with electron-rich organometallic species $(C_5R_5)(CO)_2Mn(THF)$ $R = H, CH_3$ resulting in σ -coordinated complexes where one or more N atoms are coordinated to the metal atom.^{14,15} Similarly, $(CO)_5 ReFBF_3$ reacts with TCNE and TCNQ to form σ -coordinated di-nuclear and trinuclear nitrile adducts.¹⁶ The complexes $[Ru(PPh_3)_2(TCNQ)]$ and $[Cu(pdto)(TCNQ)]_2$ ($pdto = 1,8$ -di-*z*-pyridyl-3,6 -dithiaoctane) both contain a σ - η^1 -coordination modes for TCNQ and have been structurally characterized.¹⁷ In other reactions, the electron-rich and coordinatively unsaturated diphosphazene-bridged diruthenium complex $Ru_2(\mu-CO)(CO)_4(\mu-L)_2$ [$L = (RO)_2PN(Et)P(OR)_2$] reacts with TCNQ or TCNE to yield products that contain both inner and outer sphere TCNQ and TCNE; $[Ru_2(CO)_5(\mu-L)_2(\eta^1-TCNX)](TCNX)$ ($X = E, Q$).¹⁸ In addition to the aforementioned examples, several metal salts of TCNQ exhibit weakly coordinated TCNQ units.¹⁹ There have been a few examples where TCNQ was found to dimerize through σ -bonding (ca. 1.64 Å).²⁰

A serendipitous result in high T_c ferromagnetic materials resulted from the reaction of $V(C_6H_6)_2$ and TCNE that produced an insoluble amorphous solid formulated as $V(TCNE)_2 \cdot 1/2(CH_2Cl_2)$. This material is thought to contain σ -coordinated TCNE based on infrared spectroscopy, and was found to be ferromagnetic at room temperature.²¹ There are

many

TCNE

crystal

of TCN

structure

(MaTP

Miller

1978-2

To of

(M ha

were re

simen

Ring O

disov

hinde

imide

with c

C: CN

semir

dispar

varies

state e

for ch

MaTP

studie

many examples of complexes that contain σ -coordinated TCNE^{18,16,15,14,22} several of which have been characterized by X-ray crystallography.²³ The majority of products that contain bound molecules of TCNE exhibit either a σ - η^1 or σ - μ - η^2 coordination mode. The first structurally characterized linear chain complex based on TCNE, [MnTPP][TCNE] (TPP = meso-tetra-phenylporphinato), was reported by Miller *et al.*, although it was first synthesized by Basolo and co-workers in 1978.^{23(e),24} The compound was determined to be ferromagnetic with a T_c of 18 K.^{23(e)} Other examples of linear-chain materials [M(hfacac)₂][TCNE] (M = Co, Cu; hfacac = hexafluoroacetylacetonate) were reported by Wayland at about the same time.^{23(c)} Recently, a two-dimensional structure consisting of σ - μ - η^4 -TCNE units linking Rh₂(O₂CCF₃)₄, through the axial Rh sites, to form a layered material was discovered by researchers in Cotton's laboratories.^{23(f)} The quadruply bonded dimolybdenum complex Mo₂(L)₂ (L = dibenzotetraaza-[14]-annulene) forms a 1:1 charge transfer product with TCNE which reacts with dioxygen or water to form an molybdenum-oxo product and C₃(CN)₅.²⁵

Another class of cyano-containing organic acceptors that has demonstrated an ability to coordinate to metal centers are the N,N'-dicyanoquinonediimines (DCNQIs). Aumüller and Hünig reported that a variety of substituted DCNQIs could be readily synthesized from quinones; these exhibit accessible redox processes which make them good candidates for charge-transfer chemistry.²⁶ A variety of donor-acceptor complexes incorporating these molecules, including (TTF)(DCNQI), have been studied and found to exhibit electrical conductivity.²⁷ Single crystal X-ray structures of several complexes of the form M(DCNQI)₂ (M = Cu, Ag, Tl,

Lib are

reporte

R = H

C. T

I

rely on

under

three-

examp

consist

direct

R = P

of alter

which

Mr. S

the cry

propag

thence

from

three-

formul

pyridin

phenyl

metals

Li) are known and reveal layered two-dimensional sheets.²⁸ In one reported example, DM-DCNQI was used to covalently link $\text{Ru}_2(\text{O}_2\text{CR})_4$ ($\text{R} = \text{H}, \text{Et}, n\text{Pr}, \text{Ph}$) units to form linear chain materials.²⁹

C. The Design of Magnetic Materials.

In addition to the above examples of ferromagnetic materials which rely on charge transfer to form, researchers have been making important strides in assembling other types of covalent networks of one-, two- and three- dimensional magnetic materials with unpaired spins built in. For example, Gatteschi *et al.* have synthesized one dimensional magnetic chains consisting of metal hexafluoroacetylacetonates $\text{M}(\text{hfac})_2$ linked by nitronyl nitroxides (NITR) where $\text{M} = \text{Cu}, \text{Ni}, \text{Co}, \text{and Mn}$.³⁰ When $\text{M} = \text{Mn}$ and $\text{R} = i\text{Pr}$, a ferrimagnetic complex with $T_c = 7.6 \text{ K}$ is formed as the result of alternating spins of $5/2$ and $1/2$.³⁰ Kahn employed a similar approach in which ferrimagnetically coupled bimetallic chains, consisting of alternating $\text{Mn}(S = 5/2)$ and $\text{Cu}(S = 1/2)$ metals, are linked by oxamato bridges.³¹ In the crystal structure of $\text{MnCu}(\text{pbaOH})(\text{H}_2\text{O})_2$ ($\text{pbaOH} = 2\text{-hydroxy-1,3-propanediylbisoxamato}$), the ferrimagnetic chains are aligned such that the shortest interchain separations are $\text{Mn}\cdots\text{Cu}$ creating a two dimensional ferromagnetic material with a T_c of 30 K . Recently, Kahn *et al.* reported a three-dimensional compound that is magnetic below 22.5 K with the formula $(\text{rad})_2\text{Mn}_2[\text{Cu}(\text{opda})]_3(\text{DMSO})_2 \cdot 2\text{H}_2\text{O}$ ($\text{rad} = 2\text{-(4-N-methylpyridinium)-4,4,5,5-tetramethylimidazoline-1-oxyl-3-oxide}$; $\text{opda} = \text{ortho-phenylenebisoxamato}$) in which $\text{Mn(II)}_6\text{Cu(II)}_6$ hexagons are fully interlocked.³²

D. In

D

into po

[Rh CO

polymer

chelate

two-dim

metal

[Rh. B



B.

powder

medium

is used

between

distance

range

detected

polymer

B.

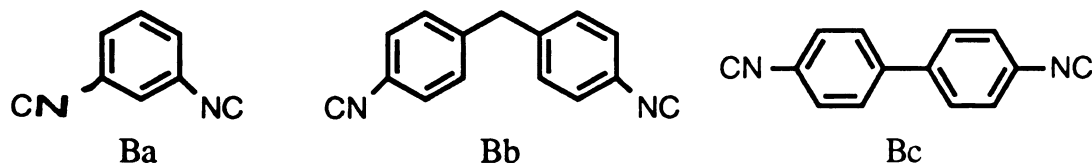
MNC-R

function

test, a

D. Inorganic-Organic Hybrid Polymers.

Diisocyanides have been very successful at assembling metal units into polymeric arrays. These ligands have been found to react with $[\text{Rh}(\text{CO})_2\text{Cl}]_2$ and $[\text{IrCl}(\text{cod})]_2$ to form insoluble two-dimensional network polymers that are formulated as $[\text{M}(\text{bridge})_2\text{Cl}]_n$ in which the non-chelating bidentate ligands act as rigid bridges between metal atoms.³³ The two-dimensional sheets are stacked in an eclipsed fashion with columnar metal chains in which Rh-Rh distances in $[\text{Rh}(\text{Ba})_2\text{Cl}]_n$ (3.21 Å), $[\text{Rh}(\text{Bb})\text{Cl}]_n$ (3.36 Å), and $[\text{Rh}(\text{Bc})\text{Cl}]_2$ (3.54 Å) were determined from



powder X-ray diffraction methods.³³ The mixed metal cobalt(II)-rhodium(I) organometallic polymer forms when 4, 4'-diisocyanobiphenyl is used as the connecting rods.³⁴ Electrical conductivity occurs within and between the sheets and is dependent on the M-M interlayer distances.^{33(c),35} Interlayer spacing of these polymers are in the same range (3 - 4 Å) as those found in the planar charge-transfer salts.³⁵ The acetonitrile complex $\text{Pd}(\text{NCCH}_3)_2(\text{BF}_4)_2$ reacts with diisocyanides to form polymers formulated as $[\text{Pd}(\text{B})_2]_n$ similar to those containing rhodium.³⁶

By taking advantage of the formation of M-CN-M and M-NC-R-CN-M linkages, Robson *et al.* have synthesized extended 3-D frameworks that contain large channels and cavities.³⁷ In fact, chains, sheets, and three dimensional structures have been observed for a variety of metal-cyanide complexes, including the Prussian blues.³⁸ An important

potenti

applied

E. M.

the val

linking

either

robust.

sample

M: O:

M: O:

determi

arrang

oxygen

read

the di

comp

out

M:

the C

reli

store

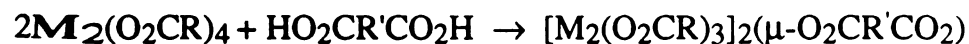
the po

positive

potential direction for these is the tailoring of structures for catalytic applications.

E. Metal-Metal Bonds in Extended Arrays.

Macromolecular chemistry based on M-M multiple bonds has been the subject of recent work by Chisholm *et al.*, particularly with regards to linking quadruply bonded molybdenum and tungsten dinuclear species in either perpendicular or parallel arrangements.^{39,40} In the quest for such robust, covalently linked, one dimensional polymers, tetranuclear complexes were synthesized by the exchange of carboxylate groups on $M_2(O_2CR)_4$ with dicarboxylates.³⁹ The choice of the R' substituent



determines whether the M_2 units align in a parallel or perpendicular arrangement.³⁹ The parallel systems exhibit interactions wherein an oxygen atom from one carboxylate ligand forms an axial interaction to the metal atom of a neighboring $M_2(O_2CR)_4$ unit in the solid state producing one dimensional arrays (which is a common occurrence for $[M_2(O_2CR)_4]_n$ complexes).^{39,41} Liquid crystalline phases containing Mo-Mo quadruple bonds were synthesized by placing long alkyl R substituents in $Mo_2(O_2CR)_4$.⁴¹ The complex $Mo_2(B\text{-diketonate})_4$, recently synthesized by the Chisholm group, consists of infinite stacks of Mo_2 units, but instead of weak intermolecular $Mo_2 \cdots O$ bonds, the origin of the stacking is due entirely to ligand-ligand interactions.⁴²

A variety of bidentate ligands have been successfully incorporated into polymeric frameworks that contain metal-metal bonded units. Pyrazine has been used to form 1:1 polymeric complexes with $M_2(O_2CR)_4$

M =
med
polym
forma
exhibi
amon
Ruc
anides
anides
Ahen
carbo
chain
phenyl
benze
produ
ship =
and pr
cord
comp
comp
comm
alt M
the re
M. C
fence

(M = Cr, Cu) via axial coordination.⁴³ Tetramethylethylenediamine (tmed) and 1,2-bis(dimethylphosphino)ethane (dmpe) both form 1:1 polymeric adducts with $\text{Mo}_2(\text{O}_2\text{CCH}_3)_4$ as the result of axial adduct formation.⁴⁴ Several diruthenium compounds of the type $\text{Ru}_2(\text{O}_2\text{CR})_4\text{Cl}$ exhibit infinite chain structure as the result of intermolecular interactions among the axial chloride ions.^{45,46} The polymeric complex $[\text{Ru}_2(\text{O}_2\text{CC}_2\text{H}_5)_4(\text{phz})][\text{BF}_4]$, where phenazine is the linking unit, displays antiferromagnetic interactions between Ru_2 units.⁴⁷ It has been shown that antiferromagnetic electronic interactions between $\text{Ru}_2^{\text{II,III}}$ ($S = 3/2$) occur when there is a linear Cl^- bridge.⁴⁶ In another example, the rhodium carboxylate compound $\text{Rh}_2(\text{O}_2\text{CC}_2\text{H}_5)_4$ is linked into one-dimensional chains by the bidentate bases phenazine or 2,3,5,6-tetramethyl-p-phenylenediamine.⁴⁸ Likewise, it is postulated that the 1:1 reaction between $\text{Rh}_2(\text{O}_2\text{CCH}_3)_4$ and adenine bases result in similar polymeric products.⁴⁹ The tetranuclear compound $[\{\text{Ru}_2(\text{chp})_4\}_2(\text{PYZ})](\text{BF}_4)_2$ ($\text{chp} = \mu\text{-6-chloro-2-hydroxypyridinato}$) was prepared from $\text{Ru}_2(\text{chp})_4\text{Cl}$ and pyrazine.⁵⁰ In general the use of pyrazine has resulted in a variety of coordination polymers including polymers that contain porphyrin complexes of Fe(II), Ru(II) and Os(II).⁵¹ Interestingly, the solvated complex $[\text{Cu}(\text{NCCH}_3)_4]^+$ reacts with pyrazine and tetramethylpyrazine forming infinite sheet and chain polymers.⁵²

Using organic polymerization methodologies, oligomeric urethanes with Mo-Mo or Fe-Fe bonds along the back-bone have been synthesized.⁵³ The reaction of the organometallic "diol" $(\text{R}_5\text{-C}_5\text{H}_4\text{C}(\text{O})\text{CH}_2\text{OH})_2\text{-Mo}_2(\text{CO})_6$ with an appropriate diisocyanate resulted in polymers that are photochemically reactive and undergo metal-metal bond photolysis.⁵³ Polymers of this type may find utility in degradable plastics.⁵³

1
bonded
array
The fir
chemis
nch
poor
X-ray
M₂-L
reaction
accepte
the syn
product
interre
Bun-N
made f
reaction
synthes
Chapter
ligands
compou
VII deal
reaction

This dissertation describes the work relating to the use of multiply bonded dimetal compounds in the preparation of extended molecular arrays. Several approaches in developing this chemistry were undertaken. The first, detailed in Chapters II, III, and IV, involves the charge transfer chemistry of a variety of dirhenium and dimolybdenum donor (electron rich) complexes with polycyano-containing organic acceptors (electron poor). In each case, covalently bonded species were formed as judged by X-ray crystallography and infrared spectroscopy. Both the oligomeric (M_2-L-M_2) and possibly polymeric ($[M_2-L]_n$) phases are formed in these reactions; these are among the first examples of covalently linked donor-acceptor complexes that incorporate dimetal units. Chapter V reports on the synthesis of the first homoleptic multiply bonded dimetal-cyanide product, $[Et_4N]_4[Mo_2(CN)_8]$. The synthesis and structure of this and other interesting dimetal-cyanide complexes, including $[Bu^n_4N]_2[Re_2(CN)_6(dppm)_2]$, that contains a rare side-on $\mu-\sigma-\pi$ -binding mode for a cyanide ligand, are reported. Preliminary results from reactions of $[Et_4N]_4[Mo_2(CN)_8]$ with solvated dimetal cations in attempts to synthesize polymeric mixed metal cyanide materials are also included. Chapter VI details a different approach to bind redox active organic ligands wherein phosphine-containing TTF ligands are reacted with dimetal compounds to give stacked and/or polymeric materials. Finally, Chapter VII deals with the novel rhenium-oxo species that form from molecular O_2 reactions of $Re_2Cl_4(dppm)_2$.

Refer

1.

2.

3.

4.

5.

6.

7.

8.

9.

10.

11.

12.

13.

14.

References

1. (a) Jérôme, D. *Science* **1991**, 252, 1509. (b) Torrance, J. B. *Acc. Chem. Res.* **1979**, 12, 79. (c) Bryce, M. R. *Chem. Soc. Rev.* **1991**, 20, 355. (d) Williams, J. M.; Schultz, A. J.; Geiser, U.; Carlson, K. D.; Kini, A. M.; Wang, H. H.; Kwok, W.-K.; Whangbo, M.-H.; Schirber, J. E. *Science* **1991**, 252, 1501.
2. Ward, M. D. *Electroanal. Chem.* **1988**, 16, 181.
3. (a) Chappell, J. S.; Bloch, A. N.; Bryden, W. A.; Maxfield, M.; Poehler, T. O.; Cowan, D. O. *J. Am. Chem. Soc.* **1981**, 103, 2442. (b) Robles-Martínez, J. G.; Salmerón-Valverde, A.; Alonso, E.; Soriano, C.; Zehe, A. *Inorg. Chim. Acta* **1991**, 179, 149.
4. (a) Cassoux, P.; Valade, L.; Kobayashi, H.; Kobayashi, A.; Clark, R. A.; Underhill, A. E. *Coord. Chem. Rev.* **1991**, 110, 115. (b) Siedle, A. R. *Ext. Linear Chain Compounds* **1982**, 2, 469.
5. Matsubayashi, G.; Yokoyama, K.; Tanaka, T. *J. Chem. Soc., Dalton Trans.* **1988**, 3059.
6. (a) Miller, J. S.; Epstein, A. *J. Am. Chem. Soc.* **1987**, 109, 3850. (b) Miller, J. S.; Zhang, J. H.; Reiff, W. M. *J. Am. Chem. Soc.* **1987**, 109, 4584. (c) Miller, J. S.; Epstein, A. J.; Reiff, W. M. *Science* **1988**, 240, 40. (d) Miller, J. S.; Calabrese, J. C.; Epstein, A. J. *Inorg. Chem.* **1989**, 28, 4230. (e) Miller, J. S.; Epstein, A. J.; Reiff, W. M. *Acc. Chem. Res.* **1988**, 21, 114. (f) Miller, J. S.; Glatzhofer, D. T.; O'Hare, D. M.; Reiff, W. M.; Chakraborty, A.; Epstein, A. J. *Inorg. Chem.* **1989**, 28, 2930. (g) Chi, K.-M.; Calabrese, J. C.; Reiff, W. M.; Miller, J. S. *Organometallics* **1991**, 10, 688. (h) Miller, J. S.; Epstein, A. J.; Reiff, W. M. *Chem. Rev.* **1988**, 88, 201. (i) Miller, J. S.; Calabrese, J. C.; Rommelmann, H.; Chittipeddi, S. R.; Zhang, J. H.; Reiff, W. M.; Epstein, A. J. *J. Am. Chem. Soc.* **1987**, 109, 769. (j) Chittipeddi, S. R.; Epstein, A. J.; Zhang, J. H.; Reiff, W. M.; Hamberg, I.; Tanner, D. B.; Johnson, D. C.; Miller, J. S. *Synth. Metals* **1987**, 19, 731.
7. Broderick, W. E.; Thompson, J. A.; Day, E. P.; Hoffman, B. M. *Science* **1990**, 249, 401.
8. Yee, G. T.; Manriquez, J. M.; Dixon, D. A.; McLean, R. S.; Groski, D. M.; Flippen, R. B.; Narayan, K. S.; Epstein, A. J. *Adv. Mater.* **1991**, 3, 309.

9. Miller, J. S.; O'Hare, D. M.; Chakraborty, A.; Epstein, A. J. *J. Am. Chem. Soc.* **1989**, *111*, 7853.
10. Eichhorn, D. M.; Skee, D. C.; Broderick, W. E.; Hoffman, B. M. *Inorg. Chem.* **1993**, *32*, 491.
11. (a) Li, S.; White, H. S.; Ward, M. D. *Chem. Mater.* **1992**, *4*, 1082. (b) Ward, M. D.; Johnson, D. C. *Inorg. Chem.* **1987**, *26*, 4213. (c) Ward, M. D.; Fagan, P. J.; Calabrese, J. C.; Johnson, D. C. *J. Am. Chem. Soc.* **1989**, *111*, 1719. (d) Ward, M. D.; Calabrese, J. C. *Organometallics* **1989**, *8*, 593.
12. Broderick, W. E.; Thompson, J. A.; Godfrey, M. R.; Sabat, M.; Hoffman, B. M. *J. Am. Chem. Soc.* **1989**, *111*, 7656.
13. Kollmar, C.; Kahn, O. *Acc. Chem. Res.* **1993**, *26*, 259.
14. (a) Gross, R.; Kaim, W. *Angew. Chem., Int. Ed. Engl.* **1987**, *26*, 251. (b) Gross-Lannert, R.; Kaim, W.; Olbrich-Deussner, B. *Inorg. Chem.* **1990**, *29*, 5046.
15. (a) Olbrich-Deussner, B.; Gross, R.; Kaim, W. *J. Organomet.Chem.* **1989**, *366*, 155. (b) Olbrich-Deussner, B.; Kaim, W.; Gross-Lannert, R. *Inorg. Chem.* **1989**, *28*, 3113. (c) Schwederski, B.; Kaim, W.; Olbrich-Deussner, B.; Roth, T. *J. Organomet.Chem.* **1992**, *440*, 145.
16. Sacher, W.; Nagel, U.; Beck, W. *Chem. Ber.* **1987**, *120*, 895.
17. (a) Ballester, L.; Barral, M. C.; Gutiérrez, A.; Jiménez-Aparicio, R.; Martínez-Muyo, J. M.; Perpiñan, M. F.; Monge, M. A.; Ruíz-Valero, C. *J. Chem. Soc., Chem. Commun.* **1991**, 1396. (b) Humphrey, D. G.; Fallon, G. D.; Murray, K. S. *J. Chem. Soc., Chem. Commun.* **1988**, 1356.
18. (a) Bell, S. E.; Field, J. S.; Haines, R. J.; Moscherosch, M.; Matheis, W.; Kaim, W. *Inorg. Chem.* **1992**, *31*, 3269. (b) Bell, S. E.; Field, J. S.; Haines, R. J.; Sundermeyer, J. *J. Organomet.Chem.* **1992**, *427*, C1.

19. (a) Shields, L. *J. Chem. Soc., Faraday Trans. 2* **1985**, *81*, 1. (b) Konno, M.; Saito, Y. *Acta Cryst.* **1974**, *B30*, 1294. (c) Hoekstra, A.; Spedler, T.; Vos, A. *Acta Cryst.* **1972**, *B28*, 14. (d) Fritchie, C. J. Jr.; Arthur, P. Jr. *Acta Cryst.* **1966**, *21*, 139. (e) Grossel, M. C.; Evans, F. A.; Hriljac, J. A.; Morton, J. R.; LePage, Y.; Preston, K. F.; Sutcliffe, L. H.; Williams, A. J. *J. Chem. Soc., Chem. Commun.* **1990**, 439.
20. (a) Harms, R. H.; Keller, H. J.; Nöthe, D.; Werner, M. *Mol. Cryst. Liq. Cryst.* **1981**, *65*, 179. (b) Dong, V.; Endres, H.; Keller, H. J.; Moroni, W.; Nöthe, D. *Acta Cryst.* **1977**, *B33*, 2428.
21. Manriquez, J. M.; Yee, G. T.; McLean, R. S.; Epstein, A. J.; Miller, J. S. *Science* **1991**, *252*, 1415.
22. (a) Rockenbauer, A.; Speier, G.; Szabó, L. *Inorg. Chim. Acta* **1992**, *201*, 5. (b) Demerseman, B.; Pankowske, M.; Bouquet, G.; Bigorgne, M.; *J. Organomet.Chem.* **1976**, *117*, C10. (c) Ittel, S. D.; Tolman, C. a.; Krusic, P. J.; English, A. D.; Jesson, J. P. *Inorg. Chem.* **1978**, *17*, 3432. (d) Booth, B. L.; McAuliffe, C. A.; Stanley, G. L. *J. Chem. Soc., Dalton Trans.* **1982**, 535. (e) Beck, W.; Schlodder, R.; Lechler, K. H. *J. Organomet.Chem.* **1973**, *54*, 303.
23. (a) Braunwarth, H.; Huttner, G.; Zsolnai, L. *J. Organomet.Chem.* **1989**, *372*, C23. (b) Ewan, A.; McQueen, D.; Blake, A. J.; Stephenson, T. A.; Schröder, M.; Yellowlees, L. J. *J. Chem. Soc., Chem. Commun.* **1988**, 1533. (c) Bunn, A. G.; Carroll, P. J.; Wayland, B. B. *Inorg. Chem.* **1992**, *31*, 1297. (d) Yee, G. T.; Calabrese, J. C.; Vazquez, C.; Miller, J. S. *Inorg. Chem.* **1993**, *32*, 377. (e) Miller, J. S.; Calbrese, J. C.; McLean, R. S.; Epstein, A. J. *Adv. Mater.* **1992**, *4*, 498. (f) Cotton, F. A.; Kim, Y. *J. Am. Chem. Soc.* (submitted 7/1993).
24. Summerville, D. A.; Cape, T. W.; Johnson, E. D.; Basolo, F. *Inorg. Chem.* **1978**, *17*, 3297.
25. (a) Giraudon, F. M.; Sala-Pala, J.; Guerchais, J. E.; Toupet, L. *Inorg. Chem.* **1991**, *30*, 891. (b) Giraudon, F. M.; Sala-Pala, J.; Guerchais, J. E.; Toupet, L. *J. Chem. Soc., Chem. Commun.* **1988**, 921.
26. (a). Aumüller, A.; Hünig, S. *Liebigs Ann. Chem.* **1986**, 142. (b) Aumüller, A.; Hünig, S. *Liebigs Ann. Chem.* **1986**, 165.

17. (C)
(C)
J
A
C

18. (C)
V
I
C
K

19. F
S

20. S
L
S
C
2
h

21. K
P
L
K
C
h
J
C
J

22. S
10

23. C
C
Fr
Fr
De
L
Ar

27. (a) Enkelmann, V. *Angew. Chem., Int. Ed. Engl.* **1991**, *30*, 1121. (b) Aumüller, A.; Hädicke, E.; Hünig, S.; Schätzle, A.; von Schütz, J.-U. *Angew. Chem., Int. Ed. Engl.* **1984**, *23*, 449. (c) Aumüller, A.; Erk, P.; Hünig, S.; von Schütz, J.-U.; Werner, H.-P.; Wolf, H. C.; Klebe, G. *Chem. Ber.* **1991**, *124*, 1445.
- 28 (a) Aumüller, A.; Hünig, S.; Von Schütz, J.-U.; Werner, H. P.; Wolf, H. C.; Klebe, G. *Mol. Cryst. Liq. Cryst. Inc. Nonlin. Opt.* **1988**, *156*, 215. (b) Kato, R.; Kobayashi, H.; Kobayashi, A. *J. Am. Chem. Soc.* **1989**, *111*, 5224. (c) Kato, R.; Kobayashi, H.; Kobayashi, A. *Synth. Met.* **1988**, *27*, B263.
29. Hockett, S. C.; Arrington, C. A.; Burns, C. J.; Clark, D. L.; Swanson, B. I. *Synth. Metals*, **1991**, *41-43*, 2769.
30. (a) Caneschi, A.; Gatteschi, D.; Renard, J. P.; Rey, P.; Sessoli, R. *Inorg. Chem.* **1989**, *28*, 3314. (b) Caneschi, A.; Gatteschi, D.; Sessoli, R. *Acc. Chem. Res.* **1989**, *22*, 392. (c) Caneschi, A.; Gatteschi, D.; Renard, J. P.; Rey, P.; Sessoli, R. *Inorg. Chem.* **1989**, *28*, 1976. (d) Caneschi, A.; Gatteschi, D.; J. P.; Rey, P.; Sessoli, R. *Inorg. Chem.* **1988**, *27*, 1756.
31. (a) Nakatani, K.; Bergerat, P.; Coddjovi, E.; Mathonière, C.; Pei, Y.; Kahn, O. *Inorg. Chem.* **1991**, *30*, 3977. (b) van Koningsbruggen, P. J.; Kahn, O.; Nakatani, K.; Pei, Y.; Renard, J. P.; Drillon, M.; Legoll, P. *Inorg. Chem.* **1990**, *29*, 3325. (c) Pei, Y.; Nakatani, K.; Kahn, O.; Sletten, J.; Renard, J. P. *Inorg. Chem.* **1989**, *28*, 3170. (d) Kahn, O.; Pei, Y.; Verdaguer, M.; Renard, J. P.; Sletten, J. *Inorg. Chem.* **1988**, *110*, 782. (e) Lloret, F.; Nakatani, K.; Journaux, Y.; Kahn, O.; Pei, Y.; Renard, J. P. *J. Chem. Soc., Chem. Commun.* **1988**, 642. (f) Pei, Y.; Verdaguer, M.; Kahn, O.; Sletten, J.; Renard, J. P. *Inorg. Chem.* **1987**, *26*, 138.
32. Stumpf, H. O.; Ouahab, L.; Pei, Y.; Grandjean, D.; Kahn, O. *Science* **1993**, *261*, 447.
33. (a) Efraty, A.; Feinstein, I.; Wackerle, L.; Frolow, F. *Angew. Chem., Int. Ed. Engl.* **1980**, *19*, 633. (b) Efraty, A.; Feinstein, I.; Frolow, F. *Inorg. Chem.* **1982**, *21*, 485. (c) Feinstein-Jaffe, I.; Frolow, F.; Wackerle, L.; Goldman, A.; Efraty, A. *J. Chem. Soc. Dalton Trans.* **1988**, 469. (d) Efraty, A.; Feinstein, I.; Wackerle, L.; Frolow, F. *J. Am. Chem. Soc.* **1980**, *102*, 6341. (e) Hahn, F. E. *Angew. Chem., Int. Ed. Engl.* **1993**, *32*, 650.

34. Lawrence, S. A.; Lott, K. A. K.; Feinstein-Jaffe, I. *Polyhedron* **1988**, *7*, 741.
35. (a) Lawrence, S. A.; Lott, K. A. K.; Sermon, P. A. Short, E. L.; Feinstein-Jaffe, I. *Polyhedron* **1987**, *6*, 2027. (b) Feinstein-Jaffe, I.; Bornstein, A.; Katz, M. *J. Am. Chem. Soc.* **1991**, *113*, 7042.
36. Feinstein-Jaffe, I.; Barash, C. *Inorganica Chimica Acta* **1991**, *185*, 3.
37. (a) Abrahams, B. R.; Hoskins, B. F.; Robson, R. *J. Chem. Soc., Chem. Commun.* **1990**, 60. (b) Abrahams, B. R.; Hoskins, B. F.; Liu, J.; Robson, R. *J. Am. Chem. Soc.* **1991**, *113*, 3045. (c) Hoskins, B. F.; Robson, R. *J. Am. Chem. Soc.* **1990**, *112*, 1546.
38. (a) Sharpe, A. G. "The Chemistry of Cyano Complexes of the Transition Metals" Academic Press, London. **1976**. (b) Ludi, A.; Güdel, H. U. *Structure and Bonding* **1973**, *14*, 1-21. (c) Shriver, D. F. *Structure and Bonding* **1966**, *1*, 32-58. (d) Griffith, W. P. *Coord. Chem. Rev.* **1975**, *17*, 177-247. (e) Iwamoto, T. in, "Inclusion Compounds: Inorganic and Physical Aspects of Inclusion" Eds., Atwood, J. L.; Davies, J. E. D.; MacNicol, D. D. Oxford University Press, Oxford. **1991**, *5*, Ch. 6, pp. 177-212. (f) Wilde, R. E.; Ghosh, S. H.; Marshall, B. J. *Inorg. Chem.* **1970**, *9*, 2512.
39. Cayton, R. H.; Chisholm, M. H.; Huffman, J. C.; Lobkovsky, E. B. *J. Am. Chem. Soc.* **1991**, *113*, 8709.
40. Cayton, R. H.; Chisholm, M. H. *J. Am. Chem. Soc.* **1989**, *111*, 8921.
41. Cayton, R. H.; Chisholm, M. H.; Darrington, F. D. *Angew. Chem., Int. Ed. Engl.* **1990**, *29*, 1481.
42. Chisholm, M. H.; Folting, K.; Putilina, E. F. *Inorg. Chem.* **1992**, *31*, 1510.
43. (a) Cotton, F. A.; Felthouse, T. R. *Inorg. Chem.* **1980**, *19*, 328. (b) Morison, B.; Hughs, R. C.; Soos, Z. G. *Acta Crystallogr. B* **1975**, *31*, 762.
44. Kerby, M. C.; Eichhorn, B. W.; Creighton, J. A.; Vollhardt, K. P. *Inorg. Chem.* **1990**, *29*, 1319.

45. (a) Bennet, M. J.; Caulton, K. G.; Cotton, F. A. *Inorg. Chem.* **1969**, 8, 1. (b) Das, B. K.; Chakravarty, A. R. *Polyhedron* **1991**, 10, 491. (c) Bino, A.; Cotton, F. A.; Felthouse, T. R. *Inorg. Chem.* **1979**, 18, 2599. (d) Martin, D. S.; Newman, A.; Vlasnik, L. M. *Inorg. Chem.* **1980**, 19, 3404.
46. Cotton, F. A.; Kim, Y.; Ren, T. *Polyhedron* **1993**, 12, 607.
47. Cotton, F. A.; Kim, Y.; Ren, T. *Inorg. Chem.* **1992**, 31, 2723.
48. Cotton, F. A.; Felthouse, T. R. *Inorg. Chem.* **1981**, 20, 600.
49. Pneumatikakis, G.; Hadjiliadis, N. *J. Chem. Soc. Dalton Trans.* **1979**, 596.
50. Cotton, F. A.; Kim, Y.; Ren, T. *Inorg. Chem.* **1992**, 31, 2608.
51. Crayston, J. A.; Cupertino, D. C.; Forster, H. S. *Synth. Metals* **1990**, 35, 365.
52. Kitagawa, S.; Munakata, M.; Tanimura, T. *Inorg. Chem.* **1992**, 31, 1714.
53. Tenhaeff, S. C.; Tyler, D. R. *Organometallics* **1991**, 10, 473.
54. O'Hare, D.; Ward, M. D.; Miller, J. S. *Chem. Mater.* **1990**, 2, 758.

CHAPTER II

REACTIVITY STUDIES OF $\text{Re}_2\text{Cl}_4(\text{dppm})_2$

WITH

TCNE, TCNQ, AND TNAP

1. Introduction

proper

material

utilized

has been

material

sample

TTF = 1

metall

TMTS

superco

of mole

synthesi

electrode

with P

tetrayl

discover

temperat

and is be

metal de

M-X: P

P: P-F

analogat

particular

electron

-

1. Introduction

The search for new materials that exhibit electrical or magnetic properties is a major challenge to researchers in materials chemistry. New materials that are easily prepared in a pure form and can be successfully utilized into new and developing technologies are sought. Recently, there has been a great deal of interest regarding the syntheses of molecular-based materials using low temperature solution techniques. The molecular-based complex TCNQ-TTF (TCNQ = 7,7,8,8-tetracyanoquinodimethane; TTF = tetrathiafulvalene), which was the first molecular crystal to exhibit metallic behavior, and the selenium-based Bechgaard salts (TMTSF)₂X (TMTSF = tetramethyltetraselenafulvalene) were among the first organic superconductors.¹ There has also been considerable emphasis on the design of molecular-based ferromagnetic materials.² Miller and others have synthesized a variety of donor-acceptor complexes with magnetically and electrically interesting properties from reactions of Cp₂*M (M = Fe, Mn) with polycyano acceptor species such as TCNQ and TCNE (tetracyanoethylene).³ In more recent work, Manriques and Miller *et al.* discovered that the reaction between V(C₆H₆)₂ and TCNE forms a room temperature ferromagnetic material formulated as V(TCNE)₂·1/2(CH₂Cl₂) and is believed to contain σ-bound TCNE.⁴ We have been exploring this metal donor organic acceptor approach with precursors of the type M₂X₄(PR₃)₄ and M₂X₄(P~P)₂ (X = Cl, Br; M = Mo, Re, W; R = Me, Et, Prⁿ; P~P = dppm, dppe) which, in addition to being coordinatively unsaturated, exhibit accessible and reversible oxidation processes.⁵ In particular, the dirhenium complex Re₂Cl₄(dppm)₂, which possesses an electron-rich Re-Re triple bond, displays two reversible oxidations at E_{1/2(ox)} = 0.35 V and E_{1/2(ox)} = 0.87 V vs Ag/AgCl, thus it is well suited

for charge-transfer chemistry with TCNQ whose first reduction potential occurs at $E_{1/2(\text{red})} = 0.28 \text{ V}$ (Figure 3).^{5(a),6} Due to the presence of a π -component in the metal-metal bonding, the incorporation of the Re_2 unit in a polymeric arrangement may allow for a conduction pathway. Thus, we set out to study the charge-transfer chemistry of the donor complex $\text{Re}_2\text{Cl}_4(\text{dppm})_2$ with organic π -acceptor molecules with well-matched redox couples.

This chapter reports the chemistry of $\text{Re}_2\text{Cl}_4(\text{dppm})_2$ with TCNQ, TCNE, and TNAP (11,11,12,12-tetracyanonaphthaquinodimethane) along with the spectroscopic and physical measurements of the resulting products.

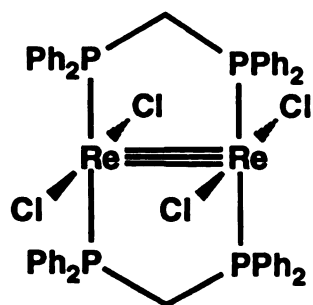
2. Experimental

A. Synthesis

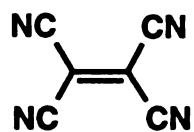
TCNQ and TCNE were purchased from Aldrich Chemicals and were sublimed prior to use. TNAP was purchased from TCI American and used as received.

(1) Preparation of $\text{Re}_2\text{Cl}_4(\text{dppm})_2$

The compound $\text{Re}_2\text{Cl}_4(\text{dppm})_2$ was prepared in an analogous procedure to that reported in the literature.⁷ In a typical reaction 25 mL of reagent grade methanol was added to a flask containing $\text{Re}_2\text{Cl}_6(\text{P}^n\text{Bu})_2$ ⁸ (0.750 g, 0.758 mmol) and dppm (1.55 g, 4.03 mmol). The mixture was refluxed for 3 h during which time a purple solid formed. The warm mixture was allowed to stand undisturbed for several minutes to allow the solid to settle out of solution. The supernatant was carefully decanted prior to filtering and the solid was washed with fresh methanol (2 x 10 mL) and then finally washed with copious amounts of diethyl ether. After vacuum drying, the yield was 0.88 g (90%). To rule out the presence of the oxidized species $\text{Re}_2\text{Cl}_5(\text{dppm})_2$ or other impurities,

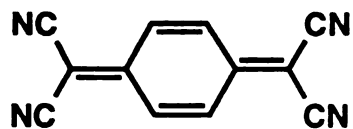

 $\text{Re}_2\text{Cl}_4(\text{dppm})_2$

$$E_{1/2(\text{ox})} = 0.35 \text{ V}$$



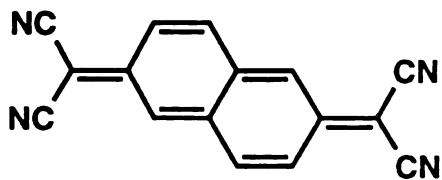
TCNE

$$E_{1/2(\text{red})} = 0.34 \text{ V}$$



TCNQ

$$E_{1/2(\text{red})} = 0.28 \text{ V}$$



TNAP

$$E_{1/2(\text{red})} = 0.31 \text{ V}$$

Figure 3. Selected precursors used for charge-transfer chemistry.

the

corr

(2)

(ii)

10 m

were

solu

chan

with

ca. 1

effect

ca. 10

colle

lined

2115

$\delta = 6$

not ch

(ii) P

Re₂O₃

10 g/l

temp

the ve

the

the cyclic voltammogram of each new batch was checked against the corresponding data for an authentic sample of the compound.

(2) 1:1 Reactions of $\text{Re}_2\text{Cl}_4(\text{dppm})_2$ with TCNQ

(i) Preparation of (1)-A

Separate solutions of $\text{Re}_2\text{Cl}_4(\text{dppm})_2$ (0.108 g, 0.084 mmol) in 10 mL of CH_2Cl_2 and TCNQ (0.0171 g, 0.084 mmol) in 10 mL of CH_2Cl_2 were cooled to -78°C using a dry ice/acetone bath. The $\text{Re}_2\text{Cl}_4(\text{dppm})_2$ solution was added to the TCNQ solution which caused an immediate color change to blue. The reaction mixture was allowed to stand for 2 h at -78°C without a noticeable change in color. The reaction volume was reduced to *ca.* 15 mL by vacuum after which time 20 mL of hexanes was added to effect precipitation of a blue solid. The volume was reduced by vacuum to *ca.* 10 mL and an additional 20 mL of hexanes was added. The solid was collected by filtration, washed with hexanes (2 x 10 mL), and vacuum dried; yield 0.115 g (92%). IR (CsI, Nujol, cm^{-1}): $\nu(\text{C}\equiv\text{N})$ 2195 (s), 2115 (m), $\nu(\text{C}=\text{C})$ 1582 (m). ^1H NMR (CDCl_3) δ = 8.12 (s, 1H), δ = 6.9 - 7.7 (m, 20H), δ = 5.51 (m, 2H) ppm. $^{31}\text{P}\{^1\text{H}\}$ NMR (CDCl_3) not observed.

(ii) Preparation of (1)-B

Dichloromethane (10 mL) was added to a flask containing $\text{Re}_2\text{Cl}_4(\text{dppm})_2$ (0.054 g, 0.042 mmol) and TCNQ (0.009 g, 0.044 mmol) to give a dark blue solution. The reaction mixture was stirred at room temperature for 24 h during which time the color changed to dark green. The volume was reduced to *ca.* 4 mL by vacuum, and diethyl ether (6 mL) was added which effected the precipitation of a green solid. The solid was collected by filtration, washed with diethyl ether (5 mL) and vacuum dried.

IR (CsI, Nujol, cm^{-1}): $\nu(\text{C}\equiv\text{N})$ 2183 (s), 2114 (s,br), 2085 (sh), $\nu(\text{C}=\text{C})$ 1571 (s).

(iii) Preparation of (1)-C

A solution consisting of $\text{Re}_2\text{Cl}_4(\text{dppm})_2$ (0.100 g, 0.078 mmol) in 10 mL of CH_2Cl_2 was added to a solution consisting of TCNQ (0.0206 g, 0.078 mmol) in 10 mL of CH_2Cl_2 . A blue solution immediately formed. The Schlenk flask was equipped with a septum and a long syringe needle which was situated just above the reaction solution. A slow purge of nitrogen was maintained until all of the methylene chloride had evaporated (*ca.* 24 h). A black metallic film, that shatters easily deposited on the bottom of the flask. IR (CsI, Nujol, cm^{-1}): $\nu(\text{C}\equiv\text{N})$ 2185 (s), 2115 (s,br), $\nu(\text{C}=\text{C})$ 1567 (s).

(iv) Preparation of (1)-D

A solution containing TCNQ (0.0320 g, 0.156 mmol) in toluene (20 mL) was added to a refluxing solution consisting of $\text{Re}_2\text{Cl}_4(\text{dppm})_2$ (0.200 g, 0.156 mmol) in toluene (40 mL) over a period of 5 minutes. The reaction mixture was refluxed with stirring for 15 minutes during which time a green precipitate formed. The hot reaction mixture was filtered and the collected solid was washed with copious amounts of toluene and dried *in vacuo*; yield 0.110 g (47%). IR (CsI, Nujol, cm^{-1}): $\nu(\text{C}\equiv\text{N})$ 2185 (s), 2085 (s,br), $\nu(\text{C}=\text{C})$ 1570 (s).

(3) Preparation of $[\text{Re}_2\text{Cl}_4(\text{dppm})_2]_2(\mu\text{-TCNQ})$ (2)

(i) Bulk Reaction

A solution containing TCNQ (0.0120 g, 0.059 mmol) in THF (15 mL) was added to a solution containing $\text{Re}_2\text{Cl}_4(\text{dppm})_2$ (0.150 g, 0.117 mmol) in THF (15 mL). The mixture was stirred for several minutes and allowed to stand overnight at room temperature to yield a crop

of black microcrystals. The product was collected by filtration, washed with THF (3 x 5 mL), and vacuum dried; yield 0.140 g (86%). *Anal.* Calcd for $C_{120}H_{108}N_4Cl_8O_2P_8Re_4$: C, 49.45; H, 3.74; Cl, 9.73. Found: C, 49.38; H, 3.48; Cl, 9.62. IR (CsI, Nujol, cm^{-1}): $\nu(C\equiv N)$ 2187 (m), 2109 (s,br), $\nu(C=C)$ 1573 (m), 1586 (w,sh). 1H NMR ($CDCl_3$) δ = 7.1 – 7.8 (m), δ = 3.73 (t), and δ = 1.83 (p) ppm; the latter two resonances are attributed to lattice THF molecules. $^{31}P\{^1H\}$ NMR ($CDCl_3$) δ = -14 ppm. Electronic spectroscopy (CH_2Cl_2): λ_{max} nm (ϵ , $M^{-1}cm^{-1}$), 1080 (2.56×10^4), 1980 (2.20×10^4).

(ii) Slow Diffusion Reaction

Separate stock solutions of $Re_2Cl_4(dppm)_2$ (0.150 g, 0.117 mmol, 15 mL of THF) and TCNQ (0.0120 g, 0.059 mmol, 15 mL of THF) were prepared; 2 mL of the $Re_2Cl_4(dppm)_2$ solution was syringed into an 8 mm O.D. Pyrex tube⁹ and carefully layered with 2 mL of THF followed by 2 mL of the TCNQ solution. The tube was flame sealed under a slight vacuum and allowed to stand undisturbed. A total of seven tubes were prepared in this way. After ten days the black crystals that had formed at the interface of the layers in each tube were harvested and washed with THF; yield 10 mg (6 %). IR (CsI, Nujol, cm^{-1}): $\nu(C\equiv N)$ 2186 (m), 2104 (s,br), $\nu(C=C)$ 1572 (m), 1586 (w,sh).

(4) 1:1 Reactions of $Re_2Cl_4(dppm)_2$ with TCNE

(i) Preparation of (3)-A

Two separate Schlenk tubes, one containing 0.111 g (0.087 mmol) of $Re_2Cl_4(dppm)_2$ and the other containing 0.011 g (0.087 mmol) of TCNE, each dissolved in 10 mL of CH_2Cl_2 , were cooled to $-78^\circ C$ using a dry ice/acetone bath. The $Re_2Cl_4(dppm)_2$ solution was transferred to the TCNE solution by cannula, and the temperature was maintained at $-78^\circ C$.

Add

add

repe

add

grad

W. L.

2121

750

iii

015

Rec C

popul

with

by R.

797

iii

was a

of TC

reflex

became

there

to

A dark blue-green solution resulted upon contact, and 5 mL of hexanes was added followed by reduction of the solution volume. This process was repeated three times and a blue-green solid was obtained. After a final addition of hexanes (15 mL) and further pumping under vacuum, the blue-green solid was collected by filtration, washed with hexanes, and dried *in vacuo*; yield 0.090 g (73%). IR (CsI, Nujol, cm^{-1}): $\nu(\text{C}\equiv\text{N})$ 2197 (s), 2121 (m). Electronic spectroscopy (CH_2Cl_2): $\lambda_{\text{max}}\text{nm}$ (ϵ , $\text{M}^{-1}\text{cm}^{-1}$), 750 (16,000).

(ii) Preparation of (3)-B

In a typical reaction, a solution consisting of TCNE (0.0198 g, 0.155 mmol) in CH_2Cl_2 (10 mL) was added to a solution consisting of $\text{Re}_2\text{Cl}_4(\text{dppm})_2$ (0.200 g, 0.155 mmol) in CH_2Cl_2 (10 mL) to give a dark purple solution. The reaction solution was reduced to *ca.* 5 mL and treated with 20 mL of diethyl ether. The resulting dark purple solid was collected by filtration, washed with diethyl ether and vacuum dried; yield 0.173 g (79%). IR (CsI, Nujol, cm^{-1}): $\nu(\text{C}\equiv\text{N})$ 2200 (s), 2128 (m).

(iii) Refluxing Reaction in Toluene

To a 100 mL Schlenk flask equipped with a condenser and stir bar was added 0.100 g (0.078 mmol) of $\text{Re}_2\text{Cl}_4(\text{dppm})_2$, 0.010 g (0.078 mmol) of TCNE, and 20 mL of toluene. The reaction mixture was stirred with refluxing for 4 h during which time the color of the reaction solution became dark green with a black precipitate. The hot reaction mixture was filtered, the product was washed with toluene (2 x 5 mL), and finally dried *in vacuo*; yield 0.041 g. The product was dissolved in 20 mL of CH_2Cl_2 , filtered, and reduced in volume to *ca.* 10 mL by vacuum. The addition of 10 mL of hexanes and further pumping to remove the CH_2Cl_2 gave a black precipitate. The product was collected by filtration, washed with hexanes

(2 x 5 mL) and vacuum dried; yield 0.038 g (34%). IR (CsI, Nujol, cm^{-1}): $\nu(\text{C}\equiv\text{N})$ 2211 (s), 2145 (m).

(5) Reactions of $\text{Re}_2\text{Cl}_4(\text{dppm})_2$ with TNAP

(i) Preparation of $[\text{Re}_2\text{Cl}_4(\text{dppm})_2](\text{TNAP})$ (4)

Methylene chloride (10 mL) was slowly added to a Schlenk tube submerged in a dry ice/acetone bath (-78°C) that contained 0.061 g (0.048 mmol) of $\text{Re}_2\text{Cl}_4(\text{dppm})_2$ and 0.012 g (0.048 mmol) of TNAP. No immediate reaction was observed as judged by the persistent purple solution color of the $\text{Re}_2\text{Cl}_4(\text{dppm})_2$ compound. The Schlenk tube was removed from the bath for 5 minutes during which time the reaction solution became dark yellow-green. The Schlenk tube was then returned to the bath, and a small aliquot was removed for an electronic absorption spectrum (CH_2Cl_2): λ_{max} nm (ϵ , $\text{M}^{-1}\text{cm}^{-1}$), 1005 (12800), 478 (7600), 374 (5800). Spectra obtained over the period of 11 h at room temperature differed only in that the absorption centered at $\lambda_{\text{max}} = 1005$ nm decreased in intensity. A infrared spectrum of the reaction solution in a CaF_2 cell exhibited $\nu(\text{C}\equiv\text{N})$ bands at 2195 (s) and 2126 (s) cm^{-1} . A spectrum of the same solution after 11 h gave a spectrum with $\nu(\text{C}\equiv\text{N})$ bands at 2186 (s), 2124 (s), and 2086 (s,br) cm^{-1} . The reaction solution maintained at -78°C was layered with 20 mL of hexanes which resulted in the precipitation of a solid that was collected by filtration, washed with hexanes (2 x 10 mL) and dried in vacuo; yield 0.058 g (80%). IR (CsI, Nujol, cm^{-1}) $\nu(\text{C}\equiv\text{N})$ 2180 (s), 2081 (s,vbr).

(ii) Preparation of $[\text{Re}_2\text{Cl}_4(\text{dppm})_2]_2(\mu\text{-TNAP})$ (5)

A quantity of CH_2Cl_2 (10 mL) was slowly added to a Schlenk tube containing 0.104 g (0.081 mmol) of $\text{Re}_2\text{Cl}_4(\text{dppm})_2$ and 0.010 g (0.041 mmol) of TNAP that was submerged in a dry ice/acetone

but

the

5 m

The

for

107

WAT

room

Am

in Ca

main

prec

wash

85%

B. X

detern

detern

AFC

$\lambda_{\alpha} =$

polariz

5000

Molec

Even 1

bath (-78°C). No reaction was observed at this temperature as judged by the lack of color change. The Schlenk tube was removed from the bath for 5 minutes during which time the reaction solution became dark blue-green. The Schlenk tube was returned to the bath and a small aliquot was removed for an electronic absorption spectrum (CH₂Cl₂): λ_{max} nm (ϵ , M⁻¹cm⁻¹), 1072 (17600). The solution color immediately turned red-brown upon warming to room temperature. Spectra obtained over the period of 1 h at room temperature differed only in the intensity of the absorption at λ_{max} = 1072 nm which decreased. A solution infrared spectrum revealed $\nu(\text{C}\equiv\text{N})$ bands at 2186 (s) and 2101 (s,br) cm⁻¹. The reaction solution maintained at -78°C was layered with 20 mL of hexanes resulting in the precipitation of a microcrystalline solid which was collected by filtration, washed with hexanes (2 x 10 mL), and dried in vacuo; yield 0.097 g (85%). IR (CsI, Nujol, cm⁻¹) $\nu(\text{C}\equiv\text{N})$ 2181 (m), 2101 (s,br).

B. X-Ray Crystallography

The structure of [Re₂Cl₄(dppm)₂]₂(μ -TCNQ)·8THF, (**2**)·8THF, was determined by application of general procedures that have been fully described elsewhere.¹⁰ Crystallographic data were collected on a Rigaku AFC6S diffractometer equipped with monochromated MoK α (λ_{α} = 0.71069 Å) radiation. All data were corrected for Lorentz and polarization effects. Calculations were performed on a VAXSTATION 4000 computer by using the Texsan crystallographic software package of Molecular Structure Corporation.¹¹ Crystallographic data for (**2**) are given in Table 1.

formu

formu

space

a. Å

b. Å

c. Å

α . deg

β . deg

γ . deg

V. Å³

Z

scale.

1 Mo

temper

time, s

R^2

R_{int}

quality

$G = \Sigma$

$R_{\text{int}} = \Sigma$

quality =

Table 1. Summary of crystallographic data for
 $[\text{Re}_2\text{Cl}_4(\text{dppm})_2]_2(\mu\text{-TCNQ})\cdot 8\text{THF}, (2)\cdot 8\text{THF}.$

formula	$\text{Re}_4\text{P}_8\text{N}_4\text{O}_8\text{C}_{144}\text{Cl}_8\text{H}_{156}$
formula weight	3347.08
space group	P-1 (#2)
a, Å	14.258(4)
b, Å	23.238(8)
c, Å	12.146(4)
α , deg	97.95(3)
β , deg	104.31(2)
γ , deg	72.64(2)
V, Å ³	3713(2)
Z	1
d_{calc} , g/cm ³	1.497
μ (Mo K α), cm ⁻¹	35.76
temperature, °C	-110
trans. factors, max., min.	0.61 - 1.00
R ^a	0.043
R _w ^b	0.066
quality-of-fit indicator	2.39

$$^a R = \sum ||F_o| - |F_c|| / \sum |F_o|.$$

$$^b R_w = [\sum w(|F_o| - |F_c|)^2 / \sum w |F_o|^2]^{1/2}; w = 1/\sigma^2(|F_o|)$$

$$^c \text{quality-of-fit} = [\sum w(|F_o| - |F_c|)^2 / (N_{\text{obs}} - N_{\text{parameters}})]^{1/2}$$

(1)

(a) 1

of

of

0.40

the

the

the

the

the

of the

decre

to ad

azim

trans

in 9

1.000

deten

DIR

refine

trans

(1) [Re₂Cl₄(dppm)₂]₂(μ-TCNQ)·8THF, (2)·8THF**(i) Data Collection and Reduction**

Crystals of (2)·8THF were grown by slow diffusion of a THF solution containing TCNQ into a THF solution containing two equivalents of Re₂Cl₄(dppm)₂. A black crystal with dimensions 0.40 x 0.36 x 0.20 mm³ was mounted on the tip of a glass fiber with silicone grease. Cell constants and an orientation matrix for data collection obtained from a least squares refinement using the setting angles of 23 carefully centered reflections in the range $35 \leq 2\theta \leq 40^\circ$ corresponded to a triclinic cell. A total of 13158 unique data were collected at $-110 \pm 1^\circ\text{C}$ using the ω -scan technique to a maximum 2θ value of 50° . The intensities of three representative reflections measured after every 150 reflections decreased by 7.3%, thus a linear correction factor was applied to the data to account for this decay. An empirical absorption correction, based on azimuthal scans of three reflections, was applied which resulted in transmission factors ranging from 0.61 to 1.00.

(ii) Structure Solution and Refinement

Based on a statistical analysis of intensity distribution and the successful solution and refinement of the structure, the space group was determined to be P-1 (#2). The structure was solved by the SHELXS¹² and DIRDIF²⁵ structure programs and refined by full matrix least-squares refinement. All non-hydrogen atoms, except C(51) and the interstitial THF atoms, were refined with anisotropic thermal parameters. Hydrogen atoms were placed in calculated positions for the final stages of refinement. The final cycle of full matrix least-squares refinement included 9435 observations with $F_o^2 > 3\sigma(F_o^2)$ and 685 variable parameters for residuals of $R = 0.043$ and $R_w = 0.066$ and a quality-of-fit index of 2.39.

3. Results and Discussion

The dirhenium donor complex $\text{Re}_2\text{Cl}_4(\text{dppm})_2$ reacts spontaneously with the polycyano organic acceptor compounds TCNQ, TCNE, and TNAP to form charge-transfer products. In reactions with TCNQ, the exact nature of the reaction products is highly dependent on the reaction conditions and stoichiometry. Different products from 1:1 stoichiometric reactions, $[\text{Re}_2\text{Cl}_4(\text{dppm})_2](\text{TCNQ})$ (1)-A, (1)-B, (1)-C, and (1)-D, are isolated depending on reaction temperature and solvent. The molecular complex $[\text{Re}_2\text{Cl}_4(\text{dppm})_2]_2(\mu\text{-TCNQ})$ (2) is produced as a crystalline solid from a careful layering of separate THF solutions of the two reactants. The structure of (2), determined by single crystal X-ray diffraction methods, reveals the presence of a novel bridging bidentate mode for TCNQ. Crystallographic data are summarized in Table 1. An ORTEP representation and packing diagrams are depicted in Figures 4, 5, and 6. A full table of positional and thermal parameters for compound (2) is located in the Appendix. Reactions of $\text{Re}_2\text{Cl}_4(\text{dppm})_2$ with TCNE produces $[\text{Re}_2\text{Cl}_4(\text{dppm})_2](\text{TCNE})$ (3)-A, at low temperatures, and (3)-B, at room temperature. Both contain σ -coordinated TCNE as evidenced by NMR and infrared spectral results. These reactions were determined not to be dependent of stoichiometry. The reactions of $\text{Re}_2\text{Cl}_4(\text{dppm})_2$ with TNAP are similar to those with TCNQ in that the products formulated as $[\text{Re}_2\text{Cl}_4(\text{dppm})_2](\text{TNAP})$ (4) and $[\text{Re}_2\text{Cl}_4(\text{dppm})_2]_2(\mu\text{-TNAP})$ (5) are produced from using 1:1 and 2:1 reaction stoichiometries.

A. Reactions of $\text{Re}_2\text{Cl}_4(\text{dppm})_2$ with TCNQ

(1) Preparation

The reaction of equimolar quantities of $\text{Re}_2\text{Cl}_4(\text{dppm})_2$ with TCNQ in CH_2Cl_2 at -78°C produces instantaneously a dark blue solution followed

by a color change to green upon warming to room temperature (see Figure 4). The blue solution is stable indefinitely at -78°C and a blue solid, $[\text{Re}_2\text{Cl}_4(\text{dppm})_2](\text{TCNQ})$ (1)-A, can be isolated by precipitation with diethyl ether. After decomposition of the blue product to the green species, one can isolate a green solid, (1)-B, by addition of diethyl ether. If benzene is used in place of CH_2Cl_2 , a blue solution persists for several days at room temperature. Attempts to grow crystals suitable for a single crystal X-ray study of either of these products were unsuccessful. However, diethyl ether layerings of the 1:1 blue solution at -78°C produces yellow-green microcrystals that turn blue upon exposure to air and with warming above -78°C . Unfortunately, repeated attempts to mount the crystals without decomposition met with failure. When equimolar CH_2Cl_2 solutions of $\text{Re}_2\text{Cl}_4(\text{dppm})_2$ and TCNQ are mixed and then evaporated to dryness, black films of (1)-C deposit on the walls of the reaction vessels. The reaction of equimolar quantities of $\text{Re}_2\text{Cl}_4(\text{dppm})_2$ with TCNQ in refluxing toluene produces (1)-D as a green solid. Using THF as the reaction solvent, the addition of one equivalent of TCNQ to two equivalents of $\text{Re}_2\text{Cl}_4(\text{dppm})_2$ produces the complex $[\text{Re}_2\text{Cl}_4(\text{dppm})_2]_2(\mu\text{-TCNQ})$ (2) which precipitates as black crystals.

(2) Spectroscopic Properties

The infrared spectral features of the aforementioned TCNQ complexes are quite unusual in comparison to other charge-transfer products of TCNQ. Selected infrared frequency values of these products are compared with TCNQ^0 and TCNQ^- in Table 2. It is clear that the prepared products are not outer-sphere charge-transfer products with TCNQ, but rather complexes containing σ -coordinated TCNQ. The determination of the X-ray crystal structure of (2) provides evidence for

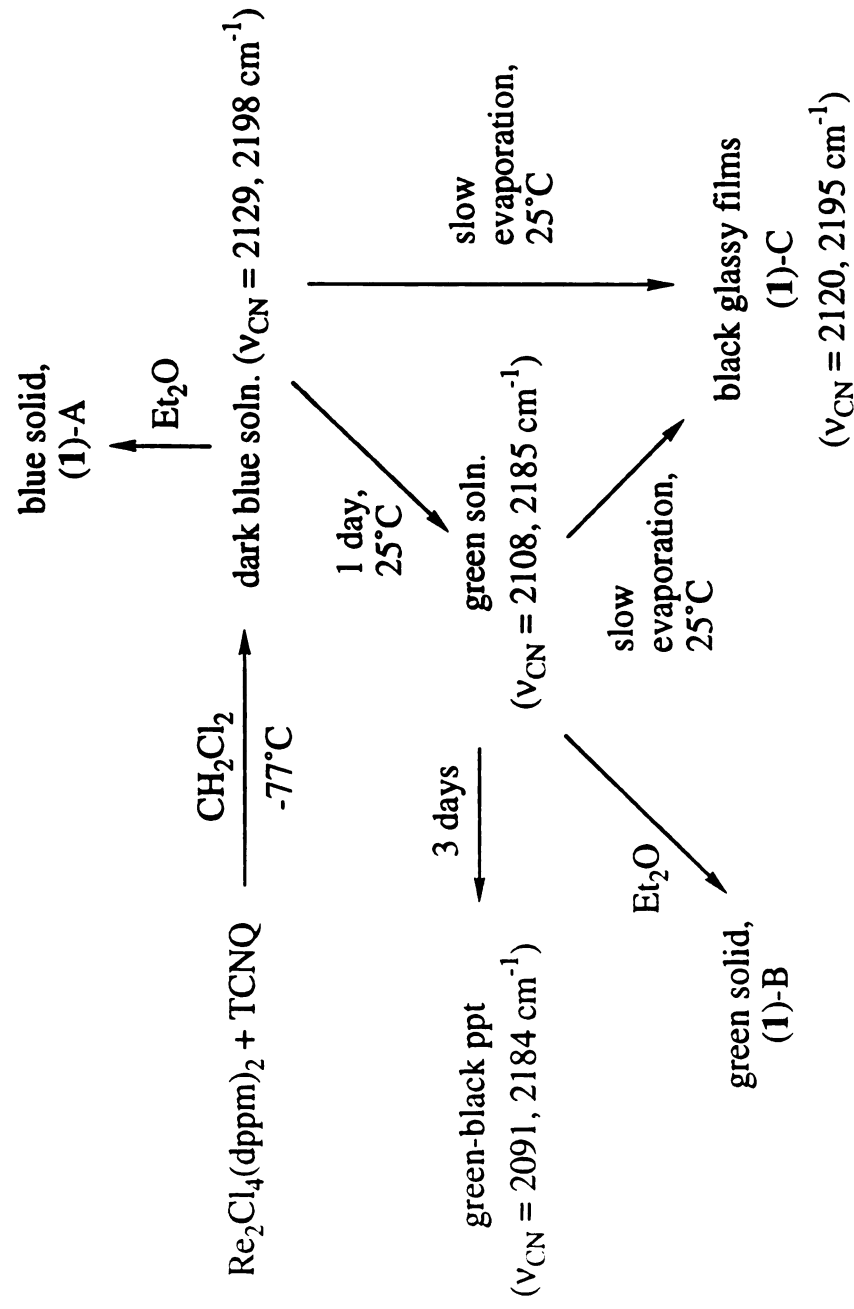


Figure 4. Pathway of the 1:1 reaction between $\text{Re}_2\text{Cl}_4(\text{dppm})_2$ and TCNQ.

Table 2. Comparison of the C≡N and C=C stretching frequencies of various TCNQ containing products.

Compound	$\nu(\text{C}\equiv\text{N})$	$\nu(\text{C}=\text{C})$	Coordination	Reference
TCNQ	2222 (vs)	1542 (s)	none	42
[Bu ₄ N] ⁺ TCNQ ⁻	2181 (s), 2156 (m)	1594 (s)	none	43
LiTCNQ	2200 (s), 2114 (s,br)	1581 (s)	none	44
(1)-A ^a	2195 (s), 2115 (m)	1582 (m)	σ -?	e
(1)-B ^a	2183 (s), 2114 (s,br), 2085 (sh)	1571 (s)	σ -?	e
(1)-C ^a	2185 (s), 2115 (s,br)	1567 (s)	σ -?	e
(1)-D ^a	2185 (s), 2085 (s,br)	1570 (s)	σ -?	e
(2) ^b	2187 (m), 2109 (s,br)	1573 (m)	σ - μ^2	e
[FeCp* ₂][TCNQ]	2179 (s), 2153 (m)	d	none	45
[CrCp* ₂][TCNQ]	2178 (s), 2153 (m)	d	none	46
[MnCp*(CO) ₂] ₂ [TCNQ]	2200 (m), 2110 (w)	1585 (m)	σ	22,23
[MnCp*(CO) ₂] ₄ [TCNQ]	2170 (w), 2105 (s)	d	σ - μ^4	22,24
[Ru ₂ (CO) ₅ L ₂ (TCNQ)](BPh ₄) ^c	2195 (m), 2145 (m), 2100 (w)	d	σ	26
{[Re ₂ (CO) ₅] ₃ (TCNQ)}(BF ₄) ₃	2265 (m), 2220 (m)	1540 (m)	σ - μ^3	47

^a(1) = "[Re₂Cl₄(dppm)₂](TCNQ)"^b(2) = [Re₂Cl₄(dppm)₂]₂(μ -TCNQ)^cL = [μ -(MeO)₂PN(Et)P(OMe)₂]^dnot reported^ethis work

this hypothesis. The infrared spectrum of (2) exhibits bands at 2186 and 2104 cm^{-1} attributed to the $\nu(\text{C}\equiv\text{N})$ of the unbound and bound CN components of TCNQ. The molecule also exhibits a stretch at 1572 cm^{-1} attributed to the C=C stretching in TCNQ. It has previously been demonstrated that the degree of charge transfer in various TCNQ complexes can be estimated from the nitrile stretching frequencies.¹³ Comparison of the $\text{C}\equiv\text{N}$ and C=C stretching frequencies of (2) with TCNQ^0 and TCNQ^- suggests the assignment of -1 to the bridging TCNQ in (2), which requires each dirhenium moiety to have a partial formal charge of 0.5+.

The strong $\nu(\text{C}\equiv\text{N})$ band at 2104 cm^{-1} attributed to the bound nitrile in (2) is shifted to lower frequency as the result of significant $d\pi-\pi^*$ back-bonding. As the $\text{C}\equiv\text{N}$ bond stretches, the π^* orbitals are lowered, and as the $\text{C}\equiv\text{N}$ lengthens, the M-N distance decreases, thus increasing the overlap of the $d\pi-\pi^*$ orbitals.¹⁴ It has been shown that metal ions with strong back-bonding interactions (a net metal-to-ligand charge transfer) exhibit an intensity enhancement of the $\text{C}\equiv\text{N}$ stretch.¹⁴

The infrared spectra of the 1:1 products (1)-A, (1)-B, (1)-C, (1)-D are also indicative of σ -coordinated TCNQ^- moieties. The major difference among these spectra is that (1)-D exhibits a strong and broad $\nu(\text{C}\equiv\text{N})$ band at 2085 cm^{-1} which is in the range for complexes that possess bridging TCNQ ligands, whereas (1)-A, (1)-B, and (1)-C exhibit nitrile stretching patterns indicative of a $\sigma-\eta^1$ coordination mode. One is able to monitor the changes during the conversion of (1)-A to (1)-B using infrared spectroscopy. The initial spectrum of the blue mixture (Figure 5), that results from the mixing of separate equimolar CH_2Cl_2 solutions

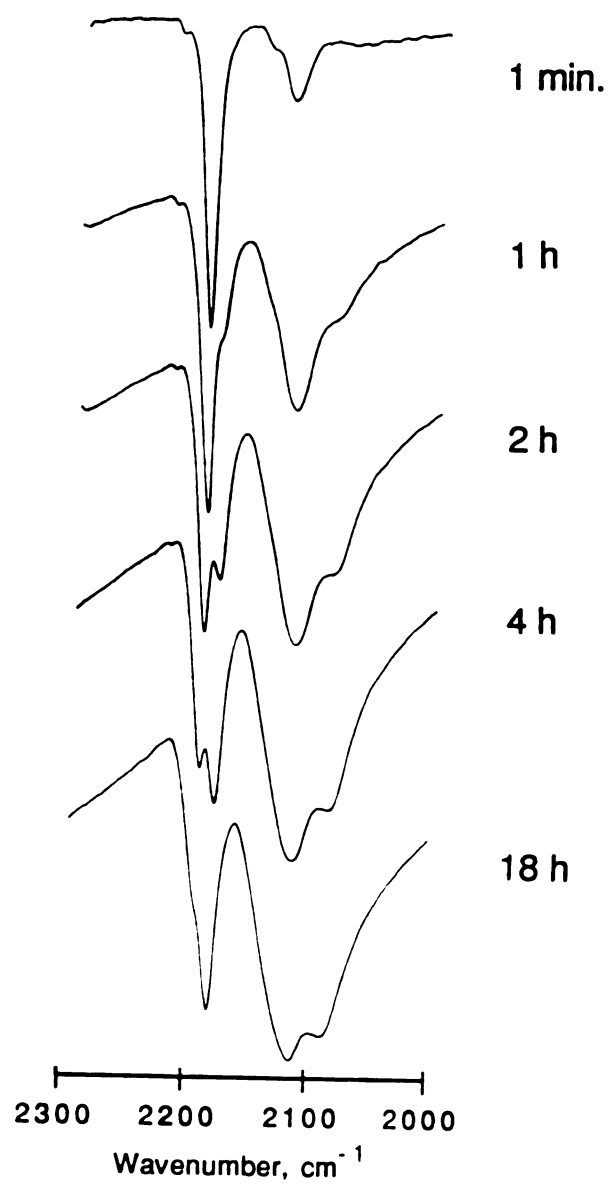


Figure 5. Infrared spectral monitoring of the conversion of (1)-A to (1)-B in CH_2Cl_2 .

containing $\text{Re}_2\text{Cl}_4(\text{dppm})_2$ and TCNQ exhibits similar $\nu(\text{C}\equiv\text{N})$ bands to that of the Nujol mull infrared spectrum of (1)-A. No apparent spectral changes occur within 1 h, although a color change to green was observed. After 1 h the spectrum exhibits an increase in intensity of the lower energy band with the onset of a shoulder occurring on each band. As the reaction progresses, the shoulders become more intense; after 4 h the solution is completely green, and after 18 h the spectrum resembles that of (1)-B. The initial infrared spectrum of the blue-gray solution (Figure 6) that results from the mixing of the two reactants in CH_2Cl_2 using a 2:1 $\text{Re}_2\text{Cl}_4(\text{dppm})_2$:TCNQ stoichiometry exhibits $\nu(\text{C}\equiv\text{N})$ bands at 2198 (m) and 2117 (s) cm^{-1} . If monitored over a two day period, a peak at 2187 cm^{-1} develops while the band at 2198 cm^{-1} disappears. The location of the stretch at 2117 cm^{-1} remains constant but broadens over this time period. If the same experiment is performed using THF as the reaction solvent, nearly identical spectra are obtained (as compared to the reaction performed in CH_2Cl_2) during the early stages of the reaction. However, as the reaction progresses, a $\nu(\text{C}\equiv\text{N})$ band at 2185 cm^{-1} appears with concomitant precipitation of a solid that results in poor spectral resolution. When the reaction between $\text{Re}_2\text{Cl}_4(\text{dppm})_2$ and TCNQ is performed in the presence of a large excess of TCNQ (at least 5 equivalents) in CH_2Cl_2 , the solution infrared spectrum exhibits a $\nu(\text{C}\equiv\text{N})$ band at 2222 (m) cm^{-1} indicative of free TCNQ^0 in addition to $\nu(\text{C}\equiv\text{N})$ bands 2195 (s) and 2120 (s) cm^{-1} that are also observed in the spectra of (1)-A.

In addition to the infrared spectra, the electronic absorption spectra (UV-visible, near and mid IR) are also helpful in distinguishing between the various phases of the reactions between $\text{Re}_2\text{Cl}_4(\text{dppm})_2$ and TCNQ. Table 3 lists the λ_{max} values from spectra of various phases along with

Table 3 Comparison of the electronic spectral data of various TCNQ and TCNE complexes.

Complex	Solvent	λ_{max} nm	ϵ , M ⁻¹ cm ⁻¹
"[Re ₂ Cl ₄ (dppm) ₂](TCNQ)" (1)-A ^a	CH ₂ Cl ₂	325	22200
		380	18500
		900	59100
		1900	16600
"[Re ₂ Cl ₄ (dppm) ₂](TCNQ)" (1)-A ^a	THF	320	16300
		370	15600
		890	45400
		1900	12900
[Re ₂ Cl ₄ (dppm) ₂] ₂ (TCNQ) (2) ^b	CH ₂ Cl ₂	1080	25600
		1980	22000
[Re ₂ Cl ₄ (dppm) ₂] ₂ (TCNQ) (2) ^a	CH ₂ Cl ₂	1080	36700
		1950	27900
[Re ₂ Cl ₄ (dppm) ₂] ₂ (TCNQ) (2) ^c	CH ₂ Cl ₂	430	15300
		1075	25600
		1975	25800
"[Re ₂ Cl ₄ (dppm) ₂](TCNQ)" (1)-D	CH ₂ Cl ₂	425	11200
		950	8000
		1950 (br)	10200
[Re ₂ Cl ₄ (dppm) ₂](TCNQ) ₂ ^a	CH ₂ Cl ₂	400	38800
		900	18000
		1850	4400
"[Re ₂ Cl ₄ (dppm) ₂] ₄ (TCNQ)" ^a	CH ₂ Cl ₂	1090	50500
		1975	41200
[Cp*(CO) ₂ Mn]TCNQ ^d	toluene	1050	e
[Cp*(CO) ₂ Mn] ₄ TCNQ ^d	toluene	14184	50200
[Cp*(CO) ₂ Mn] ₂ TCNE ^d	CH ₃ CN	720	14100
		1145	25100
[Cp*(CO) ₂ Mn]TCNE ^d	toluene	789	17000

^aSeparate solutions of the Re₂Cl₄(dppm)₂ and TCNQ compounds were mixed prior to the experiment.^bSolid product of (2) dissolved in CH₂Cl₂^cSolid product of (2) from the acetone reaction dissolved in CH₂Cl₂^dReferences 22 and 24^enot reported

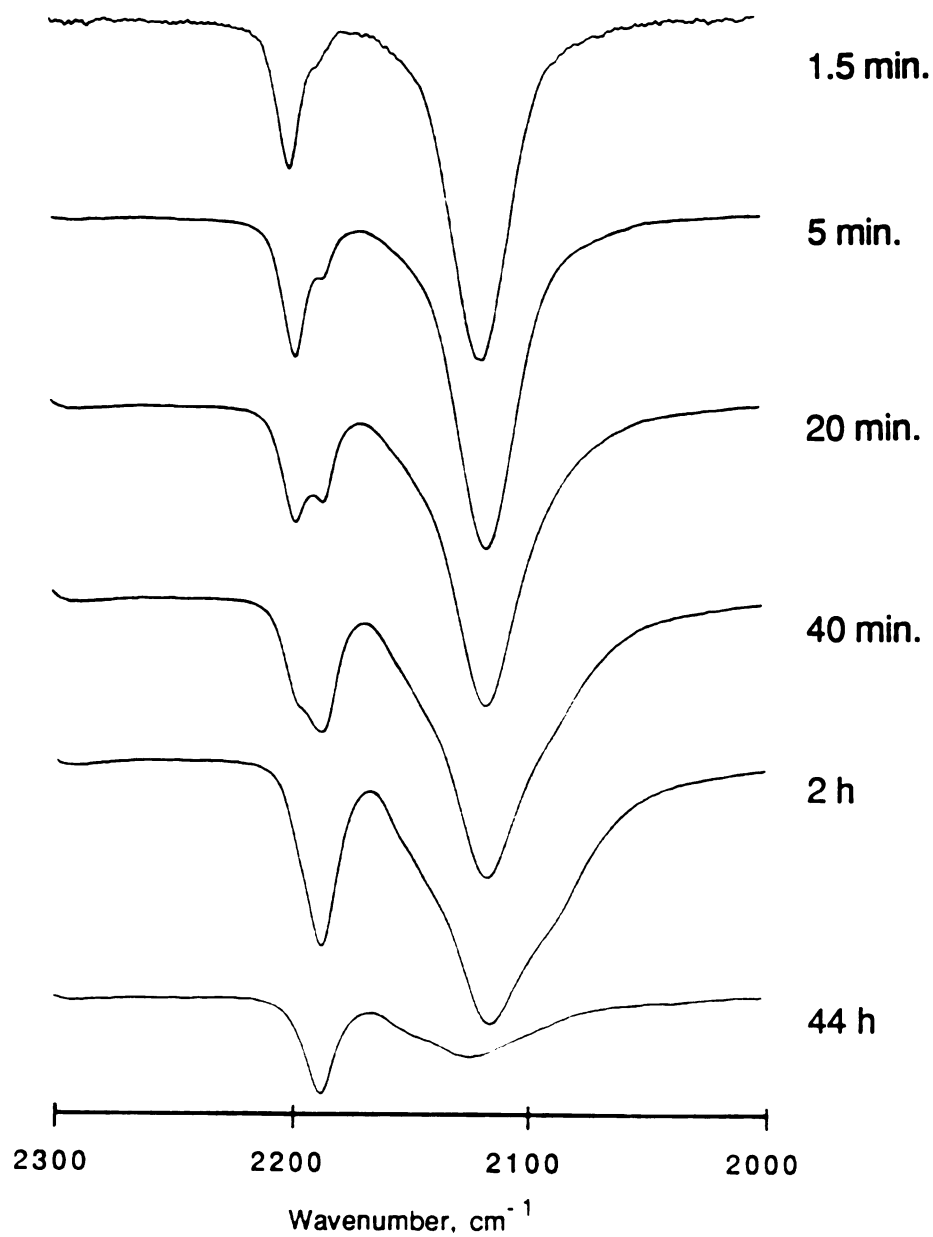


Figure 6. Infrared spectral monitoring of the decomposition of a CH₂Cl₂ solution containing [Re₂Cl₄(dppm)₂]₂(μ-TCNQ).(2).

those reported for other TCNQ-containing compounds. The spectrum of the 1:1 reaction solution between $\text{Re}_2\text{Cl}_4(\text{dppm})_2$ and TCNQ, (1)-A, in CH_2Cl_2 exhibits an intense absorption at a $\lambda_{\text{max}} = 900 \text{ nm}$ ($\epsilon = 5.91 \times 10^4 \text{ M}^{-1}\text{cm}^{-1}$) and a less intense broad absorption at $\lambda_{\text{max}} = 1900 \text{ nm}$ ($\epsilon = 1.66 \times 10^4 \text{ M}^{-1}\text{cm}^{-1}$). This spectrum also exhibits higher energy absorptions at $\lambda_{\text{max}} = 325 \text{ nm}$ ($\epsilon = 2.22 \times 10^4 \text{ M}^{-1}\text{cm}^{-1}$) and 380 nm ($\epsilon = 1.85 \times 10^4 \text{ M}^{-1}\text{cm}^{-1}$). The same behavior is also observed when THF is used as the reaction solvent (see Table 3). When more than one equivalent of TCNQ is added to $\text{Re}_2\text{Cl}_4(\text{dppm})_2$, a strong absorption appears at $\lambda_{\text{max}} = 400 \text{ nm}$, indicative of free TCNQ. The spectrum of (2) performed in CH_2Cl_2 (Figure 7) contains intense absorptions at $\lambda_{\text{max}} = 1080 \text{ nm}$ ($\epsilon = 2.56 \times 10^4 \text{ M}^{-1}\text{cm}^{-1}$) and 1980 nm ($\epsilon = 2.20 \times 10^4 \text{ M}^{-1}\text{cm}^{-1}$). A similar spectrum is obtained for the solution that results from mixing separate methylene chloride solutions of $\text{Re}_2\text{Cl}_4(\text{dppm})_2$ and TCNQ (2:1 stoichiometry). In another example, the dark green solid obtained by a 2:1 reaction between $\text{Re}_2\text{Cl}_4(\text{dppm})_2$ and TCNQ in acetone dissolved in CH_2Cl_2 , results in a similar spectrum to that of (2); in this spectrum, however, the absorption near 430 nm is stronger than the same feature observed in other spectra recorded for (2). All spectra of the 2:1 [$\text{Re}_2\text{Cl}_4(\text{dppm})_2$:TCNQ] products exhibit the absorption near 430 nm , but intensities differ from one sample to another signalling various quantities of free TCNQ. This point is better illustrated from studying the effect of prolonged reaction times on the course of the reaction. The initial UV-visible spectrum of a 2:1 mixture of $\text{Re}_2\text{Cl}_4(\text{dppm})_2$ and TCNQ in CH_2Cl_2 , exhibits a strong absorption at 1050 nm . As the blue-gray solution changes to blue-green and finally to yellow-green (*ca.* 14 h), the intensity of the absorption decreases by about 40%. At the same time, a peak near 430 nm

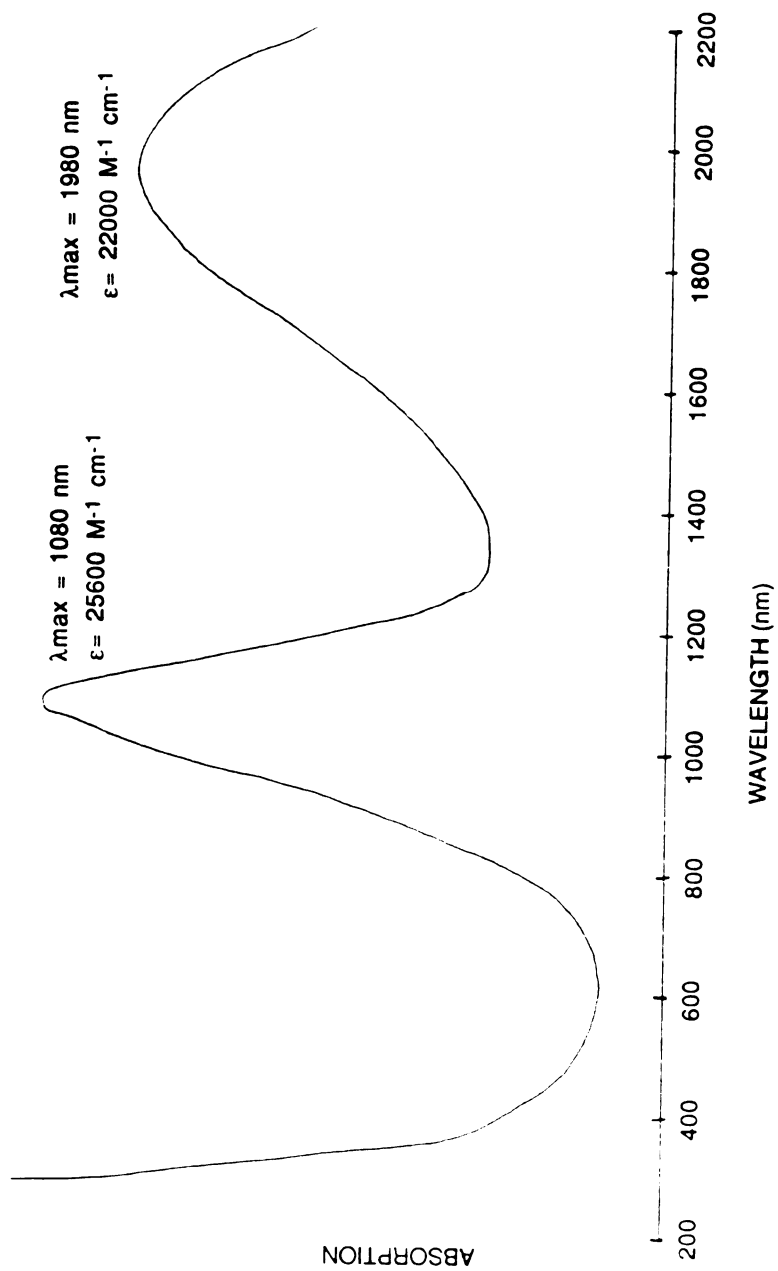


Figure 7. Electronic absorption spectrum of $[\text{Re}_2\text{Cl}_4(\text{dppm})_2]_2(\mu\text{-TCNQ})$ (2) in CH_2Cl_2 .

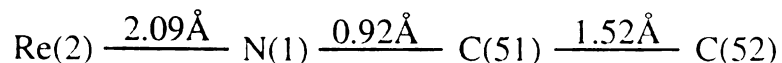
grows in. This effect of solution aging may explain why some of the previous spectra of the 2:1 products exhibit this peak at various intensity levels. In the spectrum of (1)-A in CH_2Cl_2 , the absorption at $\lambda_{\text{max}} = 900 \text{ nm}$, over a period of 7 h, decreases to about one-half its original intensity, during which time the color changes from blue (1)-A to green (1)-B.

(3) X-ray Crystal Structure of $[\text{Re}_2\text{Cl}_4(\text{dppm})_2]_2(\mu\text{-TCNQ})\cdot 8\text{THF}$, (2) $\cdot 8\text{THF}$

A single crystal X-ray study of (2) $\cdot 8\text{THF}$ confirms its 2:1 formulation, and reveals the presence of a novel bridging bidentate mode for TCNQ. The molecular structure of (2) $\cdot 8\text{THF}$, depicted in Figure 8, consists of two Re_2 units that are covalently linked through the *trans* cyanide groups of a bridging TCNQ molecule. The molecule is centrosymmetric, with the midpoint of the TCNQ moiety being situated on an inversion center.

During the refinement procedure it became necessary to fix the position of C(51). When allowed to refine unconstrained, the N(1)-C(51) distance became an unreasonably short 0.92 \AA , which is considerably less than the distance of 1.03 \AA that first appeared in the difference map. Furthermore, the C(51)-C(52) distance lengthens to an unreasonably long 1.52 \AA when unconstrained. Models that included fixing N(1), C(51), or

Unconstrained



Atom C(51) fixed

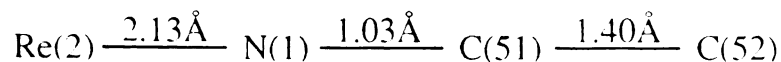


Figure 8. ORTEP representation of $[\text{Re}_2\text{Cl}_4(\text{dppm})_2]_2(\mu\text{-TCNQ})\cdot 8\text{THF}$, (2)·8THF.

b
b
k
c
s
a
r
w
c
c
c
r
v
E
s
E
M
c
c
c
h

both were examined. When only N(1) was fixed, the N(1)-C(51) distance became 0.90 Å, and when C(51) was fixed, the N(1)-C(51) distance refined to 1.03 Å. The later refinement was chosen because it was the most chemically reasonable model. In addition to the above refinements, switching the identities of the N and C atoms which would make the group an isonitrile or replacing either the N or C atom with O all led to poorer refinements. We believe that the artificially short C-N distance that refines without constraint results from librational disorder of the CN groups that distorts the thermal ellipsoid and thus prevents an accurate assignment of the atoms location for bond distance calculations. It should be noted that the unligated C(53)-N(2) moiety refines to a more realistic value of 1.12(2) Å.

The coordination geometries of the two Re atoms within each M₂L₉ dimer unit are different (see Figure 9). The nitrile-substituted metal center, Re(2), adopts an octahedral arrangement consisting of an axial chloride, Cl(2), as well as an equatorial chloride, Cl(1), and an equatorial nitrogen ligand, N(1). The geometry around Re(1) is trigonal bipyramidal which is similar to the geometries of the Re atoms in the parent complex Re₂Cl₄(dppm)₂. Distances and angles within the dirhenium unit are within the usual ranges for derivatives of Re₂Cl₄(dppm)₂.¹⁵ A list of selected bond distances and angles are given in Table 4. Of special note is the Re-Re separation of 2.2747(8) Å, which is longer than the distance of 2.234(3) Å found in the parent triply-bonded complex. In the absence of other considerations, one would predict a shorter metal-metal bond resulting from depopulation of an antibonding orbital upon oxidation (i.e. $\sigma^2\pi^4\delta^2\delta^{*2} \rightarrow \sigma^2\pi^4\delta^2\delta^{*1}$)¹⁶, but in the present system the application of an M₂L₈ bonding scheme is an oversimplification. The combined affect of

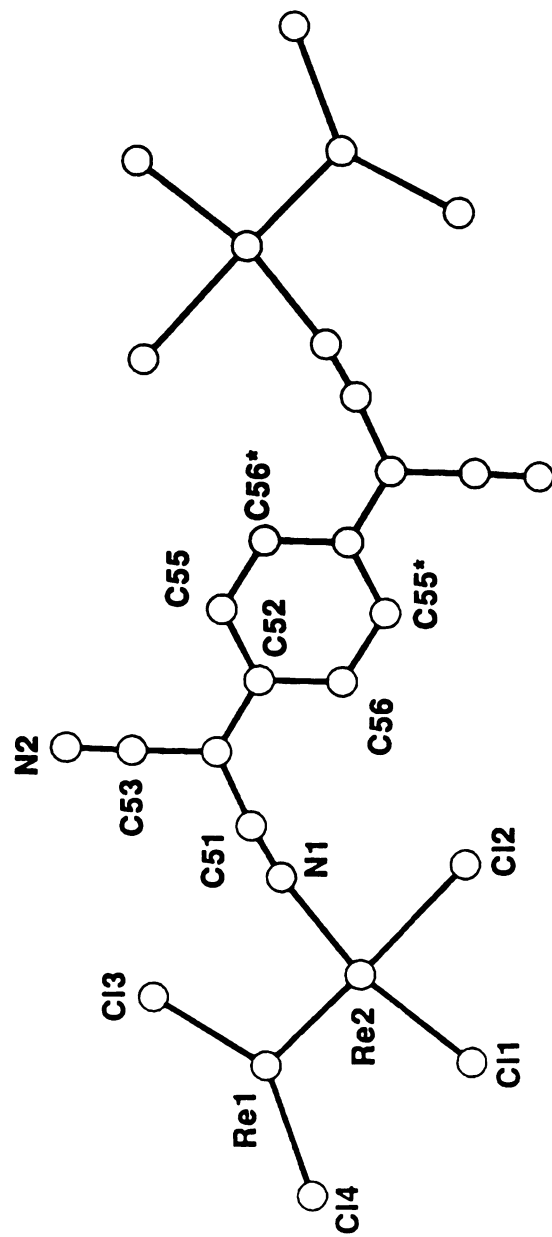


Figure 9. Pluto representation without dppm ligands of $[\text{Re}_2\text{Cl}_4(\text{dppm})_2]_2(\mu\text{-TCNQ})\cdot 8\text{THF}, (2)\cdot 8\text{THF}$.

Table 4. Selected bond distances(Å), bond angles(°) and torsion angles(°) for [Re₂Cl₄(dppm)₂]₂(μ-TCNQ)·8THF, (2)·8THF.

distances					
atom 1	atom 2	distance	atom 1	atom 2	distance
Re(1)	Re(2)	2.2747(8)	P(2)	C(49)	1.83(1)
Re(1)	Cl(3)	2.348(3)	P(3)	C(25)	1.80(1)
Re(1)	Cl(4)	2.356(3)	P(3)	C(31)	1.81(1)
Re(1)	P(2)	2.426(3)	P(3)	C(50)	1.80(1)
Re(1)	P(3)	2.432(3)	P(4)	C(37)	1.81(1)
Re(2)	Cl(1)	2.387(3)	P(4)	C(43)	1.84(1)
Re(2)	Cl(2)	2.589(3)	P(4)	C(50)	1.82(1)
Re(2)	P(1)	2.496(3)	N(1)	C(51)	1.026(8)
Re(2)	P(4)	2.493(3)	N(2)	C(53)	1.12(2)
Re(2)	N(1)	2.133(8)	C(51)	C(52)	1.40(1)
P(1)	C(1)	1.82(1)	C(52)	C(53)	1.43(2)
P(1)	C(7)	1.83(1)	C(52)	C(54)	1.42(2)
P(1)	C(49)	1.83(1)	C(54)	C(55)	1.37(2)
P(2)	C(13)	1.84(1)	C(54)	C(56)	1.43(2)
P(2)	C(19)	1.82(1)	C(55)	C(56)*	1.37(2)

torsion angles				
atom 1	atom 2	atom 3	atom 4	torsion angle
Cl(1)	Re(2)	Re(1)	Cl(3)	167.8(1)
Cl(1)	Re(2)	Re(1)	Cl(4)	10.0(1)
Cl(3)	Re(1)	Re(2)	N(1)	14.8(2)
P(1)	Re(2)	Re(1)	P(2)	15.72(9)
P(3)	Re(1)	Re(2)	P(4)	14.08(9)
C(53)	C(52)	C(54)	C(55)	5(2)

Table 4. (cont'd).

angles							
atom 1	atom 2	atom 3	angle	atom 1	atom 2	atom 3	angle
Re(2)	Re(1)	Cl(3)	106.68(8)	Cl(1)	Re(2)	P(4)	81.6(1)
Re(2)	Re(1)	Cl(4)	112.89(8)	Cl(1)	Re(2)	N(1)	166.6(2)
Re(2)	Re(1)	P(2)	99.02(7)	Cl(2)	Re(2)	P(1)	82.9(1)
Re(2)	Re(1)	P(3)	97.29(7)	Cl(2)	Re(2)	P(4)	85.09(9)
Re(2)	N(1)	C(51)	167.8(6)	Cl(2)	Re(2)	N(1)	81.8(2)
Cl(3)	Re(1)	Cl(4)	140.4(1)	P(1)	Re(2)	P(4)	167.87(9)
Cl(3)	Re(1)	P(2)	84.8(1)	P(1)	Re(2)	N(1)	85.9(2)
Cl(3)	Re(1)	P(3)	93.3(1)	P(4)	Re(2)	N(1)	94.2(2)
Cl(4)	Re(1)	P(2)	87.0(1)	N(1)	C(51)	C(52)	173.0(7)
Cl(4)	Re(1)	P(3)	84.0(1)	C(51)	C(52)	C(53)	116(1)
P(2)	Re(1)	P(3)	163.43(9)	C(51)	C(52)	C(54)	125(1)
Re(1)	Re(2)	Cl(1)	97.34(7)	C(53)	C(52)	C(54)	119(1)
Re(1)	Re(2)	Cl(2)	176.66(7)	N(2)	C(53)	C(52)	177(2)
Re(1)	Re(2)	P(1)	94.67(7)	C(52)	C(54)	C(55)	122(1)
Re(1)	Re(2)	P(4)	97.39(7)	C(52)	C(54)	C(56)	119(1)
Re(1)	Re(2)	N(1)	95.8(2)	C(55)	C(54)	C(56)	119(1)
Cl(1)	Re(2)	Cl(2)	85.21(9)	C(54)	C(55)	C(56)*	121(1)
Cl(1)	Re(2)	P(1)	95.6(1)	C(54)	C(56)	C(55)*	120(1)

structural changes and π -delocalization on the extent of Re-Re bonding must be taken into consideration. It is reasonable to argue, however, that a strong axial chloride interaction serves to weaken the σ -component of the metal-metal bond thus resulting in an overall lengthening of the Re-Re distance.

Although other M_2L_9 complexes, such as $Re_2Cl_4(dppm)_2(CO)^{17}$, have been noted before, these possess A-frame structures, whereas the structural type found in (2), in which the geometry is trigonal bipyramidal around one of the Re atoms and octahedral around the other Re atom, has been noted only in a few instances, namely in the nitrile complexes $[Re_2Cl_3(dppm)_2(NCR)_2]X$ ($X = Cl^-$, PF_6^-) ($R = Me$, Et , Ph , $4-PhC_6H_4$, $1,2-C_6H_4CN$) reported by Walton *et al.*¹⁸ These complexes contain equatorially bound nitriles and chlorides, and one axially coordinated chloride ligand. Comparisons of the Re-Re, Re-N, and Re-Cl axial distances, and P-Re-Re-P torsion angles for this structural type appear in Table 5. The values observed for (2) are quite similar to those of the $[Re_2Cl_3(dppm)_2(NCR)_2]^+$ complexes. The most notable difference appears in the torsion angles, e.g., the P-Re-Re-P twist angle (14.9°) is considerably smaller than the corresponding values in the $[Re_2Cl_3(dppm)_2(NCR)_2]^+$ complexes. This difference can be understood in terms of metal-metal bonding. The $[Re_2Cl_3(dppm)_2(NCR)_2]^+$ species are reported to be diamagnetic while for (2) there is partial oxidation of the Re_2 core that results in the destruction of some of the δ^* bonding. This introduces some δ bonding into the molecule which favors a more eclipsed conformation (a smaller P-Re-Re-P torsion angle). With a smaller P-Re-Re-P torsion angle and a longer Re-Cl axial distance, a shorter Re-Re distance in (2) than in

Table 5 Comparison of selected bond distances and angles of dirhenium complexes exhibiting an unsymmetrical M₂L₉ geometry.

Complex	Re-Re(Å)	Re-N(Å)	Re-Cl _(axial) Å	P-Re-Re-P(ave)(°)
[Re ₂ Cl ₄ (dppm) ₂] ₂ (μ-TCNQ) (2)	2.2747(8)	2.133(8)	2.589(3)	14.9
[Re ₂ Cl ₃ (dppm) ₂ (NCC ₆ H ₅) ₂] ₂ PF ₆	2.270(1)	2.066(15)	2.575(7)	22.2
[Re ₂ Cl ₃ (dppm) ₂ (NCC ₂ H ₅) ₂] ₂ PF ₆	2.2661(9)	2.01(1)	2.556(4)	30.6
[Re ₂ Cl ₃ (dppm) ₂ (1,2-C ₆ H ₄ (CN) ₂) ₂] ₂ PF ₆	2.265(1)	2.05(3)	2.492(6)	32.4
Re ₂ Cl ₅ (dppm) ₂	2.263(1)		2.575(6)	3.99

the $[\text{Re}_2\text{Cl}_3(\text{dppm})_2(\text{NCR})_2]^+$ complexes might be expected, however, the converse is true. It is interesting to note that in the structure of the mixed-valence $\text{Re}_2^{\text{II,III}}$ complex $\text{Re}_2\text{Cl}_5(\text{dppm})_2$, which also possesses the M_2L_9 structural arrangement, the Re-Re separation is 2.263(1) and the P-Re-Re-P torsion angle is 3.99° .¹⁹ The torsion angle is smaller, as expected, but the Re-Re distance is similar to other $\text{Re}_2^{\text{II,II}}$ complexes listed in Table 5. This example underscores the danger in equating the Re-Re separation with bond order or oxidation state.

Other structural features of (2) can be explored by the fact that the two rhenium atoms are electronically different which leads to different Re-Cl and Re-P distances. The Re(1)-Cl distances are about 0.04 Å shorter than the Re(2)-Cl_{equatorial} distance, and the Re(1)-P distances are about 0.07 Å shorter than the Re(2)-P distances. This same trend is also observed in the structure of $\text{Re}_2\text{Cl}_5(\text{dppm})_2$.¹⁹ Once again, these structural differences are attributed to the different coordination environments around each rhenium atom, and assignments of formal charges on either rhenium atom cannot be rationally deduced from these data.

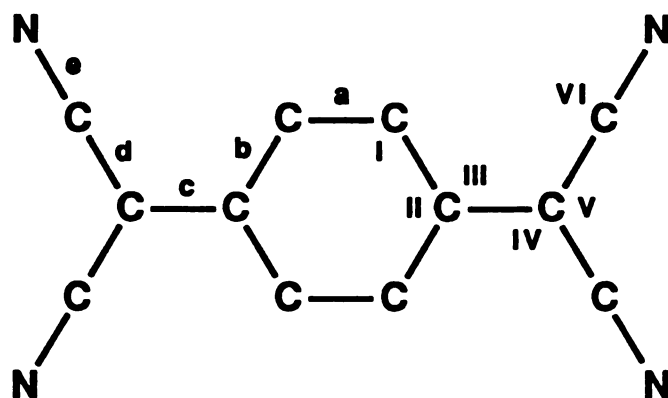
Among the vast amount of literature pertaining to the chemistry of TCNQ, there are only several reports of covalently bonded TCNQ complexes and only a few reported X-ray crystallographic structures. The crystal structures of the simple salts of the alkali metals of TCNQ display metal cations which are either octahedrally ($\text{M}^+ = \text{Na}, \text{Rb}$) or cubically ($\text{M}^+ = \text{K}, \text{Cs}$) surrounded by nitrogen atoms of TCNQ.²⁰ The metal-nitrogen distances in these structures are not very different from the sum of the van der Waals radii. In the crystal structure of AgTCNQ, however, the Ag atoms are coordinated to four nitriles in a distorted tetrahedral arrangement, with an average Ag-N distance of 2.322 Å, which is clearly

indicative of a bonding interaction and establishes precedence for a σ - μ^4 -TCNQ coordination mode.²¹ The existence of both σ -TCNQ and σ - μ^4 -TCNQ binding modes for complexes of the unstable $[\text{CpMn}(\text{CO})_2]$ fragment have been discussed in the literature, but these have not been verified by crystallography.^{22,23,24} In addition, the complex $\{[\text{Re}(\text{CO})_5]_3(\text{TCNQ})\}(\text{BF}_4)_3$ is reported to exhibit an σ - μ^3 -TCNQ ligand.²⁶ The only known example, other than (2), of a TCNQ complex that involves a metal-metal bonded dinuclear species is $\{\text{Ru}_2(\text{CO})_5[\text{M}-(i\text{PrO})_2\text{PN}(\text{Et})\text{P}(\text{O}i\text{Pr})_2]_2(\sigma\text{-TCNQ})\}$, although this complex was not structurally characterized.²⁶

The crystal structures of $[\text{Rb}^+18\text{-crown-6TCNQ}^-]_2$ and $[\text{Ru}(\text{PPh}_3)_2(\text{TCNQ})]_2$ reveal a less common type of TCNQ coordination in which a dimeric "(TCNQ)₂" unit bridges two metal centers with each metal being coordinated to two N atoms, one on each TCNQ molecule.^{27,28} In the structure of the complex $[\text{Cu}(\text{pdto})(\text{TCNQ})]_2$ (pdto = 1,8-di-2-pyridyl-3,6-dithiaoctane) the Cu atoms are coordinated to only one N atom on TCNQ and dimerization occurs via π - π interactions between adjacent TCNQ units.²⁹ The complexes $[\text{Ni}(\text{bdpa})]_2[\text{TCNQ}][\text{X}]_2$ ($\text{X} = \text{ClO}_4$, BPh_4) and $[\text{Ni}(\text{bdpa})][\text{TCNQ}][\text{ClO}_4]$ [bdpa = bis(3-dimethylarsinopropyl)phenylarsene] were not structurally characterized, but were spectroscopically determined to contain a *cis*- σ - μ^2 -TCNQ moiety rather than the *trans* arrangement depicted in the structure of (2).³⁰

The bond distances and angles within the TCNQ unit in (2) are considerably different from those found in TCNQ^0 as shown in Table 6. In comparing the bond distances in (2) and other TCNQ^- containing species to those in TCNQ^0 , bonds **a** and **c** are lengthened while bonds **b** and **d** are

Table 6. Comparison of bond distances (Å) and angle (°) of several TCNQ containing products.



Bond/ Angle	TCNQ ^a	(2)-8THF ^b	N-MePZT-TCNQ ^c	[Fe(C ₅ Et ₅) ₂]TCNQ ^d
a	1.346	1.37	1.349	1.370
b	1.446, 1.450	1.37, 1.43	1.446	1.418, 1.413
c	1.374	1.42	1.379	1.423
d	1.441, 1.440	1.43, 1.40	1.422	1.413, 1.419
e	1.141, 1.139	1.03, 1.12	1.151	1.148, 1.413
I	120.7, 121.0	120, 121	119.9	121.1, 121.5
II	118.3	119	120.1	117.4
III	120.7, 121.0	119, 122	119.9	121.2, 121.4
IV	121.8, 122.0	125, 119	122.6	121.5, 121.6
V	116.1	116	114.9	116.9
VI	179.6, 179.4	173.0, 177	177.7	179.5, 179.0

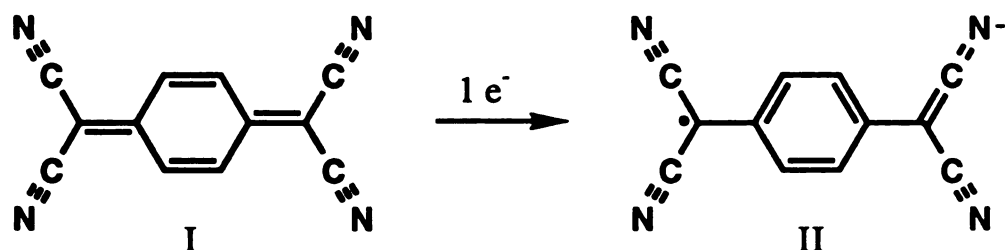
a. reference 48

b. [Re₂Cl₄(dppm)₂]₂(μ-TCNQ)

c. reference 49

d. reference 50

shortened. These changes in bond lengths are expected and can be explained by a contribution from the structure (II) for TCNQ^- . As reported in work by Hoekstra *et al.*, the charges in the reduced forms of



TCNQ reside predominately on the N atoms which explains the nucleophilic tendency of TCNQ^- .^{20(b)}

(4) Magnetic and Electrical Properties

The compounds $[\text{Re}_2\text{Cl}_4(\text{dppm})_2](\text{TCNQ})$ (1) and $[\text{Re}_2\text{Cl}_4(\text{dppm})_2]_2(\mu\text{-TCNQ})$ (2) are paramagnetic as indicated by magnetic susceptibility and EPR spectroscopy. Both (1) and (2) exhibit temperature dependent susceptibilities as a consequence of antiferromagnetic coupling. The μ_{eff} vs. temperature plots of (1)-A and (2) are displayed in Figures 10 and 11; the products exhibit room temperature values of 3.1 and 1.9 B.M., respectively, which roughly represent 2 and 1 unpaired electrons. In (1)-A, one would expect 2 unpaired electrons if complete electron transfer had occurred to form $[\text{Re}_2\text{Cl}_4(\text{dppm})_2]^+(\text{TCNQ})^-$. In the case of (2), the product $[\text{Re}_2]^{+0.5}(\mu\text{-TCNQ}^-)[\text{Re}_2]^{+0.5}$ contains strongly coupled dirhenium units which causes a net μ_{eff} value to be *ca.* 1 electron.

The EPR spectra of the 1:1 products $[\text{Re}_2\text{Cl}_4(\text{dppm})_2](\text{TCNQ})$ (1) all exhibit sharp signals centered near $g = 2.003$ indicating the presence of free TCNQ^- . This is in accord with the presence of the absorption, attributed to free TCNQ^- , in the UV-visible spectra near 400 nm for these

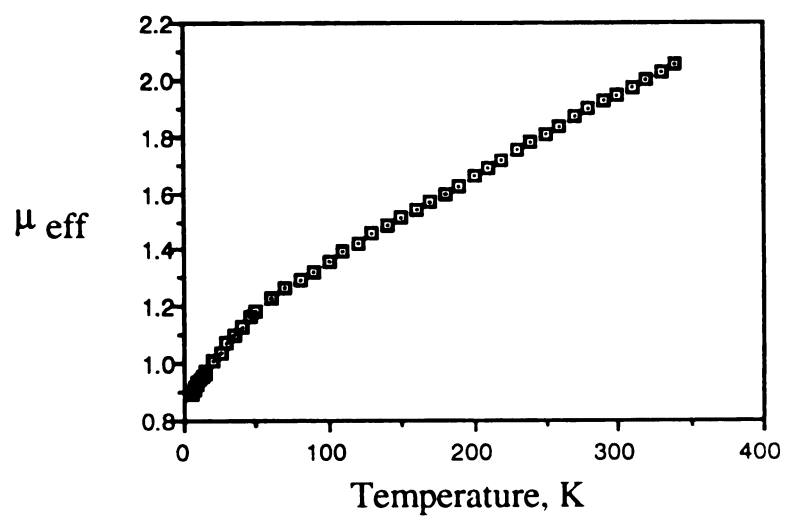


Figure 10. Plot of μ_{eff} (B.M.) vs. temperature (K) of $[\text{Re}_2\text{Cl}_4(\text{dppm})_2]_2(\mu\text{-TCNQ})$ (**2**).

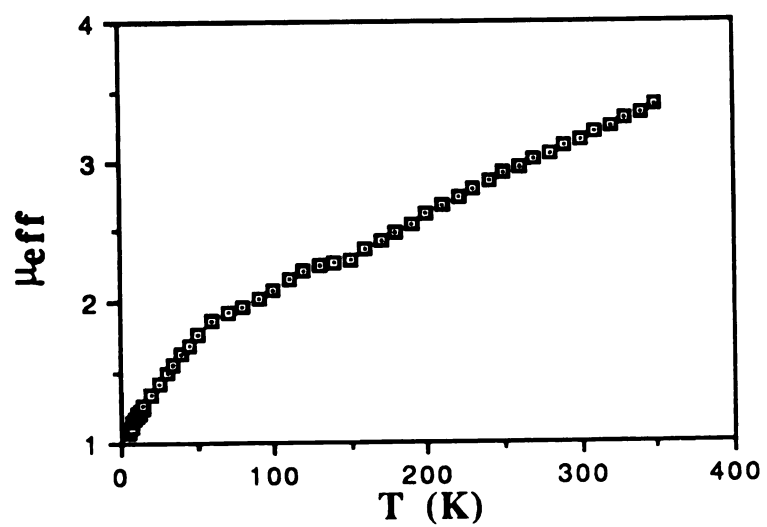


Figure 11. Plot of μ_{eff} (B.M.) vs. temperature (K) of $[\text{Re}_2\text{Cl}_4(\text{dppm})_2](\text{TCNQ})$ (**1**)-A.

complexes. Only in the spectrum of (1)-D is a weak and broad metal-based signal noticeable. On the other hand, the EPR spectrum of $[\text{Re}_2\text{Cl}_4(\text{dppm})_2]_2(\mu\text{-TCNQ})$ (2) on a crystalline sample exhibits only a broad signal centered at $g = 2.004$ (Figure 12). The EPR spectra of bulk precipitate samples of (2) exhibit the characteristic sharp signal near the free electron value due to varying amounts of TCNQ^- in the sample.

The electrical conductivities of several samples measured on pressed pellets by the four probe technique,³¹ are indicative of semiconductor behavior. The plots of $\ln R$ vs. $1/T$ of (1)-A, and (2) are linear from which band gaps of 0.50 and 0.43 eV and room temperature conductivities of 1×10^{-6} and $1 \times 10^{-5} \Omega^{-1}\text{cm}^{-1}$ are determined respectively. These values are 1/100 to 1/1000 of the expected conductivities for single crystals, unfortunately, robust crystals suitable for measurements were not obtained. Single crystals used for the X-ray study lose THF solvent of crystallization quite readily turning to powder within minutes of being removed from the mother liquid. The conductivity pathway is not likely to be through direct TCNQ-TCNQ interactions as dictated by the large separation between TCNQ moieties observed in packing diagram for (2) (Figure 13). However, close contacts between Re_2 units and the presence of solvent molecules may be responsible for the observed conductivities.

B. Reactions of $\text{Re}_2\text{Cl}_4(\text{dppm})_2$ with TCNE

(1) Preparation and Spectroscopic Properties

When solutions of $\text{Re}_2\text{Cl}_4(\text{dppm})_2$ are treated with TCNE, immediate reactions occur to produce $[\text{Re}_2\text{Cl}_4(\text{dppm})_2](\text{TCNE})$ (3) as judged by the formation of highly colored reaction solutions. When the reactions are performed at -78°C , blue-green solutions form and a blue-green solid, (3)-A, which is stable at room temperature, is obtained by

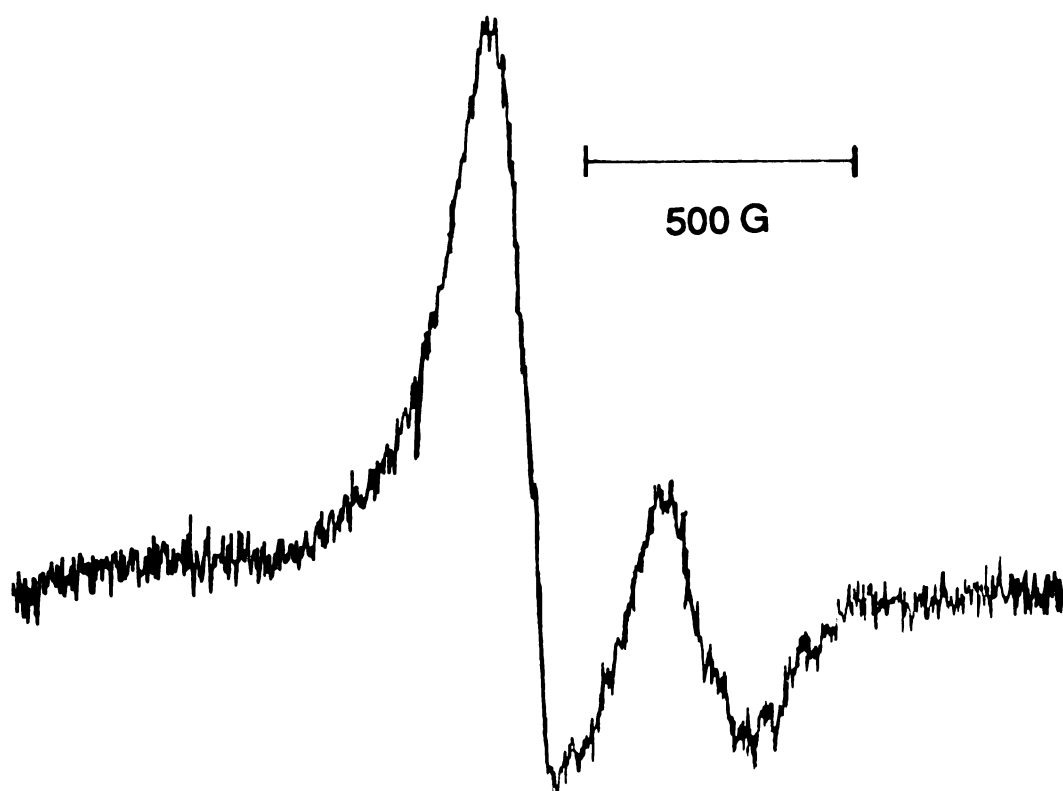


Figure 12. Single crystal EPR spectrum of $[\text{Re}_2\text{Cl}_4(\text{dppm})_2]_2(\mu\text{-TCNQ})$ (**2**) at -160°C .

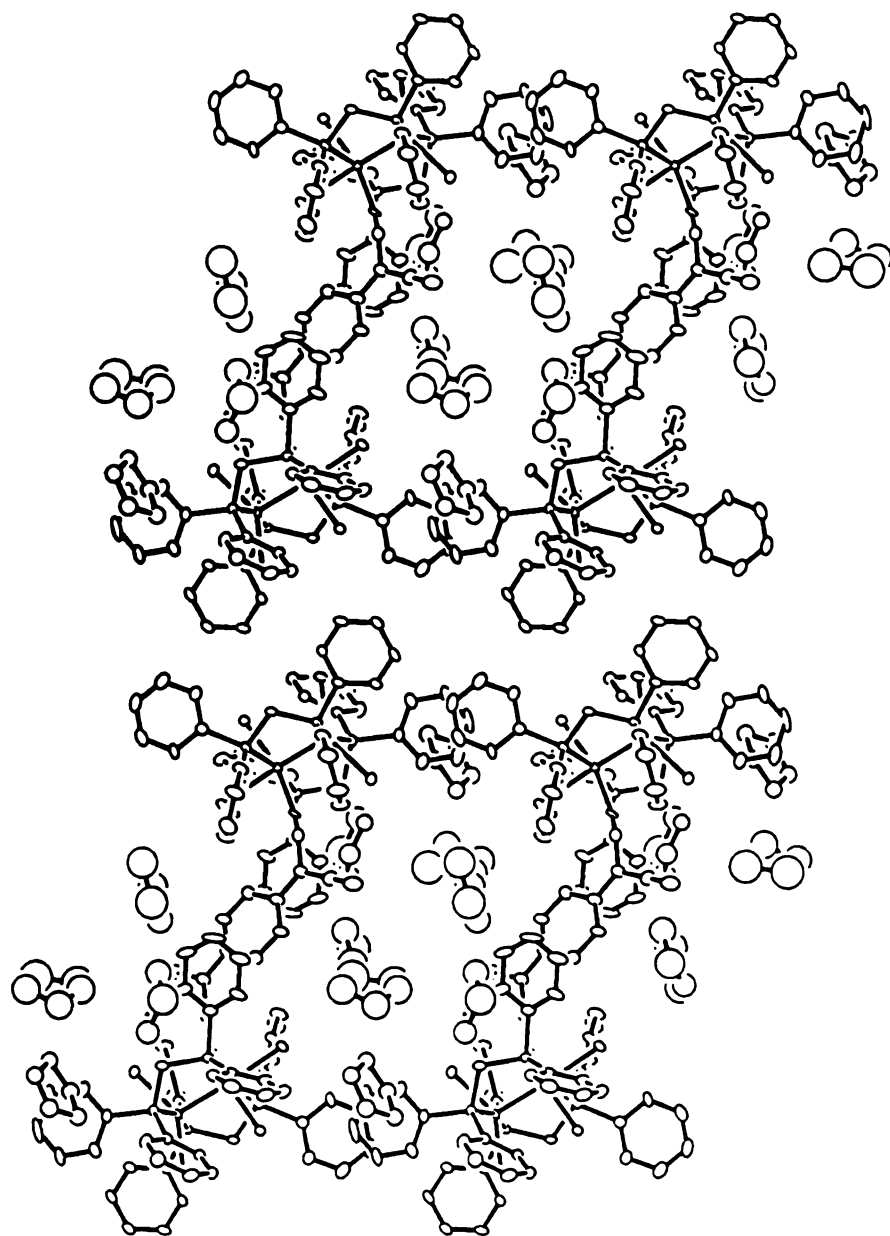


Figure 13. Packing diagram of $[\text{Re}_2\text{Cl}_4(\text{dppm})_2]_2(\mu\text{-TCNQ}) \cdot 8\text{THF}$, (2)·8THF. View down C axis.

precipitation using hexanes. When the reactions are performed at room temperature, dark purple solutions persist in which a purple solid, (3)-B, is isolated using hexanes or diethyl ether as the precipitating solvent. Infrared spectral data reveal that the blue-green and purple products, (3)-A and (3)-B, contain σ -coordinated TCNE. The $\nu(\text{C}\equiv\text{N})$ bands occur at 2197 and 2121 cm^{-1} for (3)-A and 2200 and 2128 cm^{-1} for (3)-B as compared to TCNE⁰, whose $\text{C}\equiv\text{N}$ stretches are located at 2256 and 2221 cm^{-1} . These solids are soluble in most common solvents (e.g. CH_3CN , THF, CH_2Cl_2 , acetone, toluene, benzene, and alcohols). Slow evaporation or slow diffusion of hexanes or diethyl ether into solutions of the products have not yet produced crystalline materials, thereby precluding X-ray structural determinations.

There are numerous examples of TCNE complexes in the literature with the most frequently encountered coordination mode for TCNE being the π -type as in the metallocene-TCNE complexes [i.e. $\text{M}(\text{C}_5\text{R}_5)_2\text{TCNE}$; $\text{M} = \text{Fe}, \text{Cr}, \text{Co}$; $\text{R} = \text{H}, \text{Me}, \text{Et}$] that exhibit interesting magnetic properties at low temperatures.³ In addition to the π -TCNE complexes, several σ -coordinated TCNE complexes have recently been reported, the most intriguing example being the room temperature ferromagnet $\text{V}(\text{TCNE})_2 \cdot 1/2(\text{CH}_2\text{Cl}_2)$ characterized mainly by infrared spectroscopy.⁴ Among the examples whose X-ray crystallographic structures have been determined, the complexes $\text{V}(\text{C}_5\text{H}_5)_2\text{Br}(\text{TCNE})$,^{3, 2} $\text{Os}(\text{S}_2\text{PR}_2)_2(\text{PPh}_3)(\text{TCNE})$,³³ and $\text{Mn}(\text{CO})_2(\text{C}_5\text{H}_5)(\text{TCNE})$ ³⁴ all contain TCNE which is bonded to a metal center through only one N atom on TCNE. In the structure of the complex $[\text{Ir}(\text{CO})(\text{PPh}_3)_2]_2[\text{TCNE}]$, the TCNE bridges the two Ir centers in a *trans*- $\text{M}_2\text{-N-}\sigma$ -bound arrangement as does TCNQ in the structure of (2).³⁵ The structures of the complexes

$[\text{MnTPP}\cdot\text{TCNE}]_x$ (TPP = meso-tetraphenylporphinato)³⁶ and $[\text{Cu}(\text{hfacac})_2\cdot\text{TCNE}]_x$ (hfacac = hexafluoroacetylacetonates)³⁷ contain *trans*-N- σ -bound TCNE and are polymeric. The values of the $\nu(\text{C}\equiv\text{N})$ stretching frequencies of these and other TCNE containing complexes are listed along with the values obtained for $[\text{Re}_2\text{Cl}_4(\text{dppm})_2](\text{TCNE})$ (3)-A and $[\text{Re}_2\text{Cl}_4(\text{dppm})_2](\text{TCNE})$ (3)-B in Table 7. The values of $\nu(\text{C}\equiv\text{N})$ for the $[\text{Re}_2\text{Cl}_4(\text{dppm})_2](\text{TCNE})$ products are quite comparable to those found for the crystallographically determined complex $\text{Mo}(\text{CO})_2(\text{C}_5\text{H}_5)(\text{TCNE})$ supporting the assignment of a σ -N-bound TCNE^- moiety in the $[\text{Re}_2\text{Cl}_4(\text{dppm})_2](\text{TCNE})$ products.

The electronic absorption spectrum for (3)-A exhibits a strong absorption at $\lambda_{\text{max}} = 750$ nm. This transition is assigned to a $\text{M}\rightarrow\text{TCNE}$ charge-transfer band and is observed in several M- σ -N-bound complexes.^{24,33} Complexes that do not contain σ -coordinated TCNE, but rather π -bonded TCNE as in the complex $[\text{Fe}(\text{C}_5\text{Me}_5)_2]\text{TCNE}$, exhibit electronic absorptions near 400 nm assignable to $\pi\rightarrow\pi^*$ transitions.^{3,22,38} As indicated by magnetic measurements, (3)-A is diamagnetic due to the significant $d\pi\text{-}p\pi$ interaction. This is not unusual, as diamagnetism is likewise observed in $\text{Os}(\text{S}_2\text{P}(\text{R})_2)_2(\text{P}(\text{Ph})_3)\text{TCNE}$ and $\text{V}(\text{C}_5\text{H}_5)_2\text{Br}(\text{TCNE})$.^{32,33}

The ^1H NMR(CDCl_3) spectrum of (3)-A consists of several complex multiplets between $\delta = 7.1$ to $\delta = 7.8$ ppm attributed to the phenyl protons on dppm. A set of resonances centered at $\delta = 5.68$ and $\delta = 5.61$ ppm in an ABX_4 pattern are the result of inequivalent methylene protons on the two dppm ligands, unlike the pentet which occurs at $\delta = 5.21$ ppm in an $\text{AA}'\text{X}_4$ pattern for the parent compound $\text{Re}_2\text{Cl}_4(\text{dppm})_2$.³⁹ The $^{31}\text{P}\{^1\text{H}\}$ NMR spectrum reveals two types of phosphorous nuclei in an $\text{AA}'\text{BB}'$ pattern

Table 7. Comparison of $\nu(\text{C}\equiv\text{N})$ stretching frequencies for various TCNE containing complexes.

Complex	Coordination	Charge	$\nu(\text{C}\equiv\text{N})$	Reference
TCNE		0	2256 (s), 2221 (m)	a.
$[\text{Co}(\text{C}_5\text{Me}_5)_2]_2[\text{TCNE}]^*$	π	2-	2140 (s), 2069 (s)	38
$[\text{Fe}(\text{C}_5\text{Me}_5)_2]\text{TCNE}^*$	π	1-	2183 (s), 2144 (s)	3(c)
$[\text{Re}_2\text{Cl}_4(\text{dppm})_2](\text{TCNE})$ (3)-A	σ	1-	2200 (s), 2128 (m)	this work
$[\text{Re}_2\text{Cl}_4(\text{dppm})_2](\text{TCNE})$ (3)-B	σ	1-	2197 (s), 2121 (m)	this work
$\text{V}(\text{TCNE})_2 \cdot 1/2(\text{CH}_2\text{Cl}_2)$	σ	2-	2188 (m), 2099 (s)	4
$\text{Mn}(\text{CO})_2(\text{Cp})(\text{TCNE})^*$	σ	1-	2230 (vw), 2205 (s), 2125 (m)	24,34
$[\text{Ir}(\text{CO})(\text{PPh}_3)_2]_2[\text{TCNE}]^*$	σ - μ_2	2-	2176 (m), 2097 (s)	35
$[\text{MnTPP} \cdot \text{TCNE}]_x^*$	σ - μ_2	1-	2187 (m), 2139 (m), 2126 (s)	36
$[\text{Cu}(\text{hfacac})_2 \cdot \text{TCNE}]_x^*$	σ - μ_2	0	2262, 2252, 2220 ^b	37

a. Nujol, CsI on our equipment.

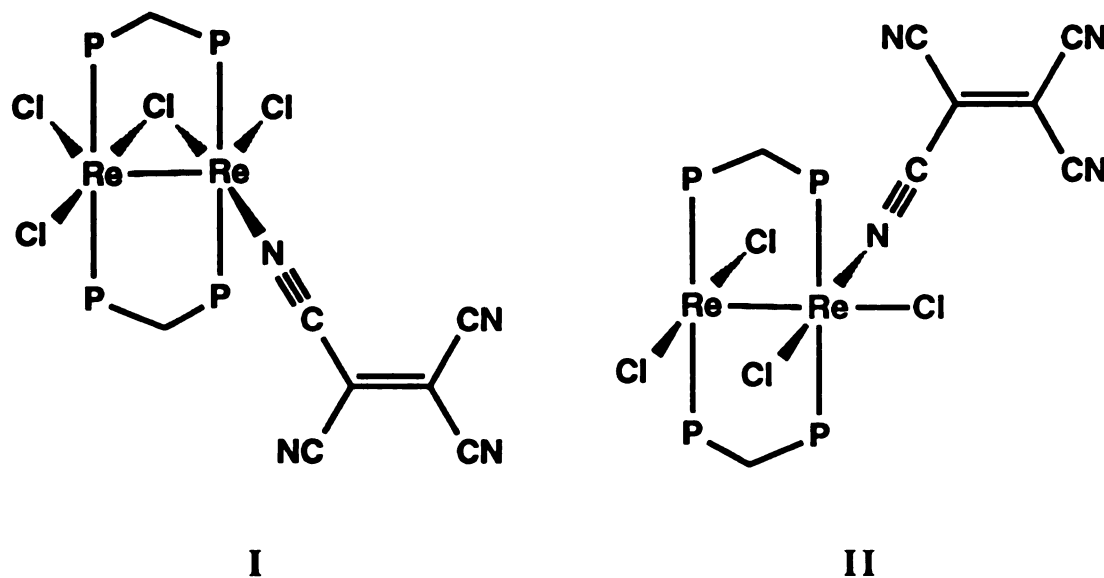
b. Relative intensities were not reported

* Structurally determined

TPP = *meso*-tetraphenylporphyrin

hfacac = hexafluoroacetylacetonate

with resonances at $\delta = -14.6$ and $\delta = -19.9$ ppm. These NMR spectral features are in accord with either an A-frame type (I) or non-A-frame type (II) seen for other complexes of the types $\text{Re}_2\text{Cl}_4(\text{dppm})_2\text{L}$, and $[\text{Re}_2\text{Cl}_3(\text{dppm})_2\text{L}_2]^+$.^{17,18,39,40} The low temperature $^{31}\text{P}\{^1\text{H}\}$ NMR



spectrum of (3)-A in CDCl_3 at -50°C , shown in Figure 14, exhibits a single broad resonance at $\delta = -21.4$ ppm which is consistent with the transformation to a more symmetrical molecule with equivalent phosphorous nuclei.

A cyclic voltammogram of (3)-A (vs. Ag/Ag^+ in 0.1M $\text{TBABF}_4/\text{CH}_2\text{Cl}_2$) exhibits a reversible reduction at $E_{1/2} = -0.10$ V which is more negative than the reduction potential for free TCNE (see Figure 15). This is consistent with metal-to-ligand electron transfer increasing the electron density on TCNE and making it more difficult to reduce.^{24,41} A reversible metal-based oxidation at $E_{1/2} = 0.72$ V is at more positive potential than the first oxidation for $\text{Re}_2\text{Cl}_4(\text{dppm})_2$. This is also a consequence of metal-to-ligand charge transfer.

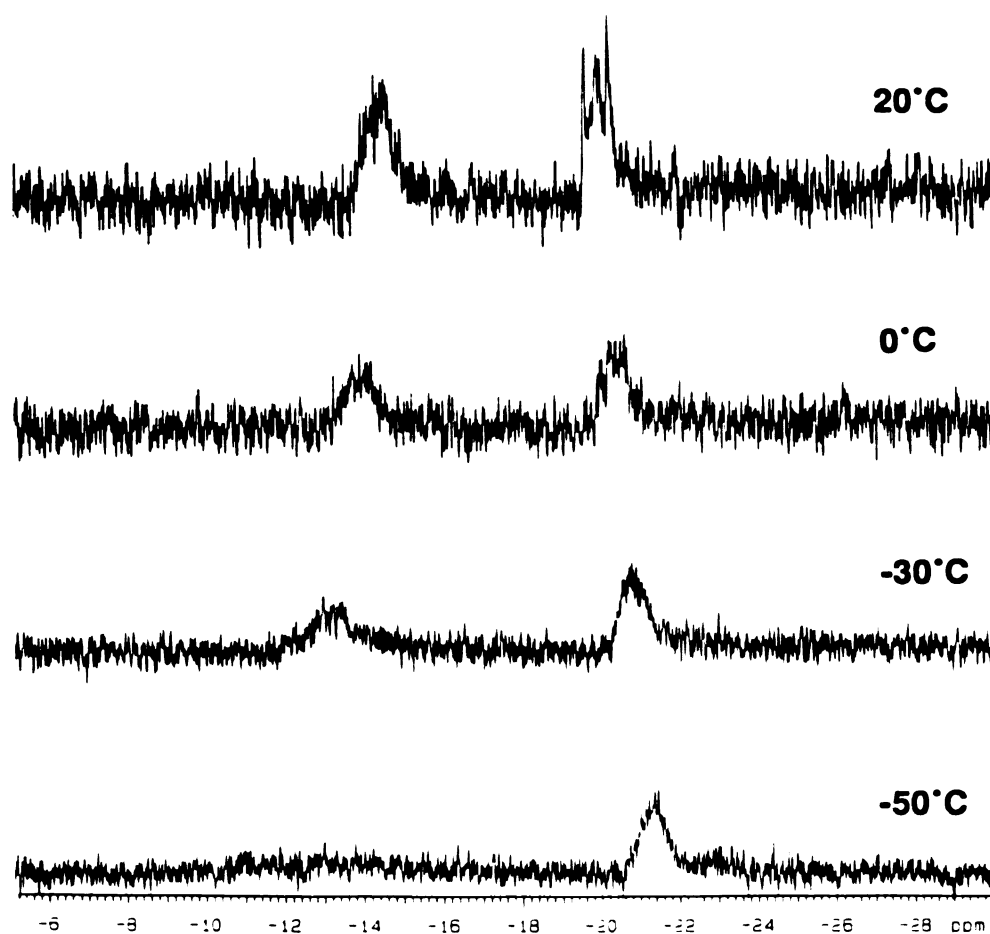


Figure 14. Variable temperature ^{31}P { ^1H } NMR (CDCl_3) spectra of $[\text{Re}_2\text{Cl}_4(\text{dppm})_2](\text{TCNE})$ (3)-A.

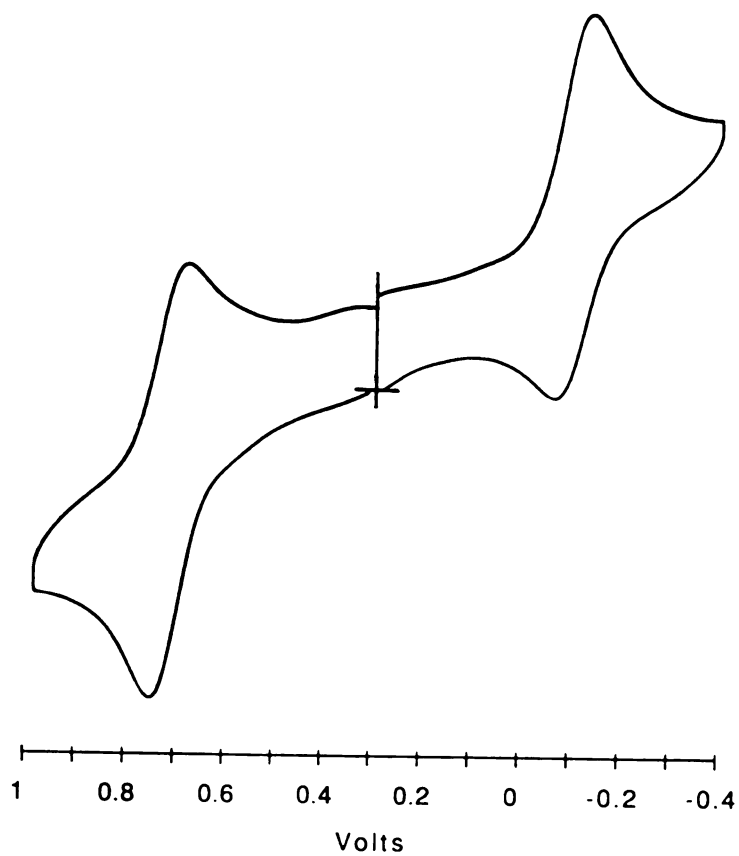


Figure 15. Cyclic voltammogram of $[\text{Re}_2\text{Cl}_4(\text{dppm})_2](\text{TCNE})$ (**3**)-A in 0.1 M TBABF₄/CH₂Cl₂ versus Ag/AgCl at a Pt disk electrode.

When a blue-green solution of (3)-A in CH_2Cl_2 is allowed to stand at room temperature over the period of *ca.* 20 h, the solution color eventually turns dark purple. UV-visible spectra during this period exhibit a feature at $\lambda_{\text{max}} = 750$ nm that decreases in intensity, and a peak that grows in near $\lambda_{\text{max}} = 500$ nm. The final spectrum exhibits absorptions at $\lambda_{\text{max}} = 518$ and 668 nm. Reactions performed with as many as 6 equivalents of TCNE yield virtually identical results. When THF is used in place of CH_2Cl_2 , these changes occur more slowly. With THF noticeable changes in the UV-visible spectrum are observed only after 48 h. The spectra of the 1:1 THF reaction solutions exhibit absorptions at $\lambda_{\text{max}} = 488$ nm with a shoulder at $\lambda_{\text{max}} = 677$ nm in addition to an intense absorption at $\lambda_{\text{max}} = 750$ nm. Over a period of 3 weeks the absorption at $\lambda_{\text{max}} = 750$ nm slowly diminishes while that at $\lambda_{\text{max}} = 488$ nm gradually becomes more intense. The absorption at $\lambda_{\text{max}} = 677$ nm, which initially becomes stronger, slowly decreases in intensity over time. The reaction between $\text{Re}_2\text{Cl}_4(\text{dppm})_2$ and 0.5 equivalents of TCNE in THF immediately produces a dark blue solution with an electronic absorption at $\lambda_{\text{max}} = 748$ nm, but within two days, the color changes to a dark olive-green and the corresponding UV-visible spectrum contains weak absorptions at $\lambda_{\text{max}} = 450$ and 650 nm.

The infrared spectra of THF solutions containing 1:5, 2:5, 1:1, and 2:1 ratios of $\text{Re}_2\text{Cl}_4(\text{dppm})_2$:TCNE all contain $\nu(\text{C}\equiv\text{N})$ bands at 2197 (s) and 2123 (m) cm^{-1} indicating that no dependence on stoichiometry. Only in the spectrum of the 1:5 solution do other peaks, attributed to free TCNE^0 , appear in the $\nu(\text{C}\equiv\text{N})$ region.

C. Reactions of $\text{Re}_2\text{Cl}_4(\text{dppm})_2$ with TNAP

(1) Preparation and Spectroscopic Properties

The reactions between $\text{Re}_2\text{Cl}_4(\text{dppm})_2$ and TNAP yield products that exhibit spectroscopic features similar to those observed for the products from the reactions between $\text{Re}_2\text{Cl}_4(\text{dppm})_2$ and TCNQ. The 1:1 reaction between $\text{Re}_2\text{Cl}_4(\text{dppm})_2$ and TNAP in CH_2Cl_2 produces an instantaneous color change to yellow-green from which $[\text{Re}_2\text{Cl}_4(\text{dppm})_2](\text{TNAP})$ (4)-A is precipitated as an olive-green solid by the addition of hexanes. The solution infrared spectrum of (4)-A exhibits $\nu(\text{C}\equiv\text{N})$ bands at 2195 and 2126 cm^{-1} which are similar to those observed for (3)-A (see Table 8). Although, judging by color, the solution appears to be stable at room temperature, the solution infrared spectrum undergoes changes. After 11 h, new $\nu(\text{C}\equiv\text{N})$ bands appear at 2183, 2114, and 2085 cm^{-1} ; these are at similar frequencies to the $\nu(\text{C}\equiv\text{N})$ bands observed in the spectra of solutions of (3)-A. The electronic absorption spectrum of (4)-A in CH_2Cl_2 exhibits absorptions at $\lambda_{\text{max}} = 374, 478, \text{ and } 1005 \text{ nm}$, with the intensity of the absorption at 1005 nm decreasing after 1 day at room temperature. The 2:1 reaction between $\text{Re}_2\text{Cl}_4(\text{dppm})_2$ and TNAP in CH_2Cl_2 produces an instantaneous blue-green solution which is stable only at low temperatures. The addition of hexanes to this solution, while kept at -78°C , affords a product formulated as $[\text{Re}_2\text{Cl}_4(\text{dppm})_2]_2(\mu\text{-TNAP})$ (5)-A as a black crystalline solid. When solutions of (5)-A are warmed to room temperature, the color quickly turns to red-brown, (5)-B, preventing solution studies of (5)-A. The solution infrared spectrum of (5)-B exhibits $\nu(\text{C}\equiv\text{N})$ bands at 2186 and 2101 cm^{-1} which are similar to those observed for (2) (see Table 8). The electronic absorption spectrum of (5)-B in

Table 8. Comparison of the infrared spectral features of the TCNQ and TNAP products.

Complex	Acceptor	$\nu(\text{C}\equiv\text{N})$ bands cm^{-1}
(3)-A	TCNQ	2195 (s), 2115 (m)
(4)-A	TNAP	2195 (s), 2126 (m)
(3)-B	TCNQ	2183 (s), 2114 (s,br) 2085 (sh)
(4)-B	TNAP	2186 (s), 2124 (s,br) 2089 (sh)
(2)	TCNQ	2187 (m), 2109 (s,br)
(5)-B	TNAP	2186 (m), 2101 (s,br)

CH_2Cl_2 exhibits one features at $\lambda_{\text{max}} = 1072$ and 2050 nm which slowly decreases in intensity with time.

References

1. (a) Ferraro, J. R.; Williams, J. M. *Introduction to Synthetic Electrical Conductors*, Academic Press, Inc. **1987**. (b) Williams, J. M.; Schultz, A. J.; Geiser, U.; Carlson, K. D.; Kini, A. M.; Wang, H. H.; Kwok, W.-K.; Whangbo, M.-H.; Schirber, J. E. *Science* **1991**, *252*, 1501. (c) Bryce, M. R. *Chem. Soc. Rev.* **1991**, *20*, 355. (d) Proceeding of the International Conference on Science and Technology of Synthetic Metals (ICSM88) Santa Fe, NM, USA (*Synth. Met.* **1988**, B1-B656).
2. (a) Kollmar, C.; Kahn, O. *Acc. Chem. Res.* **1993**, *26*, 259. (b) White, R. M. *Science*, **1985**, *229*, 11. (c) Miller, J. S.; Epstein, A. J. *Angew. Chem.* **1993**, *32*, 000. (d) Miller, J. S. *Adv. Mater.* **1992**, *4*, 298. (e) Kahn, O. *Comments Inorg. Chem.* **1984**, *3*, 105. (f) Rey, P. *Acc. Chem. Res.* **1989**, *22*, 392. (g) Caneschi, A.; Gatteschi, D.; Renard, J. P.; Rey, P.; Sessoli, R. *Inorg. Chem.* **1989**, *28*, 3314. (h) van Koningsbruggen, P. J.; Kahn, O.; Nakatani, K.; Pei, Y.; Renard, J. P.; Drillon, M.; Legoll, P. *Inorg. Chem.* **1990**, *29*, 3325.
3. (a) Miller, J. S.; Epstein, A. J. *Angew. Chem.* **1993**, *32*, 000 (b) Miller, J. S.; Epstein, A. J.; Reiff, W. M. *Chem. Rev.* **1988**, *88*, 201. (c) Miller J. S.; Calabrese, J. C.; Rommelmann, H.; Chittipeddi, S. R.; Zhang, H. H.; Reiff, W. M.; Epstein, A. J. *J. Am. Chem. Soc.* **1987**, *109*, 769. (d) Ward, M.S.; Johnson, D. C. *Inorg. Chem.* **1987**, *26*, 4213. (e) Broderick, W. E.; Thompson, J. A.; Day, E. P.; Hoffman, B M. *Science* **1990**, *249*, 401.
4. Manriquez, J. M.; Yee, G. T.; McLean, R. S.; Epstein, A. J.; Miller, J. S. *Science* **1991**, *252*, 1415.
5. (a) Zietlow, T. C.; Klendworth, D. D.; Nimry, T.; Salmon, D. J.; Walton, R. A. *Inorg. Chem.* **1981**, *20*, 947. (b) Barder, T. J.; Cotton, F. A.; Lewis, D.; Schwotzer, W.; Tetrick, S. M.; Walton, R. A. *J. Am. Chem. Soc.* **1984**, *106*, 2882.
6. Scan rate 200 mV/sec, 0.1 M TBAH, in CH₂Cl₂. The Cp₂Fe⁰/Cp₂Fe⁺ couple was refernced at +0.50 V.
7. Barder, T. J.; Cotton, F. A.; Dunbar, K. R.; Powell, G. L.; Schwotzer, W.; Walton, R. A. *Inorg. Chem.* **1985**, *24*, 2550.

8. San Filippo, J., Jr. *Inorg. Chem.* **1972**, *11*, 3140.
9. Standard procedure for thin tube layering reactions: A 6 or 8 mm outer diameter pyrex tube is cut to a length of *ca.* 16 inches and sealed at one end. The tube is connected to an apparatus consisting of a ground glass stopcock and 14/20 size female joint using a 1/2 inch piece of Tygon tubing of appropriate diameter. The glass tube is heated with a flame while under vacuum and allowed to cool prior to use. After the addition of solutions and solvents, the tube is allowed to stand for *ca.* 10 min. prior to flame sealing to allow for evaporation of solvent away from the area to be sealed. Before sealing, with the stopcock closed, a slight vacuum is created in the gas manifold by closing the nitrogen inlet and pumping and filling several times on the hose leading to the apparatus with only the mercury bubbler open. This is repeated several times until the mercury is drawn up about 2 inches. The stopcock to the thin tube is gently opened and the tube is slowly and evenly sealed using a flame at least 3 inches above the solution level. The mercury level is monitored while sealing to ensure the vacuum is not lost.
10. (a) Bino, A.; Cotton, F. A.; Fanwick, P. E. *Inorg. Chem.* **1979**, *18*, 3558. (b) Cotton, F. A.; Frenz, B. A.; Deganello, G.; Shaver, A. J. *Organomet. Chem.* **1973**, *50*, 227.
11. TEXSAN-TEXRAY Structure Analysis Package, Molecular Structure Corporation **1985**.
12. Sheldrick, G. M. In: *Crystallographic Computing 3*, Eds.; G.M. Sheldrick, C. Kruger, and R. Goddard. Oxford U.K., 1985; pp. 175 - 189.
13. Robles-Martinez, J. G.; Salmeron-Valverde, A.; Alonso, E.; Soriano, C. *Inorg. Chem. Acta* **1991**, *179*, 149.
14. Taube, H.; Johnson, A. J. *Indian Chem. Soc.* **1989**, *66*, 503
15. (a) Fanwick, P. E.; Price, A. C.; Walton, R. A. *Inorg. Chem.* **1988**, *27*, 2601. (b) Price, A. C.; Walton, R. A. *Polyhedron* **1987**, *6*, 729.
16. For a study on the effect of bond length on bond order of M₂L₈ complexes see: Cotton, F. A.; Dunbar, K. R.; Falvello, L. R.; Tomas, M.; Walton, R. A. *J. Am. Chem. Soc.* **1983**, *105*, 4950.

17. Cotton, F. A.; Dunbar, K. R.; Price, A. C.; Schwotzer, W.; Walton, R. A. *J. Am. Chem. Soc.* **1986**, *108*, 4843.
18. (a) Barder, T. J.; Cotton, F. A.; Falvello, L. R.; Walton, R. A. *Inorg. Chem.* **1985**, *24*, 1258. (b) Derringer, D. R.; Shih, K.-Y.; Fanwick, P. E.; Walton, R. A. *Polyhedron*, **1991**, *10*, 79. (c) Fanwick, P. E.; Qi, J.-S.; Shih, K.-Y.; Walton, R. A. *Inorg. Chem. Acta*, **1990**, *172*, 65.
19. Cotton, F. A.; Shive, L. W.; Stults, B. R. *Inorg. Chem.* **1976**, *15*, 2239.
20. (a) Fritchie, C. J.; Arthur, P. *Acta Cryst.* **1966**, *21*, 139. (b) Hoekstra, A.; Spoelder, T.; Vos, A. *Acta Cryst.* **1972**, *B28*, 14. (c) Konno, M.; Saito, Y.; *Acta Cryst.* **1974**, *B30*, 1294.
21. Shields, L. *J. Chem. Soc., Faraday Trans. 2* **1985**, *81*, 1.
22. Gross, R.; Kaim, W. *Angew. Chem. Int. Ed.* **1987**, *26*, 251.
23. Olbrich-Deussner, B.; Gross, R.; Kaim, W. *J. Organomet. Chem.* **1989**, *366*, 155.
24. (a) Gross-Lannert, R.; Kaim, W.; Olbrich-Deussner, B. *Inorg. Chem.* **1990**, *29*, 5046. (b) Cotton, F. A.; Daniels, L. M.; Dunbar, K. R.; Falvello, L. R.; Tetrick, S. M.; Walton, R. A. *J. Am. Chem. Soc.* **1985**, *107*, 3524.
25. DIRDIF: Direct Methods for Difference Structure, An Automatic Procedure for Phase Extension; Refinement of Difference Structure Factors. Beurskens, R. T. Technical Report, 1984.
26. Bell, S. E.; Field, J. S.; Haines, R. I.; Moscherosch, M.; Matheis, W. Kaim, W. *Inorg. Chem.* **1992**, *31*, 3269.
27. Grossel, M. C.; Evans, F. A.; Hriljac, J. A.; Morton, J. R.; LePage, Y.; Preston, K. F.; Sutcliffe, L. H.; Williams, A. J. *J. Chem. Soc., Chem. Commun.* **1990**, 439.
28. Ballester, L.; Barral, M. C.; Gutiérrez, A.; Jiménez-Aparicio, R.; Martínez-Muyo, J. M.; Perpiñán, M. F.; Monge, M. A.; Ruíz-Valero, C. *J. Chem. Soc., Chem. Commun.* **1991**, 1396.
29. Humphrey, D. G.; Fallon, G. D.; Murray, K. S. *J. Chem. Soc., Chem. Commun.* **1988**, 1356.

30. Booth, B. L.; McAuliffe, C. A.; Stanley, G. L. *J. Chem. Soc., Dalton* **1982**, 535.
31. van der Pauw, L. J. *Philips Research Reports* **1958**, 13, 1.
32. Rettig, M. F.; Wing, R. M. *Inorg. Chem.* **1969**, 8, 2685.
33. McQueen, A. E. D.; Blake, A. J.; Stephenson, R. A.; Schröder, M.; Yellowlees, L. J. *J. Chem. Soc., Chem. Commun.* **1988**, 1533.
34. Braunworth, H.; Huttner, G.; Zsolnai, L. *J. Organomet. Chem.* **1989**, 372, C23.
35. Yee, G. T.; Calabrese, J. C.; Vazquez, C.; Miller, J. S. *Inorg. Chem.* **1993**, 32, 377.
36. Miller, J. S.; Calabrese, J. C.; McLean, R. S.; Epstein, A. J. *Adv. Mater.* **1992**, 4, 498.
37. Bunn, A. G.; Carroll, P. J.; Wayland, B. B. *Inorg. Chem.* **1992**, 31, 1297.
38. Dixon, D. A.; Miller, J. S. *J. Am. Chem. Soc.* **1987**, 109, 3656.
39. Barder, T. J.; Cotton, F. A.; Lewis, D.; Schwotzer, W.; Tetrick, S. M.; Walton, R. A. *J. Am. Chem. Soc.* **1984**, 106, 2882.
40. Fanwick, P. E.; Qi, J.-S.; Walton, R. A. *Inorg. Chem.* **1990**, 29, 3787.
41. Olbrich-Duessner, B.; Kaim, W.; Gross-Lannert, R. *Inorg. Chem.* **1989**, 28, 3113.
42. TCNQ was purchased from Aldrich Chemical Co. and sublimed before using. The infrared spectra was done as a Nujol mull and obtained on our equipment.
43. Acker, D. S.; Harder, R. J.; Hertler, W. R.; Mahler, W.; Melby, L. R.; Benson, R. E.; Mochel, W. E. *J. Am. Chem. Soc.* **1960**, 82, 6408.
44. Melby, L. R.; Harder, R. J.; Hertler, W. R.; Mahler, W.; Benson, R. E.; Mochel, W. E. *J. Am. Chem. Soc.* **1962**, 84, 3374.

45. Miller, J. S.; Reiff, W. M.; Zhang, J. H.; Preston, L. D.; Reis, A. H. Jr.; Gebert, E.; Extine, M.; Troup, J.; Dixon, D. A.; Epstein, A. J.; Ward, M. D. *J. Phys. Chem.* **1987**, *91*, 4344.
46. Broderick, W. E.; Hoffman, B. M. *J. Am. Chem. Soc.* **1991**, *113*, 6334.
47. Sacher, W.; Nagel, U.; Beck, W. *Chem. Ber.* **1987**, *120*, 895.
48. Long, R. E.; Sparks, R. A.; Trueblood, K. N. *Acta Cryst.* **1965**, *18*, 932.
49. Kobayashi, H. *Bull. Chem. Soc. Japan* **1973**, *46*, 2945.
50. Chi, K.-M.; Calabrese, J. C.; Reiff, W. M.; Miller, J. S. *Organomet.* **1991**, *10*, 688.

CHAPTER III

THE USE OF N,N'-DICYANOQUINONEDIIMINES AS LINKING UNITS FOR THE DINUCLEAR COMPOUND $\text{Re}_2\text{Cl}_4(\text{dppm})_2$.

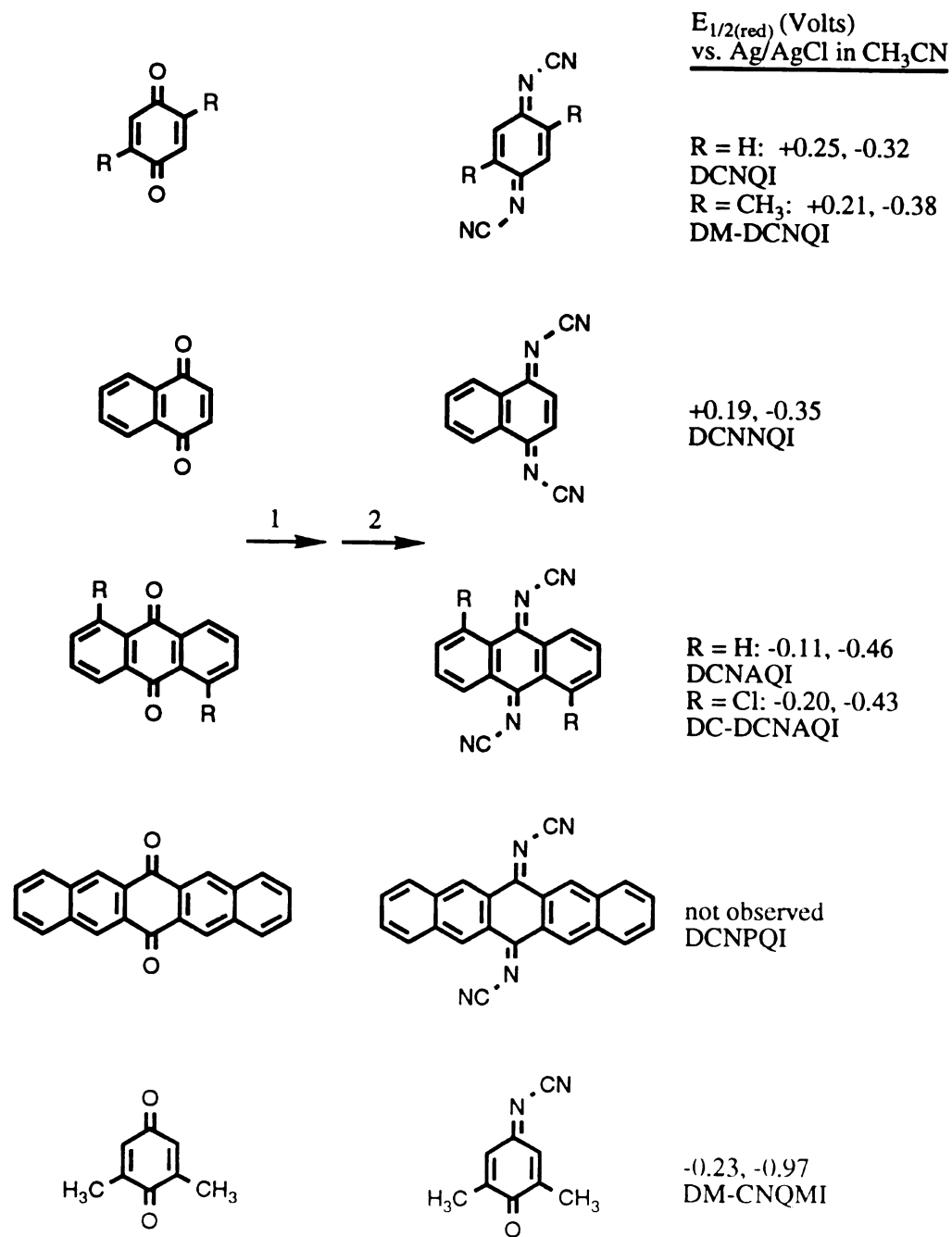
1. Introduction

The search for new molecules capable of linking dinuclear metal complexes like led us to the study of the recently discovered cyano-containing N,N'-dicyanoquinonediimines (DCNQIs). Aumüller and Hünig reported that a variety of substituted DCNQIs could be readily synthesized from quinones (see Figure 16).¹ Many of these compounds exhibit accessible redox processes which make them good candidates for charge-transfer chemistry with $\text{Re}_2\text{Cl}_4(\text{dppm})_2$.^{2,6} In particular, the electrochemical properties of 2,5-dimethyl-N,N'-dicyanoquinonediimine (DM-DCNQI) are very similar to TCNQ. The DCNQIs have the ability to form complexes which exhibit high single crystal conductivities.^{3,4} X-ray structures of a number of $\text{M}(\text{DCNQI})_2$ complexes have been determined; the cations are typically covalently linked to form layered two-dimensional sheets.^{3,5} Such structures have not been found for complexes of TCNQ, thus we sought to compare the chemistry of the DCNQIs with $\text{Re}_2\text{Cl}_4(\text{dppm})_2$ to the results for TCNQ reported in Chapter II.

2. Experimental

A. Synthesis

The compounds 2,6-dimethyl-N-cyano-1,4-benzoquinone-4-imine (DM-CNQMI), N,N'-dicyano-1,4-benzoquinonediimine (DCNQI), 2,5-dimethyl-N,N'-dicyano-1,4-benzoquinonediimine (DM-DCNQI), N,N'-dicyano-1,4-naphthaquinonediimine (DCNNQI), N,N'-dicyano-9,10-anthraquinonediimine (DCNAQI), and 1,5-dichloro-N,N'-dicyano-9,10-anthraquinonediimine (DC-DCNAQI) were synthesized according to literature procedures.¹ All of these compounds were characterized by cyclic voltammetry and IR, UV-visible, ^1H NMR, ^{13}C NMR, and GC-mass spectroscopies.



1 = TiCl_4 , 2 = $\text{Me}_3\text{SiNCNSiMe}_3$

Figure 16. Synthetic route to DCNQI molecules and their cyclic voltammetric properties.

(1) Preparation of DCNPQI

The compound N,N'-dicyano-6,13-pentacenequinonediimine, although not reported in the literature, was synthesized using a similar method described by Aumüller.¹ A quantity of pentacenequinone (0.616 g, 2.00 mmol) was added to a 100 mL Schlenk flask followed by addition of 25 mL of CH₂Cl₂. To this solution was added 5.68 mL (2.5 mmol) of bis(trimethylsilyl)carbodiimide (Me₃SiN=C=NSiMe₃) followed by 1.1 mL (10 mmol) of titanium tetrachloride forming a dark red-brown solution. The reaction was stirred at room temperature for 72 h after which time the reaction mixture was poured into a large beaker containing 500 mL of petroleum ether (boiling range: 35-60°C) to give a precipitate which was collected by gravity filtration. The solid was dissolved in *ca.* 1 L of hot benzene and filtered. The yellow filtrate was reduced in volume to *ca.* 50 mL using a rotary evaporator and an orange solid was precipitated by adding 500 mL of petroleum ether. The solid was collected by filtration and vacuum dried. A GC chromatogram of the product indicated that 3 separate components were present, thus, the product was further purified by eluting a CH₂Cl₂ (400 mL) solution of the product through a silica gel (65-200 mesh) column (12 inches long by 1 inch diameter) and the product was further eluted with CH₂Cl₂ (*ca.* 1 L) until colorless eluents were obtained. The remaining two bands, a dark brown-orange band near the top of the column and a red-pink band around the middle of the column, were not collected. The yellow CH₂Cl₂ eluent was concentrated to 50 mL using the rotary evaporator from which a bright orange solid was precipitated by adding 200 mL of petroleum ether. The solid was collected by filtration and vacuum dried; yield 0.350 g (49%). IR (CsI, Nujol, cm⁻¹): ν(C≡N) 2149 (m), 2162 (sh), 2177 (sh),

$\nu(\text{C}=\text{C})$ 1597 (s), $\nu(\text{C}=\text{N})$ 1539 (s). mass spectrum (70eV): $m/z = 356$ (100%, M^+), 330 (12%, M^+-CN), 329 (17%, M^+-HCN), 315 (7%, $\text{M}^+-\text{H}-\text{NCN}$), 302 (14%, M^+-2HCN). A cyclic voltammogram of the compound in a 0.1 M TBABF₄/CH₃CN solution did not reveal any electrochemical processes between +2.0 and -2.0 V.

(2) Reaction of $\text{Re}_2\text{Cl}_4(\text{dppm})_2$ with DM-CNQMI

A solution consisting of 0.0132 g (0.082 mmol) of DM-CNQMI dissolved in 5 mL of THF was added to a stirring solution containing 0.105 g (0.082 mmol) of $\text{Re}_2\text{Cl}_4(\text{dppm})_2$ dissolved in 10 mL of THF which resulted in the immediate production of a dark green solution. A UV-visible spectrum of the reaction solution showed an absorption at $\lambda_{\text{max}} = 812$ nm and a solution infrared spectrum (CaF₂ cells, THF reference) revealed a $\nu(\text{C}\equiv\text{N})$ band at 2195 (vs) cm^{-1} . The reaction was stirred for 4 h at room temperature with no further change in color. The reaction solution was reduced in volume by vacuum and a green solid was precipitated by the addition of hexanes (20 mL). The solid was collected by filtration, washed with copious amounts of hexanes, and vacuum dried; yield 0.061 g (51%). IR (CsI, Nujol, cm^{-1}): $\nu(\text{C}\equiv\text{N})$ 2096 (vs), $\nu(\text{C}=\text{O})$ 1645 (w), $\nu(\text{C}=\text{C})$ 1610 (w), $\nu(\text{C}=\text{N})$ 1576 (m).

(3) Reactions of $\text{Re}_2\text{Cl}_4(\text{dppm})_2$ with DCNQI

(i) Preparation of $[\text{Re}_2\text{Cl}_4(\text{dppm})_2]_2(\mu\text{-DCNQI})$

A THF (12 mL) solution containing 0.0061 g (0.039 mmol) of DCNQI was added to a THF (8 mL) solution containing 0.100 g (0.078 mmol) of $\text{Re}_2\text{Cl}_4(\text{dppm})_2$ to give a green precipitate within 5 minutes. The solid was collected by filtration, washed with THF, and vacuum dried; yield 0.073 g (69%). IR (CsI, Nujol, cm^{-1}):

$\nu(\text{C}\equiv\text{N})$ 2090 (vs), $\nu(\text{C}=\text{N})$ 1505 (vw), $\nu(\text{C}=\text{C})$ not observed. UV-visible(CH_2Cl_2) $\lambda_{\text{max}} = 1003$ and 691 nm.

(ii) 1:4 $\text{Re}_2\text{Cl}_4(\text{dppm})_2$:DCNQI Stoichiometric Reaction

Methylene chloride (20 mL) was added to a Schlenk flask that contained 0.050 g (0.039 mmol) of $\text{Re}_2\text{Cl}_4(\text{dppm})_2$ and 0.0244 g (0.156 mmol) of DCNQI resulting in the immediate formation of a dark green solution. The reaction mixture was placed in the refrigerator (-5°C) for 2 weeks during which time a dark green solid slowly precipitated. The solid was collected by filtration, washed with CH_2Cl_2 , and vacuum dried; yield 0.072 g (96%). IR (CsI, Nujol, cm^{-1}): $\nu(\text{C}\equiv\text{N})$ 2090 (vs,br), 2240 (w). The same product was obtained in slightly lower yields (0.049 g) when the reaction was performed in toluene.

(4) Reactions of $\text{Re}_2\text{Cl}_4(\text{dppm})_2$ with DM-DCNQI

(i) 1:1 Reactions

(a) Preparation of $[\text{Re}_2\text{Cl}_4(\text{dppm})_2](\text{DM-DCNQI})$ (6)-A

Methylene chloride solutions (5 mL each) of $\text{Re}_2\text{Cl}_4(\text{dppm})_2$ (0.100 g, 0.078 mmol) and DM-DCNQI (0.0143 g, 0.078 mmol) were cooled to -78°C using a dry ice/acetone bath. The $\text{Re}_2\text{Cl}_4(\text{dppm})_2$ solution was added to the DM-DCNQI solution through a cannula producing a dark blue solution with a $\nu(\text{C}\equiv\text{N})$ band at 2053 cm^{-1} . This infrared solution turned green within 5 minutes yielding a spectrum with a $\nu(\text{C}\equiv\text{N})$ band at 2082 cm^{-1} . A UV-visible spectrum of the reaction solution exhibited absorptions at $\lambda_{\text{max}} = 830$ ($\epsilon = 23100\text{ M}^{-1}\text{cm}^{-1}$) and 334 ($\epsilon = 35100\text{ M}^{-1}\text{cm}^{-1}$) nm. The solution volume was reduced to ca. 5 mL by vacuum while being maintained at low temperatures, and 30 mL of hexanes was added to precipitate a blue solid which was collected by

filtration, washed with hexanes (2 x 10 mL) and dried *in vacuo*; yield 0.096 g (84%). IR (CsI, Nujol, cm^{-1}) $\nu(\text{C}\equiv\text{N})$ 2070 (s,br).

(b) Preparation of $[\text{Re}_2\text{Cl}_4(\text{dppm})_2](\text{DM-DCNQI})$ (6)-B

A solution containing 0.0144 g (0.078 mmol) of DM-DCNQI in 8 mL of THF was transferred to a 50 mL Schlenk flask containing 0.100 g (0.078 mmol) of $\text{Re}_2\text{Cl}_4(\text{dppm})_2$ in 10 mL of THF producing an immediate dark blue solution of (6)-A. After 5 minutes, a UV-visible spectrum of the reaction solution exhibited a strong absorption at $\lambda_{\text{max}} = 812$ nm and a higher energy absorption at $\lambda_{\text{max}} = 342$ nm. The reaction mixture was stirred for 24 h at room temperature during which time the color changed to dark green. The solution volume was reduced under vacuum followed by treatment of diethyl ether (*ca.* 20 mL) which caused the precipitation of an olive-green solid of (6)-B. The solid was collected by filtration, washed with diethyl ether, and vacuum dried; yield 0.077 g (67%). IR (CsI, Nujol, cm^{-1}): $\nu(\text{C}\equiv\text{N})$ 2091 (s,br), $\nu(\text{C}=\text{C})$ 1587 (vw), $\nu(\text{C}=\text{N})$ 1576 (vw).

(c) Reaction of 1:1 $\text{Re}_2\text{Cl}_4(\text{dppm})_2$ and DM-DCNQI in Toluene

A reaction mixture containing $\text{Re}_2\text{Cl}_4(\text{dppm})_2$ (0.100 g, 0.078 mmol), DM-DCNQI (0.0143 g, 0.078 mmol), and toluene (20 mL) was refluxed causing the immediate formation of a dark-blue solution. Within 10 minutes, the solution turned dark green and a green solid precipitated. The mixture was refluxed for 45 minutes after which time a black solid was collected by filtration. The product was dissolved in CH_2Cl_2 (*ca.* 10 mL) and the green solution was filtered leaving behind an insoluble black solid. The solid was washed with CH_2Cl_2 until colorless filtrates were achieved and then dried *in vacuo*; yield 0.053 g (46%). IR (CsI, Nujol, cm^{-1}): $\nu(\text{C}\equiv\text{N})$ 2054 (s,br), $\nu(\text{C}=\text{C})$ 1588 (vw), $\nu(\text{C}=\text{N})$ 1575 (vw). The green filtrate was reduced in volume and layered with 15

5 mL of hexanes causing the eventual formation of an olive-green solid which was collected by filtration, washed with hexanes, and dried *in vacuo*; **y**ield 0.016 g (14%). IR (CsI, Nujol, cm^{-1}): $\nu(\text{C}\equiv\text{N})$ 2075 (s), $\nu(\text{C}=\text{C})$ **1** 588 (vw), $\nu(\text{C}=\text{N})$ 1574 (vw).

(i) Preparation of $[\text{Re}_2\text{Cl}_4(\text{dppm})_2]_2(\mu\text{-DM-DCNQI})$ (7)

(a) Slow Diffusion Reaction

A quantity of DM-DCNQI (0.0073 g, 0.039 mmol) was dissolved in **5** mL of THF and slowly added to a Schlenk tube containing 0.100 g (**0**.078 mmol) of $\text{Re}_2\text{Cl}_4(\text{dppm})_2$ dissolved in 5 mL of THF. The Schlenk tube was placed in the refrigerator for 2 days during which time a black crystalline solid formed. The solid was collected by filtration, washed with THF, and dried *in vacuo*; yield 0.076 g (71%). *Anal.* Calcd for $\text{C}_{110}\text{H}_{96}\text{N}_4\text{Cl}_8\text{P}_8\text{Re}_4$: C, 48.04; H, 3.52; N, 2.04. Found C, 47.98; H, 3.81; N, 2.01. ^1H NMR (CDCl_3 , ppm) $\delta = 7.0 - 7.9$ (m), $\delta = 3.73$ (t), and $\delta = 1.83$ (p). A $^{31}\text{P}\{^1\text{H}\}$ NMR signal was not observed. IR (CsI, Nujol, cm^{-1}): $\nu(\text{C}\equiv\text{N})$ 2056 (s,br), $\nu(\text{C}=\text{C})$ 1586 (w), $\nu(\text{C}=\text{N})$ 1572 (w). **E**lectronic spectroscopy (CH_2Cl_2): λ_{max} nm (ϵ , $\text{M}^{-1}\text{cm}^{-1}$), 696 (4600), **1** 035 (27000), 1800 (36000).

(b) Bulk Reaction

A solution containing 0.0073 g (0.039 mmol) of DM-DCNQI in **20** mL of benzene was slowly added to a stirring solution containing **0**. 100 g (0.078 mmol) of $\text{Re}_2\text{Cl}_4(\text{dppm})_2$ in 10 mL of benzene to form an **i**nitial dark blue solution. After 10 minutes, a black solid precipitated **w**hich was collected by filtration, washed with benzene, and vacuum dried; **y**ield 0.084 g (78%). IR (KBr pellet, cm^{-1}): $\nu(\text{C}\equiv\text{N})$ 2250 (w), 2218 (w), **2** 101 (vs), $\nu(\text{C}=\text{C})$ 1588 (w), $\nu(\text{C}=\text{N})$ 1574 (w). **E**lectronic spectroscopy

(CH₂Cl₂): λ_{max} = 702 and 1039 nm. Identical results were obtained when THF was used as the reaction solvent.

(5) Reactions of Re₂Cl₄(dppm)₂ with DCNNQI

(i) 2:1 Re₂Cl₄(dppm)₂:DCNNQI Reaction

A solution containing 0.0074 g (0.036 mmol) of DCNNQI in 10 mL of THF was slowly added to a solution consisting of 0.093 g (0.072 mmol) of Re₂Cl₄(dppm)₂ in 10 mL of THF resulting in the formation of a dark red-purple solution. A solution infrared spectrum (CaF₂ cells, THF reference) revealed two $\nu(\text{C}\equiv\text{N})$ bands at 2140 (m) and 2075 (s) cm⁻¹, and an electronic absorption spectrum exhibited absorptions at λ_{max} = 534 and 1026 nm. The reaction solution was stirred at ambient temperature for two days during which time the color changed to brown. Two 2 mL portions of the solution were layered with diethyl ether and hexanes in 8 mm outer diameter Pyrex tubes. Unfortunately no crystalline material was obtained. The remainder of the solution was reduced in volume and an olive-green solid was precipitated using diethyl ether, collected by filtration, washed with diethyl ether, and vacuum dried; yield 0.0374 g (37%). IR (CsI, Nujol, cm⁻¹): $\nu(\text{C}\equiv\text{N})$ 2100 (s), $\nu(\text{C}=\text{C})$ 1587 (w), $\nu(\text{C}=\text{N})$ 1574 (w).

(ii) 1:1 Reaction

A solution containing 0.087 g (0.068 mmol) of Re₂Cl₄(dppm)₂ dissolved in 10 mL of THF was added through a cannula to a THF (5 mL) solution containing 0.014 g (0.068 mmol) of DCNNQI producing a dark green solution. The reaction solution quickly turned dark brown. Infrared and electronic absorption spectra obtained within 5 minutes revealed $\nu(\text{C}\equiv\text{N})$ bands at 2130 (w) and 2080 (m) cm⁻¹ (CaF₂ cells, THF reference) and electronic transitions at λ_{max} = 843 and 1026 nm. The reaction

solution was reduced in volume and layered with diethyl ether (20 mL) which effected the precipitaion of a brown solid. The solid was collected by filtration, washed with diethyl ether, and dried *in vacuo*; yield 0.072 g (71%). IR (CsI, Nujol, cm^{-1}): $\nu(\text{C}\equiv\text{N})$ 2095 (s), $\nu(\text{C}=\text{C})$ 1587 (w), $\nu(\text{C}=\text{N})$ 1574 (w).

(6) Reactions of $\text{Re}_2\text{Cl}_4(\text{dppm})_2$ with DCNAQI

(i) 1:2 $\text{Re}_2\text{Cl}_4(\text{dppm})_2$:DCNAQI Reaction

Separate CH_2Cl_2 solutions of $\text{Re}_2\text{Cl}_4(\text{dppm})_2$ (0.100 g, 0.078 mmol, 10 mL of CH_2Cl_2) and DCNAQI (0.040 g, 0.156 mmol, 7.5 mL of CH_2Cl_2) were prepared and the DCNAQI solution was added to the $\text{Re}_2\text{Cl}_4(\text{dppm})_2$ solution in four equal portions (*ca.* 1.9 mL each). After each addition, a 1 mL aliquot was removed for infrared and UV-visible spectral measurements. The color of the reaction became dark green after the first addition and remained the same color throughout the reaction. The IR spectra of each aliquot exhibited strong $\nu(\text{C}\equiv\text{N})$ bands at 2080 cm^{-1} and the final spectrum exhibited a shoulder near 2170 cm^{-1} . The UV-visible spectrum of the initial solution exhibited a single strong absorption at $\lambda_{\text{max}} = 934\text{ nm}$, but with further addition of the DCNAQI solution this absorption decreased in intensity as an absorption at $\lambda_{\text{max}} = 333\text{ nm}$ appeared. The reaction solution was reduced in volume under vacuum and hexanes was added to precipitate an olive-green solid. The solid was collected by filtration, washed with hexanes, and vacuum dried; yield 0.076 g (50%). IR (CsI, Nujol, cm^{-1}): $\nu(\text{C}\equiv\text{N})$ 2068 (s,br), $\nu(\text{C}=\text{C})$ 1585 (w) and 1573 (w), $\nu(\text{C}=\text{N})$ 1560 (w).

(ii) 2:1 $\text{Re}_2\text{Cl}_4(\text{dppm})_2$:DCNAQI Reaction

A toluene (10 mL) solution containing 0.0062 g (0.024 mmol) of DCNAQI was added to a toluene solution containing 0.062 g (0.048 mmol)

of $\text{Re}_2\text{Cl}_4(\text{dppm})_2$ resulting in a green solution. This solution was filtered through a Schlenk frit and the green filtrate was slowly reduced in volume to yield a black crystalline solid which was collected by filtration, washed with toluene, and vacuum dried; yield 0.028 g (40%). IR (CsI, Nujol, cm^{-1}): $\nu(\text{C}\equiv\text{N})$ 2058 (s).

(7) 2:1 Reaction of $\text{Re}_2\text{Cl}_4(\text{dppm})_2$ with DC-DCNAQI

A solution consisting of 0.0127 g (0.039 mmol) of DC-DCNAQI and 10 mL of THF was slowly added to a Schlenk tube containing 0.100 g (0.078 mmol) of $\text{Re}_2\text{Cl}_4(\text{dppm})_2$ dissolved in 10 mL of THF resulting in the spontaneous formation of a dark green solution. A solution IR spectrum (CaF_2 cells, THF reference) exhibited a $\nu(\text{C}\equiv\text{N})$ band at 2075 cm^{-1} and an electronic transitions at $\lambda_{\text{max}} = 921\text{ nm}$. The volume of the reaction solution was reduced to *ca.* 5 mL under vacuum and Et_2O (15 mL) was added to precipitate an olive-green solid which was collected by filtration, washed with diethyl ether, and vacuum dried; yield 0.093 g (82%). IR (CsI, Nujol, cm^{-1}): $\nu(\text{C}\equiv\text{N})$ 2041 (s,br).

(8) 2:1 Reaction of $\text{Re}_2\text{Cl}_4(\text{dppm})_2$ with DCNPQI

A solution containing DCNPQI (0.0136 g, 0.038 mmol) dissolved in 10 mL of THF was slowly added to a THF (10 mL) solution containing $\text{Re}_2\text{Cl}_4(\text{dppm})_2$ (0.0983 g, 0.076 mmol) producing a dark green solution. A solution IR spectrum (CaF_2 cells, THF reference) obtained after 5 minutes exhibited a $\nu(\text{C}\equiv\text{N})$ band at 2090 cm^{-1} . The reaction solution was allowed to stand for 2 h at room temperature during which time an olive-green solid precipitated. The reaction mixture was left undisturbed for an additional 4 days to ensure that the reaction was complete. The solid was collected by filtration, washed with THF, and vacuum dried; yield

0.097 g (87%). IR (CsI, Nujol, cm^{-1}): $\nu(\text{C}\equiv\text{N})$ 2089 (vs). Electronic spectroscopy (CH_2Cl_2), $\lambda_{\text{max}} = 306$ and 845 nm.

(9) Reaction of $[\text{Re}_2\text{Cl}_4(\text{dppm})_2]_2(\text{DM-DCNQI})$ (7) with DM-CNQMI

A CH_2Cl_2 (5 mL) solution containing 0.0058 g (0.036 mmol) of DM-CNQMI was slowly added to a CH_2Cl_2 (5 mL) solution of (7) (0.053 g, 0.019 mmol) at -78°C with no observed color change. A small portion (*ca.* 1 mL) of the reaction solution was removed and a solution infrared spectrum (CaF_2 cells, THF reference) was obtained which exhibited a single $\nu(\text{C}\equiv\text{N})$ band at 2085 cm^{-1} . The reaction was warmed to room temperature, the volume was reduced to *ca.* 5 mL, and 20 mL of hexanes was added resulting in the precipitation of a brown solid. The solid was collected by filtration, washed with hexanes, and vacuum dried; yield 0.040 g (61%).

B. X-ray Crystallography

(1) $[\text{Re}_2\text{Cl}_4(\text{dppm})_2]_2(\text{DM-DCNQI})\cdot 4\text{THF}$, (7) $\cdot 4\text{THF}$

The structure of $[\text{Re}_2\text{Cl}_4(\text{dppm})_2]_2(\mu\text{-DM-DCNQI})\cdot 4\text{THF}$ (7) $\cdot 4\text{THF}$ was determined by application of general procedures that have been fully described elsewhere.⁷ Crystallographic data were collected on a Rigaku AFC6S diffractometer equipped with monochromated $\text{MoK}\alpha$ ($\lambda_\alpha = 0.71069\text{ \AA}$) radiation. The data were corrected for Lorentz and polarization effects. Calculations were performed on a VAXSTATION 4000 computer by using the Texsan crystallographic software package of Molecular Structure Corporation.⁸ Crystallographic data for (5) are given in Table 9.

Table 9. Summary of crystallographic data for
 $[\text{Re}_2\text{Cl}_4(\text{dppm})_2]_2(\mu\text{-DMDCNQI})\cdot 4\text{THF}$ (**7**)-4THF.

formula	$\text{Re}_4\text{P}_8\text{N}_4\text{O}_4\text{C}_{126}\text{Cl}_8\text{H}_{128}$
formula weight	3038.66
space group	P-1 (#2)
a, Å	14.152(5)
b, Å	22.927(8)
c, Å	12.091(4)
α , deg	96.61(3)
β , deg	104.17(3)
γ , deg	75.17(3)
V, Å ³	3713(2)
Z	1
d_{calc} , g/cm ³	1.374
μ (Mo K α), cm ⁻¹	36.08
temperature, °C	-100
trans. factors, max., min.	1.00 - 0.63
R ^a	0.089
R _w ^b	0.134
quality-of-fit indicator	3.03

$$^a R = \sum | |F_o| - |F_c| | / \sum |F_o|$$

$$^b R_w = [\sum w (|F_o| - |F_c|)^2 / \sum w |F_o|^2]^{1/2}; w = 1/\sigma^2(|F_o|)$$

$$^c \text{quality-of-fit} = [\sum w (|F_o| - |F_c|)^2 / (N_{\text{obs}} - N_{\text{parameters}})]^{1/2}$$

(i) Data Collection and Reduction

Crystals of (7) were grown by slow diffusion of a THF solution containing DM-DCNQI into a THF solution containing two equivalents of $\text{Re}_2\text{Cl}_4(\text{dppm})_2$. A black crystal with dimensions $0.30 \times 0.40 \times 0.30 \text{ mm}^3$ was mounted on the tip of a glass fiber with silicone grease. Cell constants and an orientation matrix for data collection obtained from a least squares refinement using 22 carefully centered reflections in the range $23 \leq 2\theta \leq 26^\circ$ corresponded to a triclinic cell. A total of 12940 unique data were collected at $-100 \pm 1^\circ\text{C}$ using the ω - 2θ scan technique to a maximum 2θ value of 50° . The intensities of three representative reflections measured after every 150 reflections decreased by 9.0 % thus a linear correction factor was applied to the data to account for this decay. An empirical absorption correction, using the program DIFABS,⁹ was applied which resulted in transmission factors ranging from 1.00 to 0.63.

(ii) Structure Solution and Refinement

Based on a statistical analysis of intensity distribution, and the successful solution and refinement of the structure, the space group was determined to be P-1 (#2). The structure was solved by MITHRIL¹⁰ and DIRDIF¹¹ structure programs and refined by full matrix least-squares refinement. The position of all non-hydrogen atoms, except C(49) and the interstitial THF atoms, were refined with either isotropic or anisotropic thermal parameters. Hydrogen atoms were placed in calculated positions for the final stages of refinement. The final cycle of full matrix least-squares refinement included 5175 observations with $F_o^2 > 3\sigma(F_o^2)$ and 341 variable parameters for residuals of $R = 0.089$ and $R_w = 0.134$ and a quality-of-fit index of 3.03.

3. Results

The dinuclear donor compound $\text{Re}_2\text{Cl}_4(\text{dppm})_2$ reacts with a variety of substituted DCNQIs to form covalently linked charge-transfer products as judged by infrared spectral data and X-ray crystallography. Single crystals of $[\text{Re}_2\text{Cl}_4(\text{dppm})_2]_2(\mu\text{-DM-DCNQI})$ (**7**) were synthesized from the layering of THF solutions of the starting materials and the X-ray crystal structure establishes the presence of a bridging DM-DCNQI. Crystallographic data are summarized in Table 9 and an ORTEP representation and packing diagrams are depicted in Figures 18, 19, and 20. A full table of positional and thermal parameters for complex (**7**) is located in the Appendix.

A. Reactions of $\text{Re}_2\text{Cl}_4(\text{dppm})_2$ with DM-DCNQI

(1) Preparation and spectroscopic properties

The reaction of $\text{Re}_2\text{Cl}_4(\text{dppm})_2$ with DM-DCNQI in which a 1:1 molar ratio instantaneously produces a dark blue solution of (**6**)-A which is stable only at low temperatures (-78°C). The infrared spectrum of the solution exhibits a $\nu(\text{C}\equiv\text{N})$ band at 2053 cm^{-1} and the electronic absorption spectrum shows a strong absorption at $\lambda_{\text{max}} = 830\text{ nm}$. When the solution is allowed to stand at room temperature, the color turns dark green, and the absorption at 830 nm decreases in intensity during the conversion from (**6**)-A to (**6**)-B. The infrared spectrum of (**6**)-B exhibits a single strong $\nu(\text{C}\equiv\text{N})$ band at 2091 cm^{-1} . When 2 equivalents of $\text{Re}_2\text{Cl}_4(\text{dppm})_2$ are reacted with DM-DCNQI in either THF or benzene, microcrystalline samples of $[\text{Re}_2\text{Cl}_4(\text{dppm})_2]_2(\mu\text{-DMDCNQI})$ (**7**) precipitate from solution. Single crystals are grown using slow diffusion techniques. The infrared spectrum of (**7**) exhibits a strong $\nu(\text{C}\equiv\text{N})$ band at 2056 cm^{-1} and the electronic absorption spectrum exhibits strong absorptions at $\lambda_{\text{max}} = 1035$

and 1800 nm, shown in Figure 17, indicative of a symmetrically bridged DM-DCNQI moiety. Methylene chloride solutions of (7) are not stable at room temperature as confirmed by the slow decay in intensity of the absorptions in the electronic absorption spectrum. A ^1H NMR spectrum of (7) in CDCl_3 displays a complex set of multiplets between $\delta = 7$ and 8 ppm due to phenyl protons in addition to resonances at $\delta = 3.73$ (t) and $\delta = 1.83$ (p) ppm which are attributed to the THF molecules of crystallization. A cyclic voltammogram of (7) in a 0.1 M TBABF₄/CH₂Cl₂ electrolyte solution does not exhibit any reversible oxidation or reduction processes between +1.5 and -1.5 V, although a weak quasi-reversible process appears at +0.5 V. The cyclic voltammogram of (7) is broad with numerous superimposed features as compared to the blank scan of the electrolyte solution. Increasing the concentration of (7) only serves to broaden the cyclic voltammogram. An addition of 1 equivalent of $\text{Re}_2\text{Cl}_4(\text{dppm})_2$ to an electrolyte solution containing DM-DCNQI (0.1 M TBABF₄/CH₂Cl₂) almost completely eliminates the reversible reduction process that occurs at -0.49 V for pure solutions of DM-DCNQI, while the first reduction at +0.13 V remains unchanged. The addition of a second equivalent of $\text{Re}_2\text{Cl}_4(\text{dppm})_2$ produces a cyclic voltammogram similar to that observed for (7) which has a quasi-reversible process ca. 0.5 V. Further addition of $\text{Re}_2\text{Cl}_4(\text{dppm})_2$ and subsequent scans produce featureless cyclic voltammograms.

(2) X-ray crystal structure of $[\text{Re}_2\text{Cl}_4(\text{dppm})_2]_2(\text{DM-DCNQI})\cdot 4\text{THF}$, (7)·4THF

The molecular structure of (7), depicted in Figure 18, closely resembles the structure of $[\text{Re}_2\text{Cl}_4(\text{dppm})_2]_2(\mu\text{-TCNQ})$ (2) since the DM-DCNQI moiety links together two $\text{Re}_2\text{Cl}_4(\text{dppm})_2$ molecules through the

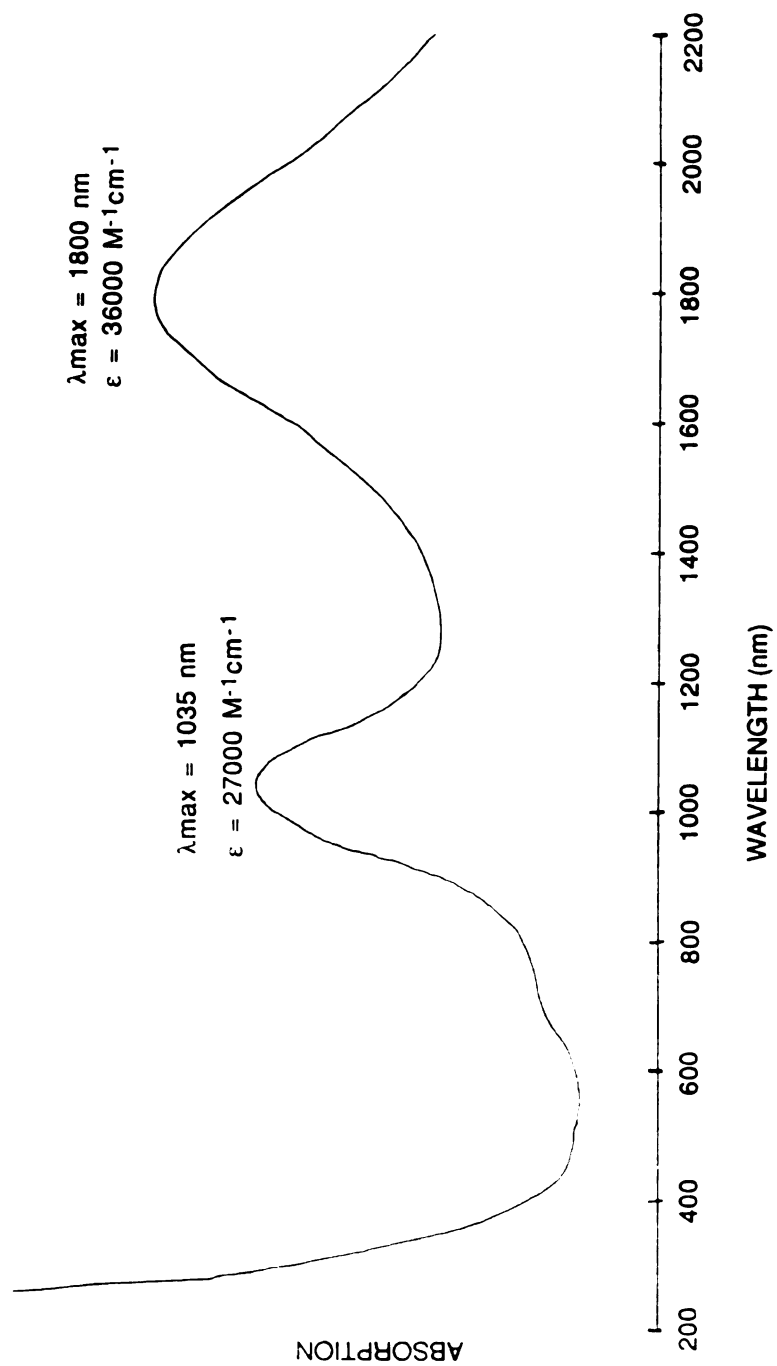


Figure 17. Electronic absorption spectrum of $[\text{Re}_2\text{Cl}_4(\text{dppm})_2]_2(\mu\text{-DM-DCNQI})$ (7) in CH_2Cl_2 .



Figure 18. ORTEP representation of $[\text{Re}_2\text{Cl}_4(\text{dppm})_2]_2(\mu\text{-DM-DCNQI})_4\text{TfH}$, (7). 4THF.

σ -coordination of its cyano groups. The molecule is centrosymmetric, with the midpoint of the DM-DCNQI moiety being situated on an inversion center. The coordination environment around Re(1) and Re(2) are octahedral and trigonal bipyramidal respectively. A list of selected bond distances and angles are given in Table 10. The Re-Re distance of 2.268(2) Å is slightly shorter than the corresponding distance found in the structure of (2) (2.275 Å) which may reflect the lower reduction potential for DM-DCNQI vs. TCNQ. The Re(1)–Cl(2) distance of 2.61(1) Å is longer than the other Re–Cl distances as a result of occupying an axial site (see Figure 19). The Re(1)–N(1) distance of 1.86(3) Å is considerably shorter than the Re–N distance found in the structure of (2) (2.133 Å). Other distances and angles in the dirhenium unit are within the range for derivatives of Re₂Cl₄(dppm)₂.¹² The packing diagram (Figure 20) shows that the molecules stack along the *a* axis in which there is a distance of *ca.* 14 Å between adjacent DM-DCNQI centers, although other closer contacts exist among atoms on the phenyl rings and solvent molecules.

(3) Magnetic properties

The complex [Re₂Cl₄(dppm)₂]₂(μ -DM-DCNQI) (7) is paramagnetic as determined by magnetic susceptibility (Figure 21) and EPR (Figure 22) measurements. The plot of μ_{eff} vs. temperature (Figure 21) shows a decrease in μ_{eff} at lower temperatures which is consistent with antiferromagnetic coupling. The room temperature effective moment is 1.8 B.M. which is indicative of *ca.* 1 unpaired electron. This is similar to the value of 1.9 B.M. exhibited for [Re₂Cl₄(dppm)₂]₂(μ -TCNQ) (2).

B. Reactions of Re₂Cl₄(dppm)₂ with other DCNQIs

The compounds DCNQI, DCNNQI, DCNAQI, DC-DCNAQI, and DCNPQI produce charge-transfer products when reacted with

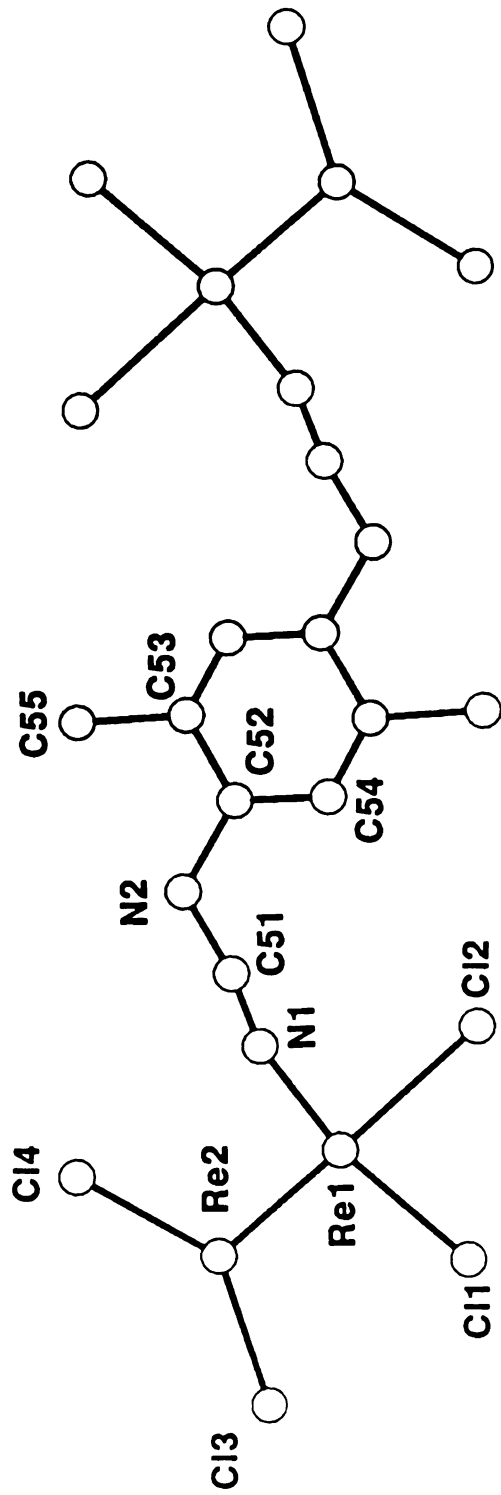


Figure 19. Pluto view without dpmm ligands of $[\text{Re}_2\text{Cl}_4(\text{dppm})_2]_2(\mu\text{-DM-DCNQI})\cdot 4\text{THF}$, (7)·4THF.

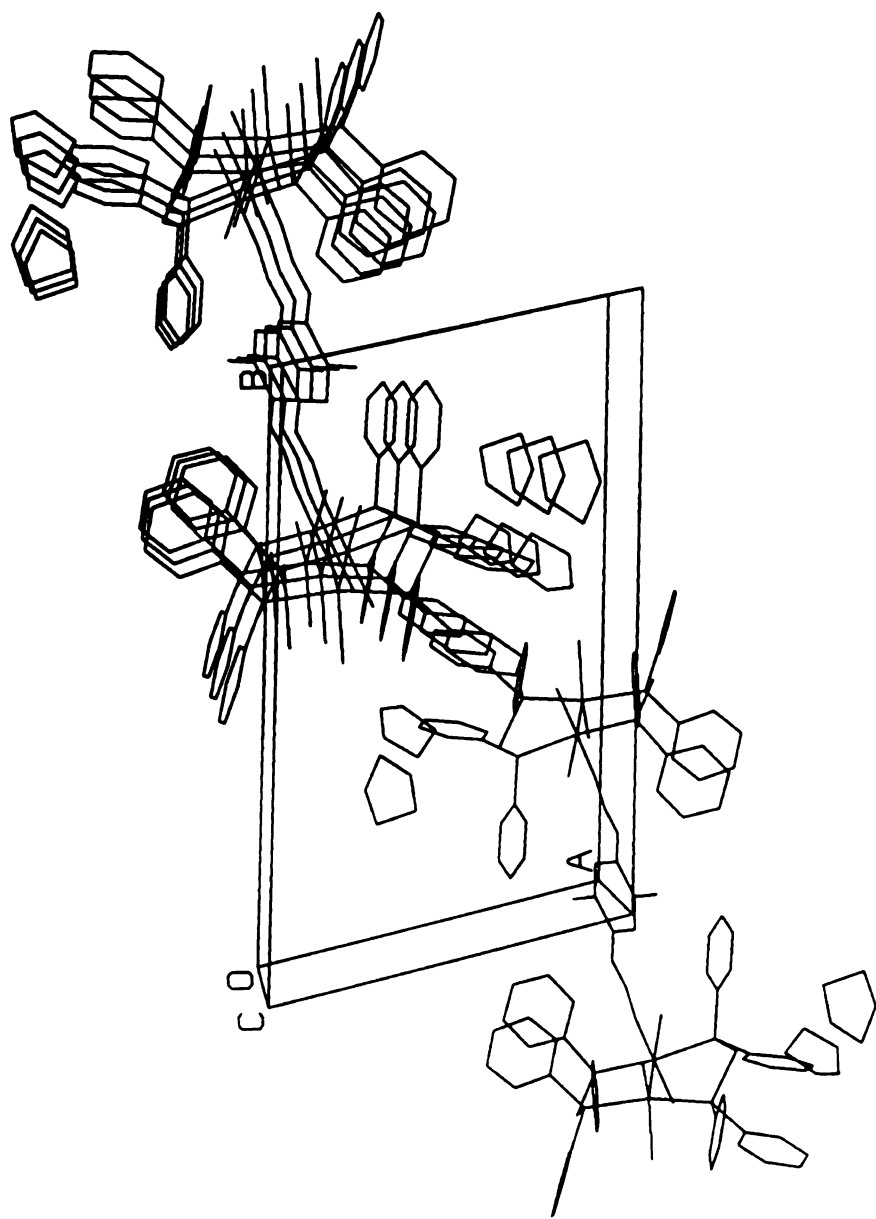


Figure 20. Stick model packing diagram of $[\text{Re}_2\text{Cl}_4(\text{dppm})_2]_2(\mu\text{-DM-DCNQI})\cdot 4\text{THF}$, $(7)\cdot 4\text{THF}$ viewed along the c axis.

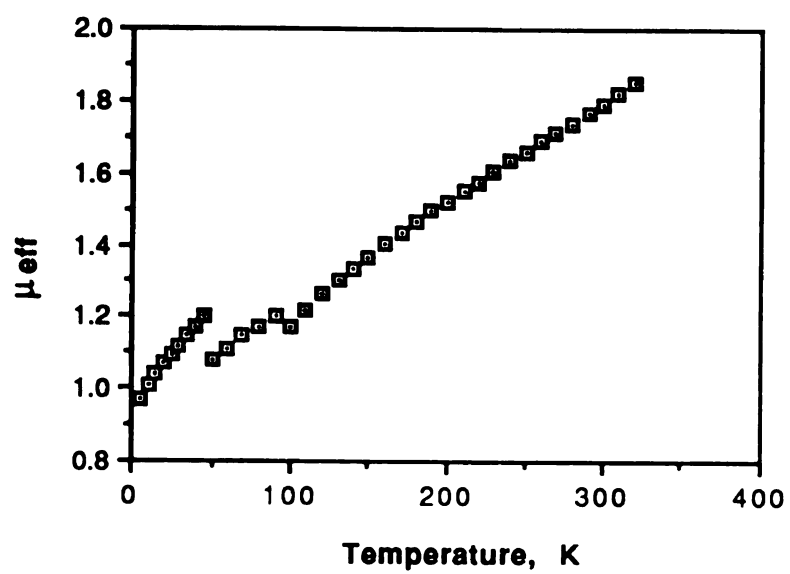


Figure 21. Plot of μ_{eff} (B.M.) vs. temperature (K) of $[\text{Re}_2\text{Cl}_4(\text{dppm})_2]_2(\mu\text{-DM-DCNQI})$ (7).

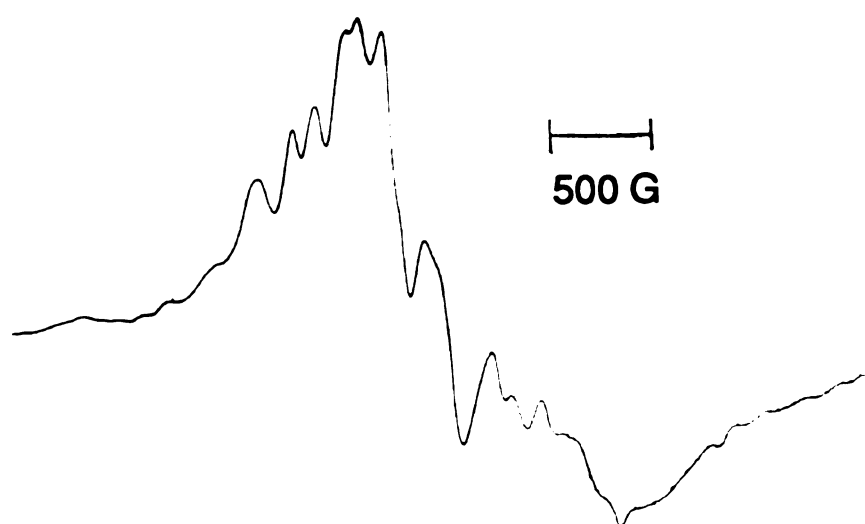


Figure 22. Solid state EPR spectrum of $[\text{Re}_2\text{Cl}_4(\text{dppm})_2]_2(\mu\text{-DM-DCNQI})$ (**7**) at -160°C .

Table 10. Selected bond distances(Å), bond angles(°) and torsion angles(°) for [Re₂Cl₄(dppm)₂]₂(μ-DM-DCNQI)·4THF, (7)·4THF.

distances					
atom 1	atom 2	distance	atom 1	atom 2	distance
Re(1)	Re(2)	2.268(2)	P(2)	C(49)	1.88(1)
Re(1)	Cl(1)	2.38(1)	P(3)	C(25)	1.82(5)
Re(1)	Cl(2)	2.61(1)	P(3)	C(31)	1.91(5)
Re(1)	P(1)	2.49(1)	P(3)	C(50)	1.87(4)
Re(1)	P(4)	2.49(1)	P(4)	C(37)	1.82(4)
Re(1)	N(1)	1.86(3)	P(4)	C(43)	1.89(4)
Re(2)	Cl(3)	2.33(1)	P(4)	C(50)	1.84(4)
Re(2)	Cl(4)	2.35(1)	N(1)	C(51)	1.11(5)
Re(2)	P(2)	2.42(1)	N(2)	C(51)	1.37(5)
Re(2)	P(3)	2.41(1)	N(2)	C(52)	1.50(5)
P(1)	C(1)	1.78(4)	C(52)	C(53)	1.44(6)
P(1)	C(7)	1.76(4)	C(52)	C(54)	1.38(5)
P(1)	C(49)	1.81(1)	C(53)	C(54)*	1.27(5)
P(2)	C(13)	1.83(4)	C(53)	C(55)	1.62(7)
P(2)	C(19)	1.92(4)			

torsion angles				
atom 1	atom 2	atom 3	atom 4	torsion angle
Re(1)	N(1)	C(51)	N(2)	152(3)
Cl(1)	Re(1)	Re(2)	Cl(3)	11.6(4)
Cl(1)	Re(1)	Re(2)	Cl(4)	167.1(4)
Cl(3)	Re(2)	Re(1)	N(1)	163(1)
Cl(4)	Re(2)	Re(1)	N(1)	18(1)
P(1)	Re(1)	Re(2)	P(2)	15.2(3)
P(3)	Re(2)	Re(1)	P(4)	16.5(4)
P(3)	Re(2)	Re(1)	N(1)	105(1)
N(2)	C(52)	C(53)	C(55)	0(6)
N(2)	C(52)	C(54)	C(53)*	180(4)
C(51)	N(2)	C(52)	C(53)	177(4)

Table 10. (cont'd).

angles							
atom 1	atom 2	atom 3	angle	atom 1	atom 2	atom 3	angle
Re(2)	Re(1)	Cl(1)	97.3(2)	Re(1)	Re(2)	P(3)	99.4(3)
Re(2)	Re(1)	Cl(2)	177.6(3)	Cl(3)	Re(2)	Cl(4)	139.7(4)
Re(2)	Re(1)	P(1)	97.4(2)	Cl(3)	Re(2)	P(2)	84.6(4)
Re(2)	Re(1)	P(4)	95.1(3)	Cl(3)	Re(2)	P(3)	87.6(4)
Re(2)	Re(1)	N(1)	94(1)	Cl(4)	Re(2)	P(2)	92.3(4)
Cl(1)	Re(1)	Cl(2)	83.8(4)	Cl(4)	Re(2)	P(3)	84.6(4)
Cl(1)	Re(1)	P(1)	82.4(4)	P(2)	Re(2)	P(3)	164.0(4)
Cl(1)	Re(1)	P(4)	95.7(4)	Re(1)	N(1)	C(51)	163(3)
Cl(1)	Re(1)	N(1)	167(1)	C(51)	N(2)	C(52)	120(3)
Cl(2)	Re(1)	P(1)	84.8(4)	N(1)	C(51)	N(2)	166(4)
Cl(2)	Re(1)	P(4)	82.7(4)	N(2)	C(52)	C(53)	120(4)
Cl(2)	Re(1)	N(1)	85(1)	N(2)	C(52)	C(54)	121(4)
P(1)	Re(1)	P(4)	167.5(3)	C(53)	C(52)	C(54)	119(4)
P(1)	Re(1)	N(1)	91(1)	C(52)	C(53)	C(54)*	122(4)
P(4)	Re(1)	N(1)	88(1)	C(52)	C(53)	C(55)	117(4)
Re(1)	Re(2)	Cl(3)	113.3(3)	C(54)	C(53)	C(55)	121(4)
Re(1)	Re(2)	Cl(4)	107.1(3)	C(52)	C(54)	C(53)*	119(4)
Re(1)	Re(2)	P(2)	96.5(2)				

$\text{Re}_2\text{Cl}_4(\text{dppm})_2$. The infrared spectra of these products, listed in Table 11, exhibit strong $\nu(\text{C}\equiv\text{N})$ bands between 2040 and 2100 cm^{-1} which are indicative of nitrile coordination. The reaction between the mono-cyano compound DM-CNQMI and $\text{Re}_2\text{Cl}_4(\text{dppm})_2$ produces a dark green solution that exhibits an absorption at $\lambda_{\text{max}} = 812 \text{ nm}$ which is identical to the spectrum of (6)-A (in THF). This supports the assignment of this transition as being a metal-to-ligand rather than a metal-to-metal charge-transfer process since a bridging arrangement is not possible for complexes containing DM-CNQMI. Reactions between DCNQI and $\text{Re}_2\text{Cl}_4(\text{dppm})_2$ mimic those between $\text{Re}_2\text{Cl}_4(\text{dppm})_2$ and DM-DCNQI as judged by infrared and electronic absorption spectra. The products from the reactions between the larger acceptors DCCNQI, DCNAQI, DC-DCNAQI, DCNPQI and $\text{Re}_2\text{Cl}_4(\text{dppm})_2$ are obtained using similar methods as described for the reactions of the other acceptor compounds. These products produce infrared and electronic absorption spectra that are characteristic of nitrile coordinated products.

4. Conclusions

The reactivity of DM-DCNQI towards $\text{Re}_2\text{Cl}_4(\text{dppm})_2$ closely resembles the reactivity of TCNQ towards $\text{Re}_2\text{Cl}_4(\text{dppm})_2$ as expected. Both TCNQ and DM-DCNQI form blue 1:1 complexes with $\text{Re}_2\text{Cl}_4(\text{dppm})_2$ at low temperatures while products (2) and (7) crystallize from THF solutions in the presence of two equivalents of $\text{Re}_2\text{Cl}_4(\text{dppm})_2$. The compound $\text{Re}_2\text{Cl}_4(\text{dppm})_2$ reacts with variety of DCNQIs and all form covalently linked complexes as judged by infrared and electronic absorption spectra.

Table 11. Tabulation of $\nu(\text{C}\equiv\text{N})$ stretching frequencies for the products from reactions of $\text{Re}_2\text{Cl}_4(\text{dppm})_2$ with DCNQIs.

Acceptor	D:A	$\nu(\text{C}\equiv\text{N})$ band cm^{-1}
DM-CNQMI	1:1	2096 (vs)
DCNQI	2:1	2090 (vs)
DCNQI	1:4	2090 (vs,br), 2240 (w)
DM-DCNQI (7)	2:1	2056 (s,br)
DM-DCNQI (6)-A	1:1	2091 (s,br)
DM-DCNQI (6)-B	1:1	2070 (s,br)
DCNNQI	2:1	2100 (s)
DCNNQI	1:1	2095 (s)
DCNAQI	1:2	2068 (s,br)
DCNAQI	2:1	2058 (s)
DC-DCNAQI	2:1	2041 (s,br)
DCNPQI	2:1	2089 (vs)

DM-CNQMI = 2,6-dimethyl-N-cyano-1,4-benzoquinone-4-imine

DCNQI = N,N'-dicyano-1,4-benzoquinonediimine

DM-DCNQI = 2,5-dimethyl-N,N'-dicyano-1,4-benzoquinonediimine

DCNNQI = N,N'-dicyano-1,4-naphthaquinonediimine

DCNAQI = N,N'-dicyano-9,10-anthraquinonediimine

DC-DCNAQI = 1,5-dichloro-N,N'-dicyano-9,10-anthraquinonediimine

References

1. Aumüller, A.; Hünig, S. *Liebigs Ann. Chem.* **1986**, 142.
2. Bartley, S. L.; Dunbar, K. R. *Angew. Chem., Int. Ed. Engl.* **1991**, 30, 448.
3. Aumüller, A.; Hünig, S.; Von Schütz, J.-U.; Werner, H. P.; Wolf, H. C.; Klebe, G. *Mol. Cryst. Liq. Cryst. Inc. Nonlin. Opt.* **1988**, 156, 215.
4. (a) Enkelmann, V. *Angew. Chem., Int. Ed. Engl.* **1991**, 30, 1121. (b) Aumüller, A.; Erk, P.; Hünig, S.; Meixner, H.; von Schütz, J.-U.; Werner, H.-P. *Liebigs Ann. Chem.* **1987**, 997. (c) Aumüller, A.; Erk, P.; Hünig, S.; von Schütz, J.-U.; Werner, H.-P.; Wolf, H. C.; Klebe, G. *Chem. Ber.* **1991**, 124, 1445.
5. (a) Kato, R.; Kobayashi, H.; Kobayashi, A. *J. Am. Chem. Soc.* **1989**, 111, 5224. (b) Kato, R.; Kobayashi, H.; Kobayashi, A. *Synth. Met.* **1988**, 27, B263.
6. Aumüller, A.; Hünig, S. *Liebigs Ann. Chem.* **1986**, 165.
7. (a) Bino, A.; Cotton, F. A.; Fanwick, P. E. *Inorg. Chem.* **1979**, 18, 3558. (b) Cotton, F. A.; Frenz, B. A.; Deganello, G.; Shaver, A. *J. Organomet. Chem.* **1973**, 50, 227.
8. TEXSAN-TEXRAY Structure Analysis Package, Molecular Structure Corporation **1985**.
9. Walker, N.; Stuart, D. *Acta Crystallogr., Sect. A: Found Crystallogr.* **1983**, A39, 158.
10. MITHRILL: Integrated Direct Methods Computer Program. Gilmore, C. *J. Appl. Crystallogr.* **1984**, 17, 42.
11. DIRDIF: Direct Methods for Difference Structure, An Automatic Procedure for Phase Extension; Refinement of Difference Structure Factors. Beurskens, R. T. Technical Report, 1984.
12. (a) Fanwick, P. E.; Price, A. C.; Walton, R. A. *Inorg. Chem.* **1988**, 27, 2601. (b) Price, A. C.; Walton, R. A. *Polyhedron* **1987**, 6, 729.

CHAPTER IV

REACTIONS OF $M_2Cl_4(PR_3)_4$, $M_2Cl_4(P\sim P)_2$ ($M = Mo, Re$; $R = Et, Pr^n$; $P\sim P = dppm, dmpm, dppe$), AND $[M_2(NCCH_3)_{10}][BF_4]_4$ ($M = Mo, Rh$) WITH POLYCYANO ACCEPTORS.

1. Introduction

After our discovery of the novel covalently linked complexes that result from the reactions of $\text{Re}_2\text{Cl}_4(\text{dppm})_2$ with TCNQ, TCNE, DCNQI's, and TNAP (Chapters II and III), further studies of analogous reactions of dinuclear molybdenum and rhenium complexes were performed to probe the generality of the approach. There exists a wide selection of metal complexes with different M-M bond orders and different chemical, redox and structural properties. Also, the fully solvated dinuclear cations e.g. $[\text{Rh}_2(\text{NCCH}_3)_{10}]^{4+}$ could be used in the preparation of inorganic-organic hybrid polymers when matched with appropriate bidentate precursors.

2. Experimental

A. Synthesis

The dinuclear metal complexes $\text{Re}_2\text{Cl}_4(\text{PEt}_3)_4$,¹ $\text{Re}_2\text{Cl}_4(\text{PPr}^n)_4$,¹ $\text{Mo}_2\text{Cl}_4(\text{PEt}_3)_4$,² $\text{Mo}_2\text{Cl}_4(\text{dppm})_2$,³ $\text{Mo}_2\text{Cl}_4(\text{dmpm})$,⁴ $\text{Mo}_2\text{Cl}_4(\text{dppe})_2$,⁵ $[\text{Rh}_2(\text{NCCH}_3)_{10}][\text{BF}_4]_4$,⁶ $[\text{Mo}_2(\text{NCCH}_3)_{10}][\text{BF}_4]_4$,⁷ $[\text{Bu}^n_4\text{N}]\text{TCNQ}$,⁸ LiTCNQ ,⁹ TCNQF_4 ,¹⁰ and DM-DCNQI ¹¹ were all prepared according to literature procedures. TCNQ and TCNE were purchased from Aldrich Chemicals and sublimed prior to use. $\text{Li}[\text{DM-DCNQI}]$ was synthesized as black needle crystals from the reaction between LiI and DM-DCNQI in boiling acetonitrile.

(1) Reactions of $\text{Re}_2\text{Cl}_4(\text{PEt}_3)_4$ with TCNQF_4

In a typical reaction $\text{Re}_2\text{Cl}_4(\text{PEt}_3)_4$ (0.050 g, 0.051 mmol), TCNQF_4 (0.05 g, 0.146 mmol), and CH_2Cl_2 (10 mL) were added to a reaction vessel and stirred for 5 h at room temperature. The initial green color of the reaction slowly changed to black with concomitant deposition of a black precipitate. The solid was collected by filtration, washed with CH_2Cl_2 and diethyl ether and vacuum dried; yield 0.041 g. IR (KBr pellet): $\nu(\text{C}\equiv\text{N})$

2202 (s,sh), 2104 (vs,br). Additional solid was obtained treating the filtrate with diethyl ether. Both solids exhibited identical infrared spectra. Many reactions employing different ratios of starting material and a variety of solvent combinations yielded solids with very similar infrared spectra.

(2) Reaction of $\text{Re}_2\text{Cl}_4(\text{PEt}_3)_4$ with TCNQ

A solution of TCNQ (0.022 g, 0.108 mmol) dissolved in 15 mL of THF was carefully layered on a CH_2Cl_2 (4 mL) solution of $\text{Re}_2\text{Cl}_4(\text{PEt}_3)_4$ (0.050 g, 0.051 mmol) which produced a dark brown solid precipitate within 20 minutes. The reaction tube was allowed to stand undisturbed for 8 days to allow for complete diffusion of the layers; the resulting solid was collected by filtration, washed with CH_2Cl_2 , and vacuum dried; yield 0.009 g. IR (CsI, Nujol, cm^{-1}): $\nu(\text{C}\equiv\text{N})$ 2189 (s), 2091 (vs,br).

(3) Reaction of $\text{Re}_2\text{Cl}_4(\text{PEt}_3)_4$ with DM-DCNQI

A THF (5 mL) solution of DM-DCNQI (0.012 g, 0.063 mmol) was slowly added to 5 mL of a THF solution of $\text{Re}_2\text{Cl}_4(\text{PEt}_3)_4$ (0.055 g, 0.056 mmol) resulting in the immediate formation of an orange-brown solution. A dark green solid precipitated after 2 h and was harvested by filtration, washed with THF, and dried *in vacuo*; yield 0.033 g. IR (CsI, Nujol, cm^{-1}): $\nu(\text{C}\equiv\text{N})$ 2105 (vs,br).

(4) Reactions of $\text{Mo}_2\text{Cl}_4(\text{dppe})_2$ with TCNQ

(i) 1:2 $\text{Mo}_2\text{Cl}_4(\text{dppe})_2$:TCNQ Reaction

Quantities of $\text{Mo}_2\text{Cl}_4(\text{dppe})_2$ (0.100 g, 0.088 mmol), 0.036 g (0.176 mmol) of TCNQ, and 25 mL of CH_2Cl_2 were combined in a Schlenk flask to give an initial green solution which turned blue within 10 minutes. A UV-visible spectrum showed an intense absorption at

$\lambda_{\text{max}} = 915$ nm. The reaction mixture was stirred at room temperature for 7 days with no further change as indicated by UV-visible spectra. The reaction volume was reduced by vacuum and treated with 30 mL of diethyl ether resulting in a blue solid precipitate which was collected by filtration, washed with diethyl ether, and vacuum dried; yield 0.074 g. IR (CsI, Nujol, cm^{-1}): $\nu(\text{C}\equiv\text{N})$ 2180 (m), 2090 (s).

(ii) 2:1 $\text{Mo}_2\text{Cl}_4(\text{dppe})_2$:TCNQ Reaction

A reaction mixture consisting of $\text{Mo}_2\text{Cl}_4(\text{dppe})_2$ (0.200 g, 0.176 mmol), TCNQ (0.018 g, 0.088 mmol), and toluene (30 mL) was refluxed for 10 minutes to give a dark green solution. The solution was refluxed for another 1 h during which time a black solid precipitated. The solid was collected by filtration, washed with toluene and diethyl ether, and dried *in vacuo*; yield 0.193 g. IR (CsI, Nujol, cm^{-1}): $\nu(\text{C}\equiv\text{N})$ 2186 (m), 2091 (s).

(iii) 4:1 [$\text{Mo}_2\text{Cl}_4(\text{dppe})_2$:TCNQ] Reaction

Toluene (10 mL) was syringed into a flask containing 0.200 g (0.176 mmol) of $\text{Mo}_2\text{Cl}_4(\text{dppe})_2$ and 0.009 g (0.044 mmol) of TCNQ. Although no immediate reaction was observed, a blue solution containing a blue solid appeared within 24 h. The reaction mixture was stirred at room temperature for 4 days after which time the blue solid was collected by filtration, washed with fresh toluene, and vacuum dried; yield 0.0192 g. IR (CsI, Nujol, cm^{-1}): 2189 (m), 2099 (s). Identical results were obtained when acetone was used as the reaction solvent.

(5) Reaction of Mo₂Cl₄(dppe)₂ with TCNE

To a 100 mL Schlenk flask was added 0.100 g (0.088 mmol) of Mo₂Cl₄(dppe)₂, 0.0227 g (0.177 mmol) of TCNE and 25 mL of CH₂Cl₂ resulting in an immediate dark blue solution to form. A UV-visible spectrum of the reaction solution exhibited a strong absorption at $\lambda_{\text{max}} = 654$ nm. The mixture was stirred at room temperature for 6 days without any detectable changes. The solution was reduced in volume by vacuum followed by the addition of 30 mL of diethyl ether producing a blue solid precipitate. The solid was collected by filtration, washed with diethyl ether, and vacuum dried. IR (CsI, Nujol, cm⁻¹): $\nu(\text{C}\equiv\text{N})$ 2200 (m), 2120 (s).

(6) Reaction of Mo₂Cl₄(dppe)₂ with TCNQF₄

Methylene chloride (20 mL) was syringed into a reaction vessel containing Mo₂Cl₄(dppe)₂ (0.100 g, 0.088 mmol) and TCNQF₄ (0.060 g, 0.176 mmol) immediately forming a black solution, which produced a black film-like solid after 4 days. The mixture was filtered through a Schlenk frit and a black solid was isolated, washed with 15 mL of CH₂Cl₂, and dried *in vacuo*; yield 0.108 g. IR (CsI, Nujol, cm⁻¹): 2199 (s), 2132 (vs,br).

(7) Reaction of Mo₂Cl₄(dppe)₂ with DM-DCNQI

Methylene chloride (10 mL) was added to a flask containing 0.210 g (0.186 mmol) of Mo₂Cl₄(dppe)₂ and 0.0085 g (0.049 mmol) of DM-DCNQI which resulted in a purple solution within 30 minutes. The reaction mixture was stirred at room temperature for 24 h during which time a red solution and a brown-red precipitate ensued. The reaction mixture was allowed to stir for an additional 24 h at which time the brown-red solid was collected by filtration, washed with CH₂Cl₂ and vacuum

drie

filter

bro

ethe

208

(8)

Mo

resu

tem

a st

min

resu

vacu

(9)

0.02

3 da

by f

2215

(10)

Ac

dried; yield 0.050 g. IR (CsI, Nujol, cm^{-1}): $\nu(\text{C}\equiv\text{N})$ 2085 (s). The red filtrate was reduced in volume and layered with diethyl ether to give a brown-red solid which was collected by filtration, washed with diethyl ether, and dried *in vacuo*; yield 0.101 g. IR (CsI, Nujol, cm^{-1}): $\nu(\text{C}\equiv\text{N})$ 2083 (m).

(8) Reaction of $\text{Mo}_2\text{Cl}_4(\text{dppm})_2$ with TCNQ

To a 100 mL Schlenk flask was added 0.100 g (0.091 mmol) of $\text{Mo}_2\text{Cl}_4(\text{dppm})_2$, 0.0240 g (0.118 mmol) of TCNQ, and 10 mL of CH_2Cl_2 resulting in a dark green solution. After stirring for 35 minutes at ambient temperature, a UV-visible absorption spectrum was recorded; this revealed a strong feature at $\lambda_{\text{max}} = 900$ nm. The reaction was stirred for 70 minutes before adding 10 mL of CH_2Cl_2 and 40 mL of diethyl ether. The resulting black solid precipitate was collected by filtration and dried *in vacuo*; yield 0.038 g IR (CsI, Nujol, cm^{-1}): 2193 (m), 2115 (s), 1968 (w).

(9) Reaction of $\text{Mo}_2\text{Cl}_4(\text{dppm})_2$ with TCNE

A mixture containing $\text{Mo}_2\text{Cl}_4(\text{dppm})_2$ (0.100 g ,0.091 mmol), 0.0232 g (0.181 mmol) of TCNE, and 30 mL of toluene was refluxed for 3 days resulting in the deposition of a black solid. The solid was collected by filtration and washed with toluene. IR (CsI, Nujol, cm^{-1}): $\nu(\text{C}\equiv\text{N})$ 2215 (s), 2130 (w).

(10) Reaction of $\text{Mo}_2\text{Cl}_4(\text{PEt}_3)_4$ with TCNQ

To a 50 mL Schlenk flask was added 0.036 g (0.045 mmol) of $\text{Mo}_2\text{Cl}_4(\text{PEt}_3)_4$, 0.012 g (0.059 mmol) of TCNQ, and 20 mL of CH_2Cl_2 . The initial blue solution slowly turned green and eventually deposited a green solid after the addition of diethyl ether. The solid was collected by filtration and washed with diethyl ether. IR (CsI, Nujol, cm^{-1}): 2188 (s), 2128 (s).

(11) Reaction of $\text{Mo}_2\text{Cl}_4(\text{PEt}_3)_4$ with TCNQF_4

A solution containing 0.021 g (0.061 mmol) of TCNQF_4 and 5 mL of acetone was carefully layered over a solution containing 0.050 g (0.061 mmol) of $\text{Mo}_2\text{Cl}_4(\text{PEt}_3)_4$ and 8 mL of CH_2Cl_2 . After one day a brown precipitate had formed at the bottom of the Schlenk tube. The solid was collected by filtration, washed with copious amounts of CH_2Cl_2 , and vacuum dried. yield 0.049 g. IR (CsI, Nujol, cm^{-1}): $\nu(\text{C}\equiv\text{N})$ 2198 (s), 2143 (s).

(12) Reaction of $\text{Mo}_2\text{Cl}_4(\text{dmpm})_2$ with TCNQ

A mixture consisting of 0.050 g (0.083 mmol) of $\text{Mo}_2\text{Cl}_4(\text{dmpm})_2$, 0.028 g (0.137 mmol) of TCNQ , and 15 mL of CH_2Cl_2 was stirred at room temperature for 5 h resulting in the formation of a grey precipitate. The solid was collected by filtration, washed with CH_2Cl_2 until colorless filtrates were obtained, and vacuum dried; yield 0.049 g. IR (KBr pellet): $\nu(\text{C}\equiv\text{N})$ 2189 (s), 2116 (vs).

(13) Reaction of $\text{Mo}_2\text{Cl}_4(\text{dmpm})_2$ with TCNE

A solution comprised of 0.0216 g (0.169 mmol) of TCNE dissolved in 10 mL of CH_2Cl_2 was slowly added to a CH_2Cl_2 solution (20 mL) of $\text{Mo}_2\text{Cl}_4(\text{dmpm})_2$ (0.0794 g, 0.131 mmol) to give a purple solution. The solution was stirred at room temperature for several hours before being reduced in volume under vacuum. Hexanes (30 mL) was added and a vacuum applied to remove additional CH_2Cl_2 until the supernatant became colorless. The purple solid was collected by filtration, washed with hexanes, and vacuum dried. IR (CsI, Nujol, cm^{-1}): 2200 (m), 2129 (m).

(14) Reaction of $\text{Re}_2\text{Cl}_4(\text{dppm})_2$ with TCNQF_4

A solution consisting of TCNQF_4 (0.0131 g, 0.038 mmol) in 10 mL of acetone was added to a solution consisting of $\text{Re}_2\text{Cl}_4(\text{dppm})_2$ (0.050 g,

0.038 mmol) dissolved in 10 mL of acetone. The initial red solution turned to green over a period of 4 days while stirring at room temperature. Diethyl ether (20 mL) was added to precipitate a green solid which was collected by filtration, washed with diethyl ether, and vacuum dried; yield 0.021 g. IR (CsI, Nujol, cm^{-1}): $\nu(\text{C}\equiv\text{N})$ 2203 (m), 2145 (s).

(15) Reaction of $\text{Re}_2\text{Cl}_4(\text{PPr}^n_3)_4$ with DM-DCNQI

A THF (5 mL) solution of DM-DCNQI (0.0042 g, 0.023 mmol) was slowly added to a THF (5 mL) solution of $\text{Re}_2\text{Cl}_4(\text{PPr}^n_3)_4$ (0.053 g, 0.046 mmol) producing an orange-brown solution. The mixture was placed in the refrigerator (-5°C) for 5 days without any noticeable change in color. The volume was reduced under vacuum and 20 mL of hexanes was added to effect the precipitation of a brown solid. The product was harvested by filtration, washed with hexanes, and vacuum dried; yield 0.015 g. IR (CsI, Nujol, cm^{-1}): $\nu(\text{C}\equiv\text{N})$ 2116 (s).

(16) Reaction of $[\text{Rh}_2(\text{NCCH}_3)_{10}][\text{BF}_4]_4$ with $[\text{Bu}^n_4\text{N}]\text{TCNQ}$

An acetonitrile (10 mL) solution of $[\text{Rh}_2(\text{NCCH}_3)_{10}][\text{BF}_4]_4$ (0.0262 g, 0.027 mmol) was added dropwise to 0.0486 g (0.108 mmol) of $[\text{Bu}^n_4\text{N}]\text{TCNQ}$ dissolved in 10 mL of acetonitrile. A dark red solid immediately precipitated. The mixture was stirred at room temperature for 30 minutes to ensure complete reaction. The product was harvested by filtration, washed with acetonitrile, and dried *in vacuo*; yield 0.029 g. IR (CsI, Nujol, cm^{-1}): $\nu(\text{C}\equiv\text{N})$ 2336 (w), 2219 (w), 2193 (w), ~ 2100 (very strong and broad stretch between 2050 and 2150 cm^{-1}).

(17) Reaction of $[\text{Rh}_2(\text{NCCH}_3)_{10}][\text{BF}_4]_4$ with LiTCNQ

A solution of $[\text{Rh}_2(\text{NCCH}_3)_{10}][\text{BF}_4]_4$ (0.0923 g, 0.096 mmol) dissolved in 10 mL of acetonitrile was slowly added to an acetonitrile (30 mL) solution containing LiTCNQ (0.0860 g, 0.408 mmol) causing the

immediate formation of a dark red precipitate. After standing undisturbed for *ca.* 12 h, the solution was filtered and the solid was washed with copious amounts of acetonitrile, and dried *in vacuo*; yield 0.097 g. IR (CsI, Nujol, cm^{-1}): 2334 (w), 2112 (w), 2190 (w), 2064 (vs,vbr).

(18) Reaction of $[\text{Rh}_2(\text{NCCH}_3)_{10}][\text{BF}_4]_4$ with LiTCNQ in H_2O

A solution consisting of 0.020 g (0.021 mmol) of $[\text{Rh}_2(\text{NCCH}_3)_{10}][\text{BF}_4]_4$ dissolved in 5 mL of H_2O was slowly added to a stirring solution containing 0.020 g (0.095 mmol) of LiTCNQ H_2O (3 mL). A dark purple solution and a black precipitate formed. The solid was collected by filtration, washed with H_2O and diethyl ether, and vacuum dried; yield 0.020 g. IR (CsI, Nujol, cm^{-1}): $\nu(\text{C}\equiv\text{N})$ 2220 (m), 2195 (m), 2145 (s).

(19) Electrochemical preparation of " $\text{Rh}(\text{TCNQ})_2$ "

In a four compartment electrochemical cell (see Figure 23) a solution consisting of 0.020 g (0.021 mmol) of $[\text{Rh}_2(\text{NCCH}_3)_{10}][\text{BF}_4]_4$, 0.020 g (0.098 mmol) of TCNQ, and 6 mL of acetonitrile was added to the working compartment. A 0.5 M TBABF_4 /acetonitrile solution was used to fill the remaining compartments. A potential of +0.1 V was applied to the cell for two days which caused the formation of a red gelatinous precipitate on the platinum gauze electrode. The product was collected by filtration, washed with acetonitrile, and vacuum dried; yield 0.013 g. IR (CsI, Nujol, cm^{-1}): $\nu(\text{C}\equiv\text{N})$ 2335 (m), 2219 (m,sh), 2190 (m,sh), 2141 (s,vbr).

(20) Reaction of $[\text{Rh}_2(\text{NCCH}_3)_{10}][\text{BF}_4]_4$ with Li[DM-DCNQI]

To a Schlenk flask containing $[\text{Rh}_2(\text{NCCH}_3)_{10}][\text{BF}_4]_4$ (0.050 g, 0.052 mmol) and Li[DM-DCNQI] (0.040 g, 0.217 mmol) was added 15 mL of acetonitrile resulting in a dark brown-red solution. The mixture was stirred with slight warming for 1 day. The solution was passed

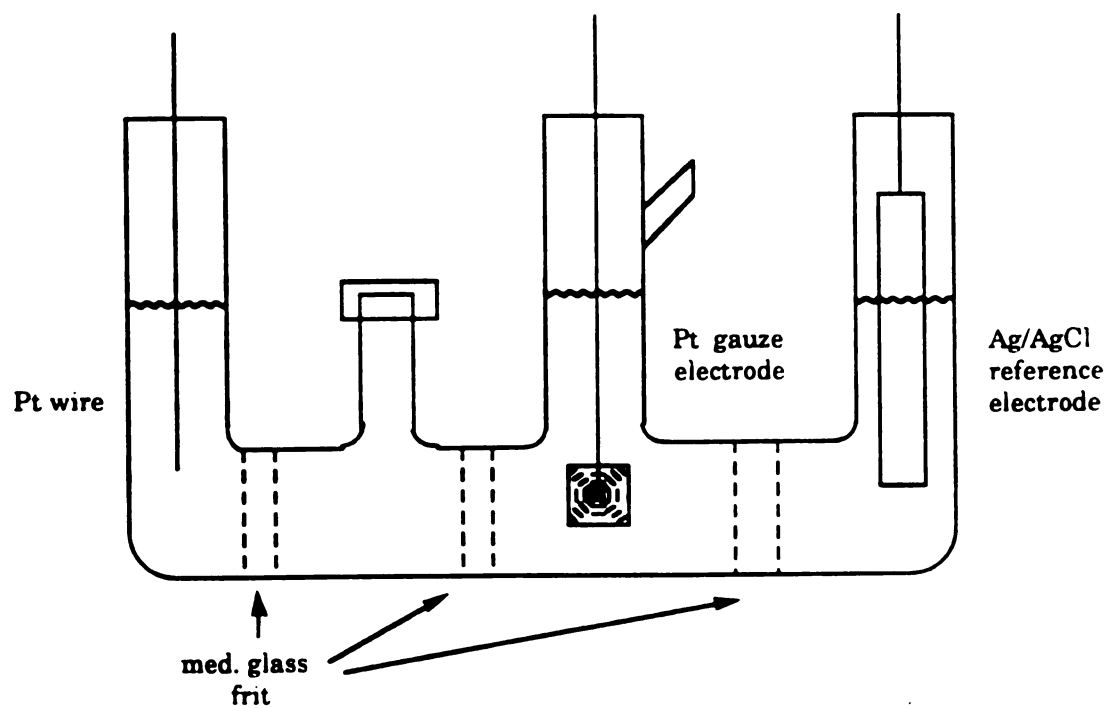


Figure 23. Schematic drawing of the electrolysis cell used in the electrochemical synthesis of " $\text{Rh}(\text{TCNQ})_2$ " and " $\text{Rh}(\text{DM-DCNQI})_2$ ".

through a frit and treated with 20 mL of CH_2Cl_2 producing a finely divided solid. The solid was collected by filtration, washed with CH_2Cl_2 , and dried *in vacuo*; yield 0.040 g black solid. The IR (CsI, Nujol) spectra of the solid exhibits a strong $\nu(\text{C}\equiv\text{N})$ band at 2050 cm^{-1} .

(21) Electrochemical Preparation of "[Rh(DM-DCNQI)₂]"

An acetonitrile (5 mL) solution containing 0.020 g (0.021 mmol) of $[\text{Rh}_2(\text{NCCH}_3)_{10}][\text{BF}_4]_4$ and 0.015g (0.083 mmol) of DM-DCNQI was added to the working electrode compartment, which consisted of a Pt wire gauze electrode, of a 4 chamber electrochemical cell (see Figure 23). The other 3 chambers were filled with a 0.01 M TBABF₄/acetonitrile electrolyte solution. A voltage of +0.05 V was applied to the cell for 24 h producing a red solid on the gauze electrode. The solid was removed from the electrode with CH_3CN washings, collected by filtration, washed with additional acetonitrile, and vacuum dried; yield 0.013 g. IR (CsI, Nujol, cm^{-1}): $\nu(\text{C}\equiv\text{N})$ 2039 (s).

(22) Reaction of $[\text{Mo}_2(\text{NCCH}_3)_{10}][\text{BF}_4]_4$ with $[\text{Bu}^n_4\text{N}][\text{TCNQ}]$

An acetonitrile (10 mL) solution containing $[\text{Mo}_2(\text{NCCH}_3)_{10}][\text{BF}_4]_4$ (0.0250 g, 0.028 mmol) was added to an acetonitrile (7 mL) solution containing $[\text{Bu}^n_4\text{N}][\text{TCNQ}]$ (0.050 g, 0.112 mmol) which resulted in the instantaneous formation of a dark green precipitate. The solid was collected by filtration, washed with acetonitrile, and vacuum dried; yield 0.022 g. IR (CsI, Nujol, cm^{-1}): $\nu(\text{C}\equiv\text{N})$ 2191 (s), 2108 (vs,br), 1986 (w).

3. Results and Discussion

A. Reactions of Dinuclear Complexes with Polycyano Acceptors

A variety of metal-metal bonded dimolybdenum and dirhenium donor complexes react with polycyano acceptors to form covalently bonded charge-transfer products. Most of these products are highly colored and

exhibit strong absorptions in their electronic spectra. Some products simply precipitate from the reaction solvent(s) used, while others require the addition of diethyl ether or hexanes. Slow diffusion reactions are not particularly useful, as the products form instantaneously resulting in finely divided solids at the interface of the layered solvents. In one example, the green filtrate from the reaction between $\text{Mo}_2\text{Cl}_4(\text{dppm})_2$ and TCNQ ($\text{CH}_2\text{Cl}_2/\text{Et}_2\text{O}$ solvents) produced disk-shaped solids that appeared to be crystalline, but were apparently not, as they did not diffract X-rays.

Infrared spectra of the products are listed in Tables 12 - 15. A common feature among these spectra is that compounds containing TCNQ, TCNE, or TCNQF_4 all exhibit two strong absorptions; one feature is sharp and in the range 2215 to 2180 cm^{-1} , but less intense than a second stretch which appears in the range 2145 to 2090 cm^{-1} . From these results we observe an apparent lack of $\nu(\text{C}\equiv\text{N})$ dependence on redox differences between the donor and acceptor molecules. For example, the TCNQ products of $\text{Mo}_2\text{Cl}_4(\text{dppe})_2$ and $\text{Re}_2\text{Cl}_4(\text{PEt}_3)_4$ (1:2 donor:acceptor) exhibit similar frequencies for $\nu(\text{C}\equiv\text{N})$ stretches although the first oxidation potential for $\text{Re}_2\text{Cl}_4(\text{PEt}_3)_4$ occurs at a 0.95 V more negative potential than $\text{Mo}_2\text{Cl}_4(\text{dppe})_2$. One would expect that a lower oxidation potential would increase the amount of charge transferred to the acceptor resulting in lowering of the observed $\nu(\text{C}\equiv\text{N})$ stretches as demonstrated previously for other charge-transfer products of TCNQ.¹² These data suggest that the most likely mechanism leading to coordination is an inner sphere rather than outer sphere charge-transfer process. As expected, however, the dimetal systems with lower oxidation potentials react faster with the acceptor species than those with higher oxidation potentials. It may then be proposed that regardless of the initial driving force for redox

Table 12. Comparison of the $\nu(\text{C}\equiv\text{N})$ stretching frequencies for products from reactions of dinuclear donor complexes with TCNQ*.

Dinuclear complex	$E_{1/2(\text{ox})}$	D/A	$\nu(\text{C}\equiv\text{N}) \text{ cm}^{-1}$
$\text{Re}_2\text{Cl}_4(\text{dppm})_2^{\text{a}}$	0.35	1:1	2195 (s), 2115 (m)
$\text{Re}_2\text{Cl}_4(\text{dppm})_2^{\text{b}}$	0.35	1:1	2183 (s), 2114 (s,br), 2085 (sh)
$\text{Re}_2\text{Cl}_4(\text{dppm})_2$	0.35	2:1	2187 (s), 2109 (s,br)
$\text{Mo}_2\text{Cl}_4(\text{dppe})_2$	0.62	1:2	2180 (m), 2090 (s)
$\text{Mo}_2\text{Cl}_4(\text{dppe})_2$	0.62	2:1	2186 (m), 2091 (s)
$\text{Mo}_2\text{Cl}_4(\text{dppe})_2$	0.62	4:1	2189 (m), 2099 (s)
$\text{Mo}_2\text{Cl}_4(\text{dppm})_2$	0.66	1:1	2193 (m), 2115 (s), 1968 (w)
$\text{Mo}_2\text{Cl}_4(\text{PEt}_3)_4$	0.61	1:1	2188 (s), 2128 (s)
$\text{Mo}_2\text{Cl}_4(\text{dmpm})_2$	0.45	1:2	2189 (s), 2116 (vs)
$\text{Re}_2\text{Cl}_4(\text{PEt}_3)_4$	-0.33	1:2	2189 (s), 2091 (vs,br)

*TCNQ⁰: $\nu(\text{C}\equiv\text{N}) = 2222 \text{ cm}^{-1}$, $E_{1/2(\text{red})} = 0.28 \text{ V}$

a. Product (1)-A

b. Product (1)-B

Table 13. Comparison of the $\nu(\text{C}\equiv\text{N})$ stretching frequencies for products from reactions of dinuclear donor complexes with TCNE*.

Dinuclear complex	$E_{1/2(\text{ox})}$	D/A	$\nu(\text{C}\equiv\text{N}) \text{ cm}^{-1}$
$\text{Re}_2\text{Cl}_4(\text{dppm})_2^{\text{a}}$	0.35	1:1	2197 (s), 2121 (m)
$\text{Re}_2\text{Cl}_4(\text{dppm})_2^{\text{b}}$	0.35	1:1	2200 (s), 2128 (m)
$\text{Re}_2\text{Cl}_4(\text{PEt}_3)_4$	- 0.33	1:1	2207 (s), 2140 (m)
$\text{Mo}_2\text{Cl}_4(\text{dppm})_2$	0.66	1:2	2215 (s), 2130 (w)
$\text{Mo}_2\text{Cl}_4(\text{dppe})_2$	0.62	1:2	2200 (m), 2120 (s)
$\text{Mo}_2\text{Cl}_4(\text{dmpm})_2$	0.45	1:1	2200 (m), 2129 (m)

*TCNE⁰: $\nu(\text{C}\equiv\text{N}) = 2256, 2221 \text{ cm}^{-1}$, $E_{1/2(\text{red})} = 0.34 \text{ V}$

a. Product (3)-A

b. Product (3)-B

Table 14 Comparison of the $\nu(\text{C}\equiv\text{N})$ stretching frequencies for products from reactions of dinuclear donor complexes with TCNQF_4^* .

Dinuclear complex	$E_{1/2(\text{ox})}$	D/A	$\nu(\text{C}\equiv\text{N}) \text{ cm}^{-1}$
$\text{Re}_2\text{Cl}_4(\text{dppm})_2$	0.35	1:1	2203 (m), 2145 (s)
$\text{Mo}_2\text{Cl}_4(\text{dppe})_2$	0.62	1:2	2199 (s), 2132 (vs,br)
$\text{Mo}_2\text{Cl}_4(\text{PEt}_3)_4$	0.61	1:1	2198 (s), 2143 (s)
$\text{Re}_2\text{Cl}_4(\text{PEt}_3)_4$	-0.33	1:3	2202 (s,sh), 2104 (vs,br)
$\text{Re}_2\text{Cl}_4(\text{PEt}_3)_4$	-0.33	1:1	2195 (m), 2100 (s)
$\text{Re}_2\text{Cl}_4(\text{PEt}_3)_4$	-0.33	1:2	2190 (m), 2100 (s)

* TCNQF_4^0 : $\nu(\text{C}\equiv\text{N}) = \text{cm}^{-1}$, $E_{1/2(\text{red})} = 0.40 \text{ V}$

Table 15. Comparison of the $\nu(\text{C}\equiv\text{N})$ stretching frequencies for products from reactions of dinuclear donor complexes with DM-DCNQI*.

Dinuclear complex	$E_{1/2(\text{ox})}$	D/A	$\nu(\text{C}\equiv\text{N}) \text{ cm}^{-1}$
$\text{Re}_2\text{Cl}_4(\text{dppm})_2$	0.35	2:1	2070 (s,br)
$\text{Mo}_2\text{Cl}_4(\text{dppe})_2$	0.62	4:1	2085 (s)
$\text{Re}_2\text{Cl}_4(\text{PEt}_3)_4$	-0.33	1:1	2105 (vs)
$\text{Re}_2\text{Cl}_4(\text{P-n-Pr}_3)_4$		2:1	2116 (s)

*DM-DCNQI⁰: $\nu(\text{C}\equiv\text{N}) = 2197 \text{ cm}^{-1}$, $E_{1/2(\text{red})} = 0.21 \text{ V}$

chemistry to occur between the two compounds, the retro charge-transfer process, which occurs upon coordination, is similar for all products. In other words, a highly charged TCNQ unit is more nucleophilic than a less charged TCNQ, and essentially behaves as a better donor, and transfers more charge in the retro charge-transfer process. Thus, net charge transfer is similar in all cases where coordination results, assuming similar D:A ratios.

All samples that were tested for magnetic properties were found to exhibit paramagnetic behavior. The majority of the samples exhibit temperature dependent paramagnetism (non-Curie-Weiss behavior). Exact values for μ_{eff} were not assigned because of ambiguities in the molecular formulae. The μ_{eff} values at 300K for the products obtained from the reactions between $\text{Re}_2\text{Cl}_4(\text{PEt}_3)_4$ and TCNQF_4 , and $\text{Mo}_2\text{Cl}_4(\text{dppm})_2$ and TCNQ, for example, are ca. 7 B.M. based on the formation of 1:1 adducts. These unusually high values may be due to either impurities or ligand loss. The latter would result in lower formula weights, thus leading to a smaller calculated μ_{eff} per molecular unit. The black solid obtained from the reaction between $\text{Mo}_2\text{Cl}_4(\text{dppm})_2$ and TCNQF_4 exhibits Curie-Weiss behavior (see Figure 24). The plot of μ_{eff} vs. temperature displays a fairly constant value for μ_{eff} consistent with a simple paramagnet $S = 1/2$ and displays a room temperature (300 K) value near that expected for one free electron.

B. Reactions of Solvated Metal Cations with Reduced Forms of Polycyano Acceptors

Another approach leading to the synthesis of complexes containing σ -bonded TCNQ involved the use of solvated metal cations. The homoleptic complexes $[\text{M}_2(\text{NCCH}_3)_{10}]^{4+}$ ($\text{M} = \text{Mo}, \text{Rh}$), in which the

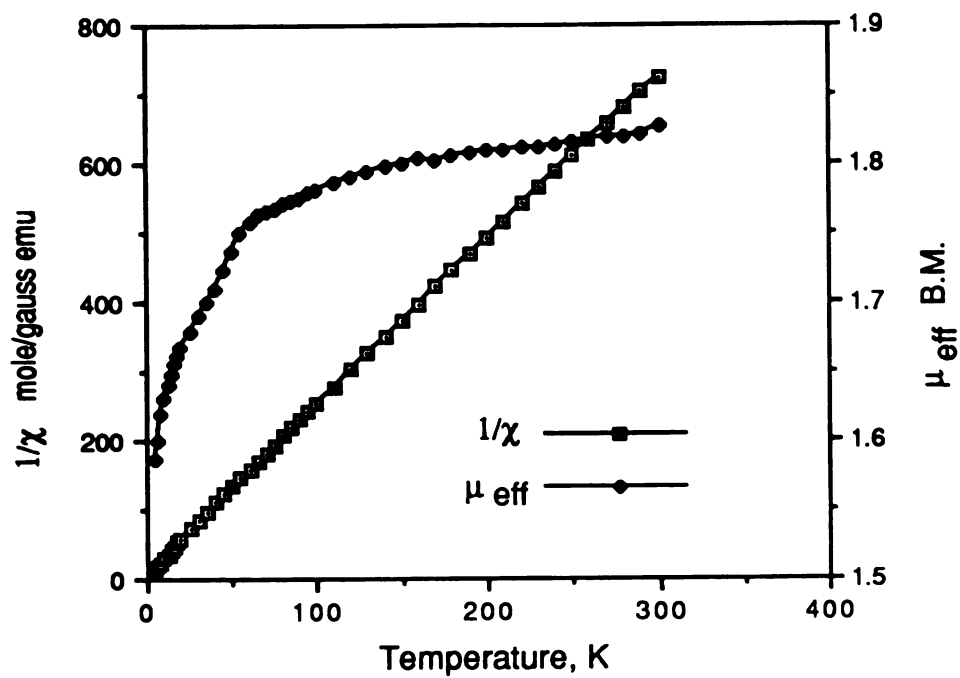


Figure 24. Plot of μ_{eff} and $1/\chi$ vs. temperature (K) of the product from the reaction of $\text{Mo}_2\text{Cl}_4(\text{dppe})_2$ with TCNQF_4 .

dinuclear metal centers are ligated by acetonitrile units, are excellent synthons for the development of macromolecular arrays. The complex $[\text{Rh}_2(\text{NCCH}_3)_{10}][\text{BF}_4]_4$ when reacted with TCNQ^- yields a product with spectroscopic features clearly indicative of Rh-TCNQ coordination. The reactions of four equivalents of LiTCNQ or $[\text{Bu}^n_4\text{N}][\text{TCNQ}]$ in acetonitrile lead to the immediate formation of dark red solids. The electrochemical reduction of TCNQ in the presence of $[\text{Rh}_2(\text{NCCH}_3)_{10}][\text{BF}_4]_4$ in acetonitrile also produces dark red solids. The infrared spectra of these complexes exhibit $\nu(\text{C}\equiv\text{N})$ bands at ~ 2335 (w), ~ 2220 (w), and ~ 2190 (w) cm^{-1} along with a strong stretch between ~ 2050 - 2150 cm^{-1} . The stretch at 2335 cm^{-1} suggests that there may still remain coordinated acetonitrile in the product. The other stretches are consistent with coordinated TCNQ^- . Based on the reaction stoichiometry, and the loss of BF_4^- ions, as indicated by infrared spectra, the product is loosely formulated as " $[\text{Rh}_2(\text{TNCQ})_4(\text{NCCH}_3)_x]$ ". The solid is soluble in dimethylformamide and partially soluble in dimethyl sulfoxide. Slow diffusion of acetonitrile solutions of $[\text{Rh}_2(\text{NCCH}_3)_{10}][\text{BF}_4]_4$ and TCNQ^- produce only amorphous solids. Controlled potential and controlled current experiments also failed to yield crystalline products. Magnetic measurements performed on the solid reveal non-Curie-Weiss behavior with an effective moment of 4.55 B.M. at 300K based on the formulation " $\text{Rh}_2(\text{TCNQ})_4$ ".

Slow addition of LiTCNQ or $[\text{Bu}^n_4\text{N}][\text{TCNQ}]$ to an acetonitrile solution of $[\text{Rh}_2(\text{NCCH}_3)_{10}][\text{BF}_4]_4$ produces dark red-orange reaction solutions. Precipitates form only when 4 or more equivalents of TCNQ^- are added. The identical reaction done at -42°C produces similar results. Adding 4 equivalents of TCNQ^- to a $[\text{Rh}_2(\text{NCCH}_3)_{10}][\text{BF}_4]_4$ solution at low temperature does not allow for crystal growth, but rather gives finely

divided solids. Reactions using solvents other than acetonitrile produce similar results, for example the reaction between $[\text{Rh}_2(\text{NCCH}_3)_{10}][\text{BF}_4]_4$ and LiTCNQ in water results in the precipitation of a black solid that exhibits a nearly identical infrared spectrum to the product obtained from acetonitrile. Electrochemical reactions between $[\text{Rh}_2(\text{NCCH}_3)_{10}][\text{BF}_4]_4$ and TCNQ, performed in nitromethane, yield similar solids to those obtained from acetonitrile and water. It should be noted that no reaction between $[\text{Rh}_2(\text{NCCH}_3)_{10}][\text{BF}_4]_4$ and TCNO^0 was observed to occur in acetonitrile.

The reaction between $[\text{Rh}_2(\text{NCCH}_3)_{10}][\text{BF}_4]_4$ and Li[DM-DCNQI] in acetonitrile produces a solid that contains σ -bonded DM-DCNQI⁻ as judged by the single, intense absorption at $\nu(\text{C}\equiv\text{N}) = 2050 \text{ cm}^{-1}$ in the infrared spectrum. Stretches attributed to acetonitrile are absent. Similar results are obtained from the electrochemical generation of DM-DCNQI⁻ in the presence of $[\text{Rh}_2(\text{NCCH}_3)_{10}][\text{BF}_4]_4$. These solids also have limited solubilities (DMSO and DMF). Controlled potential and controlled current syntheses of "Rh₂(DM-DCNQI)₄" unfortunately did not produce single crystals adequate for X-ray crystallography.

Reactions between $[\text{Mo}_2(\text{NCCH}_3)_{10}][\text{BF}_4]_4$ and $[\text{Bu}^n_4\text{N}][\text{TCNQ}]$ lead to the formation of dark green solids whose infrared spectra reveal $\nu(\text{C}\equiv\text{N})$ bands at 2191 (s) and 2108 (vs,br) cm^{-1} demonstrative of coordinated TCNQ⁻. There are no stretches present that can be attributed to acetonitrile or $[\text{BF}_4]^-$. An additional weak stretch at 1986 cm^{-1} is also observed which is likewise observed in the infrared spectra of other TCNQ complexes of dimolybdenum. The origin of this stretch is not fully understood but may be due to a π rather than a σ coordination (or a combination of the two) by the CN group on TCNQ to the metal.

The reactions between $[M_2(NCCH_3)_{10}][BF_4]_4$ ($M = Mo, Rh$) and L^- ($L=TCNQ, DM-DCNQI$) result in the formation of insoluble solids which are believed to be covalently bonded complexes having the formulations of " $M_2(L)_4$ ". The structures of these products are unknown due to our lack of success in growing crystals suitable for an X-ray structure determination, but based on infrared spectral data, it may be predicted that a two- or three-dimensional polymeric structure could exist. For example, the product " $Rh_2(DM-DCNQI)_4$ ", which may be referred to in empirical form as " $Rh(DM-DCNQI)_2$ " exhibits only one $\nu(C\equiv N)$ band in its infrared spectra which suggests that all the $C\equiv N$ moieties are equivalent. The $DM-DCNQI^-$ moiety, therefore, must be acting as a symmetrical bridge linking the rhodium units. Assuming a square planar arrangement between the rhodium for the compound as depicted in Figure 25, a two-dimensional layer structure is proposed. This would not be unprecedented since the mononuclear complexes of the type $M(DM-DCNQI)_2$ ($M=Ag, Li, Na, K, Cu, Tl$) have been crystallographically determined to exhibit this type of structure.¹³ These highly conducting materials were electrochemically synthesized as black needles using acetonitrile solutions of $[ClO_4]^-$, $[PF_6]^-$, or $[BF_4]^-$ salts of the cations under constant current conditions.^{13(a)} The crystal structures of these complexes consist of two-dimensional sheets which are layered to form three-dimensional structures having average interplanar distances between the $DCNQI$ units of *ca.* 3.2 Å. In the proposed structure of " $Rh(DM-DCNQI)_2$ ", direct Rh-Rh bonding would be limited to a minimum of *ca.* 3.2 Å if a similar structure would exist. A similar argument could be advanced for the product " $Rh(TCNQ)_2$ ". The infrared spectrum of this product supports the presence of both bound and free $C\equiv N$ units on $TCNQ$, as previously demonstrated for other complexes

of TCNQ, implying a *trans* bridging TCNQ arrangement. A structure similar to that in Figure 25 may exist, but only 1/2 of the C≡N groups would be ligated if one assumes a four-fold coordination environment about each Rh center. Again, the possibility of Rh-Rh bonding cannot be determined without further information such as structural data or raman spectroscopy. Considering the fact that products with similar spectroscopic properties are obtained by the reactions of $[\text{Mo}_2(\text{NCCH}_3)_{10}][\text{BF}_4]_4$ and $[\text{Rh}_2(\text{NCCH}_3)_{10}][\text{BF}_4]_4$ with TCNQ^- , similar structures are predicted.

Conclusions

Reactivity of a specific acceptor species with a variety of dinuclear compounds of varying oxidation potentials aided in understanding the relative unimportance of outersphere charge-transfer processes in forming covalently bonded species. The infrared spectroscopic results of the products indicate that varying the redox potentials on similar dinuclear compounds of molybdenum and rhenium does not alter the ability to form covalently bonded complexes with polycyano organic acceptors. No relationships could be established between the oxidation potential of the metal complexes and the $\nu(\text{C}\equiv\text{N})$ stretching frequencies in the infrared spectra of the products. A strong tendency was observed for polycyano acceptors to bind to unsaturated metal compounds which bodes well for the generality of this approach. In addition to the above charge-transfer reactions, reactions involving the fully solvated dinuclear compounds $[\text{Rh}_2(\text{NCCH}_3)_{10}][\text{BF}_4]_4$ and $[\text{Mo}_2(\text{NCCH}_3)_{10}][\text{BF}_4]_4$ were studied with chemically or electrochemically reduced forms of TCNQ and DM-DCNQI resulting in the synthesis of covalently bonded polymeric materials.

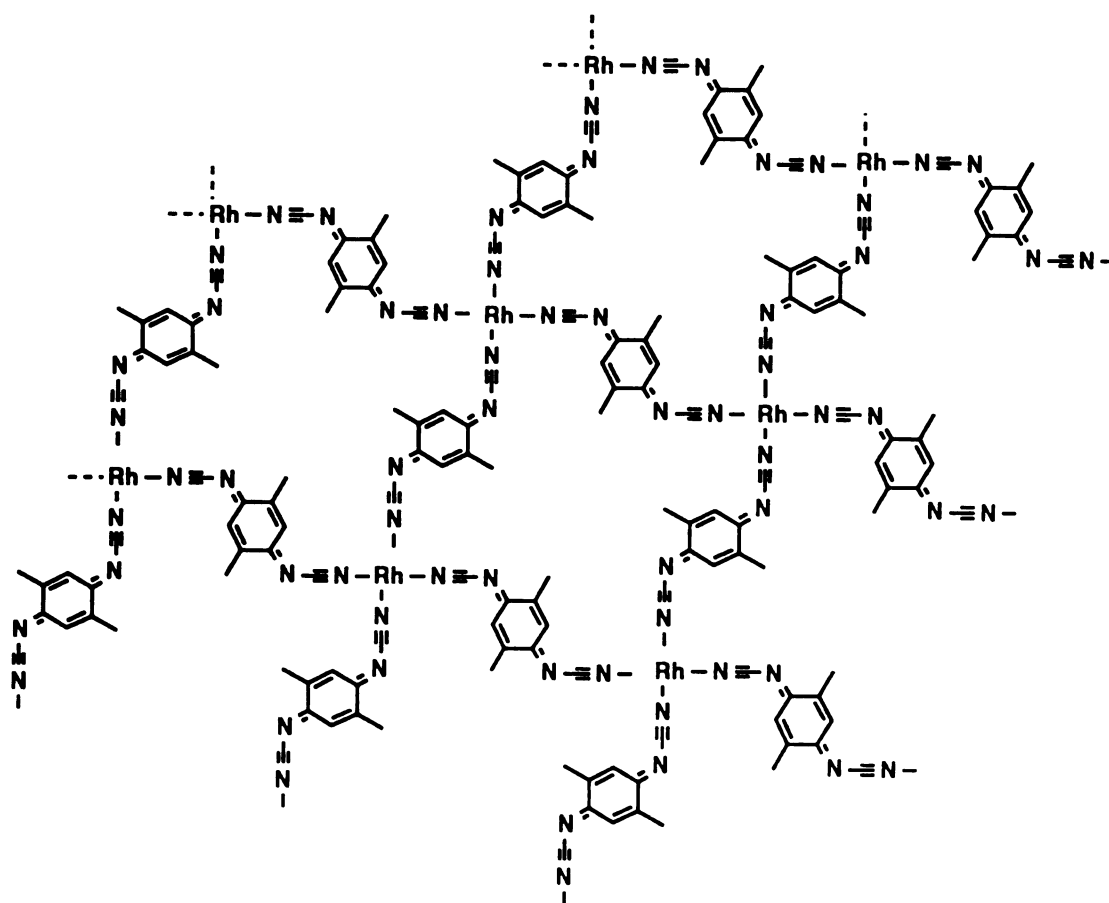


Figure 25. Proposed polymeric structure of " $\text{Rh}(\text{DM-DCNQI})_2$ ".

References

1. Brant, P.; Walton, R. A. *Inorg. Chem.* **1978**, *17*, 2674.
2. Glicksman, H. D.; Jamer, A. D.; Smith, T. J.; Walton, R. A. *Inorg. Chem.* **1976**, *15*, 2205.
3. Best, S. A.; Smith, T. J.; Walton, R. A. *Inorg. Chem.* **1978**, *17*, 99.
4. Cotton, F. A.; Falvello, L. R.; Harwood, W. S.; Powell, G. L.; Walton, R. A. *Inorg. Chem.* **1986**, *25*, 3949.
5. Agaskar, P. A.; Cotton, F. A. *Inorg. Chem.* **1984**, *23*, 3383.
6. (a) Dunbar, K. R. *J. Am. Chem. Soc.* **1988**, *110*, 8247. (b) Dunbar, K. R.; Pence, L. E. *Inorg. Synth.* **1991**, *29*, in press.
7. Cotton, F. A.; Wiesinger, K. J. *Inorg. Chem.*, **1991**, *30*, 871.
8. Acker, D. S.; Harder, R. J.; Hertler, W. R.; Mahler, W.; Melby, L. R.; Benson, R. E.; Mochel, W. E. *J. Am. Chem. Soc.* **1960**, *82*, 6408.
9. Melby, L. R.; Harder, R. J.; Hertler, W. R.; Mahler, W.; Benson, R. E.; Mochel, W. E. *J. Am. Chem. Soc.* **1962**, *84*, 3374.
10. Wheland, R. C.; Martin, E. L. *J. Org. Chem.* **1975**, *40*, 3101.
11. Aumüller, A.; Hünig, S. *Liebigs Ann. Chem.* **1986**, 142.
12. Robles-Martinez, J. G.; Salmeron-Valverde, A.; Alonso, E.; Soriano, C. *Inorg. Chem. Acta* **1991**, *179*, 149.
13. (a) Kato, R.; Kobayashi, H.; Kobayashi, A. *Synth. Met.* **1988**, *27*, B263. (b) Kato, R.; Kobayashi, H.; Kobayashi, A. *J. Am. Chem. Soc.* **1989**, *111*, 5224. (c) Enkelmann, V. *Angew. Chem. Int. Ed. Engl.* **1991**, *30*, 1121. (d) Aumüller, A.; Erk, P.; Hünig, S.; Meixner, H.; von Schütz, J.-U.; Werner, H.-P. *Liebigs Ann. Chem.* **1987**, 997. (e) Aumüller, A.; Erk, P.; Hünig, S.; von Schütz, J.-U.; Werner, H.-P.; Wolf, H. C.; Klebe, G. *Chem. Ber.* **1991**, *124*, 1445. (f) Kobayashi, A.; Mori, T.; Inokuchi, H.; Kato, R.; Kobayashi, H. *Synth. Met.* **1988**, *27*, B275. (g) Kato, R.; Kobayashi, H.; Kobayashi, A.; Mori, T.; Inokuchi, H. *Chem. Lett.* **1987**, 1579. (h) Aumüller, A.; Erk, P.; Klebe, G.; Hünig, S.; von Schütz, J.-U.; Werner, H.-P. *Angew. Chem. Int. Ed. Engl.* **1986**, *25*, 740.

- (i) Erk, P.; Gross, H.-J.; Hünig, S.; Langohr, U.; Meixner, H.; Werner, H.-P.; von Schütz, J.-U.; Wolf, H. C. *Angew. Chem. Int. Ed. Engl.* **1989**, 28, 1245. (j) Aumüller, A.; Erk, P.; Hünig, S.; von Schütz, J.-U.; Werner, H.-P.; Wolf, H. C.; Klebe, G. *Mol. Cryst. Liq. Cryst. Inc. Nonlin. Opt.* **1988**, 156, 215. (k) Hünig, S.; Aumüller, A.; Erk, P.; Meixner, H.; von Schütz, J.-U.; Gross, H.-J.; Langohr, U.; Werner, H.-P.; Wolf, H. C.; Burschka, C.; Klebe, G.; Peters, K.; Schnering, H. G. *Synth. Met.* **1988**, 27, B181.

CHAPTER V

**METAL-METAL BONDED COMPOUNDS
WITH CYANIDE LIGANDS.**

1. Introduction

Controlled self assembly reactions can lead to infinite frameworks in which the structure property relationships are easily tailored by altering the precursors. Extended 3-D frameworks with channels and cavities can be designed if rodlike units are used such as the approach being popularized by Mochl *et al.* in their "molecular lego" chemistry involving rigid staffane linking metal centers.¹ Recently, unique "scaffoldings" have been created by Robson *et al.* by utilizing M-CN-M likages.² In fact, chains, sheets, and three dimensional structures exist for a variety of metal-cyanide complexes, the most notable being the Prussian blues.³ There is a wealth of cyanide chemistry of the transition metals,³ but little pertains to metal-metal bonded complexes.⁴ In the search for suitable linking units to span dimetal compounds, the simple CN⁻ ligand was chosen because of its bifunctionality. If CN⁻ ligands are placed on dimetal units, then under the right conditions, spontaneous self assembly could occur to produce polymeric materials. The non-aqueous chemistry of metal-metal bonded systems with cyanide ion was investigated.

2. Experimental

A. Synthesis

(1) Starting Materials

The compounds Mo₂(O₂CCH₃)₄,⁵ Mo₂(O₂CCF₃)₄,⁶ [Rh₂(NCCH₃)₁₀][BF₄]₄,⁷ [Mo₂(NCCH₃)₁₀][BF₄]₄,⁸ [Re₂(NCCH₃)₁₀][BF₄]₄,⁹ [Fe(NCCH₃)₆][BF₄]₂,¹⁰ and Re₂Cl₄(dppm)₄¹¹ were prepared according to literature methods. The cyanide salt [Et₄N]CN was prepared by standard procedures.¹² The reagent [Buⁿ₄N]CN was purchased from Aldrich Chemicals and used without further purification. For the cyanide chemistry, all glassware was flame dried under vacuum prior to use.

(2) Synthesis of $[\text{Bu}^n_4\text{N}]_4[\text{Mo}_2(\text{CN})_8]$ (8)

A CHCl_3 (8 mL) solution containing $[\text{Bu}^n_4\text{N}]\text{CN}$ (0.534 g, 1.99 mmol) was added to $\text{Mo}_2(\text{O}_2\text{CCH}_3)_4$ (0.106 g, 0.248 mmol) dissolved in 4 mL of CHCl_3 to give a dark purple reaction solution which was stirred at room temperature for 5 days during which time the color changed to blue. Addition of hexanes (5 mL) followed by cooling to 0°C for 2 days led to the precipitation of a bright blue crystalline solid. After a second addition of hexanes (2 mL) and chilling at 0°C for 1 day, the product was collected by filtration, washed with hexanes (3 x 3 mL) and dried *in vacuo*; yield 0.133 g (40%). *Anal.* Calcd for $\text{C}_{72}\text{H}_{144}\text{N}_{12}\text{Mo}_2$: C, 63.13; H, 10.60; N, 12.27. Found: C, 61.63; H, 10.75; N, 11.54. The low values for the carbon and nitrogen analyses are attributed to residual CHCl_3 trapped in the crystalline form of the sample; this is supported by X-ray data that reveal the presence of 8 CHCl_3 molecules per $[\text{Mo}_2(\text{CN})_8]^{4-}$ anion in the crystal form. IR (CsI, Nujol mull, cm^{-1}): 2095 (s), 1153 (m), 1107 (w), 1060 (w), 1030 (w), 968 (w), 887 (m), 801 (w).

(3) Synthesis of $[\text{Bu}^n_4\text{N}]_3[\text{Mo}_2(\text{O}_2\text{CCH}_3)(\text{CN})_6]$ (9)

In a typical reaction, a solution consisting of $[\text{Bu}^n_4\text{N}]\text{CN}$ (1.427 g, 5.31 mmol) in 10 mL of THF was slowly added to a sample of $\text{Mo}_2(\text{O}_2\text{CCH}_3)_4$ (0.379 g, 0.88 mmol) in 10 mL of THF to give a dark purple solution. The reaction was stirred at room temperature for 5 min during which time a red-purple solid precipitated. Additional product was harvested in the form of red-purple microcrystals that appeared after the reaction mixture was left undisturbed for 12 h; the crystals were collected by filtration, washed with THF (2 x 10 mL), and vacuum dried; yield 0.93 g (92%). *Anal.* Calcd for $\text{C}_{56}\text{H}_{111}\text{N}_9\text{O}_2\text{Mo}_2$: C, 59.29; H, 9.86; N, 11.11. Found: C, 59.05; H, 9.63; N, 10.78. IR (CsI, Nujol mull, cm^{-1}):

2105 (m), 2099 (m), 1604 (w), 1531 (w), 1154 (m), 1026 (w), 887 (m), 673 (m). UV-visible spectrum (CH_2Cl_2): λ_{max} nm (ϵ , $\text{M}^{-1}\text{cm}^{-1}$), 557 (2.5×10^3), 276 (5.4×10^3).

(4) Synthesis of $[\text{Et}_4\text{N}]_4[\text{Mo}_2(\text{CN})_8]$ (10)

(i) Method i

To a flask charged with $\text{Mo}_2(\text{O}_2\text{CCH}_3)_4$ (0.100 g, 0.234 mmol) and $[\text{Et}_4\text{N}]\text{CN}$ (0.488 g, 3.12 mmol) was added 10 mL of CH_2Cl_2 which resulted in the formation of a blue solution. The reaction mixture was stirred at room temperature for 3 h, during which time a bright blue precipitate formed. The solid was collected by filtration, washed with CH_2Cl_2 (3 x 5 mL) and dried *in vacuo*; yield 0.172 g (80%). The compound is soluble in EtOH, CH_3CN , and H_2O , and was recrystallized from CH_3CN to insure complete removal of $[\text{Et}_4\text{N}][\text{O}_2\text{CCH}_3]$. IR (CsI, Nujol mull, cm^{-1}): 2095 (s), 1490 (m), 1323 (w), 1176 (s), 1003 (m), 788 (m), 666 (w), 390 (w), 358 (w), 293 (w). UV-visible spectrum (CH_2Cl_2): λ_{max} nm (ϵ , $\text{M}^{-1}\text{cm}^{-1}$), 601 (3.0×10^3), 277 (4.9×10^3).

(ii) Method ii

A CH_2Cl_2 (10 mL) solution consisting of 0.200 g (0.31 mmol) of $\text{Mo}_2(\text{O}_2\text{CCF}_3)_4$ was added to a stirred CH_2Cl_2 (10 mL) solution consisting of 0.436 g (2.79 mmol) of $[\text{Et}_4\text{N}]\text{CN}$ causing a blue reaction mixture to form. The mixture was allowed to stand undisturbed for 2 h during which time a blue solid floated to the top of a dark green solution. The blue product was collected by filtration, washed with CH_2Cl_2 (3 x 3 mL) and Et_2O (3 x 3 mL), and dried *in vacuo*; yield 0.232 g (81%).

(iii) Method iii

A flask containing $[\text{Bu}^n_4\text{N}]_3[\text{Mo}_2(\text{O}_2\text{CCH}_3)(\text{CN})_6]$ (**2**) (0.100 g, 0.088 mmol), $[\text{Bu}^n_4\text{N}]\text{CN}$ (0.095 g, 0.35 mmol) and 10 mL of CH_2Cl_2 was

treated with $[\text{Et}_4\text{N}]\text{Cl}$ (0.146 g, 0.88 mmol) in 5 mL of CH_2Cl_2 . A reaction swiftly ensued with the deposition of a bright blue precipitate. The reaction mixture was stirred for 12 h at room temperature after which time the solid was collected by filtration and washed with CH_2Cl_2 (3 x 5 mL); yield 0.071 g (88%).

(5) Synthesis of $[\text{Bu}^n_4\text{N}]_2[\text{Re}_2(\text{CN})_6(\text{dppm})_2]$ (11)

The salt $[\text{Bu}^n_4\text{N}]\text{CN}$ (0.133 g, 0.050 mmol) in 5 mL of CH_2Cl_2 was added to a solution of $\text{Re}_2\text{Cl}_4(\text{dppm})_2$ (0.100 g, 0.078 mmol) in 10 mL of CH_2Cl_2 leading to the formation of a green solution with the concomitant deposition of a bright green microcrystalline solid within 5 minutes. The solution was reduced in volume to 5 mL and the product was collected by filtration, washed with toluene (3 x 5 mL), and dried *in vacuo*; yield 0.093 g (67%). IR (CsI, Nujol mull, cm^{-1}): 2091 (m,sh), 2078 (s), 1906 (s), 1588 (w), 1574 (w), 1433 (m,sh), 1277 (m), 1126 (w), 1094 (s), 1028 (m), 785 (s), 758 (w), 737 (m), 718 (m), 691 (s), 523 (s), 490 (s), 419 (s). The compound is soluble in acetonitrile and only sparingly soluble in CH_2Cl_2 . The product was recrystallized from CH_2Cl_2 as the CH_2Cl_2 solvate $[\text{Bu}^n_4\text{N}]_2[\text{Re}_2(\text{CN})_6(\text{dppm})_2] \cdot 8\text{CH}_2\text{Cl}_2$. ^1H NMR (ppm, CD_3CN , 22°C, 300 MHz): $\delta = 7.48$ (mult, 16H, Ph); $\delta = 6.96$ (mult, 24H, Ph); $\delta = 5.44$ (s, 16H, CH_2Cl_2); $\delta = 3.30$ (pentet, 4H, $-\text{CH}_2-$); Bu^n_4N : $\delta = 3.05$ (mult, 16H); $\delta = 1.58$ (mult, 16H); $\delta = 1.33$ (sextet, 16H), $\delta = 0.95$ (triplet, 24H). $^{31}\text{P}\{^1\text{H}\}$ NMR (CD_3CN , 22 °C relative to 85% H_3PO_4): $\delta = -11.39$ (s) ppm. UV-visible (CH_3CN): λ_{max} nm (ϵ , $\text{M}^{-1}\text{cm}^{-1}$), 969 (2.5×10^2), 694 (1.4×10^2).

(6) Preparation of " $\text{Mo}_2(\text{CN})_4(\text{NCCH}_3)_x$ "

A CH_3CN (10 mL) solution containing $[\text{Bu}^n_4\text{N}]\text{CN}$ (0.487 g, 1.81 mmol) was added to a CH_3CN (30 mL) solution containing

$[\text{Mo}_2(\text{NCCH}_3)_{10}][\text{BF}_4]_4$ (0.400 g, 0.45 mmol) to give a green precipitate. The solid was collected by filtration, washed with CH_3CN (2 x 10 mL), and dried *in vacuo*; yield 0.243 g. IR (CsI, Nujol, cm^{-1}): 2317 (m), 2288 (m), 2249 (w), 2188 (w), 2110 (s,br), 1067 (s), 1034 (w,sh), 511 (w), 484 (w,br).

(7) Reaction of $[\text{Et}_4\text{N}]_4[\text{Mo}_2(\text{CN})_8]$ with $[\text{Rh}_2(\text{NCCH}_3)_{10}][\text{BF}_4]_4$

A CH_3CN (5 mL) solution containing 0.050 g (0.054 mmol) of $[\text{Et}_4\text{N}]_4[\text{Mo}_2(\text{CN})_8]$ was added to a CH_3CN (5 mL) solution containing 0.052 g (0.054 mmol) of $[\text{Rh}_2(\text{NCCH}_3)_{10}][\text{BF}_4]_4$ to give a black solid precipitate. The solid was collected by filtration, washed with CH_3CN (2 x 10 mL), and dried *in vacuo*; yield 0.031 g. IR (CsI, Nujol, cm^{-1}): 2334 (m), 2112 (s,br), 1647 (m), 1306 (w), 1175 (w), 914 (w), 968 (m), 787 (w), 461 (w,br).

(8) Reaction of $[\text{Et}_4\text{N}]_4[\text{Mo}_2(\text{CN})_8]$ with $[\text{Re}_2(\text{NCCH}_3)_{10}][\text{BF}_4]_4$

A CH_3CN (5 mL) solution containing 0.050 g (0.054 mmol) of $[\text{Et}_4\text{N}]_4[\text{Mo}_2(\text{CN})_8]$ was added to a CH_3CN (5 mL) solution containing 0.062 g (0.054 mmol) of $[\text{Re}_2(\text{NCCH}_3)_{10}][\text{BF}_4]_4$ to give a green precipitate. The solid was collected by filtration, washed with CH_3CN (2 x 10 mL), and dried *in vacuo*; yield 0.042 g of the final black solid. IR (CsI, Nujol, cm^{-1}): 2209 (m), 2095 (s,br), 1651 (w), 1196 (m), 968 (m), 788 (w), 461 (w,br).

(9) Reaction of $[\text{Et}_4\text{N}]_4[\text{Mo}_2(\text{CN})_8]$ with $[\text{Fe}(\text{NCCH}_3)_6][\text{BF}_4]_2$

Acetonitrile (15 mL) was added to a Schlenk tube containing 0.0968 g (0.105 mmol) of $[\text{Et}_4\text{N}]_4[\text{Mo}_2(\text{CN})_8]$ and 0.100 g (0.210 mmol) of $[\text{Fe}(\text{NCCH}_3)_6][\text{BF}_4]_2$ resulting in the immediate precipitation of a dark green solid. The solid was collected by filtration, washed with CH_3CN

(2 x 10 mL), and dried *in vacuo*; yield 0.069 g. IR (CsI, Nujol, cm^{-1}): 2311 (w), 2280 (w), 2211 (w), 2096 (s,br).

(10) Reaction of $[\text{Bu}^n_4\text{N}]_3[\text{Mo}_2(\text{O}_2\text{CCH}_3)(\text{CN})_6]$ with $[\text{Rh}_2(\text{NCCH}_3)_{10}][\text{BF}_4]_4$

A 10 mL solution containing 0.157 g (0.138 mmol) of $[\text{Bu}^n_4\text{N}]_3[\text{Mo}_2(\text{O}_2\text{CCH}_3)(\text{CN})_6]$ was added to a 10 mL solution containing 0.100 g (0.103 mmol) of $[\text{Rh}_2(\text{NCCH}_3)_{10}][\text{BF}_4]_4$ to give a black precipitate. The solid was collected by filtration, washed with CH_3CN (2 x 10 mL), and dried *in vacuo*; yield 0.093 g. IR (CsI, Nujol, cm^{-1}): 2325 (w), 2286 (w), 2249 (w), 2110 (s,br), 2042 (s,br), 1521 (w), 1030 (m), 972 (w), 679 (s), 621 (w), 473 (w).

(B). X-ray Crystallography

Structures were determined by application of general procedures fully described elsewhere.¹³ Crystallographic data for $[\text{Bu}^n_4\text{N}]_4[\text{Mo}_2(\text{CN})_8] \cdot 8\text{CHCl}_3$, (8) $\cdot 8\text{CHCl}_3$, $[\text{Bu}^n_4\text{N}]_3[\text{Mo}_2(\text{OCCH}_3)(\text{CN})_8]$, (9), and $[\text{Bu}^n_4\text{N}]_2[\text{Re}_2(\text{CN})_6(\text{dppm})_2] \cdot 8\text{CH}_2\text{Cl}_2$, (11) $\cdot 8\text{CH}_2\text{Cl}_2$ were collected on a Rigaku AFC6S diffractometer with monochromated $\text{MoK}\alpha$ ($\lambda_\alpha = 0.71069 \text{ \AA}$) radiation. All data were corrected for Lorentz and polarization effects. Calculations were performed on a VAXSTATION 4000 computer by using the Texsan crystallographic software package of Molecular Structure Corporation.¹⁴ Crystallographic data for the three compounds are compiled in Tables 16, 17, and 18.

(1) $[\text{Bu}^n_4\text{N}]_4[\text{Mo}_2(\text{CN})_8] \cdot 8\text{CHCl}_3$ (8) $\cdot 8\text{CHCl}_3$

(i) Data Collection and Reduction

Suitable crystals of $[\text{Bu}^n_4\text{N}]_4[\text{Mo}_2(\text{CN})_8] \cdot 8\text{CHCl}_3$ were grown by slow diffusion of hexanes into a CHCl_3 solution of the compound in a flame sealed 8 mm O.D. glass tube at 25°C . A blue crystal of approximate

Table 16. Summary of crystallographic data for
 $[\text{Bu}_4^n\text{N}]_4[\text{Mo}_2(\text{CN})_8] \cdot 8\text{CHCl}_3 (8) \cdot 8\text{CHCl}_3$.

formula	$\text{Mo}_2\text{C}_{80}\text{N}_{12}\text{Cl}_{24}\text{H}_{152}$
formula weight	2324.84
space group	Pbca (#61)
a, Å	20.526 (8)
b, Å	28.122 (5)
c, Å	19.855 (7)
α , deg	90
β , deg	90
γ , deg	90
V, Å ³	11461 (4)
Z	4
d_{calc} , g/cm ³	1.347
μ (Mo K α), cm ⁻¹	8.20
temperature, °C	-100
trans. factors, max., min.	1.00, 0.68
R ^a	0.082
R _w ^b	0.083
quality-of-fit indicator	4.03

$$^a R = \sum ||F_o| - |F_c|| / \sum |F_o|$$

$$^b R_w = [\sum w(|F_o| - |F_c|)^2 / \sum w |F_o|^2]^{1/2}; w = 1/\sigma^2(|F_o|)$$

$$^c \text{quality-of-fit} = [\sum w(|F_o| - |F_c|)^2 / (N_{\text{obs}} - N_{\text{parameters}})]^{1/2}$$

Table 17. Summary of crystallographic data for
[Bu₄ⁿN]₃[Mo₂(O₂CCH₃)(CN)₆] (9).

formula	Mo ₂ C ₅₆ N ₉ O ₂ H ₁₁₁
formula weight	1134.43
space group	P2 ₁ (#4)
a, Å	12.046 (3)
b, Å	16.05 (1)
c, Å	16.854 (3)
α, deg	90
β, deg	94.11 (2)
γ, deg	90
V, Å ³	3250 (2)
Z	2
d _{calc} , g/cm ³	1.159
μ (Mo Kα), cm ⁻¹	4.16
temperature, °C	-100
trans. factors, max., min.	1.00, 0.20
R ^a	0.067
R _w ^b	0.067
quality-of-fit indicator	2.89

$$^aR = \sum ||F_o| - |F_c|| / \sum |F_o|$$

$$^bR_w = [\sum w(|F_o| - |F_c|)^2 / \sum w |F_o|^2]^{1/2}; w = 1/\sigma^2(|F_o|)$$

$$^c\text{quality-of-fit} = [\sum w(|F_o| - |F_c|)^2 / (N_{\text{obs}} - N_{\text{parameters}})]^{1/2}$$

Table 18. Summary of crystallographic data for
 $[\text{Bu}_4^n\text{N}]_2[\text{Re}_2(\text{CN})_6(\text{dppm})_2] \cdot 8\text{CH}_2\text{Cl}_2$, (**11**) $\cdot 8\text{CH}_2\text{Cl}_2$

formula	$\text{Re}_2\text{Cl}_{16}\text{P}_4\text{C}_9\text{N}_8\text{H}_{132}$
formula weight	2461.70
space group	P-1 (#2)
a, Å	13.835 (2)
b, Å	18.172 (2)
c, Å	12.261 (1)
α , deg	106.788 (8)
β , deg	107.850 (9)
γ , deg	93.894 (9)
V, Å ³	2767.5 (6)
Z	1
d _{calc} , g/cm ³	1.477
μ (Mo K α), cm ⁻¹	27.06
temperature, °C	-100
trans. factors, max., min.	1.00, 0.64
R ^a	0.041
R _w ^b	0.045
quality-of-fit indicator	1.94

$$^a\text{R} = \Sigma ||F_o| - |F_c|| / \Sigma |F_o|$$

$$^b\text{R}_w = [\Sigma w(|F_o| - |F_c|)^2 / \Sigma w|F_o|^2]^{1/2}; w = 1/\sigma^2(|F_o|)$$

$$^c\text{quality-of-fit} = [\Sigma w(|F_o| - |F_c|)^2 / (N_{\text{obs}} - N_{\text{parameters}})]^{1/2}$$

dimensions $0.40 \times 0.50 \times 0.40 \text{ mm}^3$ was mounted on a glass fiber. Cell constants and an orientation matrix for data collection obtained from a least squares refinement using the setting angles of 25 carefully centered reflections in the range $15 \leq 2\theta \leq 24^\circ$ corresponded to an orthorhombic cell. A total of 10963 data were collected at $-100 \pm 1^\circ\text{C}$ using the ω -scan technique to a maximum 2θ value of 50° . The intensities of three representative reflections measured after every 150 reflections decreased by 6.1% thus a linear correction factor was applied to the data to account for this decay. A correction for secondary extinction was applied (coefficient = $0.19919\text{E-}07$).

(ii) Structure Solution and Refinement

The systematic absences in the data led to the space group Pbca. The structure was solved by MITHRIL¹⁵ and DIRDIF¹⁶ structure programs and refined by full matrix least-squares refinement. All non-hydrogen atoms were refined with anisotropic thermal parameters whereas hydrogen atoms were placed in calculated positions for the final stages of refinement. After isotropic convergence had been achieved, an empirical absorption correction was applied using the program DIFABS,¹⁷ which resulted in transmission factors ranging from 0.68 to 1.00. The final cycle of full matrix least-squares refinement included 4972 observed reflections with $F_o^2 > 3\sigma(F_o^2)$ and 533 variable parameters to give $R = 0.082$ and $R_w = 0.083$ and a quality-of-fit index of 4.03.

(2) $[\text{Bu}^n_4\text{N}]_3[\text{Mo}_2(\text{O}_2\text{CCH}_3)(\text{CN})_6]$ (9)

(i) Data Collection and Reduction

Large red-purple crystals of $[\text{Bu}^n_4\text{N}]_3[\text{Mo}_2(\text{O}_2\text{CCH}_3)(\text{CN})_6]$ were grown by slow diffusion of diethyl ether into a CH_2Cl_2 solution of the compound in a flame sealed 8 mm O.D. glass tube at room temperature.

A crystal of approximate dimensions $0.72 \times 0.23 \times 0.47 \text{ mm}^3$ was mounted on the tip of a glass fiber and secured with silicone grease. Cell constants and an orientation matrix for data collection, obtained from a least squares refinement using the setting angles of 16 carefully centered reflections in the range $20 \leq 2\theta \leq 27^\circ$, corresponded to a monoclinic cell. A total of 6240 reflections were measured at $-100 \pm 1^\circ\text{C}$ to a maximum 2θ value of 50° using the ω - 2θ scan technique. The crystal diffracted poorly due to a large mosaic spread and only 3108 unique reflections were of the intensity $F_o^2 > 3\sigma(F_o^2)$. Three check reflections measured every 200 data points declined by 1.3 % which was accounted for by a linear correction factor. A correction for secondary extinction was also applied (coefficient = $0.13791\text{E-}06$).

(ii) Structure Solution and Refinement

The space group $P2_1$ was selected on the basis of systematic absences. The unique Mo atom was located by SHELX-S86¹⁸ and the remaining atoms were established by DIRDIF¹⁶ structure programs and refined by full matrix least-squares refinement. After all non-hydrogen atoms had been refined isotropically, an empirical absorption correction was applied using the program DIFABS.¹⁷ Hydrogen atoms were included in the refinement in calculated positions. The final cycle of full matrix least-squares refinement was based on 3108 observed reflections with $F_o^2 > 3\sigma(F_o^2)$ and 497 variables to give $R = 0.067$ and $R_w = 0.067$ and a quality-of-fit index of 2.89. Both enantiomorphs were refined and the difference in R values led to a 99% level of confidence by the Hamilton significance test, favoring the assignment of the original enantiomorph.

(3) [Buⁿ₄N]₂[Re₂(CN)₆(dppm)₂]·8CH₂Cl₂ (11)·8CH₂Cl₂**(i) Data Collection and Reduction**

Suitable crystals of [Buⁿ₄N]₂[Re₂(CN)₆(dppm)₂]·8CH₂Cl₂ were obtained by slowly cooling a saturated CH₂Cl₂ solution of the compound. A crystal of approximate dimensions 0.52 x 0.26 x 0.16 mm³ was mounted on the end of a glass fiber with the aid of silicone grease. A least squares refinement using the setting angles of 19 carefully centered reflections in the range $20 \leq 2\theta \leq 30^\circ$ gave cell constants that correspond to a triclinic crystal system. A total of 10184 data were collected at a temperature of $-100 \pm 1^\circ\text{C}$ using the ω - 2θ scan technique in the range $7 \leq 2\theta \leq 50^\circ$ and were corrected for secondary extinction (coefficient = 0.86499E-07). The intensities of three representative reflections which were measured after every 150 reflections decayed by only 0.25%. An absorption correction based on three ψ -curves with a χ value near 90° were used as the basis for an absorption correction and resulted in transmission factors ranging from 0.64 to 1.00.

(ii) Structure Solution and Refinement

The structure was solved by MITHRIL¹⁵ and DIRDIF¹⁶ structure programs and refined by full matrix least-squares refinement. All non-hydrogen atoms were refined with anisotropic thermal parameters with the exception of atoms in the CH₂Cl₂ interstitial solvent; hydrogen atoms were included in calculated positions. The final cycle of full matrix least-squares refinement was based on 7767 observed reflections with $F_o^2 > 3\sigma(F_o^2)$ and 801 variable parameters to give $R = 0.041$ and $R_w = 0.045$ and a quality-of-fit index of 1.94.

3. Results and Discussion

A. Preparation of Cyanide Compounds from Carboxylate and Chloride Compounds.

(1) Preparation of Dimolybdenum-cyanide Complexes.

In spite of the rich chemistry involving the cyanide ligand,³ the preparation of low valent cyanide complexes with metals that form strong M-M interactions has not been pursued to any great extent. With the exception of $[\text{Et}_4\text{N}]_4[\text{Mo}_2(\text{CN})_8]$, formulated on the basis of IR and elemental data,¹⁹ there are no reports of homoleptic dinuclear cyanide compounds in the literature to our knowledge. We wondered if the lack of activity in this area was due to the fact that metal-metal bond chemistry is typically performed in non-aqueous solvents whereas classical cyanide chemistry is carried out under aqueous conditions or in liquid ammonia. To test this assumption, we set out to synthesize cyanide and mixed ligand cyanide compounds beginning with dinuclear starting materials. Initially, reactions between dimolybdenum tetracarboxylates and Me_3SiCN led to black solids and oils that exhibited $\nu(\text{C}\equiv\text{N})$ bands ranging from 2140 to 1970 cm^{-1} . Subsequently, reactions of $\text{Mo}_2(\text{O}_2\text{CR})_4$ ($\text{R} = \text{CH}_3$, or CF_3) with $[\text{R}_4\text{N}]\text{CN}$ ($\text{R} = \text{Et}$, Bu^n) were found to proceed rapidly in organic media to give $[\text{Bu}^n_4\text{N}]_4[\text{Mo}_2(\text{CN})_8] \cdot 8\text{CHCl}_3$ (8) and $[\text{Bu}^n_4\text{N}]_3[\text{Mo}_2(\text{O}_2\text{CCH}_3)(\text{CN})_6]$ (9). Chemistry of $\text{Mo}_2(\text{O}_2\text{CR})_4$ ($\text{R} = \text{CH}_3$, or CF_3) with eight equivalents of $[\text{Bu}^n_4\text{N}]\text{CN}$ or $[\text{Et}_4\text{N}]\text{CN}$ in CH_2Cl_2 produces the blue octacyanide anion $[\text{Mo}_2(\text{CN})_8]^{4-}$, with the highest yield obtained from $[\text{Et}_4\text{N}]\text{CN}$ and $\text{Mo}_2(\text{O}_2\text{CCH}_3)_4$. Substitutions involving $[\text{Bu}^n_4\text{N}]\text{CN}$ are less desirable, as these reactions invariably lead to intractable oily products contaminated with the purple intermediate $[\text{Bu}^n_4\text{N}]_3[\text{Mo}_2(\text{O}_2\text{CCH}_3)(\text{CN})_6]$, (9). The anion in (9),

$[\text{Mo}_2(\text{O}_2\text{CCH}_3)(\text{CN})_6]^{3-}$, was rationally prepared by reaction of six equivalents of $[\text{Bu}^n_4\text{N}]\text{CN}$ with $\text{Mo}_2(\text{O}_2\text{CCH}_3)_4$ in THF and subsequently converted to $[\text{Mo}_2(\text{CN})_8]^{4-}$ by addition of $[\text{Bu}^n_4\text{N}]\text{CN}$ to a solution of the compound in CH_2Cl_2 . The final product is difficult to isolate as the $[\text{Bu}^n_4\text{N}]^+$ salt, but it can be precipitated as $[\text{Et}_4\text{N}]_4[\text{Mo}_2(\text{CN})_8]$ when treated with $[\text{Et}_4\text{N}]\text{Cl}$. Attempts to prepare the mono- or bis-substituted anions $[\text{Mo}_2(\text{O}_2\text{CCH}_3)_3(\text{CN})_2]^-$ and $[\text{Mo}_2(\text{O}_2\text{CCH}_3)_2(\text{CN})_4]^{2-}$ by an analogous procedure produced only mixtures of $[\text{Bu}^n_4\text{N}]_3[\text{Mo}_2(\text{O}_2\text{CCH}_3)(\text{CN})_6]$ and $\text{Mo}_2(\text{O}_2\text{CCH}_3)_4$ as judged by NMR spectroscopic monitoring of reactions performed in deuterated solvents. Attempts at synthesizing $\text{Mo}_2(\text{CN})_4(\text{PR}_3)_4$ compounds using similar synthetic procedures as in the syntheses of $\text{Mo}_2\text{Cl}_4(\text{PR}_3)_4$ compounds have so far led to only to samples of $[\text{Mo}_2(\text{CN})_8]^{4-}$.²⁰

(2) Preparation of $[\text{Bu}^n_4\text{N}]_2[\text{Re}_2(\text{CN})_6(\text{dppm})_2]$ (11).

As part of the generality of our approach, we sought to demonstrate that Cl^- ligands of multiply-bonded compounds also readily exchange with CN^- in non-aqueous solvents. The reaction of purple $\text{Re}_2\text{Cl}_4(\text{dppm})_2$ with excess CN^- in toluene or CH_2Cl_2 proceeds at ambient temperatures with precipitation of green $[\text{Bu}^n_4\text{N}]_2[\text{Re}_2(\text{CN})_6(\text{dppm})_2]$ (11), the first example of a M-M bonded anion of the type $[\text{M}_2\text{L}_{10}]^{2-}$. No evidence for the formation of partially substituted compounds or the simple adduct $[\text{Re}_2\text{Cl}_4(\text{CN})_2(\text{dppm})_2]^{2-}$ was observed. $[\text{Re}_2(\text{CN})_6(\text{dppm})_2]^{2-}$ is quite stable in air, and, indeed, is inert to CO under prolonged reflux conditions in CH_2Cl_2 , further underscoring the stability of this dinuclear unit supported by six cyanide ligands.

B. Spectroscopy

The electronic spectra of $[\text{Mo}_2(\text{CN})_8]^{4-}$ and $[\text{Mo}_2(\text{O}_2\text{CCH}_3)(\text{CN})_6]^{3-}$ exhibit transitions in the visible region characteristic of $\delta \rightarrow \delta^*$ transitions at λ_{max} values of 601 and 557 nm respectively. The value for the octacyanide complex is considerably lower in energy than the corresponding transitions in homoleptic quadruply bonded Mo_2^{4+} compounds with halide ligands, e.g. $[\text{Mo}_2\text{Cl}_8]^{4-}$ exhibits a $\delta \rightarrow \delta^*$ transition at 530 nm.²¹ Clearly the energy separation of the δ and δ^* molecular orbitals is considerably smaller in the presence of cyanide ligands acting as strong donors. The infrared spectrum of $[\text{Bu}^n_4\text{N}]_4[\text{Mo}_2(\text{CN})_8]$ reveals two $\nu(\text{C}\equiv\text{N})$ stretches at 2095 cm^{-1} and 2103 cm^{-1} in the solid state and one stretch at 2096 cm^{-1} in CH_2Cl_2 solution. Two bands, $a_{2u} + e_u$, are expected in the absence of solid-state splitting effects for a molecule of D_{4h} symmetry, and the $I_{e_u}/I_{a_{2u}}$ is approximately 8.4 based on $(1/2)\tan^2(\theta)$, where θ is the C-Mo-Mo angle (103.7 ave.).²² The high energies of the cyanide stretches indicate that the cyanide groups are acting as strong donors and not as π -acceptors. The anion $[\text{Mo}_2(\text{O}_2\text{CCH}_3)(\text{CN})_6]^{3-}$ exhibits $\nu(\text{C}\equiv\text{N})$ stretches at 2099 and 2105 cm^{-1} for two distinct types of $\text{C}\equiv\text{N}$ in a C_{2v} symmetry environment. As in $[\text{Mo}_2(\text{CN})_8]^{4-}$, these stretching frequencies are higher than free CN^- for which $\nu(\text{C}\equiv\text{N})$ occurs at 2050 cm^{-1} in $[\text{Bu}^n_4\text{N}]\text{CN}$. The ^1H NMR spectrum of $[\text{Bu}^n_4\text{N}]_4[\text{Mo}_2(\text{CN})_8]$ in CD_2Cl_2 displays only resonances at $\delta = 0.98, 1.49, 1.72, 3.42\text{ ppm}$ (3:2:2:2 integration) for the butyl substituents of the $[\text{Bu}^n_4\text{N}]^+$ groups. When $\text{Mo}_2(\text{O}_2\text{CCF}_3)_4$ is used in synthesis of $[\text{Et}_4\text{N}]_4[\text{Mo}_2(\text{CN})_8]$, ^{19}F NMR is useful in determining the complete loss of the $\text{O}_2\text{C-C-F}_3^-$ groups. For $[\text{Bu}^n_4\text{N}]_3[\text{Mo}_2(\text{O}_2\text{CCH}_3)(\text{CN})_6]$, the ^1H NMR spectrum in CDCl_3 exhibits a singlet at $\delta = 2.60\text{ ppm}$ for the methyl group of $(\mu\text{-O}_2\text{CCH}_3)$ in addition to

the $[\text{Bu}^n_4\text{N}]^+$ resonances at $\delta = 0.92, 1.47, 1.68, 3.36$ ppm (3:2:2:2 integration).

$[\text{Bu}^n_4\text{N}]_2[\text{Re}_2(\text{CN})_6(\text{dppm})_2]$, (**11**), displays $\nu(\text{C}\equiv\text{N})$ stretches indicative of terminal (2097 and 2081 cm^{-1}) and bridging cyanide ligands (1935 cm^{-1}). The compound exhibits very low solubility in nearly all solvents except acetonitrile, in which it is sufficiently soluble to allow for solution measurements. A $^{31}\text{P}\{^1\text{H}\}$ spectrum of (**11**) recorded in CD_3CN at 22 $^\circ\text{C}$ relative to 85% H_3PO_4 contained a singlet at -11.39 ppm which is in the range of chemical shifts observed for Re_2^{4+} complexes containing *trans* dppm ligands.²⁴ ^1H NMR spectral properties of the anion are typical for symmetrical bis-dppm complexes of $\text{Re}(\text{II})$; (^1H NMR, CD_3CN , 22 $^\circ\text{C}$, 300 MHz): δ 7.48 (mult, 16H, Ph); 6.96 (mult, 24H, Ph); 5.44 (s, 16H, CH_2Cl_2); 3.30 (pentet, 4H, $-\text{CH}_2-$). The pentet for the methylene bridgehead group arises from four equivalent methylene protons undergoing virtual coupling with four equivalent P nuclei ($J(\text{P-H}) = 3.9$ Hz). Electronic d-d transitions for $[\text{Re}_2(\text{CN})_6(\text{dppm})_2]^{2-}$ occur at 969 and 694 with ϵ values in the $1\text{-}2 \times 10^2$ range. Since no other unambiguous examples of an Re_2^{4+} unit in an edge-sharing bioctahedral (ESBO) geometry exist, these transitions cannot be assigned on the basis of analogous systems. Electrochemical studies of (**11**) in CH_3CN revealed that the anion does not undergo any redox processes in the range +1.8 to -1.8 V vs Ag/AgCl. In contrast, Re_2^{4+} complexes of the M_2L_8 type ($\sigma^2\pi^4\delta^2\delta^{*2}$) exhibit two reversible or quasi-reversible oxidations corresponding to loss of the δ^* electrons.^{23,24} The situation is quite different in the present case, however, as the orbital overlap scheme of an ESBO compound places the last two electrons in a π^* level

$(\sigma^2\pi^2(\delta\delta^*)^4\pi^*2)$. There is, therefore, no justification for correlating the redox properties of the two different geometries.

C. Molecular Structures

(1) Crystal structure of $[\text{Bu}^n_4\text{N}]_4[\text{Mo}_2(\text{CN})_8] \cdot 8\text{CHCl}_3$, (8) $\cdot 8\text{CHCl}_3$.

The structure of $[\text{Bu}^n_4\text{N}]_4[\text{Mo}_2(\text{CN})_8] \cdot 8\text{CHCl}_3$ constitutes the first crystallographically determined dinuclear homoleptic cyanide complex. An ORTEP diagram of the molecular anion is depicted in Figure 26. A list of selected bond distances and angles for the compound is given in Table 19. This anion constitutes an important example of an unsupported metal-metal quadruple bond in the presence of π -acceptor ligands. For comparative purposes, the Mo-Mo distances of unsupported homoleptic dimolybdenum compounds are listed in Table 20 along with those of compounds (8) and (9). Among the unbridged compounds, $[\text{Mo}_2(\text{CN})_8]^{4-}$, (8), possesses the shortest M-M interaction, a rather surprising finding, as π -acceptor CN^- ligands would be expected to produce the opposite effect. As the infrared data in the $\nu(\text{C}\equiv\text{N})$ indicated, the ligands in compound (8) appear to be serving purely as donors for the Mo_2^{4+} core, thereby increasing the electron density at the metal centers and therefore M-M overlap. Other important metric parameters are $\text{Mo}-\text{C}_{\text{av}} = 2.21 \text{ \AA}$, $\text{C}-\text{N}_{\text{av}} = 1.14 \text{ \AA}$, $\angle\text{Mo}-\text{Mo}-\text{C}_{\text{av}} = 103.7^\circ$ and $\angle\text{Mo}-\text{C}-\text{N}_{\text{av}} = 174^\circ$; all are within expected ranges.

(2) Crystal structure of $[\text{Bu}^n_4\text{N}]_3[\text{Mo}_2(\text{O}_2\text{CCH}_3)(\text{CN})_6]$ (9).

The structure of $[\text{Bu}^n_4\text{N}]_3[\text{Mo}_2(\text{O}_2\text{CCH}_3)(\text{CN})_6]$ is unusual in that the anion possesses only one bridging acetate group, a situation that is rarely encountered.²⁹ As the ORTEP in Figure 27 clearly shows, the molecular anion approximates an eclipsed M_2L_8 unit with a torsion angle $\chi = 3.5 [7]^\circ$. The Mo-Mo bond distance of $2.114(2) \text{ \AA}$ is shorter by

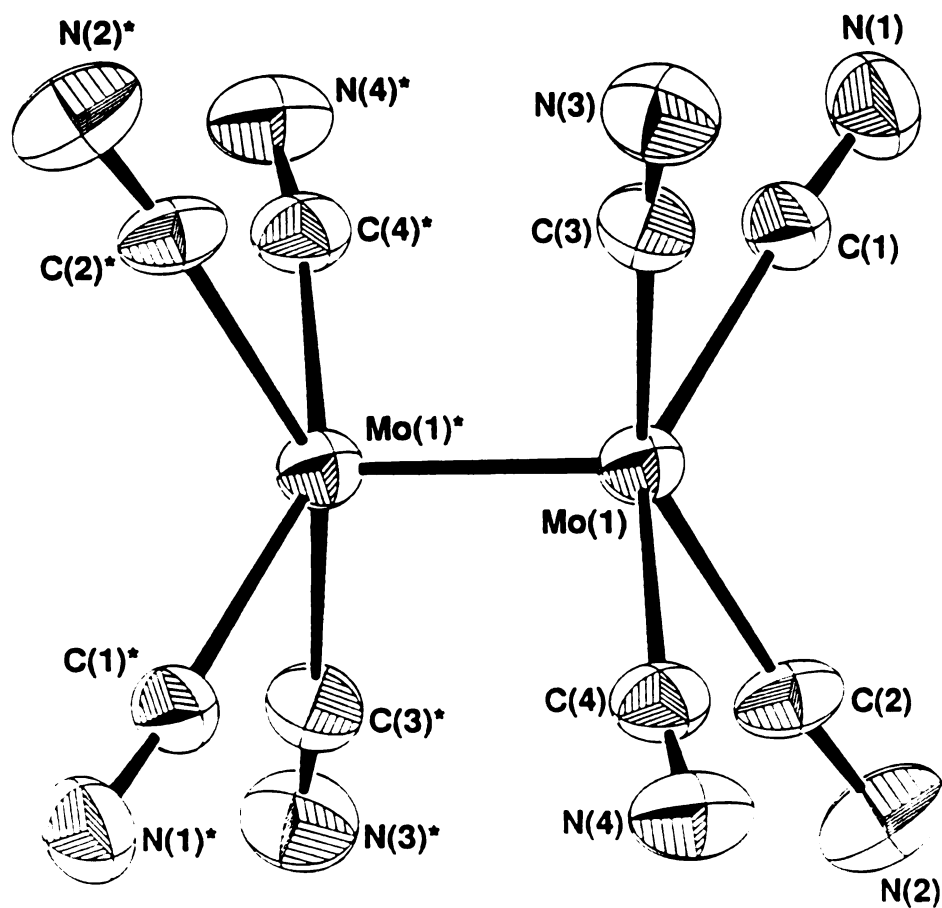


Figure 26. ORTEP depiction of the molecular anion $[\text{Mo}_2(\text{CN})_8]^{4-}$ with atoms represented by their 50% probability ellipsoids.

Table 19. Selected Bond Distances (Å) and Bond Angles (°) for $[\text{Bu}^n_4\text{N}]_4[\text{Mo}_2(\text{CN})_8] \cdot 8\text{CHCl}_3$

distances		
atom 1	atom 2	distance
Mo(1)	Mo(1)*	2.122 (2)
Mo(1)	C(1)	2.19 (1)
Mo(1)	C(2)	2.19 (1)
Mo(1)	C(3)	2.21 (1)
Mo(1)	C(4)	2.23 (1)
N(1)	C(1)	1.14 (1)
N(2)	C(2)	1.15 (1)
N(3)	C(3)	1.14 (1)
N(4)	C(4)	1.12 (1)

angles							
atom 1	atom 2	atom 3	angle	atom 1	atom 2	atom 3	angle
Mo(1)*	Mo(1)	C(1)	103.4 (3)	C(2)	Mo(1)	C(3)	153.6 (4)
Mo(1)*	Mo(1)	C(2)	102.0 (3)	C(2)	Mo(1)	C(4)	87.3 (4)
Mo(1)*	Mo(1)	C(3)	104.4 (3)	C(3)	Mo(1)	C(4)	85.9 (4)
Mo(1)*	Mo(1)	C(4)	105.0 (3)	Mo(1)	C(1)	N(1)	175 (1)
C(1)	Mo(1)	C(2)	87.4 (4)	Mo(1)	C(2)	N(2)	174 (1)
C(1)	Mo(1)	C(3)	86.6 (4)	Mo(1)	C(3)	N(3)	175 (1)
C(1)	Mo(1)	C(4)	151.6 (4)	Mo(1)	C(4)	N(4)	173 (1)

Table 20. Comparison of the Mo-Mo bond distances of selected quadruply bonded dimolybdenum complexes.

Compound	Mo-Mo distance Å	reference
[Bu ⁿ ₄ N] ₄ [Mo ₂ (CN) ₈]·8CHCl ₃	2.122 (2)	this work
K ₄ Mo ₂ Cl ₈	2.139 (4)	13
[NH ₄] ₄ [Mo ₂ (NCS) ₈]·4H ₂ O	2.162 (1)	6(a)
[Mo ₂ (MeCN) ₁₀][BF ₄] ₄ ·2MeCN	2.187 (1)	5
[Bu ⁿ ₄ N] ₄ [Mo ₂ (CN) ₈]·8CHCl ₃	2.114 (2)	this work
Mo ₂ (O ₂ CCH ₃) ₄	2.0934 (8)	15

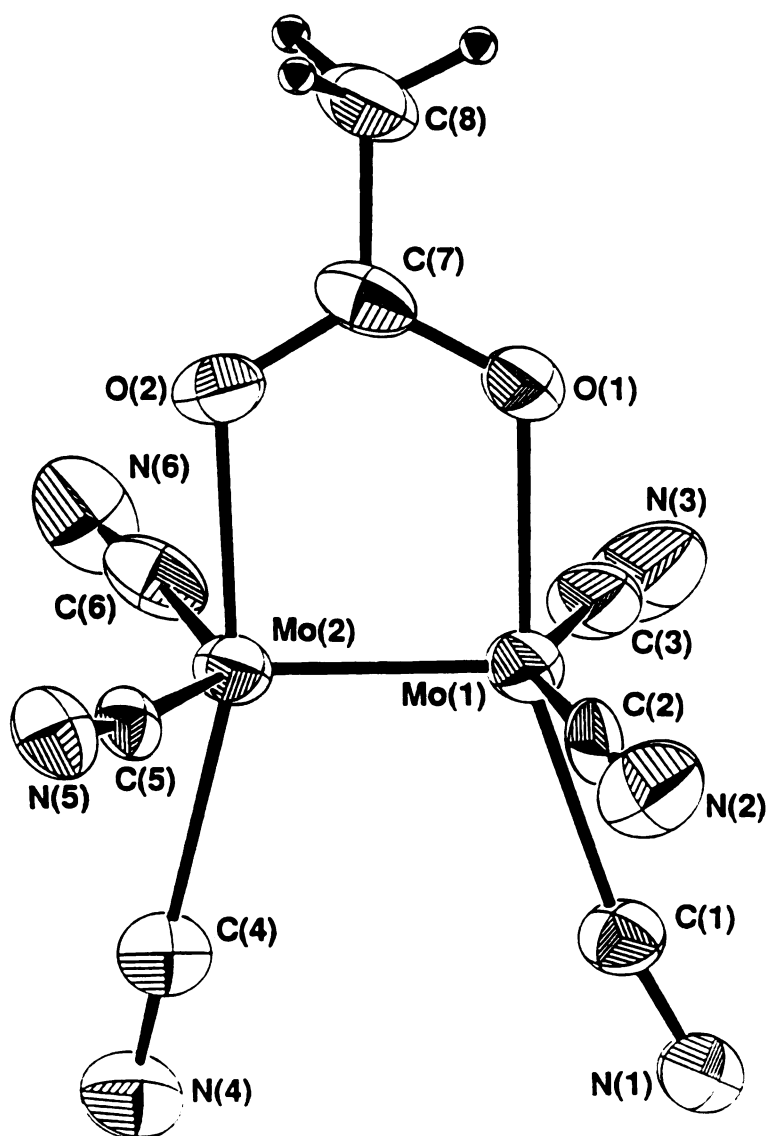


Figure 27. Molecular structure of [Mo₂(O₂CCH₃)(CN)₆]³⁻ with the atom labeling scheme. With the exception of the H atoms, the atoms are represented by their 50% probability ellipsoids.

~ 0.08 Å than that in $[\text{Mo}_2(\text{CN})_8]^{4-}$, but slightly longer than the corresponding distance in $\text{Mo}_2(\text{O}_2\text{CCH}_3)_4$. The $\text{C}\equiv\text{N}$ bond distances in (9), none of which are related by crystallographic symmetry, vary from 1.09 Å to 1.19 Å. These differences are ascribed to packing influences of the anion with the tetrabutylammonium cations, as evidenced by close contacts (2.4 - 2.8 Å) between two $[\text{Bu}^n_4\text{N}]^+$ cations and the N atoms of several cyanide ligands. Important bond distances and angles for (9) are provided in Table 21.

(3) Crystal structure of $[\text{Bu}^n_4\text{N}]_2[\text{Re}_2(\text{CN})_6(\text{dppm})_2]\cdot 8\text{CH}_2\text{Cl}_2$, (11) $\cdot 8\text{CH}_2\text{Cl}_2$

The single crystal X-ray structure of $[\text{Bu}^n_4\text{N}]_2[\text{Re}_2(\text{CN})_6(\text{dppm})_2]\cdot 8\text{CH}_2\text{Cl}_2$ is quite unusual for several reasons. Firstly, it is the only example of an edge-sharing compound that clearly falls into the category of a $\text{Re}_2^{\text{II,II}}$ rather than a $\text{Re}_2^{\text{III,III}}$ species, secondly the anion $[\text{Re}_2(\text{CN})_6(\text{dppm})_2]^{2-}$ is the first $[\text{M}_2\text{L}_{10}]^{2-}$ species to be reported, and thirdly it contains a very rare mode of coordination for the cyanide ligand. The full ORTEP is depicted in Figure 28, and a skeletal viewpoint of the equatorial plane is provided in Figure 29. Selected bond distances and angles are provided in Table 22. The drawing in Figure 29 clearly shows that the four terminal cyanide and two bridging cyanide ligands are arranged in a pseudo-edge sharing bioctahedral arrangement. The bridging cyanide ions are bound to the Re-Re unit in an η^2 fashion consisting of a σ bond between C(1) and Re(1) and a π -interaction between the $\text{C}(1)\equiv\text{N}(1)$ moiety and $\text{Re}(1)^*$. This type of situation has been crystallographically documented in only one previous instance, namely in the dimolybdenum complex $[\text{Bu}^n_4\text{N}][\text{Cp}_2\text{Mo}_2(\text{CO})_4(\text{CN})]$.^{4(a)} This asymmetrical bridging CN mode has been documented in the complexes

Table 21. Selected Bond Distances (Å) and Bond Angles (°) for [Buⁿ₄N]₃[Mo₂(O₂CCH₃)(CN)₆]

distances					
atom 1	atom 2	distance	atom 1	atom 2	distance
Mo(1)	Mo(2)	2.114 (2)	O(1)	C(7)	1.29 (2)
Mo(1)	O(1)	2.13 (1)	O(2)	C(7)	1.26 (2)
Mo(1)	C(1)	2.16 (2)	N(1)	C(1)	1.16 (2)
Mo(1)	C(2)	2.23 (3)	N(2)	C(2)	1.13 (3)
Mo(1)	C(3)	2.21 (2)	N(3)	C(3)	1.11 (2)
Mo(2)	O(2)	2.13 (1)	N(4)	C(4)	1.09 (2)
Mo(2)	C(4)	2.22 (2)	N(5)	C(5)	1.16 (2)
Mo(2)	C(5)	2.17 (2)	N(6)	C(6)	1.19 (2)
Mo(2)	C(6)	2.14 (2)	C(7)	C(8)	1.49 (3)

Table 21. (cont'd)

angles							
atom 1	atom 2	atom 3	angle	atom 1	atom 2	atom 3	angle
Mo(2)	Mo(1)	O(1)	91.3 (4)	O(2)	Mo(2)	C(6)	84.4 (6)
Mo(2)	Mo(1)	C(1)	107.3 (5)	C(4)	Mo(2)	C(5)	89.7 (7)
Mo(2)	Mo(1)	C(2)	104.5 (5)	C(4)	Mo(2)	C(6)	89.8 (8)
Mo(2)	Mo(1)	C(3)	101.5 (6)	C(5)	Mo(2)	C(6)	143.7 (7)
O(1)	Mo(1)	C(1)	161.4 (6)	Mo(1)	O(1)	C(7)	118 (1)
O(1)	Mo(1)	C(2)	91.9 (7)	Mo(2)	O(2)	C(7)	119 (1)
O(1)	Mo(1)	C(3)	89.8 (6)	Mo(1)	C(1)	N(1)	169 (2)
C(1)	Mo(1)	C(2)	84.6 (7)	Mo(1)	C(2)	N(2)	170 (2)
C(1)	Mo(1)	C(3)	85.5 (6)	Mo(1)	C(3)	N(3)	174 (2)
C(2)	Mo(1)	C(3)	153.9 (7)	Mo(2)	C(4)	N(4)	179 (2)
Mo(1)	Mo(2)	O(2)	91.1 (4)	Mo(2)	C(5)	N(5)	170 (1)
Mo(1)	Mo(2)	C(4)	104.5 (6)	Mo(2)	C(6)	N(6)	169 (2)
Mo(1)	Mo(2)	C(5)	108.7 (5)	O(1)	C(7)	O(2)	119 (2)
Mo(1)	Mo(2)	C(6)	106.5 (6)	O(1)	C(7)	C(8)	117 (2)
O(2)	Mo(2)	C(4)	164.4 (7)	O(2)	C(7)	C(8)	123 (2)
O(2)	Mo(2)	C(5)	86.4 (5)				

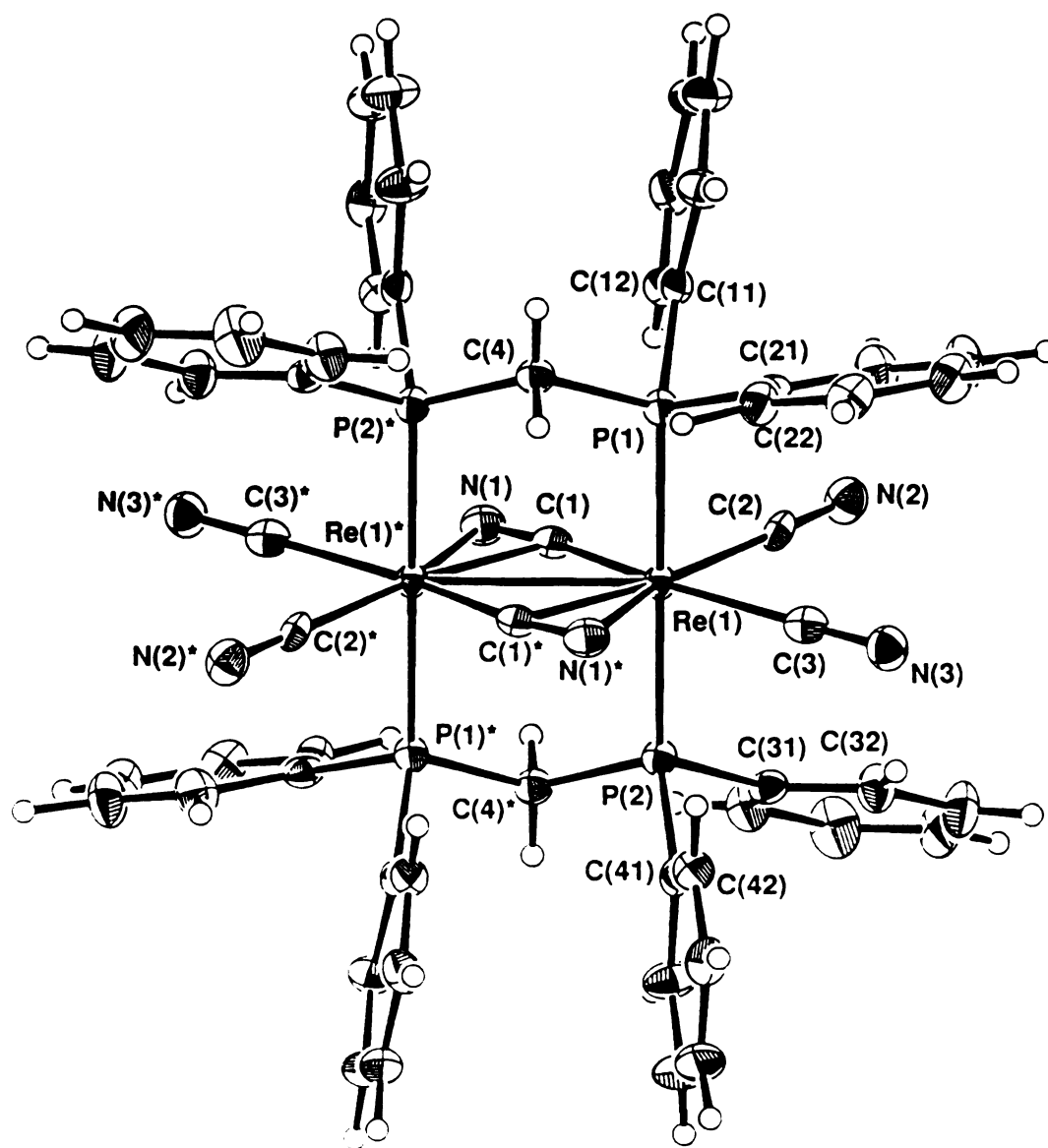


Figure 28. ORTEP plot of a molecule of [Re₂(CN)₆(dppm)₂]²⁻ with non-hydrogen atoms represented by their 50% probability ellipsoids.

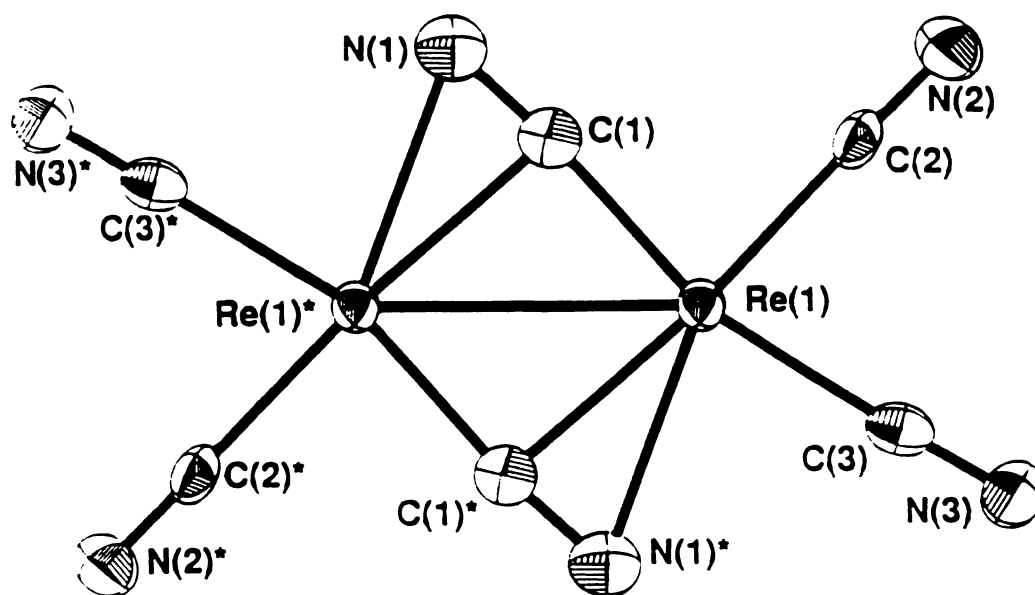


Figure 29. View looking down on the equatorial plane of the anion $[\text{Re}_2(\text{CN})_6(\text{dppm})_2]^{2-}$ emphasizing the unsymmetrical arrangement of the bridging CN group.

Table 22. Selected Bond Distances (Å) and Bond Angles (°) for [Buⁿ₄N]₂[Re₂(CN)₆(dppm)₂]·8CH₂Cl₂.

distances					
atom 1	atom 2	distance	atom 1	atom 2	distance
Re(1)*	Re(1)	3.0505 (6)	P(1)	C(11)	1.834 (6)
Re(1)	P(1)	2.369 (2)	P(1)	C(21)	1.819 (7)
Re(1)	P(2)	2.379 (2)	P(2)	C(4)*	1.838 (7)
Re(1)	N(1)*	2.486 (6)	P(2)	C(31)	1.834 (6)
Re(1)	C(1)	2.002 (7)	P(2)	C(41)	1.830 (7)
Re(1)	C(1)*	2.311 (6)	N(1)	C(1)	1.177 (8)
Re(1)	C(2)	2.070 (7)	N(2)	C(2)	1.155 (8)
Re(1)	C(3)	2.105 (7)	N(3)	C(3)	1.161 (8)
P(1)	C(4)	1.836 (7)			

Table 22. (cont'd)

angles							
atom 1	atom 2	atom 3	angle	atom 1	atom 2	atom 3	angle
Re(1)*	Re(1)	P(1)	89.90 (4)	C(2)	Re(1)	C(3)	79.3 (2)
Re(1)*	Re(1)	P(2)	90.08 (4)	Re(1)	P(1)	C(4)	113.6 (2)
Re(1)*	Re(1)	C(1)	49.3 (2)	Re(1)	P(1)	C(11)	122.6 (2)
Re(1)*	Re(1)	C(1)*	41.0 (2)	Re(1)	P(1)	C(21)	112.5 (2)
Re(1)*	Re(1)	C(2)	133.8 (2)	C(4)	P(1)	C(11)	101.3 (3)
Re(1)*	Re(1)	C(3)	146.9 (2)	C(4)	P(1)	C(21)	103.4 (3)
P(1)	Re(1)	P(2)	179.56 (6)	C(11)	P(1)	C(21)	101.1 (3)
P(1)	Re(1)	C(1)	93.5 (2)	Re(1)	P(2)	C(4)*	112.9 (2)
P(1)	Re(1)	C(1)*	86.9 (2)	Re(1)	P(2)	C(31)	116.2 (2)
P(1)	Re(1)	C(2)	88.5 (2)	Re(1)	P(2)	C(41)	120.2 (2)
P(1)	Re(1)	C(3)	91.9 (2)	C(4)*	P(2)	C(31)	102.0 (3)
P(2)	Re(1)	C(1)	86.8 (2)	C(4)*	P(2)	C(41)	103.6 (3)
P(2)	Re(1)	C(1)*	92.8 (2)	C(31)	P(2)	C(41)	99.2 (3)
P(2)	Re(1)	C(2)	91.9 (2)	Re(1)	C(1)	Re(1)*	89.7 (2)
P(2)	Re(1)	C(3)	87.9 (2)	Re(1)	C(1)	N(1)	173.4 (6)
C(1)	Re(1)	C(1)*	90.3 (2)	Re(1)	C(1)*	N(1)*	84.2 (4)
C(1)	Re(1)	C(2)	84.8 (2)	Re(1)	C(2)	N(2)	178.1 (6)
C(1)	Re(1)	C(3)	163.0 (2)	Re(1)	C(3)	N(3)	178.2 (6)
C(1)*	Re(1)	C(2)	173.0 (2)	P(1)	C(4)	P(2)*	112.3 (3)
C(1)*	Re(1)	C(3)	106.1 (2)				

$[\text{Rh}_2(\mu\text{-CN})(\mu\text{-CO})(\text{CO})_2(\text{dppm})_2]\text{ClO}_4$ and $[\text{Mn}_2\text{H}(\mu\text{-CN})(\text{CO})_4(\text{dppm})_2]$ but full structural details were not available.^{4(b),(c)} In the Mo structure, however, a disorder associated with the bridging cyanide precluded the reliable determination of bond distances and angles associated with this unusual mode of CN^- binding. The bridging angle $\angle\text{Re}(1)\text{-C}(1)\text{-N}(1)$ is $173.4(6)^\circ$ in $[\text{Re}_2(\text{CN})_6(\text{dppm})_2]^{2-}$ compared to the angle $\angle\text{Mo-C-N}_{\text{bridge}} = 170^\circ$ in $[\text{Cp}_2\text{Mo}_2(\text{CO})_4(\text{CN})]^-$. Other salient features in (11) are $\text{Re}(1)\text{-C}(1) = 2.002(7) \text{ \AA}$, $\text{Re}(1)^*\text{-C}(1) = 2.311(6)$, $\text{Re}(1)^*\text{-N}(1) = 2.486(6) \text{ \AA}$, and $\text{C}(1)\text{-N}(1) = 2.177(8) \text{ \AA}$. It is interesting to note that the unstable phosphorous analog of the $\text{C}\equiv\text{N}^-$ ligand, $\text{C}\equiv\text{P}^-$, has recently been documented as a bridging moiety in the complex $(\text{Cl})(\text{PEt}_3)_2\text{Pt}(\mu\text{-C}\equiv\text{P})\text{Pt}(\text{PEt}_3)_2$.³¹ There are major differences in the present example and the Pt case, however, as the $\text{C}\equiv\text{P}^-$ ligand does not span a M-M bonding interaction and the Pt-C-P angle (144.0°) is bent, unlike the Re-C-N angle, (173.4°). The Re-Re distance in $[\text{Re}_2(\text{CN})_6(\text{dppm})_2]^{2-}$ of $3.0505(6) \text{ \AA}$ is in accord with a Re-Re single bond ($\sigma^2\pi^2(\delta^2\delta^{*2})\pi^{*2}$); magnetic and NMR data are in perfect agreement with this assignment (vide supra).

D. Reactivity of $\text{Mo}_2(\text{CN})_8^{4-}$ towards solvated metal cations.

Reactions of $[\text{Et}_4\text{N}]_4[\text{Mo}_2(\text{CN})_8]$ with the solvated metal cations $[\text{Fe}(\text{NCCH}_3)_6][\text{BF}_4]_2$, $[\text{Rh}_2(\text{NCCH}_3)_{10}][\text{BF}_4]_4$, and $[\text{Re}_2(\text{NCCH}_3)_{10}][\text{BF}_4]_4$ in the appropriate ratios result in the formation of insoluble solids that are believed to be polymeric. Infrared spectra of these products show the presence of $\nu(\text{C}\equiv\text{N})$ bands, listed in Table 23, attributed to coordinated CH_3CN (*ca.* 2300 cm^{-1}) and CN^- (*ca.* 2100 cm^{-1}) ligands. The $\nu(\text{C}\equiv\text{N})$ bands that occur for the CN^- ligand are shifted to slightly higher energies as compared to 2095 cm^{-1} exhibited in the spectrum of $[\text{Et}_4\text{N}]_4[\text{Mo}_2(\text{CN})_8]$ which is expected in bridging cyano complexes.^{3(d)} Thermogravimetric

Table 23. Comparison of $\nu(\text{C}\equiv\text{N})$ bands for mixed metal cyanide materials prepared in this study

Compound	$\nu(\text{C}\equiv\text{N})$ band
$[\text{Rh}_2\text{Mo}_2(\text{CN})_8(\text{MeCN})_x]$	2334 (m), 2112 (s,br)
$[\text{Re}_2\text{Mo}_2(\text{CN})_8(\text{MeCN})_x]$	2209 (m), 2095 (s,br)
$[\text{Mo}_2(\text{CN})_4(\text{MeCN})_x]$	2317 (m), 2288 (m), 2249 (w), 2188 (w), 2110 (s,br)
$[\text{Fe}_2\text{Mo}_2(\text{CN})_8(\text{MeCN})_x]$	2311 (w), 2280 (w), 2211 (w), 2096 (s,br)

analyses (TGA) performed on $[\text{Mo}_2(\text{CN})_4(\text{CH}_3\text{CN})_x]$, $[\text{Rh}_2\text{Mo}_2(\text{CN})_8(\text{CH}_3\text{CN})_x]$, and $[\text{Re}_2\text{Mo}_2(\text{CN})_8(\text{CH}_3\text{CN})_x]$ shown in figures 30, 31 and 32 exhibit weight losses of 46%, 43% and 35% respectively. The infrared spectra of the solids, after being heated to at least 500°C under a flow of N_2 gas, show no $\nu(\text{C}\equiv\text{N})$ bands. Assuming the complete loss of CH_3CN and CN^- ligands, the amount of CH_3CN (x) in each product is calculated to be *ca.* 3.2, 0.9 and 2.3 equivalents respectively. The TGA of $[\text{Fe}_2\text{Mo}_2(\text{CN})_8(\text{MeCN})_x]$ (shown in Figure 33) under similar conditions exhibits a weight loss of only 31% which would account for only 5.2 equivalents of CN^- , and no CH_3CN . But this is not possible since the infrared spectrum prior to the TGA clearly shows the presence of $\nu(\text{C}\equiv\text{N})$ bands attributed to CH_3CN . The color of the solid after the TGA is orange-brown (not black as seen for the other solids) and the infrared spectrum exhibits a very strong and broad band at 835 cm^{-1} indicating that a new product has formed as the result of performing the TGA. No $\nu(\text{C}\equiv\text{N})$ bands are present in the spectrum. The TGA exhibited a 2% weight increase between 500 and 600°C indicating a reaction with the N_2 gas or possibly O_2 (if the TGA system is not absolutely free of O_2 contaminant). The decomposed materials would be expected to be highly reactive to O_2 forming M-O products.

The complex $[\text{Bu}^n_4\text{N}]_3[\text{Mo}_2(\text{O}_2\text{CCH}_3)(\text{CN})_6]$ reacts with $[\text{Rh}_2(\text{NCCH}_3)_{10}][\text{BF}_4]_4$ to form a black solid precipitate whose infrared spectrum exhibits two intense and broad $\nu(\text{C}\equiv\text{N})$ bands at 2110 and 2042 cm^{-1} . Since there are two types of CN^- ligands in $[\text{Bu}^n_4\text{N}]_3[\text{Mo}_2(\text{O}_2\text{CCH}_3)(\text{CN})_6]$, nonequivalent M-CN-M' linkages could occur to give different $\nu(\text{C}\equiv\text{N})$ bands.

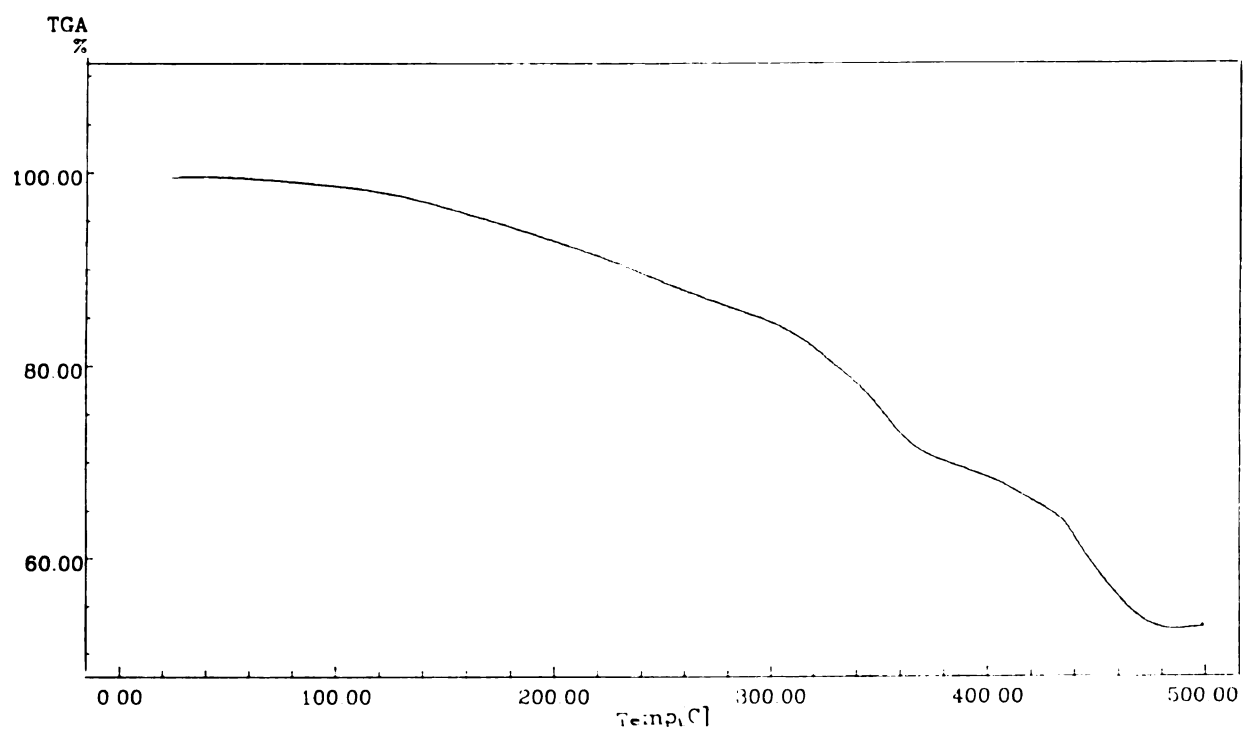


Figure 30. Thermogravimetric analysis of " $\text{Mo}_2(\text{CN})_4(\text{NCCH}_3)_x$ ".

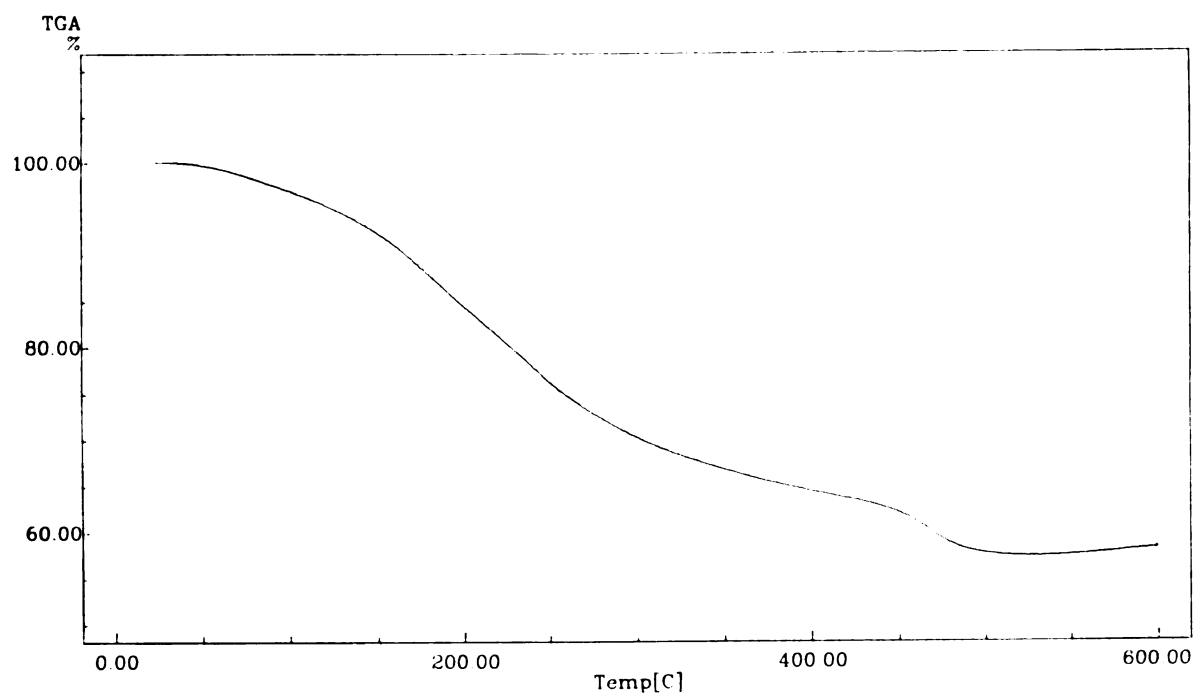


Figure 31. Thermogravimetric analysis of " $\text{Rh}_2\text{Mo}_2(\text{CN})_8(\text{NCCH}_3)_x$ ".

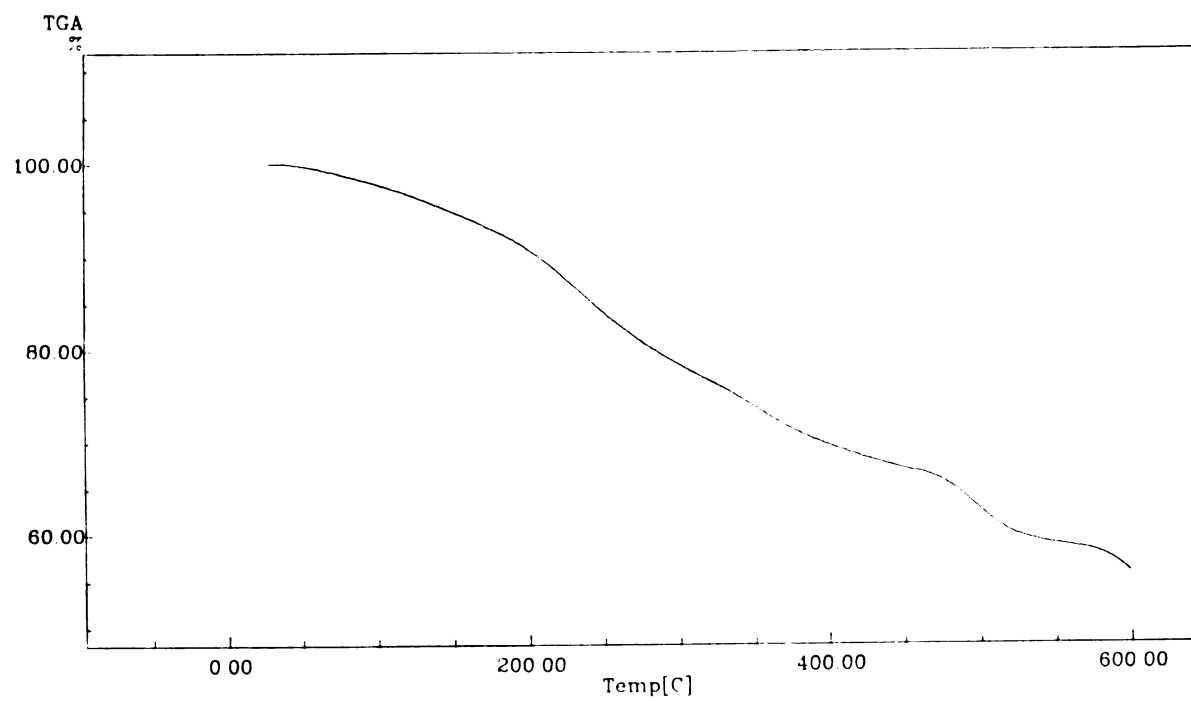


Figure 32. Thermogravimetric analysis of " $\text{Re}_2\text{Mo}_2(\text{CN})_8(\text{NCCH}_3)_x$ ".

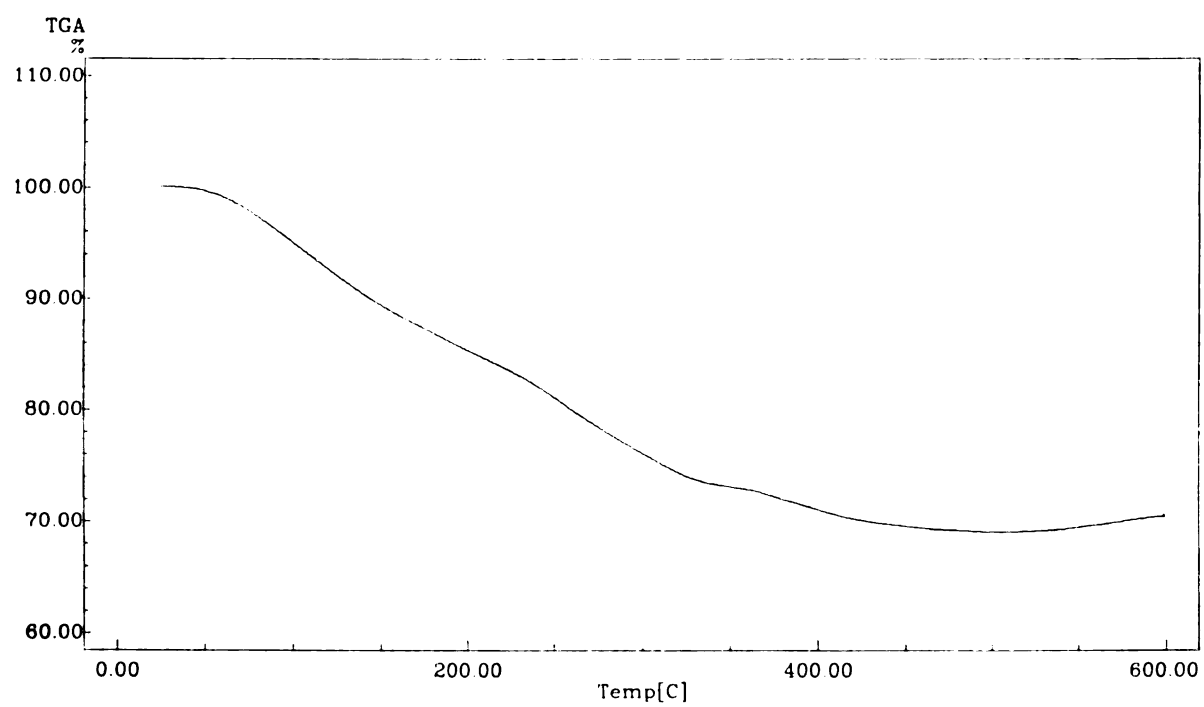


Figure 33. Thermogravimetric analysis of " $\text{Fe}_2\text{Mo}_2(\text{CN})_8(\text{NCCH}_3)_x$ ".

References

1. Michl, J. *Science* **April 26, 1991**, 511.
2. (a) Abrahams, B. R.; Hoskins, B. F.; Robson, R. *J. Chem. Soc., Chem. Commun.* **1990**, 60. (b) Abrahams, B. R.; Hoskins, B. F.; Liu, J.; Robson, R. *J. Am. Chem. Soc.* **1991**, *113*, 3045. (c) Hoskins, B. F.; Robson, R. *J. Am. Chem. Soc.* **1990**, *112*, 1546.
3. (a) Sharpe, A. G. "*The Chemistry of Cyano Complexes of the Transition Metals*" Academic Press, London. **1976**. (b) Ludi, A.; Güdel, H. U. *Structure and Bonding* **1973**, *14*, 1-21. (c) Shriver, D. F. *Structure and Bonding* **1966**, *1*, 32-58. (d) Griffith, W. P. *Coord. Chem. Rev.* **1975**, *17*, 177-247. (e) Iwamoto, T. in, "*Inclusion Compounds: Inorganic and Physical Aspects of Inclusion*" Eds., Atwood, J. L.; Davies, J. E. D.; MacNicol, D. D. Oxford University Press, Oxford. **1991**, *5*, Ch. 6, pp. 177-212. (f) Wilde, R. E.; Ghosh, S. H.; Marshall, B. J. *Inorg. Chem.* **1970**, *9*, 2512.
4. (a) Curtis, D. M.; Han, K. R.; Butler, W. M. *Inorg. Chem.* **1980**, *16*, 2096. (b) Aspinall, H. C.; Deeming, A. J.; Donovan-Mtunzi, S. *J. Chem. Soc. Dalton Trans.*, **1983**, 2669. (c) Deraniyagala, S. P.; Grundy, K. R. *Inorg. Chim. Acta*, **1984**, *84*, 205.
5. Brignole, A. B.; Cotton, F. A. *Inorg. Synth.* **1972**, *13*, 81.
6. Cotton, F. A.; Norman, J. G.; *Coord. Chem.* **1971**, *1*, 14.
7. Dunbar, K. R.; Pence, L. E. *Inorg. Synth.* **1992**, *29*, 182.
8. Cotton, F. A.; Wiesinger, K. J. *Inorg. Chem.* **1991**, *30*, 871.
9. Bernstein, S. N.; Dunbar, K. R. *Angew. Chem. Int. Ed. Engl.* **1992**, *31*, 1359.
10. Hathaway, B. J.; Holah, D. G.; Underhill, A. E. *J. Chem. Soc.* **1962**, 2444.
11. Barder, T. J.; Cotton, F. A.; Dunbar, K. R.; Powell, G. L.; Schwotzer, W.; Walton, R. A. *Inorg. Chem.* **1985**, *24*, 2550.
12. Andreades, S.; Zahnow, E. W. *J. Am. Chem. Soc.* **1969**, *91*, 4181.

13. (a) Bino, A.; Cotton, F. A.; Fanwick, P. E. *Inorg. Chem.* **1979**, *18*, 3558. (b) Cotton, F. A.; Frenz, B. A.; Deganello, G.; Shaver, A. J. *Organomet. Chem.* **1973**, 227.
14. TEXSAN-TEXRAY Structure Analysis Package, Molecular Structure Corporation **1985**.
15. MITHRIL: Integrated Direct Methods Computer Program, Gilmore, C. J. *J. Appl. Cryst.* **1984**, *17*, 42.
16. DIRDIF: Direct Methods for Difference Structure, An Automatic Procedure for Phase Extension; Refinement of Difference Structure Factors. Beurskens, R. T. Technical Report **1984**.
17. DIFABS: Walker, N.; Stuart, D. *Acta Cryst.* **1983**, *A39*, 158-166.
18. Sheldrick, G. M. in, "*Crystallographic Computing 3*", Eds. G. M. Sheldrick, C. Kruger, and R. Goddard, Oxford University Press **1985**, pp. 175 - 189.
19. Garner, C. D.; Senior, R. G. *J. C. S. Dalton* **1975**, 1171
20. Baker, S. L.; Dunbar, K. R. work in progress.
21. Fanwick, P. E.; Martin, D. S.; Cotton, F. A.; Webb, T. R. *Inorg. Chem.* **1977**, *16*, 2103.
22. Cotton F. A. Chemical Applications of Group Theory, Third addition, Wiley Interscience, **1990**.
23. Anderson, L. B.; Barder, T. J.; Cotton, F. A.; Dunbar, K. R.; Falvello, L. R.; Walton, R. A. *Inorg. Chem.* **1986**, *25*, 3629.
24. Barder, T. J.; Cotton, F. A.; Lewis, D.; Schwotzer, W.; Tetrick, S. M.; Walton, R. A. *J. Am. Chem. Soc.* **1984**, *106*, 2882.

CHAPTER VI

**REACTIONS OF METAL-METAL BONDED COMPLEXES
WITH PHOSPHINE-FUNCTIONALIZED
TETRATHIAFULVALENE DONORS**

1. Introduction

Since reactions of polycyano-organic acceptor species (i.e. TCNQ and DM-DCNQI) with dinuclear metal complexes led to the formation of covalently linked complexes¹, examples in which dinuclear metal complexes are linked to organic donor molecules were thought to be feasible targets. In one reported example, the complex $[\text{Rh}_2(\text{O}_2\text{CCH}_3)_4(\text{TTF})_2]$ contains two axially σ -bound TTF (tetrathiafulvalene) donor molecules.² Other examples in which mononuclear metal complexes are covalently linked to TTF molecules have been reported, but are rare.³ Recently, Fourmiqué and Batail have successfully synthesized a variety of TTF containing phosphines, $\text{PPh}_n\text{TTF}_{3-n}$ ($n = 0-3$), $\text{Me}_2(\text{PPh}_3)_2\text{TTF}$, and $(\text{PPh}_3)_4\text{TTF}$.⁴ Realizing the ability of phosphine ligands to stabilize dimetal centers, we set out to explore the chemistry of these newly synthesized TTF-phosphines with dinuclear metal compounds. We rationalized that the combination of the stacking ability and redox capabilities of TTF coupled with the rich redox properties of metal-metal bonded units could result in new materials with interesting magnetic or electrical properties. The products from the reactions of these redox-active TTF-phosphines with various dinuclear species have resulted in a variety of metal/P-TTF complexes. The X-ray crystal structure of $[\text{Rh}\{\text{Me}_2(\text{PPh}_2)_2\text{TTF}\}_2][\text{BF}_4]$ (**12**) was determined and revealed close intermolecular TTF-TTF contacts in the solid state.

2. Experimental

A. Synthesis

The metal complexes $[\text{Rh}_2(\text{NCCH}_3)_{10}][\text{BF}_4]_4$,⁵ $[\text{Bu}_4^n\text{N}]_2\text{Re}_2\text{Cl}_8$,⁶ $\text{Re}_2\text{Cl}_6(\text{PBu}_3^n)_2$,⁷ $\text{Mo}_2(\text{O}_2\text{CCH}_3)_4$,⁸ $\text{Mo}_2(\text{O}_2\text{CCF}_3)_4$,⁹ $[\text{Mo}_2(\text{NCCH}_3)_{10}][\text{BF}_4]_4$ ¹⁰ and $[\text{V}(\text{NCCH}_3)_6][\text{BPh}_4]_2$,¹¹ were synthesized according to literature

procedures. The phosphines $\text{Me}_3(\text{PPh}_2)\text{TTF}$, $\text{Me}_2(\text{PPh}_2)_2\text{TTF}$, and $(\text{PPh}_2)_4\text{TTF}$ were generously provided by Patrick Batail and Marc Fourmiqué.¹²

(1) Preparation of $[\text{Rh}\{\text{Me}_2(\text{PPh}_2)_2\text{TTF}\}_2][\text{BF}_4]$ (12)

A warm solution containing 0.250 g (0.416 mmol) of $\text{Me}_2(\text{PPh}_2)_2\text{TTF}$ and 20 mL of CH_3CN was slowly added to a stirred solution containing 0.100 g (0.104 mmol) of $[\text{Rh}_2(\text{NCCH}_3)_{10}][\text{BF}_4]_4$ and 10 mL of CH_3CN whereupon a green solution and a yellow crystalline solid were observed to form. The reaction was stirred for 4 h at room temperature and the yellow solid was collected by filtration, washed with CH_3CN (3 x 5 mL) and vacuum dried; yield 0.200 g (69%). The initial green filtrate was heated to reflux for a total of 48 h producing an additional 20 mg of yellow solid; total yield 0.220 g (76%). *Anal.* Calcd for $\text{C}_{64}\text{H}_{52}\text{B}_1\text{F}_4\text{P}_4\text{S}_8\text{Rh}_1$: C, 55.28; H, 3.77. Found: C, 55.34; H, 4.06. IR (CsI, Nujol, cm^{-1}): 1505 (w), 1100 (m), 1062 (s), 925 (w), 797 (m), 700 (m), 528 (m), 517 (m), 483 (w), 455 (w), 420 (w). ^1H NMR (CD_2Cl_2 , ppm) $\delta = 7.46$ (t, C_6H_5), $\delta = 7.20$ (t, C_6H_5), $\delta = 7.11$ (d, C_6H_5), $\delta = 1.82$ (s, $-\text{CH}_3$). $^{31}\text{P}\{^1\text{H}\}$ NMR (CD_2Cl_2 , ppm) $\delta = 50.4$ (d). $^{19}\text{F}\{^1\text{H}\}$ NMR (CD_2Cl_2 , ppm) $\delta = -154.9$ (s). Electronic absorption spectrum (CH_2Cl_2) $\lambda_{\text{max}} = 270, 318, \text{ and } \sim 420 \text{ nm}$. MS m/z : 1303 (M^+ , 60).

(2) Preparation of $\text{ReCl}_2[\text{Me}_2(\text{PPh}_2)_2\text{TTF}]_2$ (13)

A quantity of $[\text{Bu}_4^{\text{n}}\text{N}]_2\text{Re}_2\text{Cl}_8$ (0.030 g, 0.026 mmol), 0.0340 g (0.057 mmol) of $\text{Me}_2(\text{PPh}_2)_2\text{TTF}$ and 10 mL of ethanol was added to a 100 mL Schlenk flask equipped with a condenser. The mixture was refluxed for 30 min during which time a red precipitate formed. The solid was collected by filtration, washed with ethanol (40 mL) followed by CH_3CN (30 mL) to remove any unreacted $[\text{Bu}_4^{\text{n}}\text{N}]_2\text{Re}_2\text{Cl}_8$, washed with

diethyl ether (20 mL) to remove any unreacted $\text{Me}_2(\text{PPh}_2)_2\text{TTF}$, and vacuum dried; yield 0.029 g (71% based on $\text{Me}_2(\text{PPh}_2)_2\text{TTF}$). IR (CsI, Nujol, cm^{-1}): 1100 (m), 745 (m), 695 (m), 520 (s), 330 (m). ^1H NMR (CDCl_3) broad unresolved resonances at $\delta = 9.18$, 7.99, and 2.44 ppm. $^{31}\text{P}\{^1\text{H}\}$ NMR (CDCl_3) not observed. Electronic absorption spectrum (CH_2Cl_2) $\lambda_{\text{max}} = 276$, 322, 448, and 976 nm. MS m/z : 1457 (M^+ , 40).

(3) Reactions of $\text{Mo}_2(\text{O}_2\text{CCR}_3)_4$ ($\text{R} = \text{H}, \text{F}$) with $\text{Me}_2(\text{PPh}_2)_2\text{TTF}$

In a typical reaction 0.020 g (0.047 mmol) of $\text{Mo}_2(\text{O}_2\text{CCH}_3)_4$, 0.056 g (0.093 mmol) of $\text{Me}_2(\text{PPh}_2)_2\text{TTF}$, and 10 mL of toluene were added to a 100 mL Schlenk flask followed by the addition of 25 μL (0.19 mmol) of Me_3SiCl . No immediate color changes were observed, thus the reaction mixture was heated to reflux for 24 h resulting in the formation of a red precipitate. The solid was collected by filtration, washed with toluene and diethyl ether, and vacuum dried; yield 0.034 g. IR (CsI, Nujol, cm^{-1}): 1190 (w), 1160 (w), 1095 (m), 780 (w), 745 (s), 700 (s), 515 (s), 473 (m). ^1H NMR (CDCl_3) $\delta = 6.8 - 7.8$ ppm (complicated set of multiplets) $\delta = 1.92$ ppm (broad unresolved resonance). $^{31}\text{P}\{^1\text{H}\}$ NMR (CDCl_3) $\delta = 27.1$ ppm (s). Electronic absorption spectrum (CH_2Cl_2) $\lambda_{\text{max}} = 280$, 329, and 433 nm. A similar reaction involving $\text{Mo}_2(\text{O}_2\text{CCF}_3)_4$ and diethyl ether as the reaction solvent under the same reaction conditions and stoichiometries also produced a red solid with similar spectroscopic properties.

(4) Reaction of $[\text{Rh}_2(\text{NCCH}_3)_{10}](\text{BF}_4)_4$ with $\text{Me}_3(\text{PPh}_2)\text{TTF}$

To a 50 mL Schlenk tube was added 0.025 g (0.026 mmol) of $[\text{Rh}_2(\text{NCCH}_3)_{10}](\text{BF}_4)_4$, 0.045 g (0.104 mmol) of $\text{Me}_3(\text{PPh}_2)\text{TTF}$ and 10 mL of CH_3CN causing an instantaneous dark green solution to form. The mixture was stirred at room temperature for 1 day without any

noticeable change in color. Diethyl ether (30 mL) was carefully layered over the solution which effected the precipitation of a black solid. The solid was collected by filtration, washed with diethyl ether, and vacuum dried. IR (CsI, Nujol, cm^{-1}): 1050 (s,br), 890 (w), 750 (w), 720 (m), 695 (m), 530 (s), 475 (m). Electronic absorption spectroscopy (CH_2Cl_2) $\lambda_{\text{max}} = 510$ and 600 nm.

(5) Reaction of $[\text{Bu}_4^n\text{N}]_2\text{Re}_2\text{Cl}_8$ with $\text{Me}_3(\text{PPh}_2)\text{TTF}$

To a 50 mL Schlenk flask was added 0.050 g (0.044 mmol) of $[\text{Bu}_4^n\text{N}]_2\text{Re}_2\text{Cl}_8$, 0.077 g (0.179 mmol) of $\text{Me}_3(\text{PPh}_2)\text{TTF}$, 5 mL of ethanol and 5 mL of CH_2Cl_2 . The reaction mixture was refluxed for 16 h at which time it was deduced that no reaction had yet occurred. A quantity of NaBH_4 (0.045 g) was dissolved in 5 mL of methanol and added to the reaction mixture to aid in reuction of the Re_2 unit which is common in the synthesis of $\text{Re}_2^{\text{II,II}}\text{Cl}_4(\text{PR}_3)_4$ compounds from $[\text{Bu}_4^n\text{N}]_2\text{Re}_2^{\text{III,III}}\text{Cl}_8$. The resulting mixture was refluxed for 10 minutes whereupon a brown solution and a black precipitate were produced. The solid was collected by filtration, washed with methanol and diethyl ether, and dried *in vacuo*; yield 0.012 g. IR (CsI, Nujol, cm^{-1}): 1307 (w), 1157 (w), 1170 (w), 1095 (w), 908 (s), 747 (w), 723 (m), 693 (m), 546 (w), 519 (w).

(6) Reaction of $[\text{Rh}_2(\text{NCCH}_3)_{10}][\text{BF}_4]_4$ with $(\text{PPh}_2)_4\text{TTF}$

A quantity of $[\text{Rh}_2(\text{NCCH}_3)_{10}][\text{BF}_4]_4$ (0.054 g, 0.056 mmol) was dissolved in 10 mL of CH_3CN and added to a solution of $(\text{PPh}_2)_4\text{TTF}$ (0.112 g, 0.119 mmol) in 5 mL of CH_2Cl_2 resulting in the immediate formation of a dark brown-yellow solution. The reaction solution was stirred for several days without any noticeable color change. A UV-visible spectrum of the solution exhibited a single absorption band at $\lambda_{\text{max}} = 310$ nm. The solution was reduced in volume by vacuum and

layered with 20 mL of diethyl ether which effected the precipitation of a brown solid. The solid was collected by filtration, washed with diethyl ether, and vacuum dried. A ^1H NMR (CD_3CN) revealed a set of broad resonances between $\delta = 7.0$ and 7.8 ppm attributed to the phenyl protons in addition to resonances due to residual diethyl ether. A $^{31}\text{P}\{^1\text{H}\}$ NMR spectrum displayed a doublet centered at $\delta = 51.2$ ppm with $J_{\text{Rh-P}} = 134.7$ Hz which support the equivalencies of the phosphorous nuclei. The solid was dissolved in CH_3CN , filtered, and the filtrate was layered with diethyl ether which gave only finely divided solids.

(7) Reaction of $\text{Re}_2\text{Cl}_6(\text{PBu}_3^n)_2$ with $(\text{PPh}_2)_4\text{TTF}$

A flask charged with $\text{Re}_2\text{Cl}_6(\text{PBu}_3^n)_2$ (0.052 g, 0.053 mmol), $(\text{PPh}_2)_4\text{TTF}$ (0.100 g, 0.106 mmol) and methanol (10 mL) was refluxed for 3 days. The mixture was filtered and the resulting yellow-orange solid was washed with methanol and diethyl ether. It was quickly evident that all of the $\text{Re}_2\text{Cl}_6(\text{PBu}_3^n)_2$ had reacted as judged by the colorless diethyl ether in which $\text{Re}_2\text{Cl}_6(\text{PBu}_3^n)_2$ is soluble. The solid was recrystallized from THF; yield 0.090 g. ^1H NMR (CDCl_3) $\delta = 7 - 8$ ppm (complex multiplets due to the phenyl protons). $^{31}\text{P}\{^1\text{H}\}$ NMR (CDCl_3) $\delta = 23.1$ (s) ppm. There was no evidence of $-\text{PBu}_3^n$ in the NMR indicating complete substitution of these ligands.

B. X-ray Crystallography

The structure of $[\text{Rh}\{\text{Me}_2(\text{PPh}_2)_2\text{TTF}\}_2][\text{BF}_4]$ (**12**) was determined by application of general procedures that have been fully described elsewhere.¹³ Crystallographic data were collected on a Rigaku AFC6S diffractometer equipped with monochromated $\text{MoK}\alpha$ ($\lambda_\alpha = 0.71069$ Å) radiation and were corrected for Lorentz and polarization effects. Calculations were performed on a VAXSTATION 4000 computer by using

the Texsan crystallographic software package of Molecular Structure Corporation.¹⁴

(i) Data Collection and Reduction

Crystals of $[\text{Rh}\{\text{Me}_2(\text{PPh}_2)_2\text{TTF}\}_2][\text{BF}_4]$ (**12**) were grown from slow evaporation of a CH_2Cl_2 solution of the product. A yellow crystal with dimensions of $0.30 \times 0.20 \times 0.10 \text{ mm}^3$ was mounted on the tip of a glass fiber with silicone grease and cooled to -90°C in a cold stream attached to the goniometer. Cell constants and an orientation matrix for data collection obtained from a least squares refinement using the setting angles of carefully centered reflections in the range $20 \leq 2\theta \leq 29^\circ$ corresponded to a monoclinic cell. A total of 6465 unique data were collected at -90°C using the ω -scan technique to a maximum 2θ value of 50° . The intensities of three representative reflections measured after every 300 reflections decreased by 4.11% thus a linear correction factor was applied to the data to account for this decay. An empirical absorption correction based on azimuthal scans of 3 reflections was applied which resulted in transmission factors ranging from 0.88 to 1.00.

(ii) Structure Solution and Refinement

Based a statistical analysis of intensity distribution the space group was determined to be $\text{C}2/c$. The structure was solved by SHELXS¹⁵ and DIRDIF¹⁶ structure programs and refined by full matrix least-squares refinement. The location of the $[\text{BF}_4]^-$ moiety was ambiguous which resulted in a poor overall refinement of the structure. Residuals R and R_w remained at high values of 0.17 and 0.24 respectively. Repeated attempts higher quality crystals met with failure. A full description of the crystallographic results will, therefore, not be presented, nevertheless

valuable information is still available from the refinement in its present form.

3. Results and Discussion

The phosphine derivatized TTF compounds $\text{Me}_3(\text{PPh}_2)\text{TTF}$, $\text{Me}_2(\text{PPh}_2)_2\text{TTF}$, and $(\text{PPh}_2)_4\text{TTF}$ have been found to react with a variety of dinuclear metal complexes. Data from $^{31}\text{P}\{^1\text{H}\}$ NMR spectroscopy, FAB mass spectroscopy, and X-ray crystallography for the compound $[\text{Rh}\{\text{Me}_2(\text{PPh}_2)_2\text{TTF}\}_2][\text{BF}_4]$ (**12**), all support the existence of metal-phosphorous bonding. Results from cyclic voltammetry experiments performed on $\text{M}[\text{Me}_2(\text{PPh}_2)_2\text{TTF}]$ products are also consistent with coordinated $\text{Me}_2(\text{PPh}_2)_2\text{TTF}$ substituents. The structure of $[\text{Rh}\{\text{Me}_2(\text{PPh}_2)_2\text{TTF}\}_2][\text{BF}_4]$ (**12**) was determined by X-ray crystallography and displayed a square planar arrangement of the coordinated diphosphines. A Pluto representation and a packing diagram are depicted in Figures 34 and 35. A full table of positional parameters for compound (**12**) is located in the Appendix.

A. Synthesis and Spectroscopy.

(1) Reactions of $\text{Me}_2(\text{PPh}_2)_2\text{TTF}$

The phosphine $\text{Me}_2(\text{PPh}_2)_2\text{TTF}$ reacts with a variety of metal complexes including $[\text{Rh}_2(\text{NCCH}_3)_{10}][\text{BF}_4]_4$, $[\text{Mo}_2(\text{NCCH}_3)_{10}][\text{BF}_4]_4$, $[\text{Bu}_4^{\text{n}}\text{N}]_2\text{Re}_2\text{Cl}_8$, $\text{Re}_2\text{Cl}_6(\text{P}^{\text{n}}\text{Bu}_3)_2$, $\text{Re}_2(\text{O}_2\text{CC}_3\text{H}_7)_4\text{Cl}_2$, $\text{Mo}_2(\text{O}_2\text{CCH}_3)_4$, $\text{Mo}_2(\text{O}_2\text{CCF}_3)_4$, and $[\text{V}(\text{NCCH}_3)_6][\text{BPh}_4]_2$. The reaction of 4 equivalents of $\text{Me}_2(\text{PPh}_2)_2\text{TTF}$ with $[\text{Rh}_2(\text{NCCH}_3)_{10}][\text{BF}_4]_4$ in CH_3CN affords the mononuclear complex $[\text{Rh}\{\text{Me}_2(\text{PPh}_2)_2\text{TTF}\}_2][\text{BF}_4]$ (**12**) as yellow microcrystals. The yellow solid is insoluble in most common solvents and exhibits only limited solubility in CH_2Cl_2 and acetone. The infrared spectrum of (**12**) displays bands attributed to the phosphine ligand along

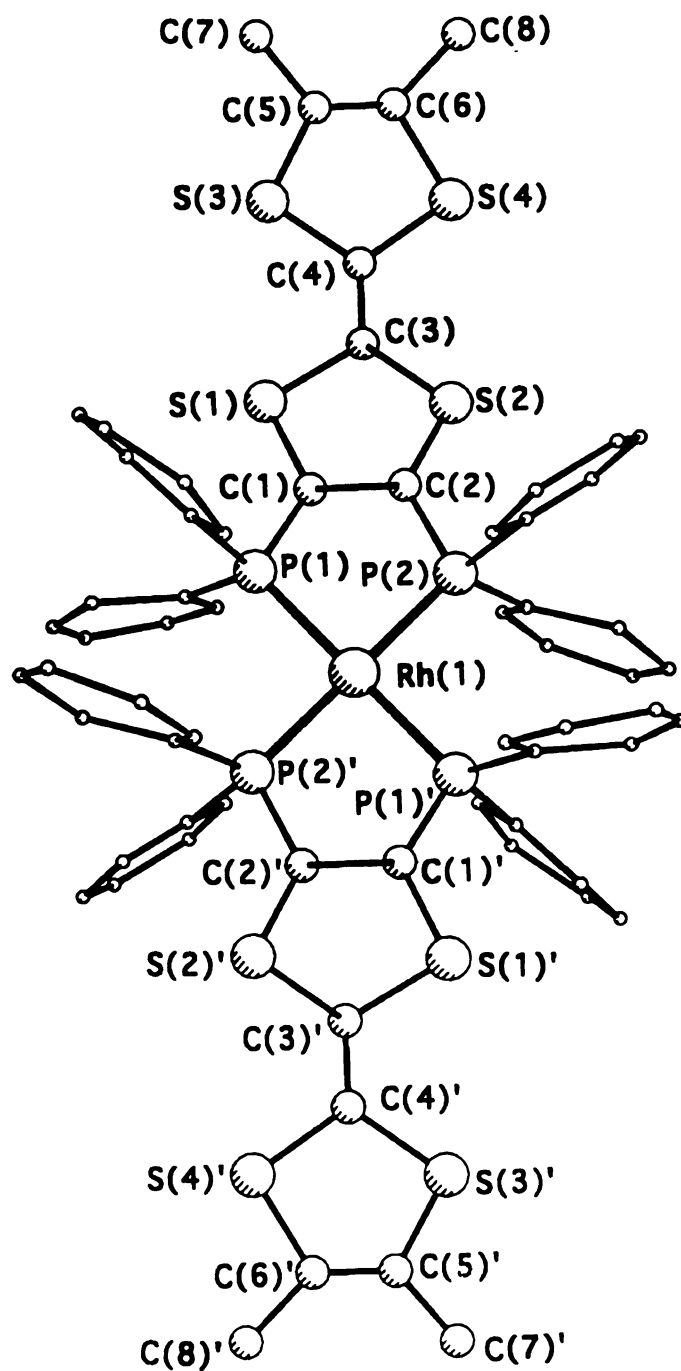


Figure 34. Pluto representation of [Rh{Me₂(Ph₂P)₂TTF}₂][BF₄] (**12**).

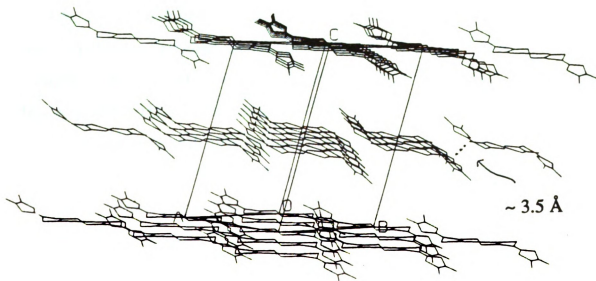


Figure 35. Stick packing diagram of [Rh{Me₂(Ph₂P)₂TTF}₂][BF₄] (12).

with stretches assignable to $[\text{BF}_4]^-$ ions. The absence of $\nu(\text{C}\equiv\text{N})$ stretches supports the loss of all CH_3CN ligands. A FAB mass spectrum exhibits a peak with $m/z = 1303$ (M^+) representing the $\text{Rh}[\text{Me}_2(\text{PPh}_2)_2\text{TTF}]_2^+$ fragment. A $^{19}\text{F}\{^1\text{H}\}$ NMR spectrum exhibits a singlet at $\delta = -154.9$ ppm which is in the range expected for $[\text{BF}_4]^-$ ion.¹⁷ The ^1H NMR spectrum of (12) contains resonances assignable only to protons of the $\text{Me}_2(\text{PPh}_2)_2\text{TTF}$ ligands, which includes a set of resonances between $\delta = 7.0$ and 7.5 ppm due to the phenyl protons, and a singlet at $\delta = 1.82$ ppm due to the methyl protons. The $^{31}\text{P}\{^1\text{H}\}$ spectrum displays a doublet at $\delta = 50.4$ ppm with $J_{\text{Rh-P}} = 134.3$ Hz. These values are within the range observed for other $\text{Rh}^{\text{I}}\text{-P}$ complexes and also compare well to the value reported for the complex $\text{NiCl}_2[\text{Me}_2(\text{PPh}_2)_2\text{TTF}]$ characterized by Fourmigué and Batail.⁴ A cyclic voltammogram (CH_2Cl_2 , 0.1 M TBABF_4) of (12) (Figure 36) exhibits two reversible oxidations at $E_{1/2(\text{ox})} = 0.63$ and $E_{1/2(\text{ox})} = 1.01$ V compared to the cyclic voltammogram of $\text{Me}_2(\text{PPh}_2)_2\text{TTF}$ under the same conditions which exhibits oxidations at $E_{1/2(\text{ox})} = 0.41$ and $E_{1/2(\text{ox})} = 0.85$ V. The shift to more positive potentials of the values in (12) is the result of strong phosphorous-to-rhodium coordination.

The reaction of $\text{Me}_2(\text{PPh}_2)_2\text{TTF}$ and $[\text{Rh}_2(\text{NCCH}_3)_{10}][\text{BF}_4]_4$ produces the mononuclear product $[\text{Rh}\{\text{Me}_2(\text{PPh}_2)_2\text{TTF}\}_2][\text{BF}_4]$ (12) as a result of reduction of Rh^{II} (d^7) to Rh^{I} (d^8). Thus, a metal-metal bonded complex is unfavorable because a $d^8\text{-}d^8$ electronic configuration in a typical M_2L_8 bonding scheme (i.e. $\sigma^2\pi^4\delta^2\delta^*2\pi^*4\sigma^*2$) results in a zero bond order. As expected, the d^8 Rh^{I} compound is diamagnetic.

The reaction of quadruply bonded $\text{Re}_2\text{Cl}_6(\text{P}^i\text{Bu}_3)_2$ with $\text{Me}_2(\text{PPh}_2)_2\text{TTF}$ in methanol, by a similar approach to that employed with $\text{Re}_2\text{Cl}_4(\text{dppm})_2$ in the attempted synthesis of $\text{Re}_2\text{Cl}_4[\text{Me}_2(\text{PPh}_2)_2\text{TTF}]_2$

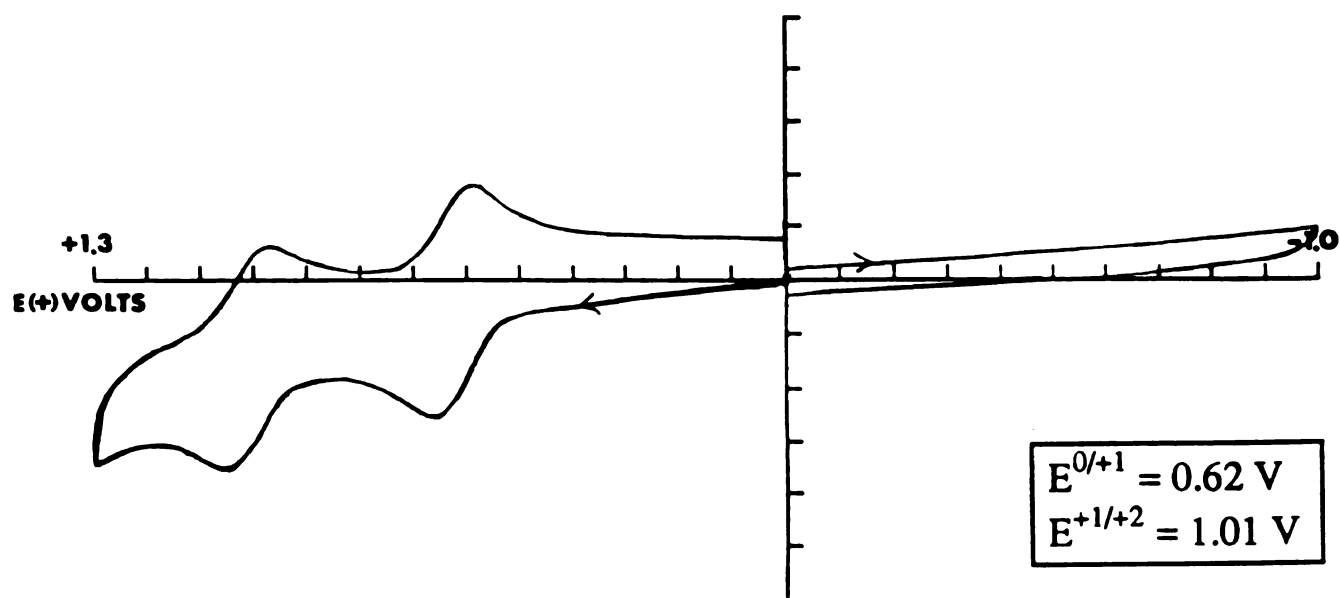


Figure 36. Cyclic voltammogram of $[\text{Rh}\{\text{Me}_2(\text{Ph}_2\text{P})_2\text{TTF}\}_2][\text{BF}_4]$ (**12**) in 0.1 M TBABF₄/CH₂Cl₂ vs Ag/AgCl at a Pt disk electrode.

does not occur. The reaction of $[\text{Bu}_4^n\text{N}]_2\text{Re}_2\text{Cl}_8$ with $\text{Me}_2(\text{PPh}_2)_2\text{TTF}$ in refluxing ethanol, however, readily produces a red precipitate. The infrared spectrum confirms the presence of the TTF-phosphine unit along with a possible $\nu(\text{Re}-\text{Cl})$ band located at 330 cm^{-1} . The infrared spectrum lacks bands that could be attributed to $[\text{Bu}_4^n\text{N}]^+$ cations. The cyclic voltammogram (0.1 M TBABF₄, CH₂Cl₂) is indicative of a product that contains coordinated phosphine with a reversible oxidation at $E_{1/2(\text{ox})} = +0.69\text{ V}$ and a quasi-reversible oxidation at $E_{1/2(\text{ox})} = +1.02\text{ V}$. A reversible reduction at $E_{1/2(\text{red})} = -0.01\text{ V}$ and an irreversible reduction at $E_{1/2(\text{red})} = -0.82\text{ V}$ are also observed. A FAB mass spectrum of this product displays the highest mass peak at $m/z = 1457$ up to 2500. This is consistent with the formulation of the product as being $\text{ReCl}_2[\text{Me}_2(\text{PPh}_2)_2\text{TTF}]_2$, which would be a rare example of a Re^{II} compound. This Re^{II} (d^5) product is paramagnetic which explains the unresolved ^1H NMR spectrum and the apparent absence of a ^{31}P NMR resonance. Reactions of $[\text{Bu}_4^n\text{N}]_2\text{Re}_2\text{Cl}_8$ with $\text{Me}_2(\text{PPh}_2)_2\text{TTF}$ in either acetone or CH₂Cl₂ fail to produce a reaction product, even under refluxing conditions.

The reaction between $\text{Me}_2(\text{PPh}_2)_2\text{TTF}$ and $\text{Mo}_2(\text{O}_2\text{CCR}_3)_4$ ($\text{R} = \text{H}, \text{F}$) in the presence of Me_3SiCl causes the precipitation of red solids whose infrared spectra are indicative of the substitution of all four acetate groups by the TTF-phosphine ligand. The $^{31}\text{P}\{^1\text{H}\}$ NMR spectrum reveals a resonance at $\delta = 27.1\text{ ppm}$ which is shifted considerably from the value observed for unreacted $\text{Me}_2(\text{PPh}_2)_2\text{TTF}$. The cyclic voltammogram exhibits two reversible oxidations at $E_{1/2(\text{ox})} = +0.67\text{ V}$ and $E_{1/2(\text{ox})} = +1.03\text{ V}$. No reaction was observed between $[\text{Mo}_2(\text{NCCH}_3)_{10}][\text{BF}_4]_4$ and $\text{Me}_2(\text{PPh}_2)_2\text{TTF}$ in refluxing CH₃CN.

Likewise, no reaction was observed between $\text{Me}_2(\text{PPh}_2)_2\text{TTF}$ and $\text{V}(\text{NCCH}_3)_6(\text{BPh}_4)_2$.

(2) Reactions of $\text{Me}_3(\text{PPh}_2)\text{TTF}$

The reaction between $[\text{Bu}_4^{\text{n}}\text{N}]_2\text{Re}_2\text{Cl}_8$ and $\text{Me}_3(\text{PPh}_2)\text{TTF}$, which does not occur under normal conditions, is facilitated by the addition of NaBH_4 which is commonly used as a reducing agent in the synthesis of $\text{Re}_2\text{Cl}_4(\text{PR}_3)_4$ complexes from $[\text{Bu}_4^{\text{n}}\text{N}]_2\text{Re}_2\text{Cl}_8$. Unfortunately, the formulation of the resulting black product is not yet known. The reaction between $[\text{Rh}_2(\text{NCCH}_3)_{10}][\text{BF}_4]_4$ and $\text{Me}_3(\text{PPh}_2)\text{TTF}$ results in the formation of a dark green solution from which a black solid is obtained by precipitation using diethyl ether. Infrared spectra suggest that $[\text{BF}_4]^-$ is still present and the solid is believed to be paramagnetic because of the broad unresolved resonances that occur in the ^1H NMR spectra.

(3) Reactions of $(\text{PPh}_2)_4\text{TTF}$

The reaction between $[\text{Rh}_2(\text{NCCH}_3)_{10}][\text{BF}_4]_4$ and $(\text{PPh}_2)_4\text{TTF}$ results in the instantaneous formation of a brown-yellow solution from which a solid is isolated by precipitation using diethyl ether. A $^{31}\text{P}\{^1\text{H}\}$ NMR spectrum exhibits a doublet at $\delta = 51.2$ ppm with $J_{\text{Rh-P}} = 134.7$ Hz. This suggests that the phosphorous nuclei are all equivalent and bound to a rhodium center, possibly forming a polymeric framework. A similar result was obtained from the reaction of $\text{Re}_2\text{Cl}_6(\text{PBu}_3^{\text{n}})_2$ with $(\text{PPh}_2)_4\text{TTF}$. The $^{31}\text{P}\{^1\text{H}\}$ NMR of the yellow-orange product in CDCl_3 exhibits only one resonance at $\delta = 23.1$ ppm, supporting equivalent, coordinated phosphorous nuclei. The assignment of these products as solids with extended interactions or as polymers is valid considering the strong evidence for the existence of $\text{ReCl}_2[\text{Me}_2(\text{PPh}_2)_2\text{TTF}]_2$ (**13**), and the crystallographically determined structure of $\text{Rh}[\text{Me}_2(\text{PPh}_2)_2\text{TTF}]_2$ (**12**).

No reaction was observed to occur with $[\text{Bu}_4^{\text{n}}\text{N}]_2\text{Re}_2\text{Cl}_8$ and $(\text{PPh}_2)_4\text{TTF}$, while the reaction between $\text{Mo}_2(\text{O}_2\text{CCF}_3)_4$ and $(\text{PPh}_2)_4\text{TTF}$ eventually occurs with the addition of Me_3SiCl , but produces only oily products.

B. X-ray Crystal Structure

The X-ray crystal structure of $[\text{Rh}\{\text{Me}_2(\text{PPh}_2)_2\text{TTF}\}_2][\text{BF}_4]$ (**12**) depicted in Figure 34 reveals a square planar arrangement of ligands around the Rh(I) center. The average Rh-P distance is 2.29 Å and the P(1)-Rh-P(2) angle is 85.2° while the P(1)-Rh-P(1)' angle is 90° as determined by symmetry. The position of the BF_4^- ion was not located in the difference map, although attempts at placing it in as a rigid group were tried. The packing diagram of (**12**) shown in Figure 35 reveals close intermolecular interactions of ~ 3.5 Å between the C(3) atoms on the TTF moieties on neighboring molecules resulting in a one-dimensional arrangement. It is apparent from examining the packing diagram that there is considerable bending of the TTF ligands away from the Rh-P plane to accommodate for this interaction. Although not shown in the packing diagram, the bulky phenyl rings prevent a perfect planar TTF-TTF intermolecular interaction. The structure of $\text{NiBr}_2[\text{Me}_2(\text{PPh}_2)_2\text{TTF}]_2$ reported by Batail *et al.*, unlike that of (**12**), exhibits a planar structural arrangement with respect to the Ni-P₂-TTF plane.⁴ There was no report of intermolecular interactions occurring in the nickel complex.

References

1. Bartley, S. L.; Dunbar, K. R. *Angew. Chem. Int. Ed. Engl.* **1991**, 448.
2. Matsubayashi, G.; Yokoyama, K; Tanaka, T. *J. Chem. Soc. Dalton Trans.* **1988**, 3059.
3. Siedle, A. R. in '*Extended Linear Chain Compounds*,' ed. Miller, J. S. Plenum Press, 1982; Ch. 11, pp 477-478.
4. Fourmigué, M.; Batail, P. *Bull. Soc. Chim. Fr.* **1992**, 129, 29.
5. Dunbar, K. R.; Pence, L. E. *Inorg. Synth.* **1992**, 29, 182.
6. Barder, T. J.; Walton, R. A. *Inorg. Synth.* **1985**, 23, 116.
7. San Filippo, J., Jr. *Inorg. Chem.* **1972**, 11, 3140.
8. Brignole, A. B.; Cotton, F. A. *Inorg. Synth.* **1972**, 13, 81.
9. Cotton, F. A.; Norman, J. G.; *Coord. Chem.* **1971**, 1, 14.
10. Cotton, F. A.; Wiesinger, K. J. *Inorg. Chem.* **1991**, 30, 871.
11. Anderson, S. J.; Wells, F. J.; Wilkinson, G.; Hussain, B.; Hursthouse, M. B. *Polyhedron* **1988**, 7, 2615.
12. Laboratoire de Physique des Solides Associé au CNRS(URA 02) Bât. 510, Université Paris-Sud, 91405 Orsay, France.
13. (a) Bino, A.; Cotton, F. A.; Fanwick, P. E. *Inorg. Chem.* **1979**, 18, 3558. (b) Cotton, F. A.; Frenz, B. A.; Deganello, G.; Shaver, A. J. *Organomet. Chem.* **1973**, 50, 227.
14. TEXSAN-TEXRAY Structure Analysis Package, Molecular Structure Corporation **1985**.
15. Sheldrick, G. M. In: *Crystallographic Computing 3* , Eds.; G.M. Sheldrick, C. Kruger, and R Goddard. Oxford U.K., 1985; pp. 175 - 189.

16. DIRDIF: Direct Methods for Difference Structure, An Automatic Procedure for Phase Extension; Refinement of Difference Structure Factors. Beurskens, R. T. Technical Report, 1984.
17. Matonic, J. H.; Chen, S.-J.; Pence, L. E.; Dunbar, K. R. *Polyhedron* **1992**, *11*, 541.

CHAPTER VII

REACTIONS OF THE ELECTRON-RICH TRIPLY BONDED COMPOUND

$\text{Re}_2\text{Cl}_4(\text{dppm})_2$ WITH DIOXYGEN.

1. Introduction

The electron-rich triply bonded species $\text{Re}_2\text{Cl}_4(\text{dppm})_2$ is easily oxidized rendering it useful in the reductive coupling of organic molecules,¹ in oxidative addition reactions across the triple bond,² and in the formation of charge-transfer complexes.³ In the course of our investigations of $\text{Re}_2\text{Cl}_4(\text{dppm})_2$ in reactions with organocyanide acceptor molecules, we observed that solutions containing $\text{Re}_2\text{Cl}_4(\text{dppm})_2$ undergo a color change with eventual production of crystalline solids after exposure to air for several days. To probe this chemistry more carefully, solutions of $\text{Re}_2\text{Cl}_4(\text{dppm})_2$ were deliberately exposed to moist air and dry O_2 . Both experiments led to the formation of $\text{Re}_2(\mu\text{-O})(\mu\text{-Cl})\text{OCl}_3(\text{dppm})_2$ (**14**) and ultimately to $\text{Re}_2(\mu\text{-O})\text{O}_2\text{Cl}_4(\text{dppm})_2$ (**15**) which have been spectroscopically and structurally characterized. Coincidentally, these same experiments were being performed at the same time by researchers in the Walton group at Purdue University, therefore a collaborative effort was undertaken to jointly report our results. Only the part of the research carried out at Michigan State is provided in this chapter. Details of additional studies can be found in a joint publication.¹⁸

2. Experimental Section

A. Synthesis

The dirhenium complex, $\text{Re}_2\text{Cl}_4(\text{dppm})_2$, was prepared as described in the literature.⁴ Glassclad 18 glass treatment to remove surface H_2O from silica was purchased from Hüls America Inc. The O_2 gas was passed through a gas purifier purchased from Alltech Associates Applied Science Labs.

(1) Synthesis of $\text{Re}_2(\mu\text{-O})(\mu\text{-Cl})\text{OCl}_3(\text{dppm})_2$ (14)**(i) Method A**

In a typical reaction, a solution of $\text{Re}_2\text{Cl}_4(\text{dppm})_2$ (0.100 g, 0.078 mmol) in acetone (20 mL) was purged with O_2 gas for 2 h. During this period, the solution color changed from purple then to red-wine with deposition of a brown microcrystalline solid. The mixture was allowed to stand undisturbed for 12 h during which time the solution color changed to yellow-brown. The resulting gold-brown precipitate was collected by suction filtration, washed with acetone (3 x 5 mL), and vacuum dried; yield 0.071 g (69%). Anal. Calcd for $\text{C}_{50}\text{H}_{44}\text{Cl}_4\text{O}_2\text{P}_4\text{Re}_2$: C, 45.67; H, 3.35. Found: C, 46.21; H, 3.39. IR (CsI, Nujol, cm^{-1}): 1707 (m), 1219 (m), 1096 (s), 899 (s), 775 (s), 689 (s), 516 (m), 480 (m). Identical results were obtained in benzene and toluene. In a separate reaction $\text{Re}_2\text{Cl}_4(\text{dppm})_2$ (0.050 g, 0.039 mmol) in CH_2Cl_2 (10 mL) was purged with O_2 for 2 h resulting in a red-wine solution. A sample of (14) was obtained by treating the reaction solution with Et_2O (20 mL), filtering, washing with acetone (3 x 5 mL), and vacuum drying; yield 0.049 g (95%). IR (CsI, Nujol, cm^{-1}): 1710 (m), 1095 (s), 907 (s), 775 (m), 692 (s), 520 (m), 482 (m).

(ii) Method B

A 50 mL Schlenk tube containing a quantity of $\text{Re}_2\text{Cl}_4(\text{dppm})_2$ (0.100 g, 0.078 mmol) in acetone (20 mL) was exposed to the laboratory atmosphere through an open stopcock for 10 days. During this period of time, large brown crystals of (14) deposited on the bottom of the vessel. The crystals were separated from the green filtrate by suction filtration, washed with acetone (3 x 5 mL), and vacuum dried; yield 0.070 g (68%). Anal. Calcd for $\text{C}_{50}\text{H}_{44}\text{Cl}_4\text{O}_2\text{P}_4\text{Re}_2$: C, 45.67; H, 3.35. Found: C, 44.92;

H, 3.03. IR (CsI, Nujol, cm^{-1}): 1705 (s), 1100 (s), 908 (s), 778 (s), 694 (s), 522 (m), 484 (m).

(2) Synthesis of $\text{Re}_2(\mu\text{-O})\text{O}_2\text{Cl}_4(\text{dppm})_2$ (15)

(i) Method A

A Schlenk tube containing $\text{Re}_2\text{Cl}_4(\text{dppm})_2$ (0.100 g, 0.078 mmol) in CH_2Cl_2 (20 mL) was purged with O_2 gas for 1.5 h resulting in an opaque red-wine solution. The solution was set aside whereupon it slowly transformed to a deep olive-green color over a four day period. The solution volume was reduced to *ca.* 5 mL and then treated with 20 mL of acetone. Within 12 h, a mixture of block-shaped green crystals and feathery green crystals had formed. The feathery crystals slowly redissolved within 3 days. The crop of large green crystals was filtered from the yellow-brown filtrate, washed with a minimal amount of cold acetone, and dried *in vacuo*; yield 0.05 g (45%). To eliminate any contamination of product (2) with (14), the solid was recrystallized by dissolving the solid in *ca.* 100 mL of hot acetone, filtering, slowly reducing the filtrate volume, and finally chilling the filtrate to 0°C overnight. The green microcrystalline solid was collected by filtration and vacuum dried; yield 0.02 g (18%). Anal. Calcd for $\text{C}_{56}\text{H}_{50}\text{Cl}_4\text{O}_3\text{P}_4\text{Re}_2$: C, 46.68; H, 3.50. Found: C, 46.23; H, 3.50. IR (CsI, Nujol, cm^{-1}): 1700 (s), 127 (m), 1154 (m), 1098 (s), 785 (s), 716 (s), 690 (m), 519 (s), 484 (m).

(ii) Method B

A total of 400 μL of purified H_2O was added to a 50 mL Schlenk tube containing a quantity of $\text{Re}_2\text{Cl}_4(\text{dppm})_2$ (0.100 g, 0.078 mmol) in acetone (20 mL). A stream of O_2 gas was bubbled through the solution for 2 h. The reaction mixture was allowed to stand for 5 days during which time a large crop of bright green crystals formed. The crystals were

collected by filtration, washed with chilled acetone (3 x 5 mL) and vacuum dried; yield 0.074 g (72%). The product was recrystallized from hot acetone (100 mL) to eliminate trace quantities of (14); yield 0.052 g (52%).

(iii) Rigorous Exclusion of H₂O

For this study, all glassware was treated with a 1% solution Glassclad 18 glass treatment⁵ and oven dried. Tetrahydrofuran was selected as the reaction solvent because it is easily purified by distillation from sodium/potassium benzophenone ketyl radical which is highly effective in eliminating H₂O. Also, the O₂ gas was passed through a gas purifier. A 50 mL Schlenk tube containing 60 mg of Re₂Cl₄(dppm)₂ and 10 mL of THF was purged with O₂ gas for 1.5 h. The solution color turned red-wine. With the reaction mixture kept sealed from atmospheric air over the course of 60 days, the solution color changed from red-wine, to orange-brown, to pale-pink, and finally to a pale yellow solution. This resulting yellow solution was reduced in volume by vacuum and layered with diethyl ether (20 mL) producing a white solid. In a separate reaction, a 50 mL Schlenk tube containing 0.035 g (0.027 mmol) of Re₂Cl₄(dppm)₂, 10 mL of THF, and 150 µL of H₂O was purged with O₂ gas for 1.5 h. This solution also turned red-wine, but after 24 h a large crop of green feathery crystals of (15) resulted. These two reactions clearly demonstrate the requirement for H₂O in the synthesis of (15).

B. X-ray Crystallographic Procedures

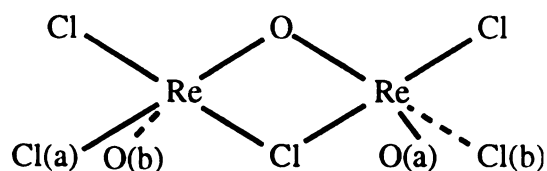
The structures of Re₂(µ-O)(µ-Cl)OCl₃(dppm)₂·(CH₃)₂CO (14)·(CH₃)₂CO and Re₂(µ-O)O₂Cl₄(dppm)₂·2(CH₃)₂CO (15)·2(CH₃)₂CO were determined by application of general procedures fully described elsewhere.⁶ Crystallographic data were collected on a Rigaku AFC6S

diffractometer with monochromated MoK α ($\lambda\alpha = 0.71069 \text{ \AA}$) radiation and were corrected for Lorentz and polarization effects. Calculations were performed on a VAXSTATION 4000 computer by using the Texsan crystallographic software package of Molecular Structure Corporation.⁷

(1) $\text{Re}_2(\mu\text{-O})(\mu\text{-Cl})\text{OCl}_3(\text{dppm})_2 \cdot (\text{CH}_3)_2\text{CO}$ (14) $\cdot (\text{CH}_3)_2\text{CO}$.

A single crystal of (14) was carefully selected from the crop of crystals resulting from the reaction in method B. A gold-brown parallelepiped with dimensions $0.30 \times 0.20 \times 0.30 \text{ mm}^3$ was mounted in a quartz capillary tube and sealed with epoxy cement. Indexing and refinement of 20 reflections in the range $6 \leq 2\theta \leq 12$ from an automatic search routine gave unit cell parameters for a triclinic crystal system. The cell was further refined by a least-squares fit of 24 reflections in the range $25 \leq 2\theta \leq 29^\circ$. Data were collected at $23 \pm 1^\circ\text{C}$ by using the $\omega - 2\theta$ scan technique. A total of 10777 unique data were collected in the range $4 \leq 2\theta \leq 50^\circ$. Intensity measurements of three standard reflections every 150 data points indicated the crystal had not decayed. An empirical absorption correction based upon azimuthal scans of 3 reflections was applied to the data and resulted in transmission factors ranging from 1.00 to 0.73. The structure of (14) was solved by SHELXS-86⁸ and DIRDIF⁹ structure solution programs within the Texsan software package and was refined by full-matrix least-squares refinement. Hydrogen atoms were not included in the refinement. All non-hydrogen atoms were refined with anisotropic thermal parameters with the exception of O(2b) and the interstitial acetone molecule. Early in the refinement procedure, it became apparent that a disorder exists between the terminal O atom and a Cl atom. This is not surprising in view of the pseudo-symmetry of the molecule. In light of this symmetry, we were curious as to whether the crystal belonged to a

monoclinic system rather than a triclinic system, but data collected on two independent crystals (one at Michigan State U. and one at Purdue U.) gave no indication of a higher symmetry cell. Furthermore, we employed several cell reduction programs including the Delaunay reduction TRACER¹⁰ and the program MISSYM¹¹, neither of which transformed the cell to monoclinic. The Re-O and Re-Cl distances are quite different, therefore the two peaks appearing in the map in the same approximate vicinity near each Re center were easily assigned. In the case of O(2b), since it tended to be "absorbed" by the Cl atom after several cycles of refinement, we chose to fix the position as determined in the original difference map after the other atoms had been located. Refinement of the occupancy of the disordered positions of the Cl atom led to an exact 0.5/0.5 population between the two sites. After establishment of this ratio for the Cl atom, the occupancies for the disorderd O atom were then fixed to 0.5. The following scheme depicts the arrangement of atoms in the equatorial plane containing the metal atoms:



One phenyl ring showed some high thermal parameters for certain carbon atoms which may be a manifestation of the disorder in the equatorial plane being transferred to the dppm ligands. After successful modeling of the Cl/O disorder and location of the other non-hydrogen atoms in the Re₂ unit, a region of electron density appeared in the lattice which was readily assigned as an acetone molecule and fixed after several cycles because of

large shifts in positions; presumably this is due to the usual lack of precise packing that occurs for solvent molecules. We did not, however, observe any alternative orientations of the acetone unit that could be modeled. Several peaks above $1\text{e}/\text{\AA}^3$ were left unassigned, as there were no chemically sensible relationships among them and the peaks were very low (the highest of them was $1.3\text{ e}/\text{\AA}^3$). After the least squares refinement had converged, the refinement statistics were as follows: $R = 0.068$, $R_w = 0.082$ and the highest peak = $1.3\text{ e}/\text{\AA}^3$ for 6553 data with $F_o^2 > 3\sigma(F_o^2)$ and 568 parameters. Other data collection and refinement parameters may be found in Table 24.

The Re(1)-O(2b) and Re(2)-O(2a) distances of 1.63 \AA and 1.65 \AA , respectively are perfectly reasonable for terminal rhenium-oxo bond distances; likewise the Re(1)-Cl(4a) and Re(2)-Cl(4b) separations of 2.33 \AA and 2.30 \AA are within the expected range. The presence of the Re=O terminal moiety is further supported by the observation of a $\nu(\text{Re}=\text{O})$ stretch at 907 (s) cm^{-1} in the infrared spectrum of (14).

(2) $\text{Re}_2(\mu\text{-O})\text{O}_2\text{Cl}_4(\text{dppm})_2 \cdot 2(\text{CH}_3)_2\text{CO}$ (15) $\cdot 2(\text{CH}_3)_2\text{CO}$

Green crystals of (2) were grown by slow evaporation of the yellow-green filtrate from the synthesis of $\text{Re}_2(\mu\text{-O})(\mu\text{-Cl})\text{Cl}_3(\text{H}_2\text{O})(\text{dppm})_2$ (14) (method B). A crystal with dimensions $0.50 \times 0.40 \times 0.40\text{ mm}^3$, was carefully selected from the crop of crystals that were grown and was sealed in a quartz capillary tube. Indexing and refinement of 20 reflections in the range $10 \leq 2\theta \leq 13$ from an automatic search routine gave unit cell parameters for a triclinic crystal system. An accurate cell was obtained by a least-squares fit of 23 reflections in the range $20 \leq 2\theta \leq 28^\circ$. Data were collected at $23 \pm 2^\circ\text{C}$ by using the $\omega - 2\theta$ scan technique. A total of 5151 unique data were collected in the range $4 \leq 2\theta \leq 50^\circ$. Intensity

Table 24. Summary of crystallographic data for
 $\text{Re}_2(\mu\text{-O})(\mu\text{-Cl})(\text{O})\text{Cl}_3(\text{dppm})_2 \cdot (\text{CH}_3)_2\text{O}$, (14) $\cdot (\text{CH}_3)_2\text{O}$.

formula	$\text{Re}_2\text{Cl}_4\text{P}_4\text{O}_3\text{C}_{53}\text{H}_{50}$
formula weight	1373.1
space group	P-1 (#2)
a, Å	16.069(6)
b, Å	16.540(5)
c, Å	12.214(2)
α , deg	109.18(2)
β , deg	99.09(3)
γ , deg	101.01(3)
V, Å ³	2923(2)
Z	2
d_{calc} , g/cm ³	1.560
μ (Mo K α), cm ⁻¹	45.23
temperature, °C	23
trans. factors, max., min.	1.00 - 0.73
R ^a	0.068
R _w ^b	0.082
quality-of-fit indicator	4.68

$$^a R = \sum ||F_o| - |F_c|| / \sum |F_o|$$

$$^b R_w = [\sum w(|F_o| - |F_c|)^2 / \sum w |F_o|^2]^{1/2}; w = 1/\sigma^2(|F_o|)$$

$$^c \text{quality-of-fit} = [\sum w(|F_o| - |F_c|)^2 / (N_{\text{obs}} - N_{\text{parameters}})]^{1/2}$$

measurements of three standard reflections every 150 data points indicated no crystal decay. An empirical absorption correction based upon azimuthal scans of 3 reflections was applied to the data and resulted in transmission factors ranging from 1.00 to 0.64. The structure was solved by MITHRIL¹² and DIRDIF⁹ structure solution programs and refined by full-matrix least-squares refinement. With the exception of the six carbon atoms of the acetone molecules in the lattice, all non-hydrogen atoms were refined with anisotropic thermal parameters. A total number of 4449 observations with $F_o^2 > 3\sigma(F_o^2)$ were used to fit 302 parameters to give $R = 0.029$ and $R_w = 0.058$. The quality-of-fit index was 2.581, and the peak of highest electron density in the final difference map was $1.349 \text{ e}/\text{\AA}^3$.

Crystallographic parameters for $\text{Re}_2(\mu\text{-O})\text{O}_2\text{Cl}_4(\text{dppm})_2$ (**15**) are summarized in Table 25. Positional parameters with the isotropic equivalents of the thermal parameters for (**14**) and (**15**) are located in the Appendix.

3. Results and Discussion

A. Synthesis

The reaction of $\text{Re}_2\text{Cl}_4(\text{dppm})_2$ with O_2 in acetone swiftly leads to the formation of $\text{Re}_2(\mu\text{-O})(\mu\text{-Cl})\text{OCl}_3(\text{dppm})_2$ (**14**) as brown crystals. The deliberate addition of H_2O to an acetone solution of $\text{Re}_2\text{Cl}_4(\text{dppm})_2$ followed by purging with O_2 aids in the solubilization of the initial product (**1**) which then goes on to form $\text{Re}_2(\mu\text{-O})\text{O}_2\text{Cl}_4(\text{dppm})_2$ (**15**) as green

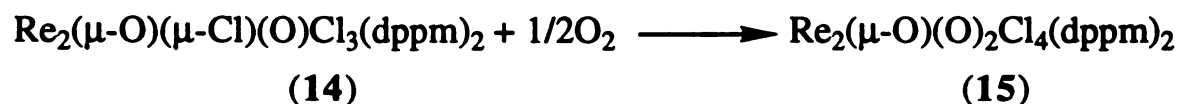
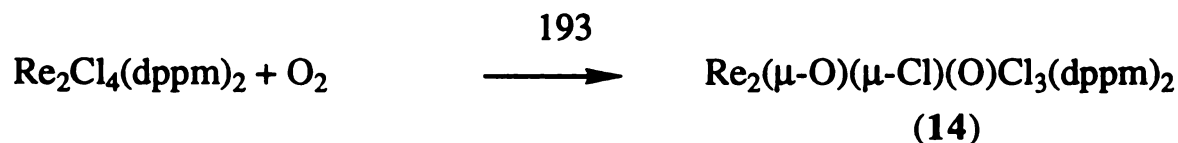
Table 25. Summary of crystallographic data for
 $\text{Re}_2(\mu\text{-O})(\text{O})_2\text{Cl}_3(\text{dppm})_2 \cdot 2(\text{CH}_3)_2\text{O}$, (15) $\cdot 2(\text{CH}_3)_2\text{O}$.

formula	$\text{Re}_2\text{Cl}_4\text{P}_4\text{O}_5\text{C}_{56}\text{H}_{50}$
formula weight	1441.0
space group	P-1 (#2)
a, Å	11.193(2)
b, Å	12.882(2)
c, Å	10.892(2)
α , deg	101.95(1)
β , deg	113.30(1)
γ , deg	75.52(1)
V, Å ³	1386.3(4)
Z	1
d_{calc} , g/cm ³	1.726
μ (Mo K α), cm ⁻¹	47.75
temperature, °C	23
trans. factors, max., min.	1.00 - 0.64
R ^a	0.029
R _w ^b	0.058
quality-of-fit indicator	2.58

$$^a R = \sum ||F_o| - |F_c|| / \sum |F_o|$$

$$^b R_w = [\sum w(|F_o| - |F_c|)^2 / \sum w |F_o|^2]^{1/2}; w = 1/\sigma^2(|F_o|)$$

$$^c \text{quality-of-fit} = [\sum w(|F_o| - |F_c|)^2 / (N_{\text{obs}} - N_{\text{parameters}})]^{1/2}$$



crystals in high yield. If CH_2Cl_2 is used in place of acetone under similar conditions to those described above, the reaction proceeds to form a persistent olive-green solution containing primarily (15). The intermediate, compound (14), which is soluble in CH_2Cl_2 and therefore does not precipitate during the course of this reaction, can be isolated by treating the reaction solution with acetone after 2 h of O_2 purging. As far as we could tell, in none of the aforementioned systems was water found to be the source of the oxygen in complexes (14) and (15). In one experiment, to rule out the possibility of water being the oxygen atom source for (14), carefully deoxygenated water was deliberately added to a Schlenk tube containing $\text{Re}_2\text{Cl}_4(\text{dppm})_2$ in acetone with strict exclusion of O_2 . After a period of 60 days, it was evident that no reaction had occurred as indicated by a persistence of the characteristic purple color of the parent complex. When this mixture was then exposed to air, large bright green crystals of (15) formed within several days. Furthermore, work done at Purdue University showed that when a sample of (14) was dissolved in CD_2Cl_2 and treated with a trace of H_2O , H_2 was not evolved, thereby ruling out the occurrence of the redox reaction $(14) + \text{H}_2\text{O} \rightarrow (15) + \text{H}_2$ as being the origin of the conversion of (14) to (15). The reaction of $\text{Re}_2\text{Cl}_4(\text{dppm})_2$ and O_2 in THF produced mixtures of (14) and (15), but only in the presence of trace amounts of water. In the absence of H_2O under rigorous moisture-free conditions, the reaction of $\text{Re}_2\text{Cl}_4(\text{dppm})_2$ with O_2 in THF proceeds by an entirely different route. In this case, the

solution changes slowly over the course of 60 days from the initial purple color, through red-wine, orange-brown, pale pink, and finally to a pale yellow solution from which a white solid can be isolated. In one instance, the red-wine solution was reduced in volume and a brown microcrystalline solid of (14) obtained. Identical behavior was found when preformed (14) was reacted with O₂ in THF under these exact same anhydrous conditions. The other intermediates in this moisture-free route are currently being investigated. In the absence of O₂, compound (14) dissolved in THF and with water added maintained a red-wine color as if no reaction occurred. It is evident from these results that H₂O plays an important role in the transformation of Re₂Cl₄(dppm)₂ to complex (15), but the mechanistic interpretation is uncertain.

B. Spectroscopy

The infrared spectrum of Re₂(μ-O)(μ-Cl)OCl₃(dppm)₂ (14) exhibits characteristic ν(Re=O) and ν(Re-O-Re) modes at 905 (s) and 775 (m) cm⁻¹. If the infrared sample of (14) is prepared in air, or if the reaction was carried out in less than moisture-free conditions, the spectra of (14) exhibit an absorption at *ca.* 3630 cm⁻¹ due to lattice H₂O. The cyclic voltammogram of Re₂(μ-O)(μ-Cl)OCl₃(dppm)₂ (14), shown in Figure 37, exhibits three reversible electrochemical processes; one reversible oxidation at +0.47 V, and two reversible reductions at -0.85 V and -0.99 V vs Ag/AgCl. A SQUID measurement on a sample of Re₂(μ-O)(μ-Cl)OCl₃(dppm)₂ (14) indicated that it is weakly paramagnetic. The data indicated antiferromagnetic coupling with a μ_{eff} value of 1.13 B.M. at 280 K. The lowest temperature measured (5 K) gave a value of 0.42 B.M. In accord with this behavior we were unable to locate the phosphorus resonance in the ³¹P{¹H} NMR spectrum of the complex, while the ¹H

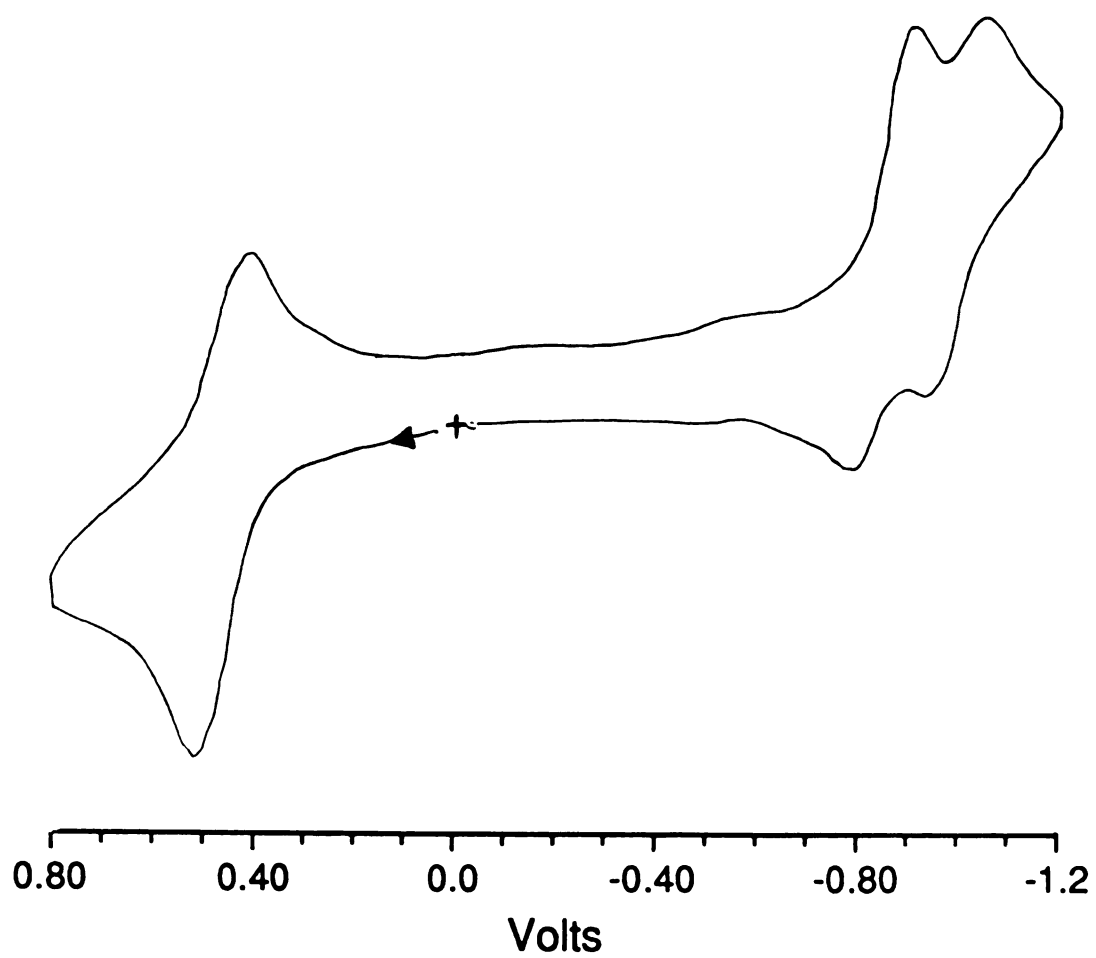


Figure 37. Cyclic voltammogram of $\text{Re}_2(\mu\text{-O})(\mu\text{-Cl})\text{OCl}_3(\text{dppm})_2$ (**14**) in 0.1 M $\text{TBABF}_4/\text{CH}_2\text{Cl}_2$ vs Ag/AgCl at a Pt disk electrode.

NMR spectrum of $\text{Re}_2(\mu\text{-O})(\mu\text{-Cl})\text{OCl}_3(\text{dppm})_2$ (**14**) in CD_2Cl_2 displayed some discernible features at $\delta = 12.2$, 11.3, and 6.2 ppm, but in general the signals are overlapping in the range of $\delta = 6 - 12$ ppm. These features are consistent with a Knight-shifted spectrum. Variable temperature spectra down to -90°C did not improve the resolution of the signals.

The infrared spectrum of $\text{Re}_2(\mu\text{-O})\text{O}_2\text{Cl}_4(\text{dppm})_2$ (**15**), like (**14**), shows $\nu(\text{Re}=\text{O})$ and $\nu(\text{Re-O-Re})$ bands at 785 (s) and 716 (s) cm^{-1} . The cyclic voltammogram for (**15**), shown in Figure 38, exhibits a reversible oxidation at $E_{1/2(\text{ox})} = +1.34$ V and in irreversible reduction process at $E_{p,c} = -0.78$ V vs Ag/AgCl with a coupled $E_{p,a}$ process at -0.70 V ($i_{p,a} < i_{p,c}$). There is an additional process at $E_{p,c} = -0.12$ V due to the formation of a chemical product following the irreversible reduction at -0.78 V. Although well separated, the relationship between the cathodic and anodic processes is supported by an absence of the wave at -0.12 V when a cyclic scan is taken at potentials positive of the cathodic process. The ^{31}P NMR spectrum of (**15**) in CD_2Cl_2 consists of a singlet at $\delta = -14.2$ ppm, while its ^1H NMR spectrum in CDCl_3 showed complex multiplets at ca. $\delta = 7.2$ and $\delta = 7.7$ ppm attributed to the phenyl protons and a pentet at $\delta = 4.10$ ppm for the $-\text{CH}_2-$ resonance of the dppm ligands. Additional resonance at $\delta = 2.15$ ppm were assigned to acetone of crystallization.

The electronic spectra of both compounds recorded in CH_2Cl_2 in quartz cells exhibit two transitions in the visible region. Characteristic features for complex (**14**) are located at $\lambda_{\text{max}} = 431$ nm ($5300 \text{ M}^{-1} \text{ cm}^{-1}$) and $\lambda_{\text{max}} = 537$ nm ($2700 \text{ M}^{-1} \text{ cm}^{-1}$). The electronic spectrum of (**15**) consists of an intense transition located at $\lambda_{\text{max}} = 441$ nm ($8800 \text{ M}^{-1} \text{ cm}^{-1}$) and a less intense feature at $\lambda_{\text{max}} = 693$ nm ($930 \text{ M}^{-1} \text{ cm}^{-1}$).

C. Crystal Structures

The X-ray structure of $\text{Re}_2(\mu\text{-O})(\mu\text{-Cl})\text{OCl}_3(\text{dppm})_2 \cdot (\text{CH}_3)_2\text{CO}$ (**14**) $\cdot (\text{CH}_3)_2\text{CO}$ (Figure 39), is that of an edge-shared bioctahedron in which the $\text{Re}_2(\mu\text{-dppm})_2$ unit is preserved. There is one bridging O and one bridging Cl atom. The three remaining Cl atoms and one O atom are situated in the terminal positions with the O atom lying trans to the bridging O atom. The chlorine atom Cl(4) and terminal oxygen atom O(2) were disordered which is a well recognized phenomenon.¹³ However, we were able to model this disorder satisfactorily. Selected bond distances and angles are listed in Table 26. The terminal and bridging Re-O bonds had distances of *ca.* 1.63 and *ca.* 1.92 Å, respectively. Two trans dppm ligands span the two rhenium centers which are separated by an unusually long distance of 3.363(2) Å and is in accord with the absence of any direct Re-Re interaction. This distance is longer than the Re-Re separation of 2.5221(1) Å determined for the symmetric dirhenium(IV) complex $\text{Re}_2(\text{O}_2\text{CC}_2\text{H}_5)(\mu\text{-O})(\mu\text{-Cl})\text{Cl}_4(\text{PPh}_3)_2$ in which there is a strong Re-Re bond.¹⁴ In the di- μ -oxo bridged dirhenium(IV) complexes $\text{K}_4[\text{Re}_2(\mu\text{-O})_2(\text{C}_2\text{O}_4)_4] \cdot 3\text{H}_2\text{O}$,¹⁵ $[\text{Re}_2(\mu\text{-O})_2\text{Cl}_2\text{L}_2]\text{I}_2 \cdot 2\text{H}_2\text{O}$,¹⁶ and $[\text{Re}_2(\mu\text{-O})_2\text{I}_2\text{L}_2]\text{I}_2 \cdot 2\text{H}_2\text{O}$,¹⁷ where L is 1,4,7-triazacyclononane, the Re-Re distances are even shorter at 2.362(1), 2.376(2), and 2.381(1) Å, respectively.

Work carried out in Professor Waltons group at Purdue University has demonstrated that (**14**) (represented as I) can be derivatized with isocyanide ligands and acetonitrile to produce the unsymmetrical compounds (II) in which the two metal centers are in quite disparate ligand environments.¹⁸ The structure of II (L = xyCN) has been determined

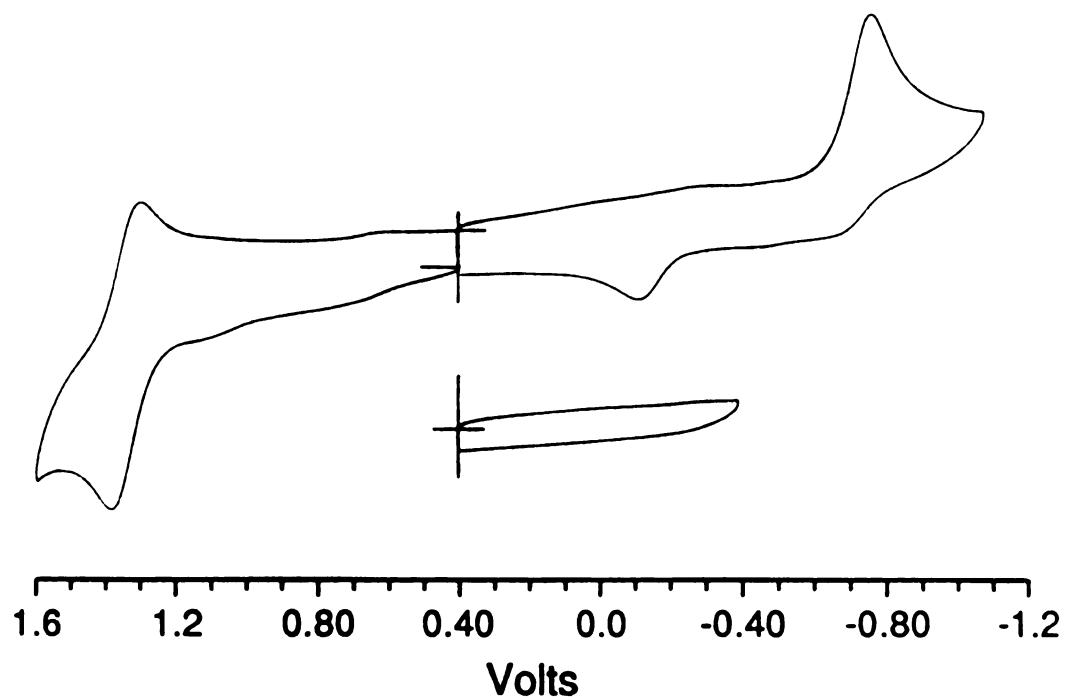


Figure 38. Cyclic voltammogram of $\text{Re}_2(\mu\text{-O})\text{O}_2\text{Cl}_4(\text{dppm})_2$ (**15**) in 0.1 M $\text{TBABF}_4/\text{CH}_2\text{Cl}_2$ vs Ag/AgCl at a Pt disk electrode.

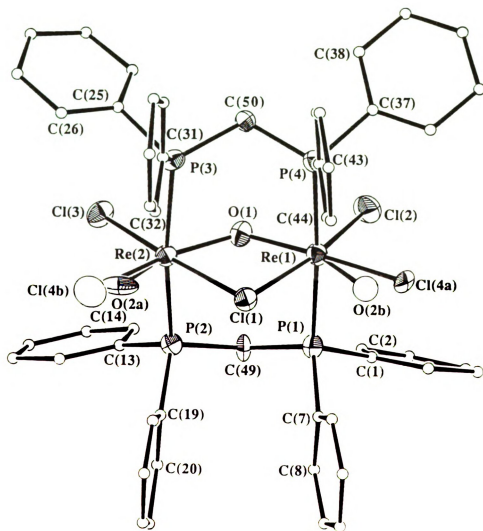


Figure 39. ORTEP representation of $\text{Re}_2(\mu\text{-O})(\mu\text{-Cl})\text{OCl}_3(\text{dppm})_2 \cdot (\text{CH}_3)_2\text{CO}$ (**14**) $\cdot (\text{CH}_3)_2\text{CO}$ with 35% probability ellipsoids. Phenyl ring atoms are shown as 0.1 Å radius spheres.

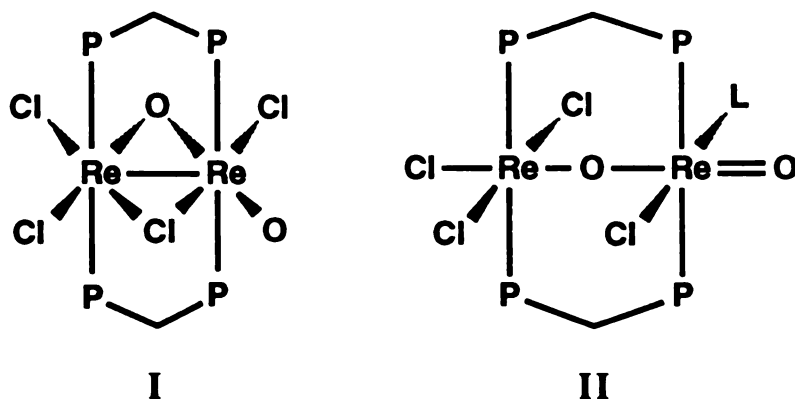
Table 26. Selected Bond Distances (Å) and Bond Angles (°) for $\text{Re}_2(\mu\text{-O})(\mu\text{-Cl})\text{OCl}_3(\text{dppm})_2\cdot(\text{CH}_3)_2\text{O}$, (14)· $(\text{CH}_3)_2\text{O}$.

distances					
atom 1	atom 2	distance	atom 1	atom 2	distance
Re(1)	Cl(1)	2.493(6)	Re(1)	Re(2)	3.361(2)
Re(1)	Cl(2)	2.337(6)	P(1)	C(1)	1.86(2)
Re(1)	Cl(4a)	2.331(9)	P(1)	C(7)	1.84(2)
Re(1)	P(1)	2.441(6)	P(1)	C(49)	1.84(2)
Re(1)	P(4)	2.460(7)	P(2)	C(13)	1.77(2)
Re(1)	O(1)	1.91(1)	P(2)	C(19)	1.81(2)
Re(1)	O(2b)	1.634(1)	P(2)	C(49)	1.84(1)
Re(2)	Cl(1)	2.557(5)	P(3)	C(25)	1.83(2)
Re(2)	Cl(3)	2.314(5)	P(3)	C(31)	1.78(2)
Re(2)	Cl(4b)	2.30(2)	P(3)	C(50)	1.87(2)
Re(2)	P(2)	2.466(6)	P(4)	C(37)	1.81(2)
Re(2)	P(3)	2.481(6)	P(4)	C(43)	1.85(2)
Re(2)	O(1)	1.93(1)	P(4)	C(50)	1.84(2)
Re(2)	O(2a)	1.65(4)			

Table 26. (cont'd).

angles							
atom 1	atom 2	atom 3	angle	atom 1	atom 2	atom 3	angle
Cl(1)	Re(1)	Cl(2)	169.4(2)	Cl(1)	Re(2)	Cl(3)	175.6(2)
Cl(1)	Re(1)	Cl(4a)	96.8(3)	Cl(1)	Re(2)	Cl(4b)	91.4(7)
Cl(1)	Re(1)	P(1)	88.0(2)	Cl(1)	Re(2)	P(2)	90.4(2)
Cl(1)	Re(1)	P(4)	90.1(2)	Cl(1)	Re(2)	P(3)	90.3(2)
Cl(1)	Re(1)	O(1)	78.0(4)	Cl(1)	Re(2)	O(1)	76.2(4)
Cl(1)	Re(1)	O(2b)	81.9(1)	Cl(1)	Re(2)	O(2a)	83(2)
Cl(2)	Re(1)	Cl(4a)	93.7(3)	Cl(3)	Re(2)	Cl(4b)	93.0(7)
Cl(2)	Re(1)	P(1)	90.0(2)	Cl(3)	Re(2)	P(2)	89.1(2)
Cl(2)	Re(1)	P(4)	91.3(2)	Cl(3)	Re(2)	P(3)	89.4(2)
Cl(2)	Re(1)	O(1)	91.5(5)	Cl(3)	Re(2)	O(1)	99.4(4)
Cl(2)	Re(1)	O(2b)	108.3(2)	Cl(3)	Re(2)	O(2a)	102(2)
Cl(4a)	Re(1)	P(1)	92.8(3)	Cl(4b)	Re(2)	P(2)	95.0(8)
Cl(4a)	Re(1)	P(4)	90.3(3)	Cl(4b)	Re(2)	P(3)	94.6(8)
Cl(4a)	Re(1)	O(1)	174.7(5)	Cl(4b)	Re(2)	O(1)	167.6(6)
P(1)	Re(1)	P(4)	176.6(2)	P(2)	Re(2)	P(3)	170.3(2)
P(1)	Re(1)	O(1)	88.3(4)	P(2)	Re(2)	O(1)	85.3(4)
P(1)	Re(1)	O(2b)	85.0(1)	P(2)	Re(2)	O(2a)	95(2)
P(4)	Re(1)	O(1)	88.5(4)	P(3)	Re(2)	O(1)	85.5(4)
P(4)	Re(1)	O(2b)	97.6(1)	P(3)	Re(2)	O(2a)	95(2)
O(1)	Re(1)	O(2b)	159.0(4)	O(1)	Re(2)	O(2a)	159(2)
Re(1)	O(1)	Re(1)	122.3(7)	Re(1)	Cl(1)	Re(2)	83.4(2)

further supporting our assignments in the structure of (14).



The molecular structure of the dirhenium(V) complex $\text{Re}_2(\mu\text{-O})\text{O}_2\text{Cl}_4(\text{dppm})_2 \cdot 2(\text{CH}_3)_2\text{CO}$ (**15**) $\cdot 2(\text{CH}_3)_2\text{CO}$ (Figure 40), is that of a corner-shared bioctahedron with a linear O-Re-O-Re-O unit. The Cl atoms are nearly perfectly trans to each other in the equatorial positions with Cl-Re-Cl angles of $174.23(8)^\circ$. The dppm ligands maintain their original bridging positions despite the Re-Re distance of 3.823 \AA . The six membered metallacycle consisted of Re-O-Re-P-C-P. Selected bond distances and angles are listed in Table 27. This is a rare example of two dppm ligands bridging a linear M-O-M unit. The only previous example cited in the literature is that of the diosmium complex $\text{Os}_2(\mu\text{-O})\text{Cl}_6(\text{dppm})_2$.¹⁹ The terminal Re-O distance is $1.708(6) \text{ \AA}$ while the bridging Re-O distance is $1.9115(5) \text{ \AA}$. These distances are well within the range observed in the structures of other linear Re(V)-O-Re(V) complexes.²⁰

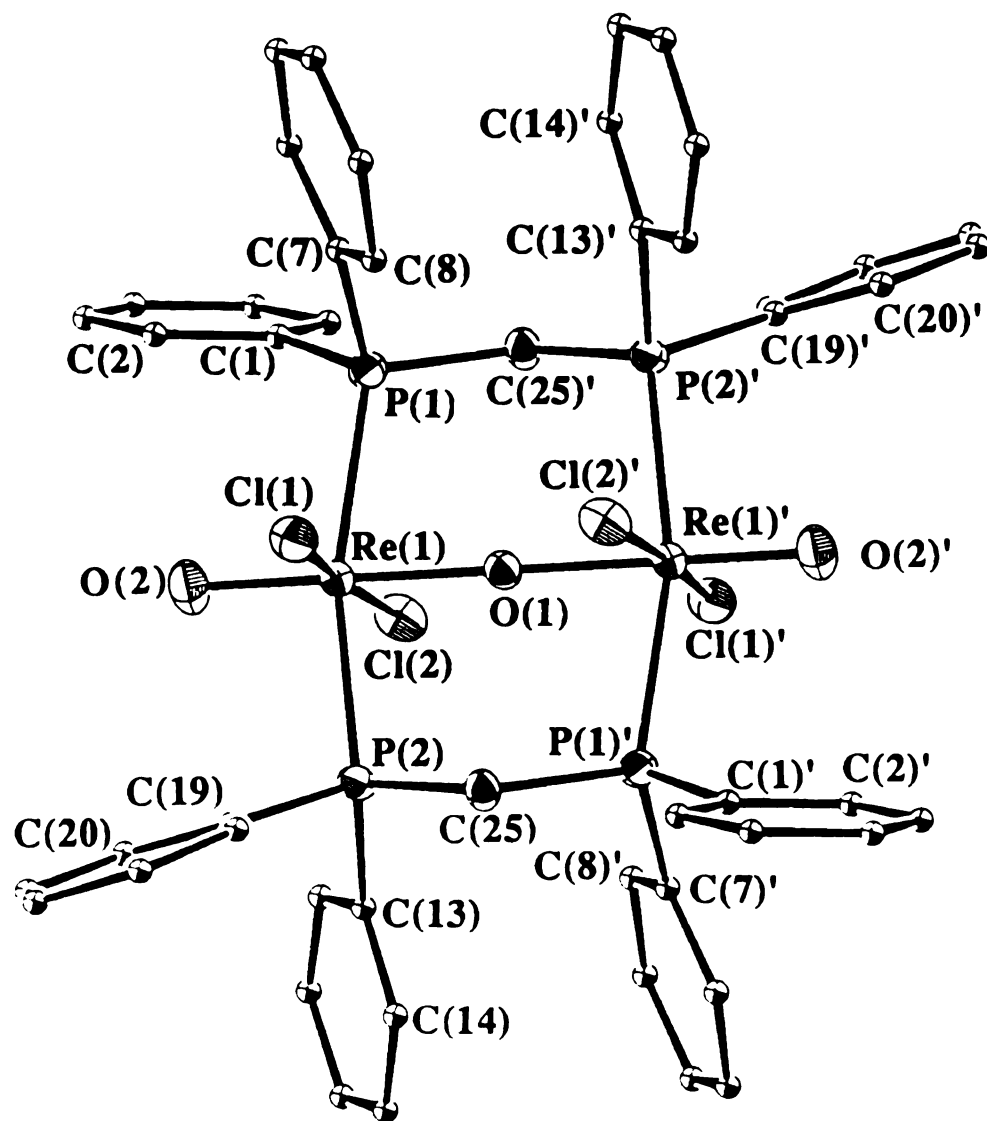


Figure 40. ORTEP representation of $\text{Re}_2(\mu\text{-O})\text{O}_2\text{Cl}_4(\text{dppm})_2 \cdot 2(\text{CH}_3)_2\text{CO}$ (**15**) $\cdot 2(\text{CH}_3)_2\text{CO}$ with 40% probability ellipsoids. Phenyl ring atoms are shown as 0.1 Å radius spheres.

Table 27 Selected Bond Distances (Å) and Bond Angles (°)
for $\text{Re}_2(\mu\text{-O})\text{O}_2\text{Cl}_4(\mu\text{-dppm})_2 \cdot 2(\text{CH}_3)\text{CO}$, (15) $\cdot 2(\text{CH}_3)\text{CO}$.

distances					
atom 1	atom 2	distance	atom 1	atom 2	distance
Re(1)	Cl(1)	2.402(2)	P(1)	C(1)	1.86(2)
Re(1)	Cl(2)	2.422(2)	P(1)	C(1)	1.836(9)
Re(1)	P(1)	2.487(2)	P(1)	C(7)	1.814(9)
Re(1)	P(2)	2.489(2)	P(1)	C(25)	1.849(8)
Re(1)	O(1)	1.9115(5)	P(2)	C(13)	1.835(9)
Re(1)	O(2)	1.708(6)	P(2)	C(19)	1.828(9)

angles			
atom 1	atom 2	atom 3	angle
Cl(1)	Re(1)	Cl(2)	174.23(8)
Cl(1)	Re(1)	P(1)	95.77(8)
Cl(1)	Re(1)	P(2)	82.61(8)
Cl(1)	Re(1)	O(1)	89.24(6)
Cl(1)	Re(1)	O(2)	92.6(2)
Cl(2)	Re(1)	P(1)	83.63(8)
Cl(2)	Re(1)	P(2)	96.58(8)
Cl(2)	Re(1)	O(1)	84.99(6)
Cl(2)	Re(1)	O(2)	93.1(2)
P(1)	Re(1)	P(2)	166.04(7)
P(1)	Re(1)	O(1)	82.24(5)
P(1)	Re(1)	O(2)	97.6(2)
P(2)	Re(1)	O(1)	83.88(5)
P(2)	Re(1)	O(2)	96.3(2)
O(1)	Re(1)	O(2)	178.1(2)
Re(1)	O(1)	Re(1)'	180.00

References

1. Esjornson, D.; Derringer, D. R.; Fanwick, P. E.; Walton, R. A. *Inorg. Chem.* **1989**, *28*, 1689.
2. (a) Qi, J.-S.; Schrier, P. W.; Fanwick, P. E.; Walton, R. A. *Inorg. Chem.* **1992**, *31*, 258. (b) Shih, K.-Y.; Fanwick, P. E.; Walton, R. A. *J. Chem. Soc., Chem. Commun.* **1992**, 375. (c) Ara, I.; Fanwick, P. E.; Walton, R. A. *Polyhedron* **1992**, *11*, 1277. (d) Ara, I.; Fanwick, P. E.; Walton, R. A. *J. Cluster Sci.* **1992**, *3*, 83.
3. Bartley, S. L.; Dunbar, K. R. *Angew. Chem. Int. Ed. Engl.* **1991**, *30*, 448.
4. Barder, T. J.; Cotton, F. A.; Dunbar, K. R.; Powell, G. L.; Schwotzer, W.; Walton, R. A. *Inorg. Chem.* **1985**, *24*, 2550.
5. This treatment provides a hydrophobic coating for glass and limits the possibility of H₂O adhering to the glass surface.
6. (a) Bino, A.; Cotton, F. A.; Fanwick, P. E. *Inorg. Chem.* **1979**, *18*, 3558. (b) Cotton, F. A.; Frenz, B. A.; Deganello, G.; Shaver, A. J. *Organomet. Chem.* **1973**, 227.
7. TEXSAN-TEXRAY Structure Analysis Package, Enraf-Nonious, Delft, The Netherlands, **1979**.
8. Sheldrick, G. M. In *Crystallographic Computing 3*, Sheldrick, G. M., Kruger, C., Goddard, R.; Oxford University Press: Oxford, U.K., **1985**; pp. 175 - 189.
9. DIRDIF: Direct Methods for Difference Structure, An Automatic Procedure for Phase Extension; Refinement of Difference Structure Factors. Beurskens, R. T. Technical Report, **1984**.
10. Lawton, S. L.; Jacobson, R. A. The Reduced Cell and Its Crystallographic Applications, United States Atomic Energy Commision, Research and Development Report, TID-4500, 1965.
11. Page, Y. L. *J. Appl. Crystallogr.* **1988**, *21*, 983.
12. MITHRIL: Integrated Direct Methods Computer Program, Gilmore, C. J. *J. appl. Cryst.* **1984**, *17*, 42.

13. (a) Calviou, L. J.; Arber, J. M.; Collison, D.; Garner, C. D.; Clegg, W. *J. Chem. Soc., Chem. Commun.* **1992**, 654. (b) Yoon, K.; Parkin, G.; Rheingold, A. L. *J. Am. Chem. Soc.* **1992**, *114*, 2210.
14. Cotton, F. A.; Foxman, B. M. *Inorg. Chem.* **1968**, *7*, 1784.
15. Lis, T. *Acta Crystallogr., Sect. B* **1975**, *31*, 1594.
16. Böhm, G.; Weighardt, K.; Nuber, B.; Weiss, J. *Angew. Chem. Int. Ed. Engl.* **1990**, *29*, 787.
17. Böhm, G.; Weighardt, K.; Nuber, B.; Weiss, J. *Inorg. Chem.* **1991**, *30*, 3464.
18. (a) Bartley, S. L.; Dunbar, K. R.; Shih, K.-Y.; Fanwick, P. E.; Walton, R. A. *Inorg. Chem.* **1993**, *32*, 1341. (b) Bartley, S. L.; Dunbar, K. R.; Shih, K.-Y.; Fanwick, P. E.; Walton, R. A. *J. Chem. Soc., Chem. Commun.* **1993**, 98.
19. Chakravarty, A. R.; Cotton, F. A.; Schwotzer, W. *Inorg. Chem.* **1984**, *23*, 99.
20. (a) Backes-Dahmann, G.; Enemark, J. H. *Inorg. Chem.* **1987**, *26*, 3960. (b) Glowiak, T.; Lis, T.; Jezowska-Trzebiatowska, B. *Bull. Pol. Sci.* **1972**, *20*, 199. (c) Lock, C. J. L.; Turner, G. *Can. J. Chem.* **1978**, *56*, 179. (d) Tisley, D. G.; Walton, R. A.; Wills, D. L. *Inorg. Nucl. Chem. Let.* **1971**, *7*, 523. (e) Fletcher, S. R.; Skapski, A. C. *J. Chem. Soc. Dalton Trans.* **1972**, 1073. (f) Shandles, R.; Schlemper, E. O.; Murman R. K. *Inorg. Chem.* **1971**, *10*, 2785.

CHAPTER VIII

CONCLUSIONS

Reactions of polycyano acceptor species with metal-metal bonded dinuclear donor compounds have led to the isolation of covalently linked complexes. The complexes $[\text{Re}_2\text{Cl}_4(\text{dppm})_2]_2(\mu\text{-L})$, where $\text{L} = \text{TCNQ}$ or DM-DCNQI , were isolated and structurally characterized and are precedence for a covalent bonding interaction. While polymeric 1:1 phases are believed to exist, the lack of suitable single crystals has prevented structural determinations. To examine the generality of this approach, a number of hybrid inorganic-organic complexes were synthesized using metal-metal bonded dinuclear complexes of molybdenum and rhenium and a variety of polycyano acceptors. In the majority of the reactions, spontaneous reactivity (as judged from the immediate and dramatic color changes that occur) was observed regardless of oxidation/reduction potentials of the precursors. This, along with the strong and shifted $\nu(\text{C}\equiv\text{N})$ bands in the infrared spectrum and intense charge-transfer bands in the electronic spectra, indicate an overwhelming tendency for these metal-metal bonded compounds to form covalent bonds with the polycyano organic molecules. Except for the complex $[\text{Re}_2\text{Cl}_4(\text{dppm})_2](\text{TCNE})$ (3)-A, all of the samples tested were found to be paramagnetic. Also, the products $[\text{Re}_2\text{Cl}_4(\text{dppm})_2](\text{TCNQ})$ (1)-A and $[\text{Re}_2\text{Cl}_4(\text{dppm})_2]_2(\mu\text{-TCNQ})$ (2) were determined to behave as semiconductors.

In addition to the reactions of the donor/acceptor type, reactions involving the fully solvated dinuclear compounds $[\text{Rh}_2(\text{NCCH}_3)_{10}][\text{BF}_4]_4$ and $[\text{Mo}_2(\text{NCCH}_3)_{10}][\text{BF}_4]_4$ were studied with chemically or electrochemically reduced forms of TCNQ and DM-DCNQI and resulted in

the synthesis of covalently bonded polymeric materials. These results clearly demonstrate the potential of constructing large molecular arrays using cyanide-containing species and are mainly attributed to the dimetal units being coordinatively unsaturated along with the bifunctional nature of the cyanide substituent.

With the intent to prepare metal-metal bonded precursors which would themselves contain bifunctional ligand sets, the cyanide-containing compounds $[\text{Bu}^n_4\text{N}]_4[\text{Mo}_2(\text{CN})_8]$ (8) and $[\text{Bu}^n_4\text{N}]_3[\text{Mo}_2(\text{O}_2\text{CCH}_3)(\text{CN})_6]$ (9) were prepared. The product $[\text{Bu}^n_4\text{N}]_4[\text{Mo}_2(\text{CN})_8]$ (8) was the first structurally characterized homoleptic cyanide complex which contained a metal-metal bonded core. These products were reacted with a variety of solvated metal complexes to form mixed metal polymeric materials. In general, it was observed that reactions of CN^- with dimetal complexes proceed readily as demonstrated in the synthesis of $[\text{Bu}^n_4\text{N}]_2[\text{Re}_2(\text{CN})_6(\text{dppm})_2]$ (11). The X-ray crystal structure of this complex revealed two bridging CN ligands in an unusual side-on σ - π - $\text{C}\equiv\text{N}$ bonding mode. This is the only well characterized compound to exhibit this bonding mode.

In other attempts to form extended molecular arrays, a variety of phosphine-functionalized TTF donors were studied. It was found that the reaction of $\text{Me}_2(\text{PPh}_2)_2\text{TTF}$ with $[\text{Rh}_2(\text{NCCH}_3)_{10}](\text{BF}_4)_4$ led to the formation of $[\text{Rh}\{\text{Me}_2(\text{PPh}_2)_2\text{TTF}\}]_2[\text{BF}_4]$ (12) which, in the solid state crystal structure, exhibits close intermolecular contacts forming an extended molecular network. Attempts to prepare polymeric materials using the tetraphosphine species $(\text{PPh}_2)_4\text{TTF}$ were also investigated.

Finally, during the course of studying reactions of $\text{Re}_2\text{Cl}_4(\text{dppm})_2$ with organic acceptors, it was observed that solutions of $\text{Re}_2\text{Cl}_4(\text{dppm})_2$

underwent color changes in air. Therefore, the chemistry of $\text{Re}_2\text{Cl}_4(\text{dppm})_2$ with air, oxygen, and water was carefully studied and led to the isolation and characterization of $\text{Re}_2(\mu\text{-O})(\mu\text{-Cl})\text{OCl}_3(\text{dppm})_2$ (**14**) and $\text{Re}_2(\mu\text{-O})\text{O}_2\text{Cl}_4(\text{dppm})_2$ (**15**). It was determined that these products are the result of reactions with molecular oxygen and not water and represent a rare example of molecular oxygen activation using a metal-metal bonded complex.

APPENDIX

Table 28. Atomic positional parameters and equivalent isotropic displacement parameters (\AA^2) and their estimated standard deviations for $[\text{Re}_2\text{Cl}_4(\text{dppm})_2]_2(\mu\text{-TCNQ})\cdot 8\text{THF}, (2)\cdot 8\text{THF}$.

atom	x	y	z	B(eq)
Re(1)	0.91930(3)	0.32564(2)	0.82133(3)	2.28(2)
Re(2)	0.89354(3)	0.28008(2)	0.96107(3)	2.31(2)
Cl(1)	0.8207(2)	0.3699(1)	1.0664(2)	3.0(1)
Cl(2)	0.8610(2)	0.2236(1)	1.1111(2)	3.5(1)
Cl(3)	0.9589(2)	0.2499(1)	0.6775(2)	3.6(1)
Cl(4)	0.8929(2)	0.4307(1)	0.8607(3)	3.4(1)
P(1)	0.7300(2)	0.2641(1)	0.8492(3)	2.8(1)
P(2)	0.7504(2)	0.3483(1)	0.7030(2)	2.8(1)
P(3)	1.0948(2)	0.3216(1)	0.9032(2)	2.6(1)
P(4)	1.0481(2)	0.2877(1)	1.1061(2)	2.7(1)
N(1)	0.9598(5)	0.1899(3)	0.9010(7)	2.2(4)
N(2)	1.153(1)	0.0434(6)	0.739(1)	8(1)
C(1)	0.6167(8)	0.3065(5)	0.900(1)	3.4(6)
C(2)	0.525(1)	0.3272(6)	0.823(1)	4.3(7)
C(3)	0.439(1)	0.3591(7)	0.864(2)	5.6(8)
C(4)	0.446(1)	0.3727(6)	0.977(2)	5.6(8)
C(5)	0.536(1)	0.3525(6)	1.052(1)	5.0(8)
C(6)	0.619(1)	0.3197(6)	1.013(1)	4.2(7)
C(7)	0.7215(9)	0.1865(5)	0.835(1)	3.9(6)
C(8)	0.765(1)	0.1443(6)	0.755(1)	5.5(8)
C(9)	0.759(2)	0.0849(7)	0.744(2)	8(1)
C(10)	0.711(1)	0.0684(7)	0.812(2)	8(1)
C(11)	0.667(1)	0.1098(8)	0.893(2)	7(1)
C(12)	0.674(1)	0.1684(6)	0.903(1)	5.3(8)
C(13)	0.6443(8)	0.4122(5)	0.732(1)	3.1(5)
C(14)	0.5592(9)	0.4313(6)	0.645(1)	4.3(6)
C(15)	0.478(1)	0.4744(6)	0.670(1)	5.2(7)
C(16)	0.479(1)	0.5005(6)	0.782(1)	4.9(7)
C(17)	0.563(1)	0.4825(5)	0.867(1)	3.8(6)
C(18)	0.6447(8)	0.4395(5)	0.842(1)	3.2(5)
C(19)	0.7505(8)	0.3575(5)	0.557(1)	3.5(6)
C(20)	0.763(1)	0.4123(6)	0.536(1)	4.5(7)
C(21)	0.768(1)	0.4222(8)	0.430(1)	6(1)
C(22)	0.760(1)	0.380(1)	0.347(1)	8(1)
C(23)	0.748(1)	0.324(1)	0.361(1)	7(1)
C(24)	0.740(1)	0.3150(7)	0.469(1)	5.3(8)
C(25)	1.1312(7)	0.3818(5)	0.861(1)	2.9(5)
C(26)	1.1429(9)	0.4326(5)	0.928(1)	3.6(6)
C(27)	1.168(1)	0.4775(5)	0.888(1)	4.8(7)
C(28)	1.182(1)	0.4727(6)	0.778(1)	4.2(7)
C(29)	1.170(1)	0.4219(6)	0.708(1)	4.5(7)
C(30)	1.1472(8)	0.3769(5)	0.749(1)	3.4(6)
C(31)	1.2026(8)	0.2577(5)	0.893(1)	3.1(5)
C(32)	1.1919(9)	0.2013(5)	0.847(1)	4.0(6)
C(33)	1.282(1)	0.1539(6)	0.841(1)	5.4(8)
C(34)	1.374(1)	0.1628(6)	0.879(2)	6.5(9)
C(35)	1.385(1)	0.2189(7)	0.927(1)	5.8(8)
C(36)	1.300(1)	0.2658(6)	0.931(1)	4.5(7)
C(37)	1.1474(8)	0.2186(5)	1.1354(9)	3.1(5)
C(38)	1.248(1)	0.2187(6)	1.164(1)	4.7(7)

Table 28. (cont'd)

atom	x	y	z	B(eq)
C(39)	1.324(1)	0.1669(7)	1.190(1)	6.0(8)
C(40)	1.301(1)	0.1149(7)	1.193(1)	7(1)
C(41)	1.200(1)	0.1138(6)	1.171(1)	6.1(9)
C(42)	1.1242(8)	0.1658(5)	1.139(1)	3.7(6)
C(43)	1.0364(8)	0.3206(5)	1.250(1)	3.5(6)
C(44)	1.028(1)	0.3806(7)	1.283(1)	5.1(8)
C(45)	1.018(1)	0.4033(7)	1.391(1)	6.0(9)
C(46)	1.012(1)	0.3678(9)	1.465(1)	6(1)
C(47)	1.016(1)	0.3092(8)	1.433(1)	6(1)
C(48)	1.027(1)	0.2850(6)	1.326(1)	4.8(8)
C(49)	0.7097(8)	0.2807(5)	0.701(1)	3.1(5)
C(50)	1.0997(8)	0.3388(4)	1.053(1)	2.9(5)
C(51)	0.9966	0.1450	0.8902	4.5(3)
C(52)	1.036(1)	0.0823(6)	0.877(1)	5.0(7)
C(53)	1.100(1)	0.0611(7)	0.797(1)	6(1)
C(54)	1.018(1)	0.0398(6)	0.937(1)	4.8(7)
C(55)	1.065(1)	-0.0207(6)	0.926(1)	5.2(8)
C(56)	0.950(1)	0.0607(6)	1.012(1)	4.6(7)
O(1)	0.3169(9)	0.3614(5)	0.204(1)	7.3(3)
C(57)	0.291(1)	0.418(1)	0.258(2)	8.5(5)
C(58)	0.361(1)	0.4218(9)	0.367(2)	8.1(5)
C(59)	0.450(1)	0.3655(9)	0.355(2)	7.8(4)
C(60)	0.405(1)	0.3239(8)	0.267(1)	7.1(4)
O(2)	0.301(2)	0.238(2)	0.580(3)	25(1)
C(61)	0.377(3)	0.186(2)	0.569(3)	19(1)
C(62)	0.472(2)	0.204(1)	0.593(2)	11.6(7)
C(63)	0.448(1)	0.2610(8)	0.555(1)	6.9(4)
C(64)	0.340(2)	0.281(1)	0.551(3)	15(1)
O(4)	0.734(3)	0.130(2)	0.267(4)	29(1)
C(69)	0.626(4)	0.173(3)	0.221(5)	24(2)
C(70)	0.605(4)	0.190(2)	0.329(5)	23(2)
C(71)	0.681(5)	0.160(3)	0.408(6)	25(2)
C(72)	0.753(6)	0.134(4)	0.409(8)	35(2)
O(3)	0.011(3)	0.127(2)	0.426(3)	30(1)
C(65)	0.116(4)	0.133(2)	0.488(3)	20(1)
C(66)	0.189(4)	0.071(3)	0.467(5)	26(2)
C(67)	0.112(3)	0.048(2)	0.396(3)	16(1)
C(68)	0.016(5)	0.060(3)	0.393(5)	31(2)
H(1)	0.5188	0.3205	0.7408	4.8
H(2)	0.3744	0.3722	0.8137	6.0
H(3)	0.3858	0.3984	1.0060	6.1
H(4)	0.5384	0.3612	1.1356	5.7
H(5)	0.6830	0.3063	1.0674	5.2
H(6)	0.8020	0.1577	0.7088	5.9
H(7)	0.7944	0.0536	0.6903	9.0
H(8)	0.7028	0.0281	0.7995	8.1
H(9)	0.6323	0.0937	0.9364	8.7
H(10)	0.6511	0.1980	0.9681	6.1
H(11)	0.5574	0.4122	0.5684	4.6
H(12)	0.4187	0.4846	0.6097	5.9

Table 28. (cont'd)

atom	x	y	z	B(eq)
H(13)	0.4199	0.5329	0.7928	5.7
H(14)	0.5640	0.5008	0.9436	4.6
H(15)	0.7037	0.4262	0.8990	3.6
H(16)	0.7707	0.4448	0.5993	5.1
H(17)	0.7789	0.4585	0.4102	6.8
H(18)	0.7591	0.3846	0.2730	7.3
H(19)	0.7397	0.2957	0.2956	7.1
H(20)	0.7304	0.2773	0.4803	6.0
H(21)	1.1329	0.4370	1.0053	4.3
H(22)	1.1798	0.5139	0.9372	5.1
H(23)	1.1980	0.5050	0.7505	4.9
H(24)	1.1772	0.4185	0.6298	5.0
H(25)	1.1407	0.3412	0.6983	3.7
H(26)	1.1254	0.1930	0.8238	4.4
H(27)	1.2758	0.1139	0.8063	5.8
H(28)	1.4324	0.1287	0.8700	7.4
H(29)	1.4524	0.2248	0.9618	6.4
H(30)	1.3066	0.3078	0.9550	5.3
H(31)	1.2644	0.2559	1.1635	5.5
H(32)	1.3947	0.1690	1.2180	6.2
H(33)	1.3588	0.0798	1.2170	8.0
H(34)	1.1829	0.0763	1.1657	7.3
H(35)	1.0532	0.1666	1.1257	4.4
H(36)	1.0299	0.4089	1.2279	5.7
H(37)	1.0173	0.4463	1.4132	6.7
H(38)	1.0065	0.3853	1.5419	6.4
H(39)	1.0090	0.2848	1.4897	6.6
H(40)	1.0305	0.2419	1.3039	5.1
H(41)	0.7470	0.2479	0.6608	3.5
H(42)	0.6396	0.2883	0.6662	3.5
H(43)	1.1684	0.3351	1.0949	3.3
H(44)	1.0622	0.3803	1.0679	3.3
H(45)	1.1115	-0.0358	0.8748	6.1
H(46)	0.9134	0.1035	1.0196	5.2
H(47)	0.2844	0.4504	0.2096	10.4
H(48)	0.2202	0.4286	0.2724	10.4
H(49)	0.3847	0.4592	0.3782	9.8
H(50)	0.3364	0.4219	0.4329	9.8
H(51)	0.4992	0.3778	0.3299	9.6
H(52)	0.4791	0.3503	0.4282	9.6
H(53)	0.3869	0.2929	0.3043	8.2
H(54)	0.4493	0.2990	0.2206	8.2
H(55)	0.3907	0.1570	0.6257	20.5
H(56)	0.3665	0.1638	0.4956	20.5
H(57)	0.5121	0.2083	0.6624	13.1
H(58)	0.5232	0.1822	0.5401	13.1
H(59)	0.4894	0.2862	0.6038	8.0
H(60)	0.4652	0.2612	0.4780	8.0
H(61)	0.3164	0.2954	0.4731	15.1
H(62)	0.3407	0.3207	0.5987	15.1

Table 28. (cont'd)

atom	x	y	z	B(eq)
H(63)	0.6181	0.1965	0.1639	25.9
H(64)	0.5803	0.1437	0.1843	25.9
H(65)	0.6204	0.2351	0.3321	26.3
H(66)	0.5420	0.2004	0.3287	26.3
H(67)	0.6862	0.1862	0.4845	22.9
H(68)	0.6533	0.1292	0.4277	22.9
H(69)	0.8121	0.1010	0.4010	36.7
H(70)	0.8103	0.1669	0.3884	36.7
H(71)	0.1387	0.1616	0.4425	19.1
H(72)	0.1316	0.1523	0.5639	19.1
H(73)	0.2633	0.0588	0.4529	30.8
H(74)	0.2203	0.0412	0.5450	30.8
H(75)	0.1375	0.0626	0.3329	15.6
H(76)	0.1588	0.0032	0.3910	15.6
H(77)	0.0167	0.0332	0.4403	25.3
H(78)	-0.0060	0.0515	0.3164	25.3

Table 29. Atomic positional parameters and equivalent isotropic displacement parameters (\AA^2) and their estimated standard deviations for $[\text{Re}_2\text{Cl}_4(\text{dppm})_2](\mu\text{-DMDCNQI})\cdot 4\text{THF} (7)\cdot 4\text{THF}$.

atom	x	y	z	B(eq)
Re(1)	0.1165(1)	0.71910(8)	0.5307(1)	2.7(1)
Re(2)	0.0892(1)	0.67145(7)	0.6701(1)	2.6(1)
Cl(1)	0.1863(8)	0.6310(4)	0.4255(8)	3.2(5)
Cl(2)	0.153(1)	0.7761(6)	0.377(1)	4.9(7)
Cl(3)	0.1073(8)	0.5677(4)	0.630(1)	4.1(5)
Cl(4)	0.0541(8)	0.7450(5)	0.8162(9)	4.1(6)
P(1)	-0.0396(8)	0.7120(5)	0.386(1)	3.0(5)
P(2)	-0.0874(8)	0.6777(5)	0.589(1)	2.9(5)
P(3)	0.2564(8)	0.6487(5)	0.788(1)	3.3(5)
P(4)	0.2802(8)	0.7370(5)	0.642(1)	3.4(6)
N(1)	0.055(2)	0.796(1)	0.582(3)	3(2)
N(2)	-0.017(3)	0.904(1)	0.619(3)	4(2)
C(1)	-0.026(3)	0.677(2)	0.249(3)	3.0(8)
C(2)	-0.018(4)	0.717(2)	0.170(4)	5(1)
C(3)	-0.014(4)	0.686(3)	0.045(5)	7(1)
C(4)	-0.003(5)	0.614(3)	0.028(6)	9(2)
C(5)	-0.004(4)	0.584(2)	0.101(5)	6(1)
C(6)	-0.017(4)	0.617(2)	0.221(4)	5(1)
C(7)	-0.134(3)	0.779(2)	0.367(4)	4(1)
C(8)	-0.107(5)	0.830(3)	0.355(6)	10(2)
C(9)	-0.183(4)	0.889(2)	0.323(4)	5(1)
C(10)	-0.278(5)	0.889(3)	0.299(5)	7(1)
C(11)	-0.308(4)	0.830(3)	0.289(5)	7(1)
C(12)	-0.232(3)	0.776(2)	0.324(4)	4(1)
C(13)	-0.130(3)	0.618(2)	0.637(4)	3.8(9)
C(14)	-0.139(4)	0.563(2)	0.556(4)	6(1)
C(15)	-0.180(4)	0.523(2)	0.608(4)	6(1)
C(16)	-0.187(3)	0.529(2)	0.719(3)	3.6(9)
C(17)	-0.177(4)	0.586(2)	0.799(4)	6(1)
C(18)	-0.144(4)	0.627(2)	0.751(4)	6(1)
C(19)	-0.191(3)	0.750(2)	0.587(4)	4(1)
C(20)	-0.171(3)	0.803(2)	0.632(4)	4(1)
C(21)	-0.250(3)	0.850(2)	0.641(4)	5(1)
C(22)	-0.349(4)	0.841(2)	0.615(4)	5(1)
C(23)	-0.366(4)	0.780(2)	0.570(4)	5(1)
C(24)	-0.289(4)	0.741(2)	0.555(4)	5(1)
C(25)	0.260(3)	0.640(2)	0.937(4)	5(1)
C(26)	0.249(4)	0.580(3)	0.954(5)	7(1)
C(27)	0.228(4)	0.568(3)	1.061(5)	7(1)
C(28)	0.238(4)	0.611(3)	1.130(5)	8(1)
C(29)	0.261(3)	0.660(2)	1.127(4)	4(1)
C(30)	0.264(3)	0.682(2)	1.021(4)	5(1)
C(31)	0.359(3)	0.580(2)	0.758(4)	5(1)
C(32)	0.448(4)	0.565(2)	0.844(4)	5(1)
C(33)	0.526(3)	0.527(2)	0.814(4)	5(1)
C(34)	0.518(4)	0.503(2)	0.718(4)	5(1)
C(35)	0.435(3)	0.513(2)	0.629(4)	5(1)
C(36)	0.361(3)	0.559(2)	0.658(4)	5(1)
C(37)	0.285(3)	0.816(2)	0.664(4)	4(1)
C(38)	0.329(4)	0.838(2)	0.598(4)	6(1)

Table 29. (cont'd)

atom	x	y	z	B(eq)
C(39)	0.338(4)	0.895(3)	0.599(5)	7(1)
C(40)	0.297(4)	0.930(2)	0.693(4)	5(1)
C(41)	0.242(4)	0.920(3)	0.749(5)	7(1)
C(42)	0.240(4)	0.855(2)	0.732(4)	5(1)
C(43)	0.394(3)	0.689(2)	0.593(4)	5(1)
C(44)	0.479(3)	0.676(2)	0.667(4)	4(1)
C(45)	0.562(5)	0.646(3)	0.596(6)	10(2)
C(46)	0.561(3)	0.632(2)	0.496(4)	5(1)
C(47)	0.467(3)	0.646(2)	0.428(4)	3.9(9)
C(48)	0.383(3)	0.679(2)	0.469(4)	4(1)
C(49)	-0.0857	0.6550	0.4348	5(1)
C(50)	0.309(3)	0.716(2)	0.791(4)	3.9(9)
C(51)	0.032(3)	0.846(2)	0.597(3)	4(2)
C(52)	-0.008(3)	0.953(2)	0.554(4)	4(1)
C(53)	-0.063(3)	1.015(2)	0.572(4)	5(1)
C(54)	0.058(3)	0.942(2)	0.482(3)	3.2(8)
C(55)	-0.135(5)	1.026(3)	0.662(5)	8(2)
H(1)	-0.0143	0.7612	0.1940	6.2
H(2)	-0.0186	0.7095	-0.0172	7.9
H(3)	0.0055	0.5961	-0.0489	10.3
H(4)	0.0018	0.5410	0.0814	7.1
H(5)	-0.0117	0.5900	0.2820	7.3
H(6)	-0.0260	0.8159	0.3797	15.0
H(7)	-0.1569	0.9234	0.3167	5.4
H(8)	-0.3290	0.9310	0.2931	9.0
H(9)	-0.3772	0.8284	0.2506	8.4
H(10)	-0.2514	0.7368	0.3234	5.2
H(11)	-0.1217	0.5554	0.4748	8.2
H(12)	-0.2085	0.4917	0.5581	7.0
H(13)	-0.1950	0.4936	0.7525	4.1
H(14)	-0.1914	0.5925	0.8764	7.7
H(15)	-0.1316	0.6643	0.7950	6.4
H(16)	-0.1028	0.8077	0.6592	5.4
H(17)	-0.2405	0.8916	0.6608	5.3
H(18)	-0.4050	0.8748	0.6292	6.1
H(19)	-0.4342	0.7724	0.5515	5.8
H(20)	-0.2984	0.7031	0.5172	6.0
H(21)	0.2501	0.5482	0.8884	8.1
H(22)	0.2121	0.5311	1.0777	8.1
H(23)	0.2283	0.6054	1.2059	8.9
H(24)	0.2758	0.6857	1.1967	4.8
H(25)	0.2677	0.7239	1.0113	6.0
H(26)	0.4494	0.5807	0.9223	6.3
H(27)	0.5907	0.5183	0.8681	5.4
H(28)	0.5761	0.4748	0.7003	6.2
H(29)	0.4277	0.4906	0.5523	5.6
H(30)	0.3047	0.5768	0.5973	5.1
H(31)	0.3635	0.8062	0.5498	6.6
H(32)	0.3622	0.9112	0.5421	8.3
H(33)	0.3148	0.9681	0.7157	6.3

Table 29. (cont'd)

atom	x	y	z	B(eq)
H(34)	0.2036	0.9495	0.7983	8.5
H(35)	0.2019	0.8394	0.7789	6.4
H(36)	0.4865	0.6839	0.7517	5.4
H(37)	0.6310	0.6340	0.6499	11.1
H(38)	0.6203	0.6133	0.4678	5.9
H(39)	0.4575	0.6351	0.3450	4.6
H(40)	0.3174	0.6943	0.4146	5.0
H(41)	-0.1514	0.6544	0.3919	5.1
H(42)	-0.0423	0.6163	0.4281	5.1
H(43)	0.2836	0.7489	0.8422	5.1
H(44)	0.3834	0.7059	0.8237	5.1
H(45)	0.0997	0.9004	0.4738	3.9
H(46)	-0.1826	1.0008	0.6429	8.8
H(47)	-0.0938	1.0131	0.7395	8.8
H(48)	-0.1688	1.0662	0.6726	8.8
O(1)	0.6880	0.6359	0.2798	13(1)
C(56)	0.5963	0.6770	0.2170	7(1)
C(57)	0.5527	0.6370	0.1351	8(1)
C(58)	0.7007	0.5863	0.2319	20(3)
C(59)	0.6470	0.5865	0.1251	11(2)
H(49)	0.5530	0.6962	0.2663	7.4
H(50)	0.6126	0.7069	0.1816	7.4
H(51)	0.5056	0.6223	0.1615	9.1
H(52)	0.5211	0.6552	0.0646	9.1
H(53)	0.7697	0.5721	0.2309	25.1
H(54)	0.6817	0.5599	0.2729	25.1
H(55)	0.6305	0.5487	0.1010	12.3
H(56)	0.6813	0.5962	0.0739	12.3
O(2)	0.5719	0.7396	0.9365	18(2)
C(60)	0.5568	0.7985	0.8884	18(3)
C(61)	0.6688	0.8068	0.9164	14(2)
C(62)	0.7039	0.7454	0.9202	11(2)
C(63)	0.6621	0.6939	0.9374	27(4)
H(57)	0.5291	0.7973	0.8085	18.9
H(58)	0.5148	0.8299	0.9251	18.9
H(59)	0.6849	0.8237	0.8572	14.6
H(60)	0.6873	0.8285	0.9869	14.6
H(61)	0.7217	0.7342	0.8485	11.6
H(62)	0.7630	0.7413	0.9794	11.6
H(63)	0.6916	0.6748	1.0075	23.0
H(64)	0.6588	0.6640	0.8762	23.0

Table 30. Atomic positional parameters and equivalent isotropic displacement parameters (\AA^2) and their estimated standard deviations for $[\text{Bu}_4\text{N}]_4[\text{Mo}_2(\text{CN})_8] \cdot 8\text{CHCl}_3 (8) \cdot 8\text{CHCl}_3$.

atom	x	y	z	B(eq)
Mo(1)	0.96425(4)	0.00343(3)	0.03830(5)	2.34(4)
N(1)	0.8832(5)	0.1023(3)	-0.0001(5)	3.8(6)
N(2)	1.0378(6)	0.0679(4)	0.1573(5)	4.4(6)
N(3)	0.8336(5)	-0.0562(3)	-0.0166(5)	3.8(6)
N(4)	0.9818(5)	-0.0889(4)	0.1426(5)	3.9(6)
N(5)	0.3119(5)	0.0465(3)	0.7032(5)	3.6(5)
N(6)	0.0664(5)	0.1996(3)	0.0459(6)	4.6(6)
C(1)	0.9123(6)	0.0687(4)	0.0104(6)	2.7(6)
C(2)	1.0157(6)	0.0457(4)	0.1140(6)	2.9(6)
C(3)	0.8787(6)	-0.0356(4)	-0.0012(6)	2.7(6)
C(4)	0.9794(5)	-0.0593(4)	0.1053(6)	2.8(6)
C(5)	0.2988(6)	0.0357(4)	0.6311(6)	3.3(6)
C(6)	0.2310(6)	0.0508(5)	0.6090(7)	4.9(8)
C(7)	0.2250(6)	0.0429(4)	0.5302(8)	5.1(8)
C(8)	0.1568(7)	0.0554(5)	0.5022(8)	7(1)
C(9)	0.2611(7)	0.0237(5)	0.7506(8)	5.4(8)
C(10)	0.2544(8)	-0.0294(5)	0.7487(8)	6(1)
C(11)	0.204(1)	-0.0452(7)	0.800(2)	13(2)
C(12)	0.148(2)	-0.031(1)	0.793(2)	22(3)
C(13)	0.3803(6)	0.0270(4)	0.7170(7)	4.1(7)
C(14)	0.4049(8)	0.0300(5)	0.7908(7)	5.3(8)
C(15)	0.4766(7)	0.0129(6)	0.7951(8)	7(1)
C(16)	0.5002(9)	0.0137(7)	0.8664(8)	9(1)
C(17)	0.3106(6)	0.0996(5)	0.7174(6)	4.1(7)
C(18)	0.3544(6)	0.1295(5)	0.6739(7)	4.6(8)
C(19)	0.3459(8)	0.1823(5)	0.6903(7)	6(1)
C(20)	0.389(1)	0.2140(5)	0.6487(8)	8(1)
C(21)	0.0497(7)	0.2493(6)	0.026(1)	7(1)
C(22)	0.0004(7)	0.2576(5)	-0.025(1)	7(1)
C(23)	-0.019(1)	0.3082(7)	-0.041(2)	19(2)
C(24)	0.028(2)	0.341(1)	-0.040(3)	31(5)
C(25)	0.0073(6)	0.1734(4)	0.0737(7)	4.8(8)
C(26)	-0.026(1)	0.1950(6)	0.131(1)	11(1)
C(27)	-0.0768(8)	0.1628(6)	0.162(1)	9(1)
C(28)	-0.108(1)	0.185(1)	0.223(1)	20(2)
C(29)	0.1210(7)	0.2035(6)	0.0963(9)	6(1)
C(30)	0.1473(9)	0.1583(7)	0.1214(8)	7(1)
C(31)	0.205(2)	0.164(2)	0.179(2)	17(3)
C(32)	0.185(2)	0.179(2)	0.220(3)	36(6)
C(33)	0.0873(6)	0.1710(4)	-0.0157(7)	4.0(7)
C(34)	0.1438(6)	0.1926(5)	-0.0565(8)	5.0(8)
C(35)	0.1669(7)	0.1577(5)	-0.1113(7)	5.2(8)
C(36)	0.2206(8)	0.1796(6)	-0.1545(8)	8(1)
Cl(1)	1.1089(2)	0.1276(2)	0.6880(3)	11.4(4)
Cl(2)	1.0613(3)	0.2098(2)	0.7566(3)	11.1(4)
Cl(3)	0.9757(2)	0.1555(2)	0.6756(3)	9.5(3)
Cl(4)	0.3154(2)	0.2317(1)	0.4657(3)	9.7(3)
Cl(5)	0.2221(2)	0.1824(2)	0.5506(3)	8.7(3)
Cl(6)	0.2250(2)	0.1649(2)	0.4086(3)	8.8(3)
Cl(7)	0.3075(2)	0.1582(1)	0.0221(3)	8.0(3)

Table 30. (cont'd)

atom	x	y	z	B(eq)
Cl(8)	0.3485(3)	0.0739(2)	0.0868(3)	10.2(4)
Cl(9)	0.3467(3)	0.0790(2)	-0.0559(3)	10.7(4)
Cl(10)	0.4603(5)	0.1124(3)	0.1759(4)	18.1(7)
Cl(11)	0.5964(4)	0.0974(3)	0.1631(4)	17.9(7)
Cl(12)	0.5475(5)	0.1866(3)	0.2054(5)	20.2(8)
C(37)	1.0444(8)	0.1510(5)	0.7296(8)	7(1)
C(38)	0.2701(7)	0.1787(5)	0.4812(9)	7(1)
C(39)	0.3080(7)	0.0973(5)	0.0149(8)	6(1)
C(40)	0.535(1)	0.129(1)	0.199(3)	46(5)
H(1)	0.3297	0.0521	0.6039	4.1
H(2)	0.3029	0.0025	0.6239	4.1
H(3)	0.1995	0.0322	0.6322	5.8
H(4)	0.2247	0.0835	0.6198	5.8
H(5)	0.2564	0.0623	0.5084	6.0
H(6)	0.2335	0.0104	0.5207	6.0
H(7)	0.1478	0.0881	0.5107	8.4
H(8)	0.1561	0.0500	0.4549	8.4
H(9)	0.1248	0.0363	0.5234	8.4
H(10)	0.2725	0.0322	0.7953	6.4
H(11)	0.2199	0.0368	0.7396	6.4
H(12)	0.2401	-0.0391	0.7052	7.4
H(13)	0.2952	-0.0439	0.7583	7.4
H(14)	0.2041	-0.0786	0.8022	15.1
H(15)	0.2185	-0.0330	0.8435	15.1
H(16)	0.1460	0.0027	0.7912	25.9
H(17)	0.1315	-0.0430	0.7502	25.9
H(18)	0.1202	-0.0424	0.8275	25.9
H(19)	0.3804	-0.0057	0.7043	5.1
H(20)	0.4100	0.0439	0.6895	5.1
H(21)	0.4026	0.0620	0.8056	6.3
H(22)	0.3785	0.0106	0.8186	6.3
H(23)	0.4791	-0.0190	0.7786	8.7
H(24)	0.5032	0.0328	0.7683	8.7
H(25)	0.4738	-0.0062	0.8931	10.9
H(26)	0.5441	0.0028	0.8675	10.9
H(27)	0.4984	0.0454	0.8826	10.9
H(28)	0.2671	0.1105	0.7110	4.8
H(29)	0.3230	0.1044	0.7629	4.8
H(30)	0.3986	0.1207	0.6818	5.5
H(31)	0.3441	0.1243	0.6278	5.5
H(32)	0.3017	0.1907	0.6823	7.2
H(33)	0.3558	0.1870	0.7365	7.2
H(34)	0.4332	0.2060	0.6564	10.3
H(35)	0.3789	0.2098	0.6023	10.3
H(36)	0.3816	0.2462	0.6609	10.3
H(37)	0.0353	0.2652	0.0657	8.7
H(38)	0.0891	0.2637	0.0104	8.7
H(39)	0.0146	0.2412	-0.0646	8.2
H(40)	-0.0386	0.2436	-0.0091	8.2
H(41)	-0.0148	0.3091	-0.0935	22.5

Table 30. (cont'd)

atom	x	y	z	B(eq)
H(42)	-0.0578	0.3149	-0.0297	22.5
H(43)	0.0670	0.3394	-0.0399	33.6
H(44)	0.0079	0.3737	-0.0412	33.6
H(45)	0.0238	0.3453	0.0237	33.6
H(46)	-0.0236	0.1706	0.0385	5.8
H(47)	0.0213	0.1426	0.0871	5.8
H(48)	0.0060	0.2019	0.1648	13.0
H(49)	-0.0460	0.2234	0.1169	13.0
H(50)	-0.1100	0.1574	0.1294	10.7
H(51)	-0.0571	0.1335	0.1738	10.7
H(52)	-0.0746	0.1899	0.2570	24.0
H(53)	-0.1273	0.2140	0.2125	24.0
H(54)	-0.1393	0.1635	0.2416	24.0
H(55)	0.1560	0.2204	0.0758	7.3
H(56)	0.1055	0.2209	0.1340	7.3
H(57)	0.1126	0.1406	0.1409	8.2
H(58)	0.1647	0.1410	0.0843	8.2
H(59)	0.2232	0.1338	0.1886	20.2
H(60)	0.2383	0.1844	0.1616	20.2
H(61)	0.2180	0.1824	0.2545	42.1
H(62)	0.1668	0.2088	0.2110	42.1
H(63)	0.1520	0.1582	0.2381	42.1
H(64)	0.1005	0.1404	-0.0009	4.8
H(65)	0.0508	0.1681	-0.0448	4.8
H(66)	0.1293	0.2210	-0.0773	6.1
H(67)	0.1789	0.1993	-0.0270	6.1
H(68)	0.1832	0.1298	-0.0901	6.3
H(69)	0.1311	0.1497	-0.1392	6.3
H(70)	0.2569	0.1874	-0.1267	9.5
H(71)	0.2339	0.1574	-0.1878	9.5
H(72)	0.2048	0.2076	-0.1754	9.5
H(73)	1.0342	0.1316	0.7672	8.0
H(74)	0.3003	0.1536	0.4886	8.0
H(75)	0.2644	0.0861	0.0138	7.5
H(76)	0.5368	0.1151	0.2586	32.4

Table 31. Atomic positional parameters and equivalent isotropic displacement parameters (\AA^2) and their estimated standard deviations for $[\text{Bu}_4\text{N}]_3[\text{Mo}_2(\text{O}_2\text{CCH}_3)(\text{CN})_6]$ (9).

atom	x	y	z	B(eq)
Mo(1)	0.0808(1)	0.2977	0.72110(7)	4.78(9)
Mo(2)	0.0710(1)	0.3948(2)	0.80504(7)	4.30(8)
O(1)	0.192(1)	0.229(1)	0.8005(7)	5.5(7)
O(2)	0.1786(9)	0.329(1)	0.8890(6)	5.3(7)
N(1)	-0.075(1)	0.339(1)	0.5566(8)	6(1)
N(2)	-0.132(2)	0.168(2)	0.745(1)	8(1)
N(3)	0.292(1)	0.355(2)	0.6167(9)	10(1)
N(4)	-0.092(1)	0.536(1)	0.712(1)	6(1)
N(5)	-0.121(1)	0.355(1)	0.9311(8)	5.3(9)
N(6)	0.290(1)	0.519(1)	0.800(1)	8(1)
N(7)	-0.404(1)	0.408(1)	0.7369(9)	5.7(9)
N(8)	0.098(2)	0.593(1)	0.016(1)	7(1)
N(9)	0.882(1)	0.062(2)	0.5054(8)	7(1)
C(1)	-0.021(1)	0.333(1)	0.6162(9)	5(1)
C(2)	-0.060(2)	0.214(2)	0.744(1)	5(1)
C(3)	0.223(1)	0.339(2)	0.655(1)	6(1)
C(4)	-0.037(2)	0.490(2)	0.743(1)	5(1)
C(5)	-0.061(1)	0.366(1)	0.8815(9)	4(1)
C(6)	0.213(2)	0.473(2)	0.793(1)	6(1)
C(7)	0.224(1)	0.263(2)	0.868(1)	5(1)
C(8)	0.301(2)	0.213(2)	0.923(1)	8(1)
C(9)	-0.350(1)	0.424(2)	0.822(1)	7(1)
C(10)	-0.435(2)	0.440(2)	0.884(1)	7(1)
C(11)	-0.370(2)	0.481(2)	0.957(1)	10.5(7)
C(12)	-0.451(2)	0.494(2)	1.018(2)	12.1(8)
C(13)	-0.307(1)	0.389(2)	0.686(1)	6(1)
C(14)	-0.341(2)	0.360(2)	0.603(2)	11(2)
C(15)	-0.337(3)	0.424(3)	0.551(2)	14(1)
C(16)	-0.345(3)	0.390(3)	0.459(2)	18(1)
C(17)	-0.480(1)	0.334(2)	0.738(1)	5(1)
C(18)	-0.428(2)	0.255(2)	0.768(1)	7(1)
C(19)	-0.508(2)	0.185(2)	0.754(1)	7.8(5)
C(20)	-0.473(2)	0.101(2)	0.787(1)	10.5(7)
C(21)	-0.470(2)	0.482(2)	0.706(1)	7(1)
C(22)	-0.408(2)	0.562(2)	0.702(1)	9(2)
C(23)	-0.492(3)	0.630(3)	0.678(2)	13(1)
C(24)	-0.438(3)	0.716(3)	0.682(2)	13(1)
C(25)	0.029(2)	0.604(2)	-0.058(1)	8(2)
C(26)	-0.021(3)	0.689(2)	-0.073(2)	15(2)
C(27)	-0.082(2)	0.703(2)	-0.154(1)	10.3(7)
C(28)	-0.184(2)	0.657(2)	-0.144(1)	11.0(7)
C(29)	0.023(2)	0.589(1)	0.085(1)	6(1)
C(30)	-0.072(2)	0.523(2)	0.085(2)	10(2)
C(31)	-0.112(3)	0.511(3)	0.164(2)	15(1)
C(32)	-0.197(6)	0.477(5)	0.173(4)	29(2)
C(33)	0.181(2)	0.658(1)	0.029(1)	8(1)
C(34)	0.259(2)	0.661(2)	-0.035(1)	9.2(6)
C(35)	0.348(2)	0.724(2)	-0.012(1)	10.2(7)
C(36)	0.427(2)	0.737(2)	-0.075(1)	11.2(7)
C(37)	0.445(2)	0.505(2)	0.012(1)	6(1)

Table 31. (cont'd)

atom	x	y	z	B(eq)
C(38)	0.217(2)	0.476(2)	0.084(1)	9(1)
C(39)	0.268(2)	0.393(2)	0.076(1)	8.1(5)
C(40)	0.339(2)	0.371(2)	0.157(1)	9.5(6)
C(41)	0.865(2)	0.076(1)	0.417(1)	6(1)
C(42)	0.843(3)	0.166(2)	0.389(1)	11(2)
C(43)	0.838(2)	0.178(2)	0.311(2)	12.8(9)
C(44)	0.798(2)	0.263(2)	0.282(1)	10.2(7)
C(45)	0.787(2)	0.100(2)	0.547(1)	7(1)
C(46)	0.675(2)	0.064(2)	0.518(1)	10(2)
C(47)	0.555(4)	0.120(4)	0.546(2)	21(2)
C(48)	0.574(5)	0.040(5)	0.595(3)	27(2)
C(49)	0.892(2)	-0.030(2)	0.519(1)	8(2)
C(50)	0.915(2)	-0.048(3)	0.608(2)	13(2)
C(51)	0.930(5)	-0.125(5)	0.625(3)	22(2)
C(52)	0.847(3)	-0.178(3)	0.607(2)	18(1)
C(53)	0.979(2)	0.109(2)	0.539(1)	7(1)
C(54)	1.093(2)	0.084(2)	0.508(1)	10(2)
C(55)	1.195(2)	0.133(2)	0.548(2)	10.9(8)
C(56)	1.203(3)	0.088(3)	0.629(3)	19(1)
H(1)	0.2686	0.2019	0.9737	11.8
H(2)	0.3310	0.1659	0.9039	11.8
H(3)	0.3665	0.2510	0.9411	11.8
H(4)	-0.2979	0.3793	0.8395	8.5
H(5)	-0.2994	0.4742	0.8222	8.5
H(6)	-0.4957	0.4716	0.8652	9.8
H(7)	-0.4637	0.3862	0.9035	9.8
H(8)	-0.3023	0.4537	0.9797	14.8
H(9)	-0.3396	0.5392	0.9439	14.8
H(10)	-0.4184	0.5217	1.0679	13.5
H(11)	-0.5128	0.5253	1.0004	13.5
H(12)	-0.4751	0.4402	1.0365	13.5
H(13)	-0.2605	0.4395	0.6827	8.0
H(14)	-0.2589	0.3475	0.7108	8.0
H(15)	-0.2902	0.3200	0.5826	12.7
H(16)	-0.4132	0.3388	0.5978	12.7
H(17)	-0.4021	0.4625	0.5555	18.4
H(18)	-0.2730	0.4601	0.5608	18.4
H(19)	-0.4079	0.3579	0.4480	19.5
H(20)	-0.3410	0.4342	0.4211	19.5
H(21)	-0.2788	0.3552	0.4534	19.5
H(22)	-0.5415	0.3453	0.7724	7.0
H(23)	-0.5163	0.3233	0.6859	7.0
H(24)	-0.3626	0.2389	0.7403	8.2
H(25)	-0.4056	0.2532	0.8238	8.2
H(26)	-0.5821	0.1961	0.7755	9.9
H(27)	-0.5315	0.1757	0.6956	9.9
H(28)	-0.5317	0.0580	0.7735	13.1
H(29)	-0.4103	0.0832	0.7603	13.1
H(30)	-0.4605	0.1038	0.8402	13.1
H(31)	-0.3014	0.4689	1.0532	8.0

Table 31. (cont'd)

atom	x	y	z	B(eq)
H(32)	-0.5336	0.4879	0.7388	8.9
H(33)	-0.3775	0.5704	0.7573	10.6
H(34)	-0.3542	0.5553	0.6692	10.6
H(35)	-0.5200	0.6255	0.6248	15.4
H(36)	-0.5551	0.6329	0.7113	15.4
H(37)	-0.4203	0.7278	0.7381	16.4
H(38)	-0.3857	0.7205	0.6515	16.4
H(39)	-0.5010	0.7571	0.6678	16.4
H(40)	0.0840	0.5919	-0.1039	9.3
H(41)	-0.0236	0.5597	-0.0687	9.3
H(42)	-0.0664	0.7002	-0.0268	13.7
H(43)	0.0421	0.7327	-0.0604	13.7
H(44)	-0.0983	0.7602	-0.1686	12.1
H(45)	-0.0422	0.6796	-0.1969	12.1
H(46)	-0.2248	0.6796	-0.1016	13.3
H(47)	-0.2350	0.6551	-0.1909	13.3
H(48)	-0.1684	0.5989	-0.1295	13.3
H(49)	0.0662	0.5841	0.1378	9.0
H(50)	-0.0152	0.6446	0.0914	9.0
H(51)	-0.1355	0.5377	0.0504	13.1
H(52)	-0.0442	0.4701	0.0652	13.1
H(53)	-0.0536	0.4739	0.1937	16.3
H(54)	-0.1086	0.5614	0.1910	16.3
H(55)	-0.2618	0.5073	0.1522	30.6
H(56)	-0.2068	0.4199	0.1550	30.6
H(57)	-0.2138	0.4709	0.2327	30.6
H(58)	0.1365	0.7122	0.0268	11.9
H(59)	0.2150	0.6561	0.0807	11.9
H(60)	0.2960	0.6062	-0.0376	11.9
H(61)	0.2255	0.6718	-0.0863	11.9
H(62)	0.3050	0.7754	-0.0045	14.0
H(63)	0.3800	0.7086	0.0388	14.0
H(64)	0.4712	0.6854	-0.0805	13.2
H(65)	0.3965	0.7527	-0.1235	13.2
H(66)	0.4842	0.7783	-0.0560	13.2
H(67)	0.0856	0.4643	0.0004	9.5
H(68)	0.1892	0.5020	-0.0359	9.5
H(69)	0.2795	0.5150	0.0942	10.3
H(70)	0.1760	0.4769	0.1302	10.3
H(71)	0.2056	0.3530	0.0657	10.9
H(72)	0.3092	0.3911	0.0298	10.9
H(73)	0.2971	0.3730	0.2038	12.8
H(74)	0.3744	0.3168	0.1570	12.8
H(75)	0.4007	0.4109	0.1677	12.8
H(76)	0.9298	0.0542	0.3886	8.6
H(77)	0.8028	0.0413	0.3936	8.6
H(78)	0.7803	0.1841	0.4156	13.5
H(79)	0.9074	0.1975	0.4122	13.5
H(80)	0.8974	0.1635	0.2835	14.8
H(81)	0.7723	0.1415	0.2857	14.3

Table 31. (cont'd)

atom	x	y	z	B(eq)
H(82)	0.8567	0.3034	0.3032	11.3
H(83)	0.7894	0.2714	0.2273	11.3
H(84)	0.7316	0.2815	0.3061	11.3
H(85)	0.7989	0.1024	0.6057	9.8
H(86)	0.7817	0.1626	0.5338	9.8
H(87)	0.6671	0.0547	0.4661	13.4
H(88)	0.6729	0.0060	0.5458	13.4
H(89)	0.5302	0.0222	0.6519	33.8
H(90)	0.5796	-0.0241	0.5817	33.8
H(91)	0.6559	0.0302	0.6389	33.8
H(92)	0.5649	0.1677	0.5733	22.9
H(93)	0.4894	0.1132	0.5157	22.9
H(94)	0.8234	-0.0582	0.4942	11.6
H(95)	0.9507	-0.0540	0.4856	11.6
H(96)	0.9821	-0.0203	0.6337	16.4
H(97)	0.8550	-0.0263	0.6420	16.4
H(98)	0.9782	-0.1353	0.5840	25.0
H(99)	0.9513	-0.1306	0.6726	25.0
H(100)	0.7926	-0.1756	0.6424	21.9
H(101)	0.8198	-0.1805	0.5539	21.9
H(102)	0.8863	-0.2342	0.6174	21.9
H(103)	0.9635	0.1705	0.5250	9.8
H(104)	0.9866	0.1095	0.5956	9.8
H(105)	1.1091	0.0276	0.5123	12.2
H(106)	1.0920	0.0949	0.4465	12.2
H(107)	1.2660	0.1421	0.5202	13.6
H(108)	1.1788	0.1983	0.5574	13.6
H(109)	1.1390	0.0860	0.6509	22.4
H(110)	1.2254	0.0293	0.6133	22.4
H(111)	1.2650	0.1060	0.6637	22.4

Table 32. Atomic positional parameters and equivalent isotropic displacement parameters (\AA^2) and their estimated standard deviations for $[\text{Bu}_4\text{N}][\text{Re}_2(\text{CN})_6(\text{dppm})_2] \cdot 8\text{CH}_2\text{Cl}_2 (11) \cdot 8\text{CH}_2\text{Cl}_2$.

atom	x	y	z	B(eq)
Re(1)	1.02288(2)	0.08407(1)	1.00331(2)	1.68(1)
P(1)	1.0689(1)	0.0396(1)	0.8275(1)	1.94(5)
P(2)	0.9753(1)	0.1286(1)	1.1790(1)	1.91(5)
N(1)	1.1544(4)	-0.0209(3)	1.1368(5)	2.8(2)
N(2)	1.2275(4)	0.2155(3)	1.1191(5)	3.0(2)
N(3)	0.9342(4)	0.2307(3)	0.9269(5)	3.1(2)
N(4)	0.7039(4)	0.3272(3)	0.7869(5)	2.6(2)
C(1)	1.1113(5)	0.0207(4)	1.0882(6)	2.2(2)
C(2)	1.1545(5)	0.1683(3)	1.0796(6)	2.1(2)
C(3)	0.9642(5)	0.1777(4)	0.9526(6)	2.3(2)
C(4)	1.0082(5)	-0.0611(4)	0.7328(6)	2.1(2)
C(11)	1.2036(5)	0.0383(3)	0.8342(6)	2.0(2)
C(12)	1.2815(6)	0.0447(4)	0.9412(7)	2.5(2)
C(13)	1.3811(6)	0.0395(4)	0.9416(7)	2.8(2)
C(14)	1.4031(6)	0.0278(4)	0.8372(7)	3.2(3)
C(15)	1.3273(6)	0.0227(4)	0.7308(7)	3.2(3)
C(16)	1.2277(5)	0.0286(4)	0.7294(6)	2.7(2)
C(21)	1.0266(5)	0.0952(4)	0.7248(6)	2.1(2)
C(22)	0.9364(5)	0.0747(4)	0.6275(6)	2.7(2)
C(23)	0.9057(6)	0.1241(4)	0.5597(6)	3.2(3)
C(24)	0.9670(7)	0.1950(5)	0.5904(6)	3.4(3)
C(25)	1.0590(6)	0.2162(4)	0.6866(7)	3.7(3)
C(26)	1.0883(6)	0.1679(4)	0.7535(7)	3.1(3)
C(31)	1.0510(5)	0.2205(4)	1.2934(6)	2.1(2)
C(32)	1.0441(6)	0.2881(4)	1.2625(7)	3.0(2)
C(33)	1.1000(7)	0.3598(4)	1.3451(8)	3.8(3)
C(34)	1.1626(7)	0.3643(4)	1.4587(7)	4.1(3)
C(35)	1.1715(7)	0.2983(5)	1.4903(7)	4.3(3)
C(36)	1.1158(5)	0.2263(4)	1.4090(6)	3.0(3)
C(41)	0.8457(5)	0.1501(3)	1.1656(6)	2.2(2)
C(42)	0.7717(5)	0.1450(4)	1.0565(6)	2.4(2)
C(43)	0.6754(5)	0.1622(4)	1.0506(7)	2.9(2)
C(44)	0.6483(6)	0.1844(4)	1.1531(7)	3.2(3)
C(45)	0.7198(6)	0.1893(5)	1.2631(8)	3.9(3)
C(46)	0.8169(6)	0.1726(4)	1.2688(6)	3.2(3)
C(47)	0.6410(6)	0.3906(4)	0.7697(8)	3.2(3)
C(48)	0.5413(6)	0.3867(5)	0.7968(9)	3.9(3)
C(49)	0.4930(8)	0.4567(6)	0.785(1)	5.1(4)
C(50)	0.3940(8)	0.4580(7)	0.813(1)	6.2(4)
C(51)	0.7273(6)	0.3208(4)	0.9131(6)	2.7(2)
C(52)	0.7743(7)	0.3958(5)	1.0172(7)	3.5(3)
C(53)	0.7956(7)	0.3819(5)	1.1373(7)	4.3(3)
C(54)	0.8563(8)	0.4536(6)	1.2435(9)	5.1(4)
C(55)	0.6451(6)	0.2485(4)	0.6953(7)	2.9(3)
C(56)	0.7073(6)	0.1831(4)	0.6879(8)	3.8(3)
C(57)	0.6388(7)	0.1035(5)	0.6125(8)	3.8(3)
C(58)	0.5794(8)	0.0741(6)	0.680(1)	5.3(4)
C(59)	0.8064(6)	0.3482(5)	0.7710(7)	2.9(3)
C(60)	0.8001(6)	0.3516(5)	0.6468(7)	3.8(3)
C(61)	0.9029(7)	0.3902(5)	0.6523(8)	4.3(3)

Table 32. (cont'd)

atom	x	y	z	B(eq)
C(62)	0.900(1)	0.3960(7)	0.530(1)	5.5(4)
Cl(1)	1.0697(2)	0.4335(1)	1.0633(2)	5.8(1)
Cl(2)	1.2294(2)	0.3862(1)	0.9669(3)	6.9(1)
C(63)	1.1348(6)	0.3571(5)	1.022(1)	5.0(4)
Cl(3)	0.4850(2)	0.3222(2)	0.0576(3)	6.8(1)
Cl(4)	0.3650(2)	0.2318(2)	-0.1923(3)	8.1(1)
C(64)	0.3908(8)	0.2401(5)	-0.040(1)	6.4(4)
Cl(5)	0.4572(2)	0.1381(2)	0.3056(3)	6.8(1)
Cl(6)	0.3572(2)	0.1434(2)	0.4839(2)	8.4(1)
C(65)	0.3390(7)	0.1323(6)	0.3323(8)	5.7(4)
Cl(7)	0.3541(4)	0.4439(3)	0.3571(5)	14.7(3)
Cl(8)	0.5195(7)	0.3562(3)	0.4095(6)	28.1(5)
C(66)	0.396(1)	0.3530(7)	0.363(2)	17(1)
H(1)	1.273(5)	0.053(4)	1.000(6)	2(1)
H(2)	1.435(4)	0.041(3)	1.008(5)	2(1)
H(3)	1.466(5)	0.023(4)	0.834(6)	3(1)
H(4)	1.345(5)	0.012(4)	0.659(6)	4(1)
H(5)	1.181(6)	0.029(4)	0.666(7)	4(2)
H(6)	0.887(4)	0.023(3)	0.607(5)	2(1)
H(7)	0.842(5)	0.112(4)	0.496(6)	3(1)
H(8)	0.949(5)	0.225(4)	0.546(6)	2(1)
H(9)	1.100(5)	0.274(4)	0.707(6)	3(1)
H(10)	1.151(7)	0.171(6)	0.809(9)	8(2)
H(11)	1.001(4)	0.287(3)	1.179(5)	1(1)
H(12)	1.088(6)	0.405(5)	1.321(8)	6(2)
H(13)	1.199(5)	0.413(4)	1.511(6)	3(1)
H(14)	1.209(5)	0.302(4)	1.560(7)	4(1)
H(15)	1.121(5)	0.180(4)	1.427(6)	3(1)
H(16)	0.782(5)	0.129(3)	0.984(6)	2(1)
H(17)	0.620(6)	0.158(4)	0.971(7)	6(2)
H(18)	0.587(5)	0.196(4)	1.146(6)	3(1)
H(19)	0.703(7)	0.207(6)	1.325(8)	7(2)
H(20)	0.868(5)	0.175(4)	1.355(6)	4(1)
H(21)	0.678(5)	0.440(4)	0.820(6)	2(1)
H(22)	0.627(4)	0.391(3)	0.686(5)	1(1)
H(23)	0.500(5)	0.340(4)	0.748(6)	3(1)
H(24)	0.554(5)	0.383(4)	0.878(7)	4(1)
H(25)	0.542(7)	0.515(6)	0.839(9)	8(2)
H(26)	0.456(6)	0.448(4)	0.699(7)	4(1)
H(27)	0.357(8)	0.500(6)	0.80(1)	9(1)
H(28)	0.342(7)	0.398(6)	0.759(8)	7(1)
H(29)	0.41(1)	0.470(7)	0.92(1)	13(1)
H(30)	0.666(5)	0.306(3)	0.921(5)	2(1)
H(31)	0.776(5)	0.280(4)	0.922(6)	3(1)
H(32)	0.837(6)	0.413(4)	1.021(6)	4(1)
H(33)	0.745(6)	0.447(5)	1.011(7)	5(2)
H(34)	0.748(7)	0.353(5)	1.152(8)	7(2)
H(35)	0.842(6)	0.332(5)	1.135(7)	6(2)
H(36)	0.872(8)	0.450(6)	1.31(1)	8(2)
H(37)	0.938(9)	0.475(6)	1.25(1)	11(2)

Table 32. (cont'd)

atom	x	y	z	B(eq)
H(38)	0.825(7)	0.499(5)	1.236(8)	6(2)
H(39)	0.576(6)	0.237(5)	0.715(7)	6(2)
H(40)	0.621(4)	0.257(3)	0.620(5)	2(1)
H(41)	0.760(6)	0.197(4)	0.652(7)	5(2)
H(42)	0.744(6)	0.185(5)	0.768(8)	5(2)
H(43)	0.594(5)	0.104(4)	0.536(6)	3(1)
H(44)	0.676(5)	0.055(4)	0.596(6)	4(1)
H(45)	0.537(8)	0.118(6)	0.71(1)	10(2)
H(46)	0.529(6)	0.026(5)	0.629(7)	5(1)
H(47)	0.633(8)	0.063(6)	0.76(1)	10(2)
H(48)	0.832(5)	0.403(4)	0.826(6)	4(1)
H(49)	0.850(6)	0.307(5)	0.785(7)	7(2)
H(50)	0.781(5)	0.295(4)	0.582(7)	4(1)
H(51)	0.739(6)	0.383(5)	0.616(7)	6(2)
H(52)	0.905(6)	0.440(5)	0.708(8)	6(2)
H(53)	0.964(7)	0.354(5)	0.683(8)	7(2)
H(54)	0.963(8)	0.429(6)	0.54(1)	9(2)
H(55)	0.876(6)	0.348(5)	0.471(7)	5(1)
H(56)	0.848(8)	0.427(6)	0.50(1)	8(1)
H(59)	1.1676	0.3419	1.0908	6.0
H(60)	1.0875	0.3136	0.9605	6.0
H(61)	0.4149	0.1940	-0.0284	7.9
H(62)	0.3289	0.2440	-0.0228	7.9
H(63)	0.3042	0.1726	0.3111	6.5
H(64)	0.2971	0.0831	0.2820	6.5
H(65)	0.3653	0.3341	0.4064	17.8
H(66)	0.3695	0.3193	0.2770	17.8
H(57)	0.934(5)	-0.058(3)	0.704(5)	2(1)
H(58)	1.028(4)	-0.077(3)	0.667(5)	2(1)

Table 33. Atomic positional parameters and equivalent isotropic displacement parameters (\AA^2) and their estimated standard deviations for $[\text{Rh}\{\text{Me}_2(\text{Ph}_2\text{P})_2\text{TTF}\}_2][\text{BF}_4]$ (12).

atom	x	y	z	B(eq)
Rh(1)	0	0	1/2	1.5(2)
S(1)	0.3040(8)	0.0840(6)	0.5001(6)	3.7(5)
S(2)	0.3188(7)	-0.0660(6)	0.5293(6)	3.5(5)
S(3)	0.5163(8)	0.1032(7)	0.5599(6)	4.1(6)
S(4)	0.5348(7)	-0.0444(6)	0.5885(6)	4.1(6)
P(1)	0.1029(7)	0.0846(6)	0.4974(5)	2.0(5)
P(2)	0.1183(7)	-0.0737(6)	0.5260(5)	1.9(4)
C(1)	0.131(3)	0.152(2)	0.554(2)	2.3(8)
C(2)	0.094(3)	0.137(2)	0.598(2)	3(1)
C(3)	0.119(3)	0.179(2)	0.655(2)	3(1)
C(4)	0.162(3)	0.239(3)	0.652(2)	5(1)
C(5)	0.206(3)	0.254(2)	0.602(2)	3(1)
C(6)	0.183(3)	0.207(2)	0.558(2)	3(1)
C(7)	0.089(2)	0.131(2)	0.428(2)	1.8(8)
C(8)	0.101(3)	0.095(2)	0.388(2)	3(1)
C(9)	0.088(3)	0.127(3)	0.337(2)	5(1)
C(10)	0.056(4)	0.195(3)	0.332(3)	7(2)
C(11)	0.058(3)	0.229(2)	0.376(2)	3(1)
C(12)	0.071(3)	0.206(2)	0.425(2)	2.5(9)
C(13)	0.112(3)	-0.146(2)	0.476(2)	4(1)
C(14)	0.130(3)	-0.145(3)	0.423(2)	4(1)
C(15)	0.115(2)	-0.193(2)	0.388(2)	1.9(8)
C(16)	0.085(3)	-0.264(2)	0.400(2)	3(1)
C(17)	0.073(3)	-0.278(3)	0.453(2)	4(1)
C(18)	0.091(3)	-0.220(2)	0.501(2)	2.4(9)
C(19)	0.157(3)	-0.108(2)	0.598(2)	3(1)
C(20)	0.121(3)	-0.072(2)	0.639(2)	2.7(9)
C(21)	0.145(3)	-0.091(3)	0.691(2)	5(1)
C(22)	0.210(4)	-0.148(3)	0.716(2)	6(1)
C(23)	0.241(3)	-0.179(3)	0.671(2)	5(1)
C(24)	0.210(3)	-0.155(2)	0.617(2)	2.6(9)
C(25)	0.202(3)	0.046(2)	0.502(2)	4(1)
C(26)	0.211(2)	-0.031(2)	0.522(2)	1.9(8)
C(27)	0.376(3)	0.014(2)	0.534(2)	4(1)
C(28)	0.462(2)	0.023(2)	0.559(2)	1.9(8)
C(29)	0.612(3)	0.078(3)	0.606(2)	5(1)
C(30)	0.622(3)	0.013(2)	0.621(2)	4(1)
C(31)	0.673(4)	0.135(3)	0.631(2)	6(1)
C(32)	0.697(3)	-0.030(3)	0.659(2)	5(1)

Table 34. Atomic positional parameters and equivalent isotropic displacement parameters (\AA^2) and their estimated standard deviations for $\text{Re}_2(\mu\text{-O})(\mu\text{-Cl})\text{OCH}_3(\text{dppm})_2(\text{CH}_3)_2\text{CO}(\mathbf{14})\cdot(\text{CH}_3)_2\text{CO}$.

atom	x	y	z	B(eq)
Re(1)	0.84705(3)	0.74655(4)	0.21818(4)	3.05(2)
Re(2)	0.68697(3)	0.75287(3)	0.36552(4)	2.92(2)
Cl(1)	0.6851(2)	0.6991(2)	0.1436(3)	3.4(1)
Cl(2)	0.9939(2)	0.8034(3)	0.3238(4)	5.0(1)
Cl(3)	0.7000(3)	0.8053(2)	0.5698(3)	4.3(1)
Cl(4A)	0.8820(6)	0.7036(6)	0.0302(6)	4.1(2)
Cl(4B)	0.5372(6)	0.7136(6)	0.3243(9)	5.7(3)
P(1)	0.8416(2)	0.8934(2)	0.2191(3)	3.1(1)
P(2)	0.6999(2)	0.9052(2)	0.3710(3)	3.1(1)
P(3)	0.7013(2)	0.6076(2)	0.3713(3)	3.3(1)
P(4)	0.8469(2)	0.5995(2)	0.2255(3)	3.5(1)
O(1)	0.8079(6)	0.7756(6)	0.3632(7)	3.5(3)
O(2A)	0.581(1)	0.717(1)	0.315(2)	4.2(7)
O(2B)	0.856(2)	0.708(1)	0.058(2)	4.7(8)
C(1)	0.947(1)	0.969(1)	0.234(1)	4.0(5)
C(2)	0.995(1)	1.040(1)	0.340(1)	5.0(6)
C(3)	1.075(1)	1.093(1)	0.344(2)	6.4(7)
C(4)	1.107(1)	1.071(1)	0.239(1)	6.3(7)
C(5)	1.063(1)	0.997(1)	0.140(2)	7.0(8)
C(6)	0.980(1)	0.949(1)	0.131(1)	5.6(6)
C(7)	0.7751(8)	0.903(1)	0.090(1)	3.7(5)
C(8)	0.771(1)	0.989(1)	0.096(1)	5.1(6)
C(9)	0.726(1)	0.998(1)	-0.009(2)	5.8(6)
C(10)	0.688(1)	0.925(1)	-0.113(1)	5.1(6)
C(11)	0.693(1)	0.842(1)	-0.114(1)	5.2(6)
C(12)	0.734(1)	0.828(1)	-0.014(1)	4.4(5)
C(13)	0.698(1)	0.9825(9)	0.510(1)	3.8(5)
C(14)	0.771(1)	1.040(1)	0.598(1)	5.4(6)
C(15)	0.761(1)	1.099(1)	0.708(2)	7.6(8)
C(16)	0.683(1)	1.099(1)	0.734(1)	5.6(6)
C(17)	0.608(1)	1.037(1)	0.650(1)	6.1(7)
C(18)	0.615(1)	0.980(1)	0.538(1)	5.3(6)
C(19)	0.620(1)	0.9223(9)	0.265(1)	3.5(4)
C(20)	0.621(1)	1.010(1)	0.274(1)	5.6(6)
C(21)	0.552(1)	1.021(1)	0.186(2)	7.3(7)
C(22)	0.494(1)	0.946(2)	0.104(1)	7.7(8)
C(23)	0.491(1)	0.865(1)	0.096(1)	5.5(6)
C(24)	0.555(1)	0.851(1)	0.178(1)	5.0(5)
C(25)	0.696(1)	0.5984(9)	0.516(1)	3.6(4)
C(26)	0.615(1)	0.583(1)	0.541(2)	7.5(8)
C(27)	0.611(1)	0.580(2)	0.649(2)	8.5(9)
C(28)	0.685(1)	0.604(1)	0.745(1)	5.9(7)
C(29)	0.762(1)	0.625(1)	0.722(2)	7.5(8)
C(30)	0.770(1)	0.628(1)	0.605(1)	6.6(7)
C(31)	0.625(1)	0.5075(9)	0.268(1)	3.5(4)
C(32)	0.558(1)	0.513(1)	0.179(1)	4.2(5)
C(33)	0.499(1)	0.433(1)	0.099(1)	4.8(6)
C(34)	0.501(1)	0.351(1)	0.105(1)	5.7(6)
C(35)	0.565(1)	0.346(1)	0.197(2)	7.2(8)
C(36)	0.628(1)	0.427(1)	0.274(2)	5.5(6)

Table

atom

C(37)

C(38)

C(39)

C(40)

C(41)

C(42)

C(43)

C(44)

C(45)

C(46)

C(47)

C(48)

C(49)

C(50)

O(3)

C(51)

C(52)

C(53)

Table 34. (cont'd)

atom	x	y	z	B(eq)
C(37)	0.951(1)	0.574(1)	0.243(1)	4.6(5)
C(38)	0.987(2)	0.554(2)	0.340(2)	12(1)
C(39)	1.070(2)	0.540(3)	0.363(3)	29(2)
C(40)	1.112(2)	0.543(2)	0.266(3)	12(1)
C(41)	1.086(1)	0.570(2)	0.171(3)	10(1)
C(42)	1.001(1)	0.585(1)	0.164(2)	8.1(8)
C(43)	0.779(1)	0.4985(9)	0.099(1)	3.8(5)
C(44)	0.732(1)	0.507(1)	-0.000(1)	4.6(5)
C(45)	0.682(1)	0.431(1)	-0.097(2)	6.6(7)
C(46)	0.682(2)	0.352(1)	-0.089(2)	7.8(9)
C(47)	0.731(2)	0.346(1)	0.008(2)	9(1)
C(48)	0.776(1)	0.421(1)	0.104(2)	7.5(8)
C(49)	0.8060(8)	0.9544(9)	0.353(1)	3.4(4)
C(50)	0.8094(8)	0.588(1)	0.356(1)	3.6(4)
O(3)	0.6824	0.2634	0.3987	25(1)
C(51)	0.6180	0.2569	0.4453	17(1)
C(52)	0.5973	0.3360	0.5512	30(2)
C(53)	0.5917	0.1792	0.4632	33(2)

Table 35. Atomic positional parameters and equivalent isotropic displacement parameters (\AA^2) and their estimated standard deviations for $\text{Re}_2(\mu\text{-O})\text{O}_2\text{Cl}_4(\text{dppm})_2 \cdot 2(\text{CH}_3)_2\text{CO}(\mathbf{15}) \cdot 2(\text{CH}_3)_2\text{CO}$.

atom	x	y	z	B (eq)
Re(1)	-0.16982(3)	0.04364(3)	0.01642(4)	1.82(2)
Cl(1)	-0.2719(2)	0.0212(2)	-0.2248(2)	2.8(1)
Cl(2)	-0.0456(2)	0.0611(2)	0.2567(2)	2.9(1)
P(1)	-0.1332(2)	-0.1504(2)	0.0427(2)	2.04(9)
P(2)	-0.1557(2)	0.2236(2)	-0.0212(2)	1.92(8)
O(1)	0	0	0	2.0(3)
O(2)	-0.3190(6)	0.0833(5)	0.0367(7)	3.3(3)
C(1)	-0.1969(9)	-0.1630(7)	0.169(1)	2.3(4)
C(2)	-0.115(1)	-0.1880(7)	0.296(1)	2.8(4)
C(3)	-0.169(1)	-0.1878(9)	0.390(1)	3.9(5)
C(4)	-0.304(1)	-0.1625(9)	0.355(1)	4.2(5)
C(5)	-0.385(1)	-0.1382(9)	0.228(1)	3.9(5)
C(6)	-0.334(1)	-0.1373(8)	0.137(1)	3.2(4)
C(7)	-0.1982(8)	-0.2498(7)	-0.0981(9)	2.2(3)
C(8)	-0.190(1)	-0.2469(8)	-0.221(1)	3.0(4)
C(9)	-0.230(1)	-0.3296(9)	-0.326(1)	3.8(5)
C(10)	-0.277(1)	-0.4122(9)	-0.310(1)	4.2(5)
C(11)	-0.284(1)	-0.4128(8)	-0.186(1)	4.0(5)
C(12)	-0.246(1)	-0.3331(8)	-0.080(1)	3.2(4)
C(13)	-0.1146(8)	0.3330(7)	0.117(1)	2.2(3)
C(14)	-0.084(1)	0.4234(7)	0.099(1)	2.9(4)
C(15)	-0.070(1)	0.5091(8)	0.198(1)	3.7(5)
C(16)	-0.088(1)	0.5042(9)	0.315(1)	4.0(5)
C(17)	-0.120(1)	0.4169(8)	0.331(1)	3.5(5)
C(18)	-0.132(1)	0.3309(7)	0.233(1)	2.8(4)
C(19)	-0.3136(8)	0.2907(7)	-0.134(1)	2.2(3)
C(20)	-0.411(1)	0.3395(9)	-0.080(1)	3.4(4)
C(21)	-0.531(1)	0.396(1)	-0.161(1)	4.4(5)
C(22)	-0.555(1)	0.4060(9)	-0.294(1)	4.1(5)
C(23)	-0.458(1)	0.356(1)	-0.345(1)	4.0(5)
C(24)	-0.339(1)	0.2960(8)	-0.268(1)	3.2(4)
C(25)	-0.0463(8)	0.2044(7)	-0.116(1)	2.2(3)
O(3)	0.775(1)	0.2822(9)	0.492(1)	7.0(2)
C(26)	0.714(1)	0.212(1)	0.426(1)	5.4(3)
C(27)	0.763(2)	0.096(1)	0.474(2)	6.8(4)
C(28)	0.594(2)	0.249(2)	0.294(2)	9.4(5)
H(1)	-0.0207	-0.2076	0.3172	3.1
H(2)	-0.1099	-0.2052	0.4816	4.3
H(3)	-0.3381	-0.1598	0.4248	4.9
H(4)	-0.4784	-0.1160	0.2080	4.5
H(5)	-0.3910	-0.1171	0.0483	3.8
H(6)	-0.1554	-0.1851	-0.2326	3.8
H(7)	-0.2188	-0.3267	-0.4095	5.1
H(8)	-0.3078	-0.4700	-0.3856	4.9
H(9)	-0.3172	-0.4725	-0.1734	4.7
H(10)	-0.2533	-0.3325	0.0059	3.8
H(11)	-0.0770	0.4230	0.0146	3.6
H(12)	-0.0465	0.5716	0.1869	4.6
H(13)	-0.0815	0.5584	0.3871	5.8
H(14)	-0.1429	0.4078	0.4068	4.5

Table 35. (cont'd)

atom	x	y	z	B(eq)
H(15)	-0.1500	0.2646	0.2463	3.2
H(16)	-0.3927	0.3391	0.0161	4.0
H(17)	-0.5973	0.4337	-0.1227	4.9
H(18)	-0.6331	0.4534	-0.3468	5.1
H(19)	-0.4694	0.3682	-0.4358	5.0
H(20)	-0.2722	0.2617	-0.3060	3.7